8-9-2014

Understanding the Effect of Contaminants from BOP materials on PEMFC electrode: Ex-situ studies

Mayukhee Das
University of South Carolina - Columbia

Understanding the Effect of Contaminants from BOP materials on PEMFC electrode: Ex-situ studies

By

Mayukhee Das

Bachelor of Engineering
Jadavpur University, India, 2008

Submitted in Partial Fulfillment of the Requirements

For the Degree of Doctor of Philosophy in

Chemical Engineering

College of Engineering and Computing

University of South Carolina

2013

Accepted by:

John W. Van Zee, Major Professor

James A. Ritter, Committee Member

Nicole D. Berge, Committee Member

Branko M. Popov, Committee Member

John W. Weidner, Committee Member

Lacy Ford, Vice Provost and Dean of Graduate Studies

Dedication

I dedicate this work to my parents, Mr. Madhusudan Das and Mrs. Ira Das, my siblings Mr. Mainak Das and Mrs. Maitreyee Das.

Acknowledgements

It would not have been possible to write this doctoral thesis without the help and support of the kind people around me, for example my family has given me their unequivocal support throughout, as always, for which my mere expression of thanks likewise does not suffice.

I would like to express the deepest appreciation to my committee chair and my advisor Professor and Dept. Head of Chemical and Biological Engineering Dr. Van Zee, at University of Alabama. He continually and convincingly conveyed a spirit of adventure in regard to research and scholarship, and an excitement in regard to teaching. Without his guidance and persistent help this dissertation would never have been possible. I would like to thank my committee members, Dr. John W. Weidner, Dr. Nicole Berge, Dr. James Ritter, Dr. Branko Popov, who helped me with their constructive criticism and useful reviews.

I owe my profound gratitude to our principal investigator Dr. Huyen Dinh and my colleagues at NREL: Dr. Neyerlin, Jason Christ, Clay Macomber, Dr. Shyam Kocha, Dr. Heli Wang and Jason Zack, who guided me all along till the completion of my project at NREL by providing all necessary resources. I am thankful to and fortunate enough to get constant encouragement and support from my colleagues Dr. Masoto Ohashi, Dr. Shimpalee, Hyun Seok, Md. Opu at University South Carolina.

For any errors or inadequacies that may remain in this work, of course, the responsibility is entirely my own.

Abstract

Off-the-shelf Balance of Plant (BOP) materials for proton exchange membrane fuel cell (PEMFC) systems may be more economical than custom-prepared materials. However, they pose a higher risk of decreased performance of a PEMFC by contaminating the electrodes. This dissertation contributes to the understanding of the mechanisms of electrode contamination by studying the effect of leachate extracts and model compounds from structural plastics and assembly aids that may be used as BOP materials. The effect of contamination was investigated by measuring the decrease in electrochemical surface area (ECA) of the Pt/C catalyst and the change in the oxygen reduction reaction (ORR) current using a thin film rotating disk electrode (TF-RDE) method. Experimental protocols were developed using several batches of electrodes with mass and specific activities within a narrow range of 250±10 mA/mgpt and 350±15 $\mu A/cm^2 Pt$ respectively to ensure reproducibility and quality of contamination data. Preliminary data for screening of BOP materials showed the effect of the liquid phase contamination can be correlated with the chemistry of the constituents present in the leachates.

The organic constituents found in the leachates (detected by GCMS) were tested as model compounds with varying concentrations. The results from these individual organic compounds indicated different extent of contamination (on ECA and ORR)

effects attributed to the poisoning of the catalyst or ionomer mirrored in the loss of Pt sites in the catalyst or the ORR currents. ECA losses due to the organic compounds were more than 50% in all cases at 20 mM. The experiments also offered insights on the poisoning mechanism (adsorption, absorption, parallel electrochemical reactions) by the contaminant molecules. Additional analyses were performed to measure and compare the peroxide formation during ORR experiments due to the contamination using a rotating ring disk electrode (RRDE) method. Recovery experiments were performed to assess the ability to restore the lost ECA and currents through potential cycling to higher voltages. Conclusions were drawn based on the severity of contamination (aromatics more than aliphatics) and recoverability of the electrodes.

Since the leachates were mixtures of organic and inorganic compounds, additional experiments were performed to demonstrate the effects of (1) mixture of organic compounds and (2) mixture of organic and anionic constituents identified in the leachates using TF-RDE method on Pt catalyst and ionomer. The effects of the mixtures on electrode were compared to the individual constituents' effects. Data showed large and almost irreversible losses for a mixture of aromatic model compounds. In cases of mixtures of aliphatic and aromatic organic compound the contamination pattern resembled that of aromatic compounds. The anionic species demonstrated additional ECA loss compared to any other species, which could not be attributed to ionomer poisoning by absorption. It can be concluded that the aromatic compounds shows higher contamination features than aliphatics for both the ionomer and catalyst parts of the electrode.

Table of Contents

Dedication iii

Acknowledgements iv

Abstract vi

List of Tables xi

List of Figures xiv

Chapter 1. Introduction 1

1.1. Polymer Electrolyte Membrane Fuel Cell (PEMFC) 1

1.2. PEM fuel cell fundamentals and theories 7

1.3. Background of study - effect of contamination on PEMFC 14

1.4. Experimental techniques 19

1.5. Research objectives 21

Chapter 2. Literature review 32

2.1. Overview 32

2.2. PEMFC performance degradation in presence of air impurities 32

2.3. Activity requirements for oxygen reduction catalysts 35

2.4. Electrochemical area (ECA) 36

2.5. Oxygen reduction reaction (ORR) 37

2.6. BOP materials as sources of contamination 38

2.7. Effect of contamination on ECA and ORR 39

Chapter 3. Effect of BOP structural plastics on Pt/C 48

3.1. Introduction 49

3.2. Experimental 51

3.3. Results and discussion 58

3.4. Conclusions 69

Chapter 4. Screening of assembly aids using TF-RDE method 88

4.1. Introduction 88

4.2. Experimental 92

4.3. Results and discussions 95

4.4. Conclusions 102

Chapter 5. Effect of a leachate and its constituents on Pt catalyst 134

5.1. Introduction 135

5.2. Experimental 139

5.3. Result and discussion 142

5.4. Conclusions 154

Chapter 6. Study of the effects of organic compounds on PEMFC electrode 173

6.1. Introduction 174

6.2. Experimental 177

6.3. Results and discussions 181

6.4. Conclusions 191

References 218

Appendix A. Calculation of ECA using samples data 228

Appendix B. Monolayer equivalent of leachate solution calculation 236

Appendix C. Effect of purging, hold and cycle time and DI water on ECA 240

Appendix D. Calculations for ORR mass and Pt area specific activities 250

Appendix E. Calculations of Tafel Slope 255

Appendix F. Ring-rotating disk electrode (RRDE) experiments 258

Appendix G. Characterization of leachates by TOC, GCMS and ICP-MS 261

Appendix H. Baselining with Cl^- to study effect of anions 264

List of Tables

Table 3.1. Summary of comparison of ECA loss due to CV cycles and contamination (Ultramid®, EMS Grivory® and Ryton®) on Pt/C catalyst as evaluated in this paper ... 72

Table 3.2. Summary of the average and standard deviation of mass activities during control experiments performed in three steps and after contaminating the electrolyte with 1, 5 and 20 mM of caprolactam corresponding to step 1, 2 and 3 in a different set of experiments (refer to figure 3.11 for the respective ECAs). ... 73

Table 3.3. Summary of ECA loss and ORR currents before and after adding contaminants. ... 74

Table 4.1. Organic (aromatic and aliphatic) compounds identified using GCMS in the leachates of the assembly aids tested in this paper. ... 104

Table 4.2. Inorganic constituents identified using ICP-MS in the leachates of the assembly aids tested in this paper ... 106

Table 4.3. Analysis of current and ECA loss to demonstrate the effect of contamination due to addition of Krytox lubricant.Platinum ECSAs and ORR currents were determined before and after contamination, for thin films of 46 wt.%Pt/VC, 17.4 μgPt cm^{-2}, 0.1M $HClO_4$, 25°C ... 107

Table 4.4. Analysis of current and ECA loss to demonstrate the effect of contamination due to addition of 3M silicone 8664.Platinum ECSAs and ORR currents were determined before and after contamination, for thin films of 46 wt. % Pt/VC, 17.4 μgPt cm^{-2}, 0.1M $HClO_4$, 25°C ... 108

Table 4.5. Analysis of current and ECA loss to demonstrate the effect of contamination due to addition of Loctite 39916.Platinum ECSAs and ORR currents were determined before and after contamination, for thin films of 46 wt.%Pt/VC, 17.4 μgPt cm^{-2}, 0.1M $HClO_4$, 25°C ... 109

Table 4.6. Analysis of current and ECA loss to demonstrate the effect of contamination due to addition of 4000 fast cure white. Platinum ECSAs and ORR currents determined before and after contamination, for thin films of 46 wt.%Pt/VC, 17.4 μgPt cm^{-2}, 0.1M $HClO_4$, 25°C ... 110

Table 4.7. Analysis of current and ECA loss to demonstrate the effect of contamination due to addition of Loctite 567. Platinum ECSAs and ORR currents determined before and after contamination, for thin films of 46 wt.%Pt/VC, 17.4 μgPt cm^{-2}, 0.1M $HClO_4$, 25°C 111

Table 4.8. Analysis of current and ECA loss to demonstrate the effect of contamination due to addition of Bond it b45. Platinum ECSAs and ORR currents determined before and after contamination, for thin films of 46 wt.%Pt/VC, 17.4 μgPt cm^{-2}, 0.1M $HClO_4$, 25°C 112

Table 4.9. Summary and comments on the contamination process by leachates – based on extent of ECA loss during contamination (column 3), recovery of ECA (column 4), ionomer contamination (column 5) and recovery of ionomer contamination (column 6) 113

Table 4.10. Analysis of mass activities to demonstrate the effect of contamination due to addition of leachates. Platinum ECSAs and ORR currents determined before and after contamination, for thin films of 46 wt.%Pt/VC, 17.4 μgPt cm^{-2}, 0.1M $HClO_4$, 25°C ... 114

Table 4.11. Tafel slope (in mV/decade) measured from iR-free polarization curve at 23°C in 0.1 M perchloric acid at a scan rate of 20mV/s (range of polarization being -0.01 to 1.0V) with two parts. In the higher over potentials (typically above 0.8) it is around -65 to -75 mV/decade, but in the lower over potential region it is around -118 to -130 mV/decade for carbon supported Pt..... 115

Table 5.1. Normalized mass activities of Pt/C at room temperature in 0.1 M perchloric acid before, during and after recovery of contamination..... 157

Table 5.2. Comparison of Tafel slope before and after addition of contaminants from the leachate (Bostik® 920) and the model compound (p-toluenesulfonamide) of pre-reduced Pt in higher and lower potential region (interpreted from figure 5.7) 158

Table 6.1. Organic (aromatic and aliphatic) compounds aids tested in this paper identified using GCMS in the leachates of the assembly..... 194

Table 6.2. Analysis of current and ECA loss to demonstrate the effect of contamination due to addition of 2-(2-ethoxyethoxy) ethanol. Platinum ECSAs and ORR currents determined before and after contamination, for thin films of 46 wt.%Pt/VC, 17.4 μgPt cm^{-2}, 0.1M $HClO_4$, 25°C. 196

Table 6.3. Analysis of current and ECA loss to demonstrate the effect of contamination due to addition of 2-(2-ethoxyethoxy) ethanol acetate. Platinum ECSAs and ORR currents determined before and after contamination, for thin films of 46 wt.%Pt/VC, 17.4 μgPt cm^{-2}, 0.1M $HClO_4$, 25°C..... 197

Table 6.4. Analysis of current and ECA loss to demonstrate the effect of contamination due to addition of PEG dimethacrylate. Platinum ECSAs and ORR currents determined

before and after contamination, for thin films of 46 wt.%Pt/VC, 17.4 μgPt cm^{-2}, 0.1M $HClO_4$, 25°C 198

Table 6.5. Analysis of current and ECA loss to demonstrate the effect of contamination due to addition of 2,6-DAT. Platinum ECSAs and ORR currents determined before and after contamination, wt.%Pt/VC, 17.4 μgPt cm^{-2}, 0.1M $HClO_4$, 25°C. 199

Table 6.6. Analysis of current and ECA loss to demonstrate the effect of contamination due to addition of benzyl alcohol. Platinum ECSAs and ORR currents determined before and after contamination, for thin films of 46 wt.%Pt/VC, 17.4 μgPt cm^{-2}, 0.1M $HClO_4$, 25°C 200

Table 6.7. Analysis of current and ECA loss to demonstrate the effect of contamination due to addition of p-tert butl alcohol. Platinum ECSAs and ORR currents determined before and after contamination, for thin films of 46 wt.%Pt/VC, 17.4 μgPt cm−2, 0.1M $HClO_4$, 25°C 201

List of Figures

Figure 1.1. Projected cost of an 80-kWe fuel cell system at a production rate of 500,000/year (36). 24

Figure 1.2. Schematic of PEM fuel cell with electrodes..... 25

Figure 1.3. Fuel cell components (8) 26

Figure 1.4. Polarization curve of a typical PEM fuel cell under normal operation condition showing three main regions of fuel cell polarization: Kinetic, Ohmic, and Mass transport 27

Figure 1.5. Three electrode method for voltammtric experiments using thin film RDE.. 28

Figure 1.6. The rotating ring disk electrode (37) 29

Figure 1.7. A typical cyclic voltammogram in perchloric acid, showing different adsorption and desorption peaks. 30

Figure 1.8. A typical LSV sweep (after saturating the electrolyte with oxygen) for calculating the ORR activity of the catalyst. The current at 0.9 V and the limiting current were recorded. 31

Figure 2.1. Loss in voltage at higher current density in a polarization curve due to the exposure to air contaminants (64)..... 43

Figure 2.2. Durability tests before and after SO2 contamination 44

Figure 2.3. CV showing loss of Catalyst sites after contaminating with structural plastics (BOP materials) leachate 45

Figure 2.4. Examples of plastics with generalized costs for the system..... 46

Figure 2.5. Voltage drop with time after infusing BOP leachates contaminating a fuel cell 47

Figure 3.1. Schematic of the experimental protocol to investigate the impact of the organic contaminants found in the DI water soak of the materials used in a PEMFC. The loss of ECA and ORR activity of Pt/VC were measured using three electrodes TF-RDE apparatus at room temperature. 75

Figure 3.2. Figure showing the initial cyclic voltammetry in 0.1 M HClO4 at room temperature. Conditions: scanned at 20mVs-1 without any rotation of the electrode in a well purged (with inert gas) clean electrolyte from 0.to 1.2 V after conditioning. The CV shows distinct peaks at 0.1 V cathodical (hydrogen adsorption). 76

Figure 3.3. Schematic of the caprolactam molecule showing an aliphatic closed chain organic compound with =O and –HN group attached the ring. 77

Figure 3.4. The loss in ECA after to holding the WE at 0.4 V and OCV potential (0.9V) from the initial ECA in clean 0.1 M HClO4, at room temperature recorded at intervals of 5, 10 and 20 minutes. 78

Figure 3.5. ECA loss due to contamination from the leachates at room temperature, in 0.1 M HClO4. 79

Figure 3.6. Example of the recovery of contaminated (Ultramid®) electrode at the end of potential holding at 0.75 V, 0.85 V, 0.95 V, 1.05 V in a clean electrolyte (0.1 M HClO4) purged with N2. 80

Figure 3.7. The recovery of lost ECA due to potential holding and potential cycling. The left side of the figure shows the recovery characteristic of potential holding on the lost ECA due to contamination from the fabrication plastics used in a fuel cell (Ultramid®, Ryton®) and DI water. The right side shows the further impact of potential cycling to a higher voltage (10 full CV cycles) on recovering the lost ECA after potential holding. . 81

Figure 3.8. Charge recorded during 5 minutes holds at the time of recovery in a clean electrolyte after rinsing the WE in DI water. The holds were performed at 0.75 (blue), 0.85 (red), 0.95 (green) and 1.05 (violet) V. Legend: (…….. EMS Grivory, ¬¬—— Ultramid, – ·– Ryton)..... 82

Figure 3.9. The baseline is the initial CV scans before adding any contaminants (black solid line). After the electrodes were contaminated with two leachates and recovered at higher potential, the CV scans after recovery was shown in red line for EMS Grivory®, blue line for Ultramid® and green line for Ryton®. 83

Figure 3.10. Cyclic voltammogram to determine time needed for caprolactam to adsorb on Pt sites. 1x10-3 M caprolactam was added to the electrolyte after conditioning of electrode at 1.05 V (a) and no change was observed in the Pt-O reduction region. In the first cycle (red line) the first peak (b) was observed at 0.3 V and the Hupd region (c) stayed the same. Then in the 15th cycle after the addition of caprolactam (green line), area under Pt-O region (d) as well as Hupd region (e) decreased. The arrows show the direction of cyclic voltammetry. 84

Figure 3.11. The loss in ECA during the control experiment (▲, Δ) in the clean electrolyte (0.1 M HClO4) and after injecting caprolactam (■, □). The y axis denotes normalized ECA. Sets 1 to 3 denote the three steps after contamination, which for

caprolactam were 1, 5 and 20 mM. Legend: (open symbols: available ECA, solid symbols: loss in ECA)..... 85

Figure 3.12. The effect of caprolactam on partial CV scans at room temperature. Conditions: scanned at 20 mVs-1 without any rotation of the electrode in a well purged (with inert gas) clean electrolyte..... 86

Figure 3.13. ORR polarization curves for Pt/VC in 0.1 M perchlric acid electrolyte: initial or baseline ORR (black solid line), with 1x10-3 M caprolactam (red solid line), with 5x10-3 M caprolactam (green solid line), with 2x10-2 M caprolactam (violet solid line). 87

Figure 4.1. Assembly aids selected for screening based on the contamination and recovery characteristics. The assembly aids have different groups and the assembly aids highlighted may are presented in this paper. 116

Figure 4.2. Schematic of contamination experiments consisting ECA and ORR measurement procedures..... 117

Figure 4.3. Votammograms showing effect of adding 1.2 ml of Loctite® 39916 on Pt/C (Vulcan) at room temperature in 0.1 M HClO4, scanned from 0.025 to 1.05 V 118

Figure 4.4. Contamination criteria: After selecting potential materials they were injected in the RDE electrolyte to observe the impact on the electrochemical surface area – which determined the characteristic of the leachate 119

Figure 4.5. The CV and ORR curves before (baseline) and after adding Krytox leachate (1.8 μM, 18 μM, 180 μM). Change in surface coverage by contaminants (loss of ECA due to adsorption of contaminant molecules on Pt sites) with CV cycles from 0.025 to 0.5 V at a scan rate of 20mV/s as measured under the Hupd. 120

Figure 4.6. The CV and ORR curves before (baseline) and after adding 3M silicone 8664 leachate (1.8 μM, 18 μM, 180 μM). Change in surface coverage by contaminants (loss of ECA due to adsorption of contaminant molecules on Pt sites) with CV cycles from 0.025 to 0.5 V at a scan rate of 20mV/s as measured under the Hupd. 121

Figure 4.7. Organic functional groups found in leachate of 3M Silicone 8664 using GCMS (83)..... 122

Figure 4.8. The CV and ORR curves before (baseline) and after adding Loctite leachate (1.8 μM, 18 μM, 180 μM).Change in surface coverage by contaminants (loss of ECA due to adsorption of contaminant molecules on Pt sites) with CV cycles from 0.025 to 0.5 V at a scan rate of 20mV/s as measured under the Hupd. 123

Figure 4.9. Organic functional groups found in leachate of Loctite 39916 using GCMS (83)..... 124

Figure 4.10. Changes in available ECA due to effect of contamination from the assembly aids 125

Figure 4.11. Organic functional groups found in leachate of 4000 fast cure white using GCMS (83)..... 126

Figure 4.12. Organic functional groups found in the one week soak leachate of Loctite 567 using GCMS (83)..... 127

Figure 4.13. Organic functional groups found in the one week soak leachate of Bond it b45 using GCMS (83)..... 128

Figure 4.14. Tafel plots of the log of kinetic currents, for O2 reduction during potentiodynamic scans in onPt/C after adding 3M Silicone 8664. The oxidation rate was measured in a flow cell (scan rate 20mVs−1,electrolyte as indicated in the figure). The measurements were initiated at -0.1 V and ended at 1.0V. Tafel slopes corresponding to −60 and−120mVdec−1 are shown as solid lines for comparison. 129

Figure 4.15. Tafel plots of the log of kinetic currents, for O2 reduction during potentiodynamic scans in on Pt/C after adding Loctite 39916. The oxidation rate was measured in a flow cell (scan rate 20mVs−1, electrolyte as indicated in the figure). The measurements were initiated at -0.1 V and ended at 1.0V. Tafel slopes corresponding to −60 and−120mVdec−1 are shown as solid lines for comparison. 130

Figure 4.16. Tafel plots of the log of kinetic currents, for O2 reduction during potentiodynamic scans in on Pt/C after adding 4000 fast cure white. The oxidation rate was measured in a flow cell (scan rate 20mVs−1, electrolyte as indicated in the figure). The measurements were initiated at -0.1 V and ended at 1.0V. Tafel slopes corresponding to −60 and −120mVdec−1 are shown as solid lines for comparison. 131

Figure 4.17. Tafel plots of the log of kinetic currents, for O2 reduction during potentiodynamic scans in on Pt/C after adding Loctite 567. The oxidation rate was measured in a flow cell (scan rate 20mVs−1, electrolyte as indicated in the figure). The measurements were initiated at -0.1 V and ended at 1.0V. Tafel slopes corresponding to −60 and −120mVdec−1 are shown as solid lines for comparison. 132

Figure 4.18. Tafel plots of the log of kinetic currents, for O2 reduction during potentiodynamic scans in on Pt/C after adding Bond it b45. The oxidation rate was measured in a flow cell (scan rate 20mVs−1, electrolyte as indicated in the figure). The measurements were initiated at -0.1 V and ended at 1.0V. Tafel slopes corresponding to −60 and −120mVdec−1 are shown as solid lines for comparison. 133

Figure 5.1. Schematic of the experimental protocol to investigate the impact of the organic contaminants found in the DI water soak of the materials used in a PEMFC. The loss of ECA and ORR activity of Pt/VC were measured using three electrodes TF-RDE apparatus at room temperature. 159

Figure 5.2. Votammograms showing effect of adding 28.3 µl of each of the contaminants Bostik®920 (left) and p-toluenesulfonmide (right) on Pt/C (Vulcan) at room temperature in 0.1 M HClO4, scanned from 0.025 to 1.05 V. The TOC of Bostik®920 and p-toluenesulfonmide was 110 ppm. Original concentration of p-toluenesulfonmide was 220 ppm. The final carbon molecule concentration for both molecules was 180µM inside the RDE cell. 160

Figure 5.3. The change in surface coverage by contaminants (loss of ECA due to adsorption of contaminant molecules on Pt sites) with CV cycles from 0.025 to 1.05 V at a scan rate of 100mV/s as measured under the Hupd (open symbols) and oxide region (solid symbols) of the voltammograms normalized by initial available surface in the clean electrode 161

Figure 5.4. Cyclic Voltammetry to 1.05V of uncontaminated contaminated (a. with bostik 920 and b. with 4MBSA) and contamination recovered Pt/C at room temperature in 0.1 M HClO4 at 20mVs-1 162

Figure 5.5. ORR polarization curves for Pt/VC in 0.1M HClO4 as electrolyte: initial or baseline ORR (black solid line), with 1.8x10-3 mM Bostik® (red solid line), with 18x10-3 mM Bostik® (green solid line), with 18x10-2 mM Bostik® (violet solid line). The WE was transferred to a second set of cell with clean electrolyte after contamination to attempt recovery. The blue solid line was obtained during recovery. Conditions: scanned at 20mVs-1 with electrode rotation at 1600 rpm of the electrode in a well O2 saturated electrolyte at room temperature. 163

Figure 5.6. ORR polarization curves for Pt/VC in 0.1M HClO4 as electrolyte: initial or baseline ORR (black solid line), with 1.8x10-3 mM 4MBSA (red solid line), with 18x10-3 mM 4MBSA (green solid line), with 18x10-2 mM 4MBSA (violet solid line). The WE was transferred to a second set of cell with clean electrolyte after contamination to attempt recovery. The blue solid line was obtained during recovery. Conditions: scanned at 20mVs-1 with electrode rotation at 1600 rpm of the electrode in a well O2 saturated electrolyte at room temperature. 164

Figure 5.7. Tafel plots on pre-reduced Pt after addition of (a) Bostik 920 and (b) p-toluenesulfonamide. The ORR data were corrected for mass transfer limitations, elevation effect (due to the altitude of Denver, the partial pressure of oxygen over the RDE cell is 83kPa instead of 101 kPa. Legend: black- baseline, dark blue -1.8 µM, green 18 µM, light blue -180 µM and violet- recovery. Experimental condition: pre-reduced Pt/C (17.37µgPt/cm2) i.e. 400 S at 0.4 vs. RHE before the sweep at 20mV/s from -0.01 to 1 V in oxygen saturated 0.1 M perchloric acid at 1600 rpm. 165

Figure 5.8. Cyclic Voltammetry to 1.05V of contaminated electrolyte with 1.3mM 4MBSA on Pt/C at room temperature in 0.1 M HClO4 at 20mVs-1 166

Figure 5.9. Role of 110 ppm equivalent of 4MBSA on ORR activities of Pt/C in O2 saturated 0.1 M HClO4, rotating WE at 1600 rpm. The Left hand side figure depicts the ring and disk currents during ORR and the right hand side figure shows the

corresponding fraction of hydrogen peroxide formation. The black line shows ORR in clean electrolyte, while the green line shows the LSVs in contaminated electrolyte. 167

Figure 5.10. Cyclic Voltammetry to 1.05V of contaminated electrolyte with 22 µM Cl- on Pt/C at room temperature in 0.1 M HClO4 at 20mVs-1 in a N2 saturated electrolyte. 168

Figure 5.11. Role of 22 µM Cl- on ORR activities of Pt/C in O2 saturated 0.1 M HClO4, rotating WE at 1600 rpm. The Left hand side figure depicts the ring and disk currents during ORR and the right hand side figure shows the corresponding fraction of hydrogen peroxide formation. The black line shows ORR in clean electrolyte, while the green line shows the LSVs in contaminated electrolyte. 169

Figure 5.12. Cyclic Voltammetry to 1.05V of contaminated electrolyte with 640 µM 4MBSA and 22 µM Cl-, on Pt/C at room temperature in 0.1 M HClO4 at 20mVs-1 in a N2 saturated electrolyte. 170

Figure 5.13. Role of 110 ppm equivalent of 4MBSA and 22 µM Cl- on ORR activities of Pt/C in O2 saturated 0.1 M HClO4, rotating WE at 1600 rpm. The Left hand side figure depicts the ring and disk currents during ORR and the right hand side figure shows the corresponding fraction of hydrogen peroxide formation. The black line shows ORR in clean electrolyte, while the red line shows the LSVs in contaminated electrolyte and the red line shows the recovery in a clean electrolyte after rinsing the contaminated electrode in DI water. 171

Figure 5.14. Comparison of normalized available ECA (%) and current 0.9 V (%) in pristine electrolyte with contaminated electrolytes (4MBSA, Cl-, and mixture of 4MBSA and Cl-). 172

Figure 6.1. Schematic of the experimental protocol to investigate the impact of the organic contaminants found in the 1 week DI water soak of the assembly aids used in a PEM fuel cell, on loss of ECA and ORR activities of Pt/VC using three electrodes TF-RDE at room temperature. 202

Figure 6.2. Structures of the organic compounds studied in this paper 203

Figure 6.3. Schematic of the configurations of the adsorbed organic molecule on the Pt nanoparticles (Pt (111)) 204

Figure 6.4. Example of the change in surface coverage by 2-(2-ethoxyethoxy) ethanol, and 2-(2-ethoxyethoxy) ethanol acetate (loss of ECA due to adsorption of contaminant molecules on Pt sites) with CV cycles from 0.025 to 1.05 V at a scan rate of 20mV/s as measured under the Hupd normalized by initial available surface in the clean electrode. 205

Figure 6.5. The peak at 0.8 V is a characteristic feature of both 2-(2-ethoxyethoxy) ethanol, and 2-(2-ethoxyethoxy) ethanol acetate, which is attributed to the adsorption of –

CHO species on Pt after following a series of steps involving electrochemical reactions 206

Figure 6.6. The effect of polyethylene glycol dimethacrylates (loss of ECA due to adsorption of contaminant molecules on Pt sites) with CV cycles from 0.025 to 1.05 V at a scan rate of 20mV/s as measured under the Hupd normalized by initial available surface in the clean electrode. 207

Figure 6.7. Example of effect of 2,6-DAT (loss of ECA due to adsorption of contaminant molecules on Pt sites) with CV cycles from 0.025 to 1.05 V at a scan rate of 20mV/s as measured under the Hupd normalized by initial available surface in the clean electrode 208

Figure 6.8. Example of the change in surface coverage by benzyl alcohol and p-tert butyl phenol (loss of ECA due to adsorption of contaminant molecules on Pt sites) with CV cycles from 0.025 to 1.05 V at a scan rate of 20mV/s as measured under the Hupd normalized by initial available surface in the clean electrode. 209

Figure 6.9. The ECS loss after adding organic compounds in the RDE electrolyte. 210

Figure 6.10. Recovery CV at room temperature after contaminating with 20mM of DEGEE using partial scans from 0.75, 0.85, 0.95 and 1.05 V at 20mVs-1. 211

Figure 6.11. ORR polarization curves on a Pt/VC working electrode at different concentrations of 2-(2-ethoxyethoxy) ethanol after pre-reducing the Pt at 0.4 V for 400s. The “baseline” curve denotes uncontaminated polarization curve. 212

Figure 6.12. ORR polarization curves on a Pt/VC working electrode at different concentrations of 2-(2-ethoxyethoxy) ethanol acetate after pre-reducing the Pt at 0.4 V for 400s. The “baseline” curve denotes uncontaminated polarization curve. 213

Figure 6.13. ORR polarization curves on a Pt/VC working electrode at different concentrations of polyethylene glycol dimethacrylates after pre-reducing the Pt at 0.4 V for 400s. The “baseline” curve denotes uncontaminated polarization curve. 214

Figure 6.14. ORR polarization curves on a Pt/VC working electrode at different concentrations of 2,6-DAT after pre-reducing the Pt at 0.4 V for 400s at room temperature. The “baseline” curve denotes uncontaminated polarization curve. 215

Figure 6.15. ORR polarization curves on a Pt/VC working electrode at different concentrations of benzyl alcohol after pre-reducing the Pt at 0.4 V for 400s at room temperature. The “baseline” curve denotes uncontaminated polarization curve. 216

Figure 6.16. ORR polarization curves on a Pt/VC working electrode at different concentrations of p-tert butyl alcohol after pre-reducing the Pt at 0.4 V for 400s at room temperature. The “baseline” curve denotes uncontaminated polarization curve. 217

Figure C.1. Open circuit potential before purging the electrolyte with inert gas was as high as 0.85 V due to the presence of dissolved O2 in the electrolyte (a). After purging for 15 minutes the OCV came down to 0.45 (b) and after conditioning (WE was subjected to potential cycling between 0 to 1.2 V at a rate of 100 mVs-1) the OCV further reduced to 0.3 V (c). 246

Figure C.2. Effect of DI water (left) on the partial cyclic voltammetries and baseline cyclic voltammetries during the control experiments, with no DI water added (right). CVs 1 to 6 correspond to the CVs at the performed at 10 minutes intervals. 247

Chapter 1. Introduction

1.1. Polymer Electrolyte Membrane Fuel Cell (PEMFC)

There is a growing awareness on Fuel Cell research due to the less environmental impact and decay in the reserve of fossil fuel as a supply of energy sources. Fuel cells have the potential to provide a clean and efficient energy source for transportation, stationary power, and specialty applications as sustainable and renewable energy sources. Recently efforts are being made to commercialize the PEM fuel cell running on hydrogen to minimize dependence on petroleum. Unlike batteries, fuel cells do not store energy. They can be continually fed a fuel much like an engine. One common fuel often used for fuel cells is hydrogen because it is abundant in nature and has highest energy density.

The first challenge is producing inexpensive fuel cell components. Fuel cells can be commercially used in stationary and automotive industries if the cost is prohibitively high. Current studies estimate that the cost of large scale production of fuel cells would be approximately 31 $/kW. The US Department of Energy (DOE) has targeted a production cost of $30/kW for transportation and $750/kW with for Stationary 40,000 h durability and efficiency of 42.5% by 2015 (1, 2) to make fuel cells commercially viable in the transportation market. As shown in Figure 1.1, for projected for high volume production (500,000 units/year) the cost of a hydrogen-fueled 80-kWe fuel cell power system) was calculated to be $51/kW in 2010, a $22/kW (30%) reduction from the 2008 cost of $73/kW and $10/kW (16%) reduction from the 2009 cost of $61/kW (2). But the

future targets (DOE, 2015) for vehicle applications still being $30/kW_{net}$ with the 2015 durability target of 5,000 hours (2), major system level cost lowering is required.

Currently the largest cost associated with the fuel cell is the precious metal Pt used as the catalyst for the oxygen reduction reaction (ORR) at the cathode. This cost can be decreased by finding robust electrode configurations and low concentration Pt catalyst or replacing Pt with other metal catalyst that are cheaper. New catalysts that use non precious metals are in development, but it compromises with the efficiency (3). The other major cost associated with hydrogen PEMFCs is the cost of creating and distributing hydrogen fuel.

1.1.1. History of Fuel Cell

Sir William Grove invented the first fuel cell generating electricity from gaseous fuel and called it "gaseous voltaic battery". The first practical application of polymer membrane fuel cell dates back to the end of 1960 used in the Gemini Program (US Space Program) manufactured by General Motors. Fuel cells were used in the Apollo Space Program. Fuel cell resurfaced in 1990's when Ballard Power Systems introduced fuel cell powered buses (4). It was until later 1990's that the potential of fuel cell in automobile application was realized. The fuel cell activity was funded by US Department of Energy at the end of the 1990's and most car manufacturing companies played an important part in production of a prototype car that ran on hydrogen energy. In 21st century, the scope of manufacturing and commercializing fuel cell vehicles, applying fuel cell in stationary and emergency power supply is mostly limited in North America, Japan and some of the western European countries. Even though gradual involvement of other countries have

been seen in last five years, for different environmental and economic reasons, more continuous interest and effort are needed in research of all kind of fuel cells.

Development of PEM fuel cell catalysts with superior activities has always been an important part in the history of commercialization of fuel cell. Effort to reduce precious metal (Pt) usage in manufacturing a PEMFC has opened new directions in catalyst synthesis, such as using high surface area carbon support for Pt and alloying Pt with non-noble metals like Ni, Co, Fe etc. The Pt catalyst used in a PEM fuel cell has evolved from platinum black to carbon supported platinum catalysts. Platinum black catalysts are not economically feasible due to their low surface areas, requiring higher platinum loadings to achieve realistic performance goals. In last decade, researchers have been focusing on carbon-supported platinum (Pt/C) catalysts to attain higher active surface areas. Pt/C catalysts are now available in loadings from around 20% to over 50% platinum. Enhancements in catalyst synthesis technology have allowed for production of catalysts containing over 50% platinum with very small platinum particles. For example, catalysts with 50% platinum by weight can be made with an average platinum particle size of ca. 2 to 3 nm. Typical loadings in the electrode today are about 0.4-0.8 mg platinum/cm^2, which is significantly lower than 25 mg/cm^2 with early platinum black catalysts. The US Department of Energy (DOE) has set targets of 0.3 mg/cm^2 for 2010 and 0.2 mg/cm^2 for 2015 (5).

1.1.2. Hydrogen as fuel

Hydrogen has been touted as the “fuel of the future”. Hydrogen can be created from a variety of sources independent of oil including reforming of natural gas or coal, biomass, or electrolysis of water. Hydrogen is a carbon-free fuel. Therefore no harmful

emissions are released during hydrogen consumption, which is a big concern for global warming. Water is the only byproduct of a hydrogen/oxygen fuel cell. In addition, the efficiency of fuel cells is higher than of internal combustion engines since the process of the fuel cell is electrochemical and therefore does not involve conversion of thermal to mechanical energy. For these reasons extensive research funding has been given to study, develop, and produce hydrogen PEMFCs.

Hydrogen fuel cells utilize the energy released when hydrogen and oxygen combine to form water. This reaction occurs as two separate half reactions (6):

$$2H_2 \rightarrow 4H^+ + 4e^- \qquad \text{(anode)}$$

$$O_2 + 4e^- + 4H^+ \rightarrow 2H_2O \qquad \text{(cathode)}$$

Energy is manifested as electrical potential by forcing the hydrogen half reaction products at the anode through an electrolyte that allows protons (H^+ ions) to pass through to the cathode but restricts the flow of electrons. The electrons are flows in an external path and the electrical current is obtained. The transported protons and electrons meet at the cathode where they react with oxygen to form water. These reactions are shown schematically in Figure 1.2.

Hydrogen gas is an extremely difficult to store, and transport. Currently no specific infrastructure exists for the large scale production or transportation of hydrogen fuel. Hydrogen requires special infrastructure because it has a low energy to weight density and because it causes corrosion of normal transportation pipes made of steel and other metals. Additionally, no distribution network for hydrogen currently exists. Estimates put the cost of a transport and distribution network for hydrogen in the US at

up to 1 trillion dollars. At the very least 12 billion dollars of investment is needed to provide filling stations accessible by 70% of the US population (7).

Recently a hydrogen fueling station (operated by AirPower) opened next to the Orange County waste-water treatment plant in Fountain Valley. The hydrogen fuel offers about 70 miles per gallon and the station can fuel up to 50 automobiles per day with the daily 120 kilograms of hydrogen gas produced at the plant. In order to produce the hydrogen gas, sewage is processed to collect methane. This methane is converted into hydrogen and sent into a fuel cell to power the entire plant with 250 kilowatts of electricity. The remaining hydrogen is converted into fuel grade hydrogen and sent to the fueling station for consumer use.

1.1.3. Fuel cell components

The membrane electrode assembly (MEA), consisting primarily of an anode catalyst, a cathode catalyst, and a proton exchange membrane (PEM), is the key component of PEM fuel cells (see figure 1.3). The electrocatalytic activity, selectivity, and stability of catalysts, as well as the electrochemical reactions taking place at the catalyst–PEM interface, play a crucial role in determining the performance and durability of fuel cells. At cathode, oxygen reduction is catalyzed by Pt. The other electrode, the anode, is where hydrogen oxidation occurs. Electrodes for fuel cells are usually made of platinum or other precious metal combinations. These electrodes are separated by an electrolyte. PEMFCs are fuel cells that use a solid polymer membrane as the electrolyte. These polymer electrolytes are known as ionomers. The most popular and well-studied polymer electrolyte membrane is Nafion® (Dupont. Wilmington, DE). Nafion® has a

polytetrafluoroethylene (PTFE) like backbone with sulfonic acid terminated ends (9). Polymers of this type are often called perfluorosulfonic acid (PFSA) polymers.

The strong bonds between the fluorine and the carbon make it durable and resistant to chemical attack. Another important property is that it is strongly hydrophobic, and so it is used in fuel cell electrodes to drive the product water out of the electrode, and thus it prevents flooding. The basic PTFE polymer is sulphonated – a side chain is added, ending with sulphonic acid HSO_3. The HSO_3 group added is ionically bonded, and so the end of the side chain is actually SO_3- ion that attracts H^+. The key property of sulphonic acid is that it is highly hydrophilic. The hydrophilic regions around the clusters of sulphonated side chain can lead to the absorption of large quantity of water, and increase the dry weight as much as 50%. Within the hydrated regions, the H^+ ions are relatively weakly attracted to the SO_3^- group and are able to move (10).

Necessary components in fuel cell are carbon-supported platinum layer and gas diffusion layer in the fuel cell system. Gas diffusion layers (GDL) regulate the supply of gas to the electrodes as well as help with the transport and management of the water in the fuel cell system. They must also be electrically conductive to pass the current from the electrodes to the current collectors. GDLs are generally made of carbon cloth or carbon paper and often contain PTFE to aid in water management and channeling.

There are different coating processes for the generation of catalyst layers (CL) in MEAs. The traditional mode is that the CL is applied to the GDL (catalyst gas diffusion layer, CGDL), followed by membrane addition. The other mode is that the CL is directly applied to the membrane (catalyst coated membrane, CCM) followed by GDL. Adding

the GDLs to the CCM creates a membrane electrode assembly (MEA). Multiple MEA units can be stacked together in series to provide a larger electrical potential than one MEA alone just as multiple batteries can be placed end to end to create a larger voltage. MEAs are separated by bi-polar plates which collect the current and direct gas flows in the fuel cell stack. Other system components such as gaskets, tubing, and wiring are also needed (6).

The important challenges in PEMFC research arise in the CLs because these are complex and heterogeneous. The catalyst layers need to be designed so as to generate high rates of the desired reactions and minimize the amount of catalyst necessary for reaching the required levels of power output. To meet the goal, the following requirements need to be considered:

(1) Large three-phase interface in the catalyst layer,

(2) Efficient transport of protons,

(3) Easy transport of reactant and product gases and removal of condensed water, and

(4) Continuous electronic current passage between the reaction sites and the current collector. The CL is in direct contact with the membrane and the gas diffusion layer (GDL)

1.2. PEM fuel cell fundamentals and theories

The performance of a fuel cell is governed by its Polarization Curve. This type of performance curve shows the DC voltage delivered at the cell terminals as a function of the current density (current per unit area of membrane) is drawn by the external load. In

reality fuel cells achieve their highest output voltage at open circuit (no load) conditions and the voltage drops off with increasing the voltage drops off with increasing current draw. This is known as polarization. An example of a polarization curve is shown in figure 1.4.

The fuel cell efficiently converts chemical energy to electrical energy, but the conversion is associated with some losses. There are losses to energy production associated with each of the main processes involved in the energy conversion. The losses that reduce the efficiency of fuel cells can be broken down into four main categories. These categories are open circuit losses, activation losses, Ohmic losses, and mass transport losses. These losses will often be referred to as overpotentials or polarizations. In a real process the electrodes cannot operate at their equilibrium potentials. Irreversibilities in real processes lead to efficiency losses or resistances to the process. Electrodes must shift to potentials more favorable for oxidation or reduction to overcome efficiency losses. These shifted potentials are called overpotentials.

The cell voltage V = Open circuit voltage – cathode activation losses – anode activation losses – ohmic losses – (concentration polarization or mass transport losses) (11).

Open circuit losses cause the potential of the cell at zero current to be lower than what one might expect from the theoretical thermodynamic potential of the cell. The cell potential is lower than the thermodynamic potential mainly due to use of air instead of pure oxygen, reactants crossing over from one electrode to the other and oxide formation on the electrodes (12). Activation losses are associated with the reaction and charge transfer steps. Ohmic losses account for the energy lost as ions are carried across the

electrolyte. Mass transport losses occur because the reactant concentrations are lowered as reactants are transported to the reaction site (13).

- Activation losses: Slow kinetics of reaction on electrode surface. The activation overpotential arises by virtue of the activation energy barrier that the reactants must overcome. Since cathode kinetics are slower than anode kinetics, cathode has large overpotential and anode has much smaller overpotential, so small that it is ignored for all practical purposes.

At equilibrium: Forward rxn. rate = Reverse rxn. Rate, so no net current is flowing.

- Fuel crossover and internal currents: Diffusion of fuels from anode to cathode through the electrolyte and react with oxygen without generating current and electron passes through the electrolyte. This small amount of wasted fuel that migrate through the electrolyte is known as fuel crossover.
- Ohmic losses: Electric resistance of electrode and interconnections. Ohmic losses (equation 1) occur due to resistances to the flow of ions through the electrolyte and to the flow of electrons from the electrode to the external circuit.

$$\eta_{ohmic} = \eta_{elec} + \eta_{ionic} = i(R_{elec} + R_{ionic}) \qquad [1]$$

R_{ionic} = Electrolyte resistance to ionic transport

R_{elec} = Electrical resistance in cell

- Mass transport or concentration losses: Change of reactant concentration at surface of electrode. Concentration gradient establishes at the electrode surface which prevent the fresh reactants from reaching the catalyst and reduction in reaction concentration.

The change of O_2 concentration if air is used and O_2 partial pressure in the cathode will reduce the operational voltage significantly. Since H_2 diffusion is fast across the flow field and purity of the gas is higher than air used in cathode, concentration polarization in anode is negligible. At cathode slow oxygen mass transport loss and subsequent voltage loss in the cathode, this is also called mass transport losses (11).

These losses are also dependent on the amount of current drawn from the cell. One typical way of measuring fuel cell performance is to graph the voltage of the fuel cell on the ordinate axis against the current density of the cell on the abscissa. These graphs are called polarization curves. A polarization curve has three main regions named after the overpotentials that dominate in that region. At low currents activation dominates the polarization curve. In middle potentials Ohmic losses dominate the polarization. At high currents mass transport effects come into play. These losses determine the total amount of power that can be drawn from a fuel cell. The power drawn from the cell is equal to the voltage multiplied by the current. Figure 1.4 shows a representative fuel cell polarization curve and highlights these three regions (11).

1.2.1. Fuel cell thermodynamics

The basic reactions occurring in the half cells are:

$H_2 \rightarrow 2H^+ + 2e^-$ (anode)

$O_2 + 4e^- + 4H^+ \rightarrow 2H_2O$ (cathode)

The reaction can be combined and written as:

$H_2 + 1/2O_2 \rightarrow H_2O\ (l) + 286\ kJmol^{-1}$

The reaction is exothermic, with 286 kJmol-1 heat of reaction released per molecule of hydrogen. This heat can be partially converted to electricity in a fuel cell following the Gibb's free energy (ΔG) equation (2):

$$\Delta G = \Delta H - T\Delta S \quad [2]$$

Due to the entropy (ΔS), some energy is lost as heat. At T= 25°C, out of 286 $kJmol^{-1}$, 237 $kJmol^{-1}$ can be converted to electrical energy.

Electrical work, W, in a fuel cell is given by:

$$W = nFE \quad [3]$$

n = number of electron transfer per molecule of H_2, 2

F = charge for 1 mol electron transfer (Faraday's constant), 96485

E = theoretical potential of a fuel cell

Now, maximum number of electrical energy generated in a fuel cell is the Gibb's free energy, ΔG.

Therefore, W = ΔG, or

$$E = \frac{-\Delta G}{nF} \quad [4]$$

The numerical value of E after substituting for ΔG, n and F is 1.23 Volts. So, at 25°C the theoretical potential of a fuel cell is 1.23 V.

The theoretical fuel cell efficiency is given by η:

$$\eta = \frac{\Delta G}{\Delta H} = 0.83 \text{ or } 83\% \quad [5]$$

This efficiency changes with temperature and pressure.

$$\Delta E° = -\Delta G°/ (z\ F)\text{……..}[6]$$

The general Nernst equation correlates the Gibb's Free Energy ΔG and the EMF of a chemical system known as the galvanic cell. For the reaction

$$aA + bB \leftrightarrow cC + dD$$

$$\text{and, } Q = \frac{[C]^c[D]^d}{[A]^a[B]^b}$$

It has been shown in thermodynamics that

$$\Delta G = \Delta G° + R\ T\ \ln Q \quad [7]$$

$$\Delta G = -\ z\ F\Delta E \quad [8]$$

$$-\ z\ F\ \Delta E = -\ z\ F\ \Delta E° + R\ T\ \ln Q \quad [9]$$

Where R, T, Q and F are the gas constants (8.314 J/(molK), temperature (in K), reaction quotient, and Faraday constant (96487 C), respectively). Thus, we have:

$$\Delta E = \Delta E^0 + \frac{RT}{zF}\ln\frac{[C]^c[D]^d}{[A]^a[B]^b} \quad [10]$$

$$E = E^0 + \frac{RT}{nF}ln\frac{C_{ox}}{C_{red}} \quad [11]$$

Where E^0 is the cell potential at standard condition or formal potential (potential actually measured in an electrochemical cell) (14)

This is called Nernst Equation (equation 11). Nernst equation describes how reversible cell voltages vary with chemical activity. A Carnot engine would have to have a high temperature of 1753 K, with a corresponding low temperature of 1753 K, with a corresponding low temperature of 298 K, to achieve an efficiency of 83%.

1.2.2. Fuel cell electrochemistry

In a fuel cell in cathode oxygen reduction and in anode hydrogen oxidation takes place. The net current density generated due to these electrochemical reactions and the potential of the fuel cell bears a relationship knows as Butler Volmer equation (4):

$$i = i_0 \left\{ exp\left[\frac{-\alpha_{rd} F(E-E_r)}{RT}\right] - exp\left[\frac{\alpha_{ox} F(E-E_r)}{RT}\right]\right\} \quad [12]$$

Where:

i_0 = exchange current density kinetic parameter representing the electrochemical reaction rate at equilibrium. For an electrochemical reaction, both forward and backward reactions can occur. At equilibrium, the net current density of the reaction is zero. The current density of the forward reaction equals that of the backward reaction [3]. This current density is called exchange current density. The magnitude of the exchange current density determines how rapidly the electrochemical reaction can occur.

α_{rd}, α_{ox} = transfer coefficients for reduction and oxidation reactions, is 0.5 for hydrogen fuel cell anode and 0.1 for anode α = 0.5

E_r = reversible or equilibrium potential. The reversible potential at the PEMFC anode is 0 V and 1.23 at the cathode. F is the Faraday constant, R is the gas constant, and T is the temperature in Kelvin.

$E-E_r$ is known as overpotential η. The overpotential on the anode is positives ($E > E_r$) and negative on the cathode ($E < E_r$). At large overpotential the second term in equation is negligible and the equation reduces to

$$i = i_{0,c}\left\{exp\left[\frac{\alpha_{rd,c}F(E_{ac}-E_{r,c})}{RT}\right]\right\} \quad [13]$$

Where subscript "c" denotes the cathode reaction:

$$E_{ac} - E_{r,c} = \eta_c \quad [14]$$

The plot of η_c vs. I gives a linear relationship, and the slope is given by $\frac{2.3\,RT}{\alpha F}$, which is called Tafel slope.

1.2.3. PEM fuel cell catalysts

- High intrinsic activities for fuel oxidation and O_2 reduction
- Large specific surface area (m^2/g)
- Good durability
- Good electric conductivity
- Inexpensive to make, good reproducibility

Anode Electrocatalysis:

$H_2 \rightarrow 2H^+ + 2e^-$ (E_0=0.00 V, pH=0)

$H_2 + Pt \rightarrow 2Pt\text{-}H_{ads}$

$2Pt\text{-}H_{ads} \rightarrow 2Pt + 2H^+ + 2e^-$

- Pt, Pd have high exchange current density i_0 (10^{-3} A/cm^2)
- For pure H_2, low concentration (0.05 mg/cm^2) of Pt is needed
- CO, CO_2 and H_2S degrade anode performance through poising

1.3. Background of study - effect of contamination on PEMFC

Hydrogen PEMFCs produce energy cleanly and efficiently, but three major hurdles must be overcome before PEMFCs can be a viable energy source for the future.

The three hurdles are cost, infrastructure, and durability. Each of these obstacles is an active area of research and development. These three areas are also interrelated. For instance, higher durability reduces long-term costs, but the cost of creating a better infrastructure and components to increase durability may actually increase total costs. Other factor affecting PEMFC performance and durability is contamination. Contaminants are introduced into the PEMFCs with the incoming reactant streams (fuel and oxygen) or from materials used to construct the PEMFC stack or its accessories. Contamination can be classified into following three categories based on their sources: fuel (anode side), air (cathode side) and system contaminants (15).

1.3.1. Sources of contamination

1.3.1.1 Fuel contaminants

The fuel-side contaminants originate from reformates, which the fuel (hydrogen) is derived from more cost effectively than electrolysis of water. The majority of commercial hydrogen is produced by the steam reforming of natural gas. The steam reforming process converts hydrocarbons into CO, CO_2, and H_2 (reformates). Natural gas contains many naturally occurring impurities, especially H_2S and NH_3. Even though, the reformate is purified to the desired H_2 grade, but the purification processes can leave traces of residual CO, H_2S, CH_4 and NH_3. These three fuel side contamination significantly affects the catalyst performance even at a very low concentration over a longer period of time (16, 17). Ammonia has been identified as one of the three main contaminants in hydrogen streams along with carbon monoxide and hydrogen sulfide (18, 19). Scientists are involved in setting maximum ammonia level purity standards for hydrogen fuels. Initial specifications from the Freedom Car fuel cell tech team allowed

for up to 1 ppm of NH_3 in the hydrogen feed gas (20). The Japanese Automobile Research Institute (JARI) has claimed that ammonia levels should be below 0.3 ppm. More recent specifications, such as SAE J2719 and ISO TS14687-2, state that ammonia should be limited to 0.1 ppm (18).

During the reforming process organic sulfur species can be oxidized to SO_2 or reduced to H_2S. CO is always a contaminant even at ppb level. The residual CO, H_2S, SO_2, and organic sulfur species (thiophenes, mercaptons, etc.) resulting from hydrocarbon reformation can be one of the major issues in the path of commercialization of PEMFC.

1.3.1.2 Air contaminants

Most PEMFCs use the ambient air as a source of O_2 and rendering the cathodes susceptible to airborne contaminants since using pure oxygen can be very expensive. SO_x and NO_x are two important airborne contaminants that are the subject of many studies (21-23). Contaminants can lead to permanent performance losses in PEMFC cathodes. SO_2 level of 1ppm has been reported to cause significant contamination over a period of 24 h (24).

1.3.1.3 . System contaminants

- Structural materials
- Coolants*
- Elastomers for seals
- Elastomers for (sub)gaskets
- Assembly aids (adhesives, lubricants)

- Hoses
- Membrane degradation products
- Bipolar/end plates
- Ions from catalyst alloys
- Compressor oils

Contamination coming from components of a PEMFC or stack or accessories can extensively reduce the performance and durability of hydrogen PEMFCs. Cationic impurities such as NH_4^+, Na^+, Ca^{2+}, Cs^+ present in the assembly aids, hoses, seals (25, 26) compete with protons for the sulfonic acid sites in the polymer electrolyte membrane (27-29). Also cations, such as Fe^{3+}, Ni^{2+}, Cu^{2+} and Cr^{3+} from the material of the bipolar plate can hinder the performance of the cell by attacking the membrane resulting in its chemical and mechanical degradation (17).These impurities can be present in the hydrogen feed stream. Ammonia is often a byproduct of the reforming method used to produce hydrogen. In the fuel cell environment ammonia is converted to the ammonium cations.

Hydrocarbon coolants have a strong affinity for platinum catalysts and can cause fouling of the surface (30). Plasticizers can leach out of tubing and sealing materials. Studies reported some of common materials which can be used in commercial automotive systems with PEMFCs to reduce the manufacturing cost can contaminant PEMFCs due to time associated exposure, including plastics, assembly aids, antioxidants and flame retardants (31, 32). Even the catalyst can contain contaminants, such as residual Cl^- from starting synthetic materials, and sulfur in the carbon catalyst supports (33). The impurities

can be distributed wet gas streams or water in the humidifier can collect organic and ionic impurities.

Halocarbons are proposed to be regulated as part of the International Organization for Standardization (ISO) and the Society of Automotive Engineers (SAE) fuel quality standards. The proposed limit for chlorinated compounds in both the ISO and SAE standards is 0.05 ppm of total chlorinated species (18, 34).

Contaminating cations can also access the system from the air feed in coastal environments (sodium) or where salts are used as deicing agents (calcium). Finally, they can also be introduced into the system through corrosion of gas feed lines, bipolar plates and other stack and tubing components. The corrosion products of metal bipolar plates have been studied and have shown many different cations (primarily multivalent transition metals) (31, 35).

There are significant repercussions when contaminant cations replace protons in the fuel cell ionomer. This type of replacement is of particular concern since most cationic contaminants have a higher affinity for the sulfonic acid sites than protons do (25). Cations in the membrane affect water management in the membrane and decrease the ionic conductivity of the membrane. The cations can also hinder the ability of the platinum catalyst in the cathode electrode layer to catalyze the oxygen reduction reaction (27).

Although a major amount of research has been undertaken on other modes of durability failure, relatively little research has been carried out on cationic contamination. This may be because in earlier generation fuel cells other modes have often caused device

failure before cationic contamination could seriously degrade performance. Also, fuel cells used in research settings tend to use higher quality feed streams and newer components less prone to corrosion since cost is not as much of a factor. Studying cationic contamination becomes increasingly important as the durability and marketability of PEMFCs continues to rise. Understanding exactly how and to what extent cationic contamination effects PEMFCs will allow for the development of hydrogen purity standards, understanding of acceptable corrosion rates, new modes for diagnosis, new component design, and better methods to recover fuel cell performance.

1.4. Experimental techniques

1.4.1. Three electrode method

A standard three electrode electrochemical cell can be used to study the oxidation or reduction half reactions that occur in a fuel cell (figure 1.5). In such an electrochemical cell it is possible to isolate the oxidation and reduction half reactions to study the catalyst contamination and the associated mechanisms and kinetics. For hydrogen fuel cells, the focus of this type of research is on the cathode half reaction, the reduction of oxygen, since it has a sluggish kinetics. A three electrode cell employs a *working* electrode, where the reaction of interest occurs, a *counter* electrode, through which the current flows to or from the working electrode, and a *reference* electrode, through which the potential is controlled without passing current. This configuration and the choice of electrode materials will be discussed later in greater detail. Ex-situ techniques like cyclic voltammogram, rotating disk electrode experiments, ring rotating disk electrode experiments assist greatly in isolating the poisoning effect on catalyst from membrane contamination by ion exchange.

1.4.2. Thin film rotating disk electrode (TF-RDE) method

The rotating disk electrode (RDE) or rotating ring-disk electrode (RRDE) is one of the most commonly used analytical tools in electrochemistry. An RDE is a small metal disk inlaid into an insulating cylinder having a large base. The disk is situated in the center of the base. The cylinder is mounted on a metallic shaft connected to an electric motor. The shaft is perpendicular to the base, lies in the axis of the cylinder, and is connected to a potentiostat and to the metal disk by a wire.

As shown in Figure 1.6, a disk electrode is set in an insulating rod, which is rotated at a constant frequency in a solution. Rotation of the solution induces a centrifugal force that causes radial movement. Due to the rotation convection current is set, the adsorbent species from the bulk to the electrode.

An RRDE (figure 1.6) is a double-working electrode (WE) used in hydrodynamic voltammetry, very similar to an RDE. Instead of three electrodes it employs four electrodes. The electrode rotates during experiments, inducing a flux of the electrolyte to the electrode. The difference between an RRDE and an RDE is the addition of a second WE in the form of a ring around the central disk of the first WE. The two electrodes are separated by a nonconductive barrier and connected to the potentiostat through different leads. To operate such an electrode it is necessary to use a bipotentiostat. This rotating hydrodynamic electrode is used to detect peroxide formation at the ring.

1.4.3. Cyclic voltammetry

Since electrochemistry is an interfacial science, it permits characterization of the catalyst surface and its interaction with the gases and the electrolyte. One method of characterization of the surface is cyclic voltammetry, where the potential is scanned

linearly in one direction, and then scanned in the opposite direction to generate a complete voltage vs. current scan, as shown in Figure 1.7. Cyclic voltammetry is used in half cell electrochemistry to determine the electrochemical surface area (ECSA), and the potential dependence of the contaminant oxidation or reduction reaction. In the hydrogen region, protons interact with the catalyst surface, adsorbing to the surface in the cathodic scan and desorbing in the anodic scan. In the oxygen region, hydroxide ions oxidize the surface in the anodic scan and are reduced from the surface in the cathodic scan. Between these regions is the double layer region, in which only double layer charging occurs. The increased surface area from nanoparticles (as compared with smooth polycrystalline electrodes or single crystals) results in a higher double current magnitude in this region.

1.4.4. Linear sweep voltammetry

Linear sweep voltammetry is a general term applied to any *voltammetric method* in which the potential applied to the working electrode is varied linearly in time. Hydrodynamic voltammetry to assess oxygen reduction reaction was carried out applying LSV in O_2 saturated solution with oxygen blanket on the electrolyte rotating the working electrode at 1600 rpm. LSVs were recorded from -0.01 to 1.0 V at scan rate of 20mV/s. An example of a typical LSV curve is given in figure 1.8.

The limiting current, i_{lim} was measured at the highest current at mass controlled region. The current at 0.9 V is also measured to calculate specific and mass activities.

1.5. Research objectives

The goal of this dissertation is to provide an increased understanding of fuel cell system contaminants and help provide guidance in the implementation, and where

necessary, the development of system materials that will not lead to undesirable loss of fuel cell efficiency due to contamination. In addition to that, studying ORR in presence of those contaminants will facilitate development of high performance fuel cell catalysts.

The research objectives are to determine the sequence of experiments, developing protocols to study contamination effect, establishing a stable baseline with clean electrolyte for well reproducible data, perform electrochemical testing with the BOP leachates, down select materials to perform experiments with organic compounds, analyze the data and propose recovery strategy.

A broad spectrum of BOP materials (i.e., plastics, lubricant and adhesives) commonly used in present-day vehicles are studied with the goal of providing data to the fuel cell community that may help in selecting materials which limit contamination of the electrode. In addition, we report a cost-effective analysis technique for testing electrode performance exposed to PEMFC system components that may contaminate and develop a recovery strategy to address the contamination.

The focus of the first part of the dissertation was to study effect of the BOP plastics. Then the organic functional group identified in the plastics leachates were also tested for its degradation effect. After the testing of BOP plastics, BOP assembly aids leachates were tested for their detrimental effect on the PEMFC electrode.

In the second part the organic and anions identified in the leachates of assembly aids were injected the electrolyte and the loss of ECA and ORR currents were quantified and analyzed to understand the mechanism of contamination. This part was followed up by experimenting with mixture of organic and organic and anions. The focus of this part

was to understand the impact of mixture of the organic compounds, compare them with the individual compounds. The compounds detected in the leachates in the assembly aids were tested for their effects on the ORR of Pt/VC individually. But the leachates were a mixture of the organic compounds. So there was a need of testing the mixture of model compounds.

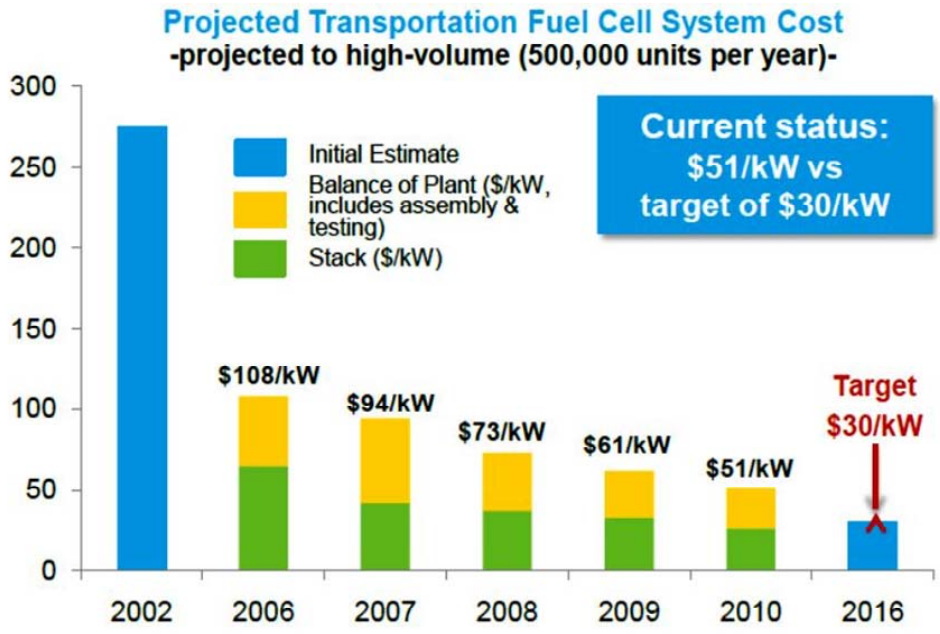

Figure 1.1. Projected cost of an 80-kWe fuel cell system at a production rate of 500,000/year (36).

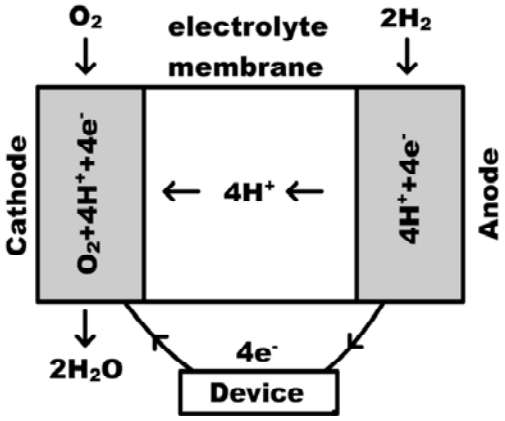

Figure 1.2. Schematic of PEM fuel cell with electrodes

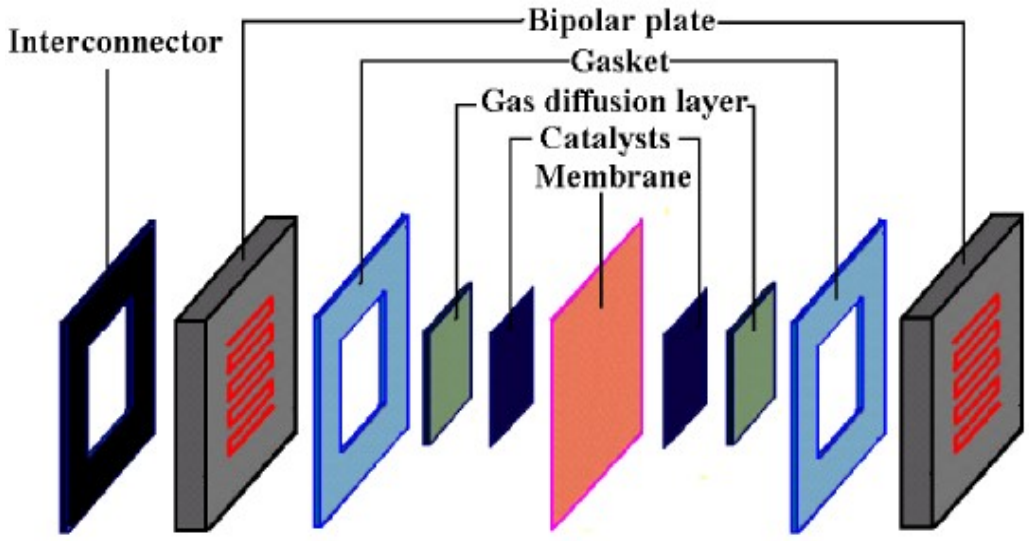

Figure 1.3. Fuel cell components (8)

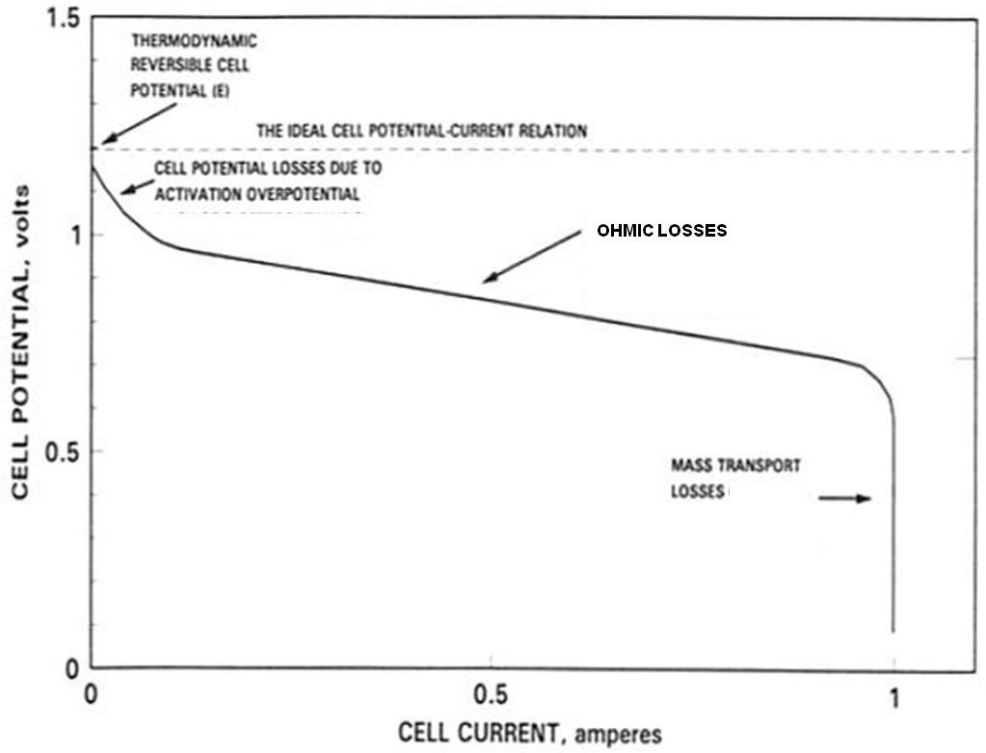

Figure 1.4. Polarization curve of a typical PEM fuel cell under normal operation condition showing three main regions of fuel cell polarization: Kinetic, Ohmic, and Mass transport

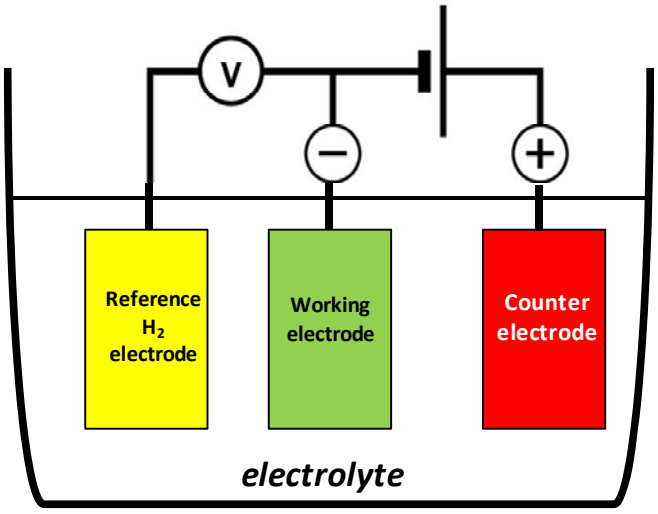

Figure 1.5. Three electrode method for voltammtric experiments using thin film RDE

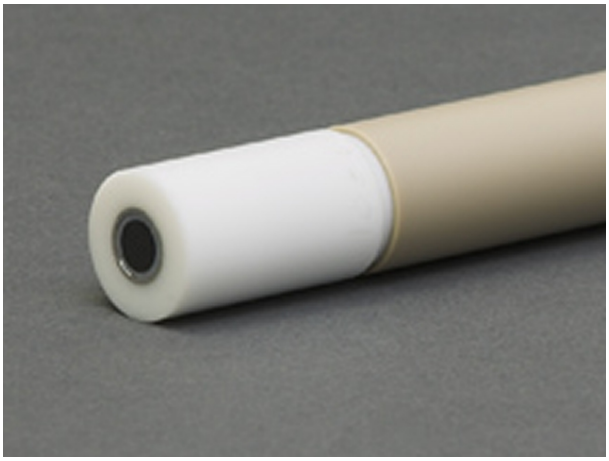

Figure 1.6. The rotating ring disk electrode (37)

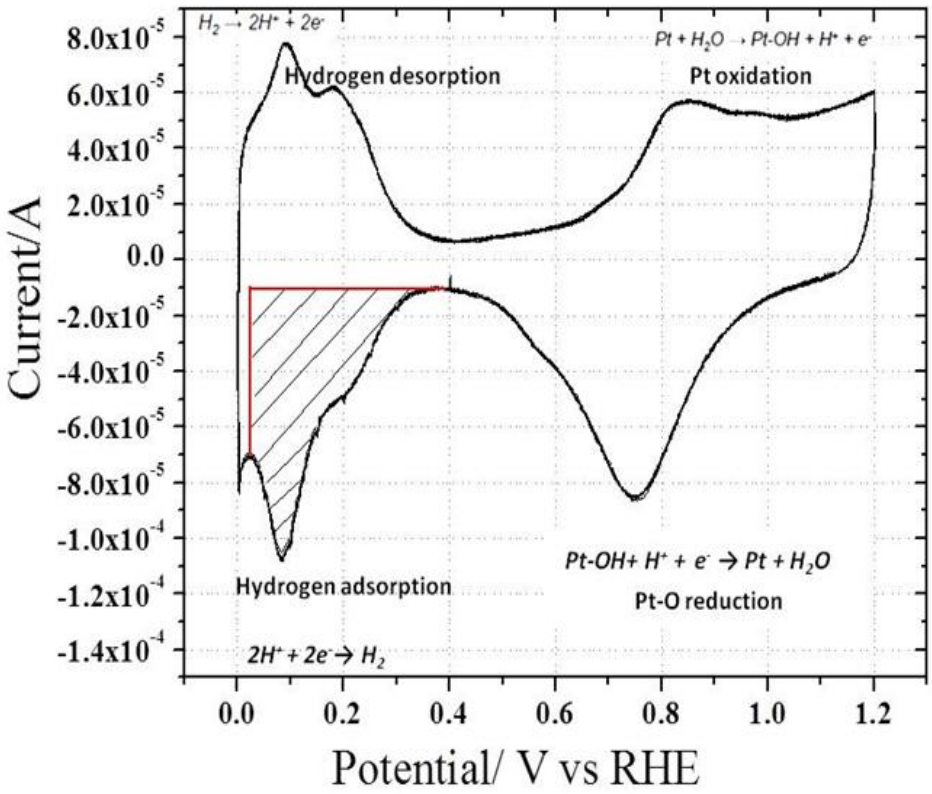

Figure 1.7. A typical cyclic voltammogram in perchloric acid, showing different adsorption and desorption peaks.

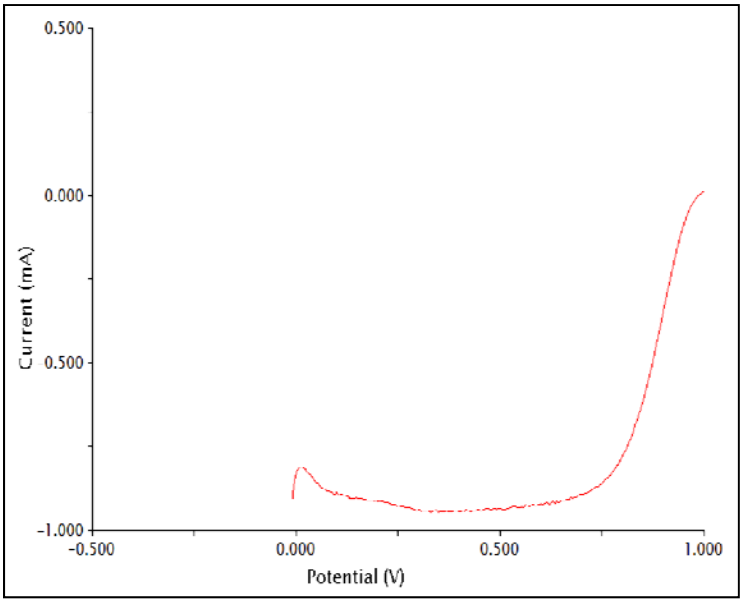

Figure 1.8. A typical LSV sweep (after saturating the electrolyte with oxygen) for calculating the ORR activity of the catalyst. The current at 0.9 V and the limiting current were recorded.

Chapter 2. Literature review

2.1. Overview

Polymer electrolyte membrane fuel cell (PEMFC) presents a promising future of clean and renewable energy for commercial automobiles and stationery applications. Although the technology has existed for almost a century, commercialization was difficult due to its higher price over conventional power sources. Proton exchange membrane fuel cell converts energy from electrochemical reaction of hydrogen and oxygen in presence of a catalyst to electric energy which is used for domestic needs, automobile and space propulsion. PEMFC uses Pt on carbon as the cathode catalyst. But Pt can be easily poisoned by any contamination that is present in the system.

The contamination can affect different functionalities of PEMFC like electrode kinetics, ionic transport, and mass transport. The electrode kinetics may be changed by poisoning electrode catalyst activity (S, CO adsorption on Pt catalyst), ionic transport may be affected by altering the protonic conductivity of catalyst layer by reducing membrane conductivity and by changing mass transport properties of gas diffusion layer (GDL) (38).

2.2. PEMFC performance degradation in presence of air impurities

In another study, Okada et al. showed effect of ammonium ions on persulfonated ionomer coated electrodes. The alkaline earth metal cations present in the PEMFC as

impurities hinder the ORR kinetics by suppressing the charge transfer through the ionomer in the fuel cell (25).

The impact of sulfur impurities present in air on cathode side of PEMFC is a matter of concern because the SO_2 tends to oxidize to a more stable state and adsorb on Pt. In a subscale fuel cell study Naghara et al showed the change of cell voltage at $1Acm^{-2}$ during continuous injection of various air contaminants (0.5 ppm SO_2, 0.6 ppm H_2S, 2 ppm NO, 2 ppm NO_2 and 5 ppm NH_3) mixed with humidified simulated air to the cathode (figure 2.1.) (39).

An exploratory study of H_2S poisoning of membrane electrode assemblies (MEAs) in proton exchange membrane fuel cells (PEMFCs) consisting of Pt and Pt-Ru alloy electrodes is presented. Steady-state polarization curves are reported for each electrode after exposure to 50 ppm H_2S at 70°C. Significant findings include (i) partial recovery of the MEA after 3.8 h of exposure to H_2S; (ii) the degree of the recovery is influenced by the electrochemical oxidation of two surface species observed during cyclic voltammetry experiments; (iii) in contrast to CO poisoning, Ru has no effect on increasing MEA tolerance toward H2S poisoning; and (iv) increasing the Pt loading by 60% appears to quadruple the partially recovered current density at 0.6 V (i.e., 0.125 A/cm^2 for Pt-Ru alloy and 0.575 A/cm^2 for Pt electrodes) after exposure to neat H-2 for 24 h.

The figure 2.2 shows the effect of sulfate species on cyclic voltammograms at 50mV/s. The orange, green and red lines denote the CV scans after injection of 2 ppm SO_2 80°C and the humidification temperatures were 80°C/80°C (100/100%RH).

It was hypothesized that sulfate species exist in the cathode catalyst layer after the *I–V* measurement since characteristics of the cyclic voltammograms are similar each other. Oxidation of sulfur adspecies to sulfate should occur during *I–V* measurement since the measurement procedure includes relatively high voltage (>0.9 V) period.

Prolonged exposure of the common cathode air impurities like NO_2, SO_2, H_2S etc has degenerative effect on fuel cell performance (Mohtadi, Lee et al. 2003). In that study, Mohtadi et al. had shown the effect of 200 ppm of H_2S for 15 hours, 2.5 and 5 ppm of NO_2 in air for 20 hours, 2.5 and 5 ppm of SO_2 in air for 20 hours. The effect of NO_2 on fuel cell performance was recoverable but for SO_2 only partial recovery by CV scans was possible because the sulfur species weakly adsorbed on the Pt catalyst (40). The fuel and air mixture supplied to a PEMFC are the sources of contamination resulting in degradation and failure of a fuel cell stack (15, 40-42). This price is affected by the loss of performance when the electrodes are exposed to contaminants. While there are many existing studies on air impurities (15, 24, 43-45) very few literature exists on the technique of studying the effect of liquid phase organic and inorganic impurities originating from different parts inside the fuel cell.

Sulfur species is adsorbed on Pt:

$$Pt–S + 4H_2O \leftrightarrow SO_4^{2-} + 8H^+ + 6e^- + Pt$$

The voltage effect on SO_2 has been reported by Swider-Lyons *et all*. The study was important because SO_2 oxidation state changes with electrode potential. As the potential was increased from 0.5 V to 0.7 V sulfur oxidation state reduces from 0 to -6 (from S to SO_2 to SO_3^- / $SO_4^=$). The sulfur coverage decreased with increasing cathode

potential, with almost zero coverage at 0.9 V (26). This study showed the potential to operate the fuel cell with contaminants present in the air stream and the analysis of mechanism gives a path forward to restricting the extent of contamination.

To study the effect of contaminants (air and liquid phase) on PEMFCs in-situ, Pt cyclic voltammetry has been used to measure poisoning of MEA (40, 44, 46). The experiments performed inside a PEMFC explain the overall poisoning effects on the electrochemical properties of MEA, but do not isolate the effect on ORR kinetics. The purpose of this report is develop electrochemical testing protocols to understand the fundamentals of oxygen reduction reaction (ORR) (47) and electrochemical area using thin-film rotating disk electrode (TF-RDE) method.

2.3. Activity requirements for oxygen reduction catalysts

Platinum nanoparticles supported on high surface area carbon are the most widely used electrocatalyst for PEM fuel cell due to its higher oxygen reduction reaction (ORR) activities at PEMFC cathode during the fuel cell operation. Unfortunately the ORR has a slow kinetics that requires increased catalyst loading which increases the manufacturing cost. In addition to that, the ORR activities of Pt electrocatalyst are adversely affected in presence of contaminants. To solve the two aforementioned problems, state of the art Pt/C catalyst manufacturing facilities are employing different techniques to characterize and study the oxygen reduction reaction to enhance the activities of the catalyst. For example, in an attempt to increase available surface area, particle size effects (48) are being studied in non-absorbing electrolytes with PFSA ionomers since higher dispersion of Pt particles can lead to higher surface area and lower Pt loading. A recent study has compared three catalysts solid Pt disk, Pt black and 46% Pt/C (TKK) to show the effect

of Pt size on the OH adsorption. The potentials for oxides adsorption and desorption shifted towards the H_2 potential (i.e. Lower potential) with dispersed Pt on carbon being the highest and Pt disk (i.e. of 46% Pt/C (TKK) > Pt black > Pt disk) (49). Therefore there is an impact of the Pt particle size on the ORR. In this study 46% TKK Pt/C was chosen as the catalyst for its high activities and lower influence on the adsorption of OH_{ads} which was believed to reduce ORR activities in 0.1 M perchloric acid (50, 51).

Theoretical studies on the HOR kinetics of Pt electrodes are based on the Tafel–Heyrovsky–Volmer mechanism:

$$H_2 + 2Pt \leftrightarrow 2Pt - H_{ads} \text{ (Tafel reaction)}$$

$$H_2 + Pt \rightarrow Pt\text{-}H_{ads} + H^+ + e^- \text{ (Heyrovsky reaction)}$$

$$Pt\text{-}H_{ads} \leftrightarrow Pt + H^+ + e^- \text{ (Volmer reaction)}$$

$$H_2 \leftrightarrow 2H^+ + 2e^- \text{ (overall reaction)}$$

2.4. Electrochemical area (ECA)

Studies have shown that alkali and alkaline earth metal cations or transition metal cations strongly hinder the kinetics of the oxygen reduction reaction (ORR) on platinum covered with perfluorinated ionomer membranes, relating to the membrane contamination and performance degradation in polymer electrolyte fuel cells. The organics from the Balance of Plant (BOP) materials can also contaminate the catalyst and the membrane and be responsible for the performance loss in a PEM Fuel Cell. The preliminary cyclic voltammetry studies done at GM and NREL (31) has showed that off-the-shelf structural plastics (BOP) like Polyamides can reduce the available Pt sites in the catalyst as shown in figure 2.3.

2.5. Oxygen reduction reaction (ORR)

Pt on Vulcan carbon was chosen as the ORR catalyst since it is known as the most commercially used catalysts in low temperature PEMFCs. It has ca. 3.4 nm diameter particles dispersed on Vulcan carbon (30%) (52) Because of it high activities. But it is also known for its susceptibility towards contamination. Many studies have been conducted to quantify and compare the catalyst ORR activities of Pt/VC prepared with different techniques and under different experimental conditions (5, 51, 53-55). Nafion® is mixed in the catalyst ink suspension so that Nafion thickness is less than 0.2 μm, to reduce film diffusion resistances become negligible so that it doesn't affect kinetic current densities (47). The significantly reduced catalyst loading used in the thin-film RDE method expands the range of experimentally accessible mass-specific current densities to values which are typically obtained in PEM fuel cells i.e. 2-3 Amg_{Pt}^{-1}, corresponding to 0.9 V.

The poisoning of Pt catalyst by air impurities such as NO_x was discussed in details with ex-situ TF-RDE studies in liquid electrolyte, conducted by Zhu et al (56). They found that the absorption of NO_x on metallic Pt is more significant than on Pt oxides, and this absorption is mainly a chemical process rather than an electrochemical process. Although the absorption of NO_x on Pt surface is not strong, exposure to NO_x contaminants can result in significant performance degradations of Pt/C catalysts. The ORR mechanism remains unchanged after the NO_x poisoning, because Tafel slope remains the same for the unpoisoned and poisoned Pt/C catalysts. This indicates that the NO_x poisoning on Pt/C catalysts is just due to the reduction of electrochemically active surface area. Since lower potentials facilitate the reduction of NO_x to water soluble NH_4^+,

reducing the working potential might mitigate the poisoning of NO_x. However, the performance loss due to the NO_x poisoning can be completely recovered by the oxidation removal, but not by the reduction.

2.6. BOP materials as sources of contamination

The BOP materials are used in different parts of PEM Fuel Cell power system as discussed in the introduction. The cost of the BOP system ($49/kW in 2012 (57)) has risen in importance. Lowering the cost is one of the most important goals before commercializing PEMFC. Therefore, use of cheap off-the-shelf BOP materials as fabrication materials (plastics), assembly aids is justified in the light of decreasing cost. Figure 2.4 shows the cost of different BOP plastics which can be used as fabrication materials in PEMFC. The materials with higher cost ($12.50 to $30.00) on the right side of the chart are currently used by the manufacturers and to decrease the BOP cost the plastics on the left side of chart should be considered for use. Therefore some of the low-priced plastics in the left side of the figure 2.4 were chosen to study for their contamination effect. However, impact of those materials on Fuel Cells under the normal operating conditions has scarcely been reported so far. Most of the studies have focused on air impurities than organic impurities from the BOP materials. Lowering the cost of PEMFC system component requires understanding of the materials used in the system components and the contaminants that are derived from them, which have been shown to affect the performance and durability of fuel cell system. Lower cost commodity polymers are suitable for larger components such as cathode air handling systems. Higher cost engineering polymers are suitable for smaller, precision components such as impellers and valves and sensors.

Results from GM experiments on 4 BOP materials depicted as Z1, Z2, Z3 and Z4 in figure 2.5 show voltage drop in in-situ studies in a 50 cm^2 fuel cell. This was one of the first studies to show the degradation effect of BOP contamination over 40 hours.

2.7. Effect of contamination on ECA and ORR

Liquid phase contaminants may adsorb on Pt on both the cathode (where ORR takes place) and the anode (where hydrogen reduction reaction or HOR takes place) in a PEMFC much like air contaminations (SO_2, NH_3, CO, CO_2, H_2S etc.) (15, 23, 24, 40, 44, 56). Since the contamination effect on the HOR is less pronounced compared to the ORR, it requires detailed investigation because its slower kinetics combined with the effects of contaminants can result in high over potential and loss in fuel cell performance (44, 58). So it will be useful to develop protocols (59) for systematic understanding of the contamination process from the liquid phase contamination such as chemicals leached out from the stack, on Pt/C using ex-situ methods like rotating disk electrode to develop commercially viable catalyst with high ORR activities with specific application in PEMFC.

2.7.1. Effect of additives in coolants

The performance of a fuel cell has been found to degrade over time in the presence of not only air contaminations but also system derived contamination in a PEMFC (11). For example, recent studies on the additives of the glycol based coolants have shown detrimental effects on Pt on Vulcan carbon catalyst. These contaminants originate from ethoxylated nonylphenol surfactant, and azole- and polyol-based corrosion inhibitors which are frequently added to the commercially available BioGlycol coolants to enhance specific functionalities. K.E. Swider Lyons et al has conducted a study with

three above mentioned additives and glycol mixtures and have observed that the lost ECA could be fully recovered in clean electrolyte for the mixture with the surfactant pure glycol-water, glycol-water-surfactant mixtures and glycol mixture containing the polyol corrosion inhibitor, while coolant mixtures with the azole corrosion inhibitor caused irreversible losses to the ECA and oxygen reduction reaction (ORR) activity. The ECA and ORR activity could be recovered to 70% of its initial values after voltammetric cycling to 1.50 V in case of azole poisoning (30).

2.7.2. Effect of Ammonia on membrane

Ammonium ions are probed for their impurity effect in PEM Fuel Cell (60). Even ppm level trace of ammonia irreversibly decreases the performance of the cell. It also replaces the detachable protons in the Nafion, decreasing the membrane conductivity. It affects the HOR in anode and ORR in cathode as well as poisons anode catalyst layer and membrane. The additives from fuel cell also inhibits ORR (61).

2.7.3. Effect anions on catalyst

In previous studies from N. M Markovic et al results from smooth polycrystalline and single crystal Pt electrodes, the ORR activity decreases in the order $ClO4^- > HSO4^- > Cl^-$, consistent with the increasing adsorption bond strength of the anions. The ORR characteristics of Pt/Vulcan in the presence of adsorbed Cl^- can be interpreted as a superposition of the individual ORR properties of the Pt(111)|Clad and Pt(100)|Cl_{ad} solid |liquid interface with respect to both the kinetic limitations and the formation of H_2O_2. This is in qualitative agreement with the proposed cubo-octahedral Pt particle shape. Although these results were obtained in liquid electrolyte, similar reduced activity and enhanced formation of H_2O_2 can be expected in a PEMFC, therefore indicating the

necessity of chloride-free MEA preparation and, more importantly, of chloride free humidified feed-streams in order to avoid performance losses and/ or membrane degradation (62).

2.7.4. Experimental approach in studying the effects of liquid phase contaminants in PEMFC using thin film RRDE

Researches had shown that the slow ORR kinetics on carbon supported Pt catalysts are the most preventive aspect in the energy conversion efficiency of state-of-the-art PEM fuel cells and the development of improved catalysts would have a dramatic impact on fuel cell. Due to the different electron yields of the two reaction paths (H_2O_2 versus H_2O formation), catalyst development for oxygen reduction catalysts requires that the electrocatalytic activity as well as the product distribution for the ORR on new catalysts can be determined quantitatively under PEMFC relevant conditions (47).

Owing to the deleterious effect of H_2O_2 on the stability of polymer electrolyte membranes, the extent of H_2O_2 formation on the cathode catalyst in the potential region above ca. 0.7 V (i.e. at the typical operating potential) is a critical criterion for the choice of suitable catalysts. This is crucial, however, not only for the ORR but also for the anode reaction. Oxygen reduction to H_2O_2 may also occur on the anode catalyst at the typical operating potential of below ca. 0.1 V, since molecular O_2 can come in contact with the anode catalyst either due to the significant O_2 cross-over through thin state-of-the-art membranes (e.g. Nafion® 112 and GORE Select) or via the air-bleed used for operation with reformates.

The oxygen reduction reaction on a typical Pt/VC catalyst in the presence of adsorbed S*x*. These electroanalytical studies of Pt poisoning with adsorbed S species support prior observations made in fuel cell studies, plus add additional insights. RRDE measurements show that the ORR activity decreases significantly as the initial coverage of S species increases > 0.37, drastically changes both the activity and the reaction pathway of the ORR on the Pt/VC catalyst from a 4-electron process to 2-electron process reaction (63).

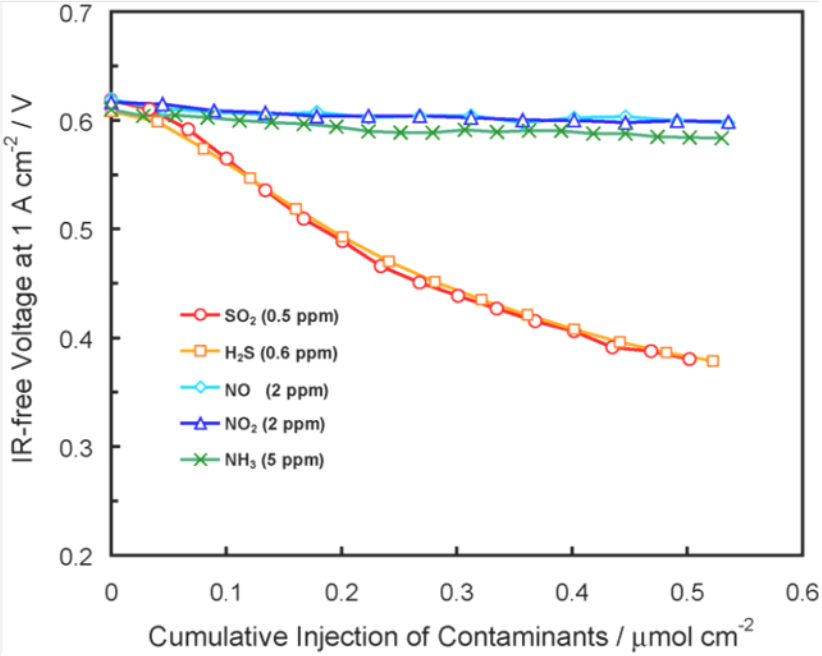

Figure 2.1. Loss in voltage at higher current density in a polarization curve due to the exposure to air contaminants (64)

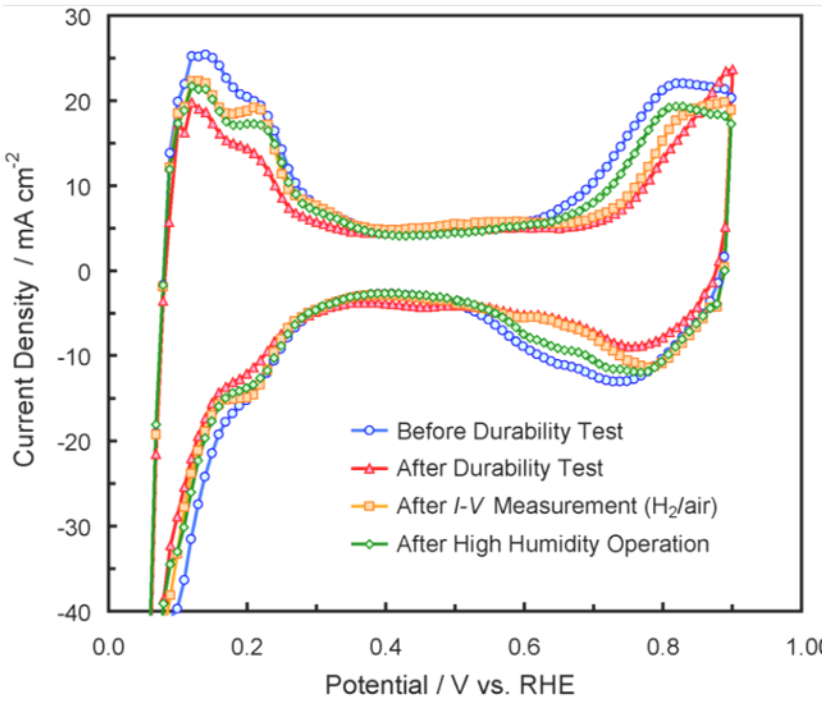

Figure 2.2. Durability tests before and after SO_2 contamination

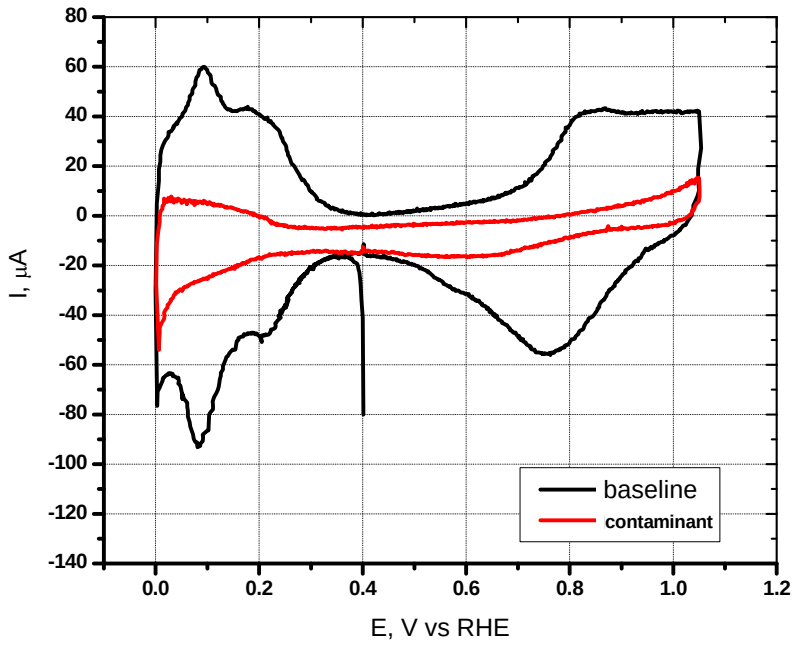

Figure 2.3. CV showing loss of Catalyst sites after contaminating with structural plastics (BOP materials) leachate

Figure 2.4. Examples of plastics with generalized costs for the system

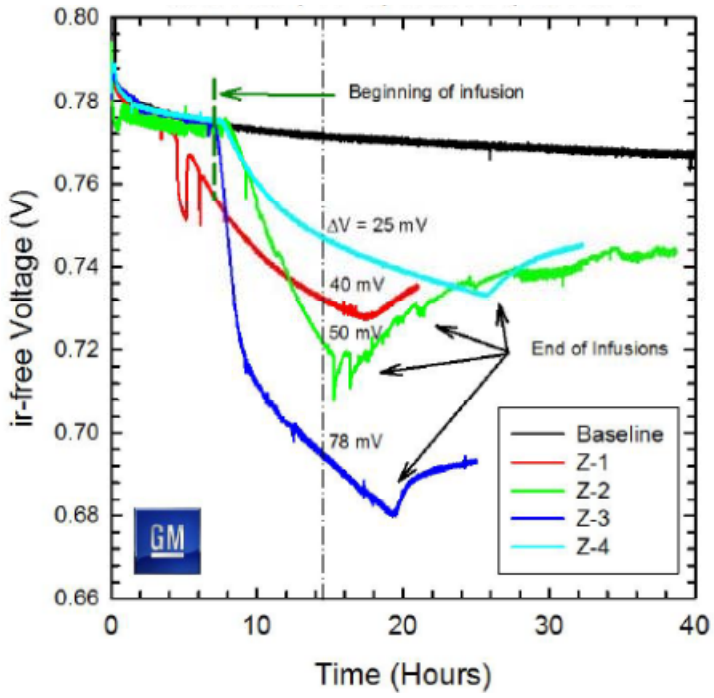

Figure 2.5. Voltage drop with time after infusing BOP leachates contaminating a fuel cell

Chapter 3. Effect of BOP structural plastics on Pt/C

In this chapter detailed experimental process in presented along with methods for establishing a stable baseline of the activities related to oxygen reduction reaction on Pt catalyst (46% Pt on XC72 Vulcan carbon). The focus of this study is to design appropriate sets of experiments to study the effect of liquid phase contaminants on Pt/C catalyst in a liquid electrolyte using thin-film rotating disk electrode (TF-RDE) method at room temperature. This ex-situ voltammetric approach quantitatively measures the loss of electrochemical surface area and oxygen reduction reaction. It also includes a route to recovery of the lost electrochemical surface area (ECSA or ECA) and oxygen reduction reaction (ORR) activities. As the part of the study the electrodes coated with 46% Pt/C were benchmarked to estimate the losses due to voltammetric cycling and other associated steps without adding any contaminants from outside source. Leachates from BOP materials that may be used in fuel cell were used as examples of contamination behavior. Loss incurred during the experiments was quantified followed by recovery experiments. The effect of the organic compound (found in the leachates) on ORR was evaluated.

The additional information on the methodology and background studies can be found in appendices A, B and C.

3.1. Introduction

Polymer electrolyte membrane fuel cell (PEMFC) presents a promising future of clean and renewable energy for commercial vehicles and stationery applications. Although the technology has existed for almost a century, commercialization has been difficult due to its higher cost over conventional power sources. This cost is also affected by the loss of performance when the electrodes are exposed to contaminants. The fuel and air mixtures supplied to a PEMFC have been shown to be a major source of contamination resulting in degradation and failure of a fuel cell stack (15, 40-42). While there are many existing studies on air contaminants (15, 24, 43-45), very little research exist on the technique of studying the effect of liquid phase organic and inorganic contaminants originating from balance of plant materials components. This type of contamination may also decrease the performance of the catalyst for the oxygen reduction reactions (ORR) activities. Furthermore, under certain operating conditions of a PEMFC, catalyst degradation may be only partially reversible.

Platinum nanoparticles supported on high surface area carbon are the most widely used electrocatalysts for PEMFC due to their higher oxygen reduction reaction (ORR) activities. Because of its slow kinetics, the oxygen reduction reaction of Pt electrocatalysts may be particularly susceptible to contaminants. State-of-the-art Pt/C catalyst manufacturing facilities are employing techniques to characterize and study the ORR to enhance the activities of the catalyst. For example, in an attempt to increase available surface area, particle size effects have been studied in non-absorbing electrolytes with perfluorosulfonic acid (PFSA) ionomers. In particular, it has been shown that higher dispersion of Pt particles can lead to higher surface area and lower Pt

loading (65). A recent study has compared three catalysts – solid Pt disk, Pt black and 46% Pt/C (TKK- Tanaka Kikinzoku Kogyo), to show the effect of Pt size on the OH adsorption. The potentials for oxides adsorption and desorption shifted towards the H_2 potential (i.e. lower potential) with dispersed Pt on carbon with the highest and Pt disk with the lowest shift (i.e.in the order of 46% Pt/C (TKK) > Pt black > Pt disk) (5). This shift of Pt-OH adsorption/desorption potential indicates that in case of 46% Pt/C (TKK) the adsorbing species from the electrolyte affect the ORR less than the Pt disk and Pt black catalysts (5). Therefore, there is an impact of the Pt particle size on the ORR. In this study, 46% TKK Pt/C (3.4 nm particle size with 30% dispersion) was chosen as the catalyst for its high activities and lower influence on the adsorption of OH_{ads} which has been shown to reduce ORR activities in 0.1 M perchloric acid (50, 51).

To study the effect of contaminants (air and liquid phase) on PEMFCs in-situ, Pt cyclic voltammetry has been used to measure poisoning of MEAs (40, 44, 46). The experiments performed with a PEMFC explain the overall poisoning effects on the electrochemical properties of MEA, but do not isolate the effect on ORR on the catalyst. The purpose of this paper is to present the development of electrochemical testing protocols to understand the effect of contamination from BOP material on ORR and electrochemical area using TF-RDE method. TF-RDE has been used as an effective tool for studying catalyst contamination for air contaminants (66, 67) since it isolates the effect on the catalyst from the MEA.

In the first part (sections 3.1 to 3.3), the study focuses on the contamination from the leachates of BOP materials (structural plastics) that may be used in fuel cell stacks. The contamination study involves holding the working electrode (WE) at a potential for a

specified period of time to allow the contaminants to adsorb on Pt sites. The study also involves recording the current scanned over a potential range (for performing CVs and LSVs) to quantify any loss of ECA and ORR activities. Therefore, any unwanted loss in ECA or ORR activities resulting from the holding and/or cycling the WE over a range of potential was determined in a clean electrolyte (control). The second part of the study (section 3.4 and 3.5) quantifies and assesses the variation of baseline loss of ECA and ORR activity resulting from preparation of different inks.

Finally, sections 3.6 and 3.7 present the poisoning characteristics of an organic compound (found in those leachates from the structural plastics) on ORR activities of Pt on Vulcan carbon. This compound is used as an example to demonstrate the role of polymer degradation product from the structural plastics that can be used in PEMFC, on contamination using three electrode rotating disk electrode (TF-RDE) method.

3.2. Experimental

A rotating disk electrode was employed in all measurements, using a three electrode cell apparatus. The electrochemical cell apparatus consisted of glassware (5 neck electrochemical cell), wires, and H_2 gas reference electrode (RE) insert.

The electro-chemical cell apparatus was initially soaked in concentrated H_2SO_4 for a minimum of 12 hours followed by soaking in a solution containing 1 package of Nochromix® in 7.6 l of concentrated H_2SO_4 and Nochromix solution for another 12-24 hours. After the acid soaking, the cell apparatus was boiled twice in DI water for 3 hours using fresh 18 MΩ water.

3.2.1. Catalyst ink and thin film electrode preparation ORR on Pt/C

Catalyst inks were prepared in a small glass vial with 7.4 mg of TEC10V50E catalyst dissolved in 7.6 ml DI water and 2.4 ml isopropyl alcohol (IPA). Note: TEC10V50E catalyst is TKK 46% Pt on Vulcan carbon (i.e. Pt/VC). Then, 40 µl of Nafion® (5wt %) was added to the vial. The ink solution was sonicated in an ice bath for 2400 s. The ice was changed every 3-4 minutes as it melted. A 5mm diameter glassy carbon tip (AFE2M050GC) on a Teflon cylinder (Pine Instruments) was used for the working electrode (WE). It was polished using a 0.05 µm alumina polish suspension and a few drops of DI water on a Buehler MicroCloth for 5 minutes followed by rinsing in DI water. The electrode was then sonicated in DI water (18 MΩ) to remove excess polish followed by sonication for 15 min in a solution of 70% by volume IPA in DI water. After sonication, 10 µL of ink was dispensed carefully at once on the electrode glassy carbon tip to build an evenly dispersed thin film. The tip was then dried in an oven at 40°C for 20 min. Thus, the Pt loading was ca. 17.4 $\mu g_{Pt} cm^{-2}$. Catalyst preparation must be very precise and the loading for this study was chosen to be ~ 18 $\mu g_{Pt} cm^{-2}$ to avoid any mass transport losses that was encountered in case of thick catalyst films.

3.2.2. Electrochemical apparatus preparation

The electrochemical glassware was filled with 0.1 M $HClO_4$ acid from GFS Chemical (highest purity perchloric acid, maximum level of chlorides of 0.00001%). A Pt wire (placed inside a glass insert and connected to hydrogen gas) served as the RE (reversible hydrogen electrode). The counter electrode (CE) was also made of Pt wire and Pt mesh spot welded on the wire. Excess O_2 was removed from the electrolyte by purging N_2 for at least 5 min. The N_2 or O_2 (research grade purity, by Air Products Ltd.) gas was

passed through water trap before entering the cell to eliminate any possible gaseous contaminates.

3.2.3. Electrode conditioning

All TF-RDE measurements were performed at room temperature using a Pine Instruments WaveNow potentiostat (model # AFTP1). Voltage ranges were measured with respect to RHE. The electrolyte (0.1 M $HClO_4$) was purged with N_2 for 20 minutes or until the OCV was < 0.4V. Note: a drop of water on the WE helps prevent accumulation of N_2 bubbles on the surface. The WE was mounted on the shaft of the electrode rotator (MSR style rotators) and slowly lowered inside the cell so that the tip was well inside the electrolyte (the vertical distance from the RHE insert to the tip being one and half times the diameter of the Teflon cylinder). The tip was maintained at the same depth for each experiment to keep the solution resistance the same across all TF-RDE experiments. The electrode was electrochemically conditioned from ~0.025 to 1.2 V at a scan rate of 100 mVs^{-1} for 100 cycles in the de-oxygenated electrolyte while rotating the electrode at 2500 rpm. The minimum potential was chosen so that the inflection point for H_{upd} region (hydrogen evolution) was clearly discernible but it was not so low as to generate a lot of hydrogen in the electrolyte.

3.2.4. Determination of time to reach equilibrium with the Pt catalyst

To determine the time by the organic molecules to reach an equilibrium adsorption state, the CVs were performed at 100 mVs^{-1} and the electrolyte was contaminated at 1.05 V in a separate set of experiments. Caprolactam was used as the model contaminate for these experiments. Completion of one full cycle (1.05 V → 0.025 V→ 1.05 V) required 20 s. Therefore, after injecting the contaminant at 1.05 V, time

taken by the contaminants to reach electrode surface could be calculated by counting the number of cycles before observing any change in the CV scan.

3.2.5. Rotating disk experiments to measure ECA and ORR activity of Pt/C

In the first part of the contamination experiments, three leachates (from structural plastics) were tested for their impact on the ECA. In the second part, an organic compound was tested for its effect on both ECA and ORR (figure 3.1).

Since the leachates from the structural plastics were a mixture of both organics and inorganics, longer time was needed for the leachates to reach equilibrium with the Pt sites. But the organic compound was injected in its pure form. So, it attained equilibrium with the Pt sites quicker than the leachates.

3.2.6. Effect of leachates to measure ECA

The electrode was conditioned as described in section 2.3. For the baseline, a full scan CV (i.e. 0.4V → 1.05 V → 0.025 V → 1.05 V → 0.4 V) and a partial CV (i.e. 0.4 V → 0.5 V → 0.025 V → 0.5 V → 0.4 V) were measured at a scan rate of 20 mVs^{-1} in an N_2 environment (i.e. the electrolyte being blanketed with N_2) with no rotation. The ECA was determined from the partial scans.

After baselines were established in clean electrolyte, the leachates were injected while holding the WE at 0.4 V for 10 mins and 3 cycles of CVs were performed to measure the ECA loss. The step was repeated six times (total 60 mins hold) to allow the contaminant molecules sufficient time to come to equilibrium with Pt sites. The contamination step was repeated for different concentrations of the leachates.

3.2.7. Effect of organic compound to measure ECA and ORR

For the second part of the experiment with organic compound, baseline CVs were established as described on section 2.5.1. After the partial baseline CV, the gas valve was switched to purge the electrolyte with O_2 for 7 mins and then an ORR was measured from -0.01 to 1 V at 20mVs^{-1}. This ORR served as the baseline for the ORRs performed after contaminating the electrolyte.

The contamination was added with a pipette while the WE was held at 0.4 V and purging with N_2 and rotating at 2500 rpm. The hold was continued for 5 mins as determined by previous experiments (section 2.4). A short CV_a (~0.025 to 0.5 V) was recorded for 3 cycles at 20 mVs^{-1}, labeled ECA_a. The ECA was calculated from this CV and a comparison with the baseline was recorded to check the change in ECA after contamination. Next, for ORR experiments the gas was switched to O_2 and after the solution was saturated with O_2, an LSV sweep (-0.01 to 1 V) was performed for comparison of ORR with baseline. The latter was used to determine the contamination effect on ORR. A short CV (~0.025 to 0.5 V) was recorded for 3 cycles at 20 mVs^{-1} after changing the gas to N_2 to allow the calculation of another ECA, label ECA_b. The difference between ECA_a and ECA_b measured any change in ECA after ORR. Finally, 3 cycles of full CV (~0.025 to 1.05 V) were recorded at 20 mVs^{-1} to measure any change in current above 0.5 V. These steps were repeated for different concentrations of organic compound.

Note that the electrolyte was well mixed (rotation speed 1600 rpm) during the addition of leachate while measuring the ORR. Note also that ORR was measured on pre-

reduced Pt that has been held at 0.4 V. This ensures no oxidation of the leachate composition. Refer to figure 3.1 for the detailed steps.

3.2.8. Recovery of contaminated electrode

The recovery process attempted to discover a potential between 0.75 and 1.05 V where the contaminants might be oxidized for the purpose of recovering the lost Pt sites in the catalyst by desorption of the contaminants. Experiments to determine the extent of recovery were performed with a clean set of electrochemical apparatus (with clean reference and counter electrodes). The electrolyte 0.1 M $HClO_4$ was purged with N_2 for 20 min. The recovery of a contaminated electrode consisted of two parts – a potential hold at 0.75, 0.85, 0.95, and 1.05 V, followed by potential cycling (10 cycles) from ~0.025 to 1.05 V in a clean electrolyte.

The WE was rinsed with DI water before transferring it to clean the electrolyte. It was then held at 0.75 V for 5 minutes. This was repeated another 3 times with holds at higher voltages (0.85, 0.95, and 1.05 V). During the holds, the electrolyte was purged with N_2 and WE was rotated at 2500 rpm. A short CV (~0.025 to 0.5 V) was recorded from the hold potential to ~0.025 and finally to 0.5 V immediately after each hold. This was repeated for 3 cycles at 20 mV/s to check the change in ECA due to recovery. In the end, the effect of residual contaminant (recovered ECA) was tested from the ECA calculated from the final CV scans (~0.025 to 1.05 V).

The flow was switched to O_2 purging (with 2500 rpm rotation) for 7 minutes. After the electrolyte was saturated with O_2, the rotation was reduced to 1600 rpm and an

LSV sweep was performed anodically from -0.01 V to 1 V. Refer to figure 3.1 for the detailed steps.

3.2.9. Preparation of contaminant solutions

Structural plastics (BOP materials) that may be used in fuel cell stacks were chosen for testing during the contamination experiments. They were selected from a wide range of commercially available plastics with varying properties and functions in a fuel cell. The effects of widely used plastics in fuel cells – Ultramid® (grade A3WG7 BK00564) and EMS Grivory® (grade GVN-35H Black) from BASF and Ryton® R4-220BL from Chevron Philips, are described in this paper as examples of contamination. Ultramid® is a poly amide 6,6 (nylon) and comparatively less expensive than Ryton® (polyphenelyne sulfide). EMS Grivory® is poly amide 6,6/6 (nylon). It is slightly more expensive than Ultramid® but less expensive than Ryton®. The contamination solution was prepared from pellets of the selected materials. The plastic pellets were measured, weighed and soaked in DI water at 90°C for 6 weeks. The wetted surface to volume ratio was 150 mm^2ml^{-1}. At the end of 6 weeks, the TOC (257 for Ultramid®, 282 ppm for EMS Grivory® and 7 for Ryton®) was measured and the leachates were analyzed using GCMS, IC and ICP-OES. For detailed chemical analysis results on the leachates, please see (68, 69).

Since the quantitative composition of the leachate extracts was unknown, the amount of solution to be injected in the electrolyte was determined based on the concentration of C atoms in the leachate based on total organic carbon (TOC) content in ppm (g of C per 10^6 g solution). Since the solution is water, the TOC in this case becomes mg of carbon per liter.

The concentrations of the leachates in terms of C atoms were 0.36, 0.18, 1.8, 3.6, 18, 36 and 180 μM of carbon for 145 ml plus contaminant volume of electrolyte. For detailed calculation please see (70).

From the GCMS analyses, caprolactam was found in the leachate of Ultramid® and dimer of caprolactam was found in EMS Grivory® but nothing was detected in the leachate of Ryton®. Therefore, caprolactam (figure 3.3) was chosen for further studies.

Caprolactam is extensively used in synthesizing Nylon 6 by the ring opening polymerization method. This explains the source of caprolactam in the leachate of Ultramid® which is a nylon 6,6. The solubility of caprolactam in DI water is very high (4560 gl^{-1}). A solution of 10,000 ppm, 10 gl^{-1} of caprolactam was prepared for the following experiments. The contamination concentration of caprolactam was for 1, 5 and 20 M in the electrolyte.

3.3. Results and discussion

All potentials reported in this paper were measured with reference to hydrogen electrode. In the subsequent sections, the results obtained from the experiments include loss of ECA due to potential holding and cycling in clean electrolyte, the time taken by contamination to reach equilibrium with the Pt electrode, extent of both contamination and recovery, and impact on ORR activities.

3.3.1. Part I. Experiments with leachates from BOP materials to determine their role in decreasing ECA

Developing a protocol to study the effect of contaminants on the Pt sites involved a complex multi-step process that emphasized details like change in ECA due to cycling

and holding in a blank electrolyte (no contaminants present), time taken by contaminants to reach equilibrium with the Pt, ECA loss due to contaminants, etc.

Figure 3.2 shows that for the CVs in $HClO_4$ there are three distinct peaks at potentials of 0.14, 0.25 and 0.8 V due to adsorption/desorption of protons and Pt-oxidation or reduction. The ECA was calculated by integrating the peak under the H_{upd} region (the hashed area shown in figure 3.2 between 0.04 and 0.4 V). The catalytic activities are greatly affected by different electrolytes-. Since bisulphate ions have greater affinity towards adsorbing on Pt than perchlorate ions, 0.1 M $HClO_4$ was chosen as the electrolyte for the CVs.

3.3.2. Effect of holding the electrode at OCV and at 0.4 V on ECA

The purpose of these experiments was to determine the effect of holding the electrode at different potentials on ECA loss. When the contaminant is injected in the electrolyte, the molecules take some time before adsorption equilibrium on the Pt is established. The transportation of the molecules depends on the rotation speed of the electrode. The latter induces a convection current inside the cell and thereby facilitates the transportation of the contaminant molecules. During this period, the electrode was held at a certain potential eliminating the chances of any electrochemical change (oxidation or reduction) of the molecules. The hold potentials were chosen to be 0.4 V and OCV (i.e. 0.85-0.9 V). At 0.4 V, the CV did not show Pt oxidization reduction peaks, but rather a double layer region (resembling capacitance) was observed. Therefore, holding at 0.4 V ensured that no contaminant molecule was oxidized or reduced and the sole effect of contamination was observed in the consecutive CV cycles. Alternatively holding at OCV may allow for oxidation of the contaminant that was not possible at 0.4

V. As shown in figure 3.4, after holding the WE at OCV for 10 min, a loss of 10% was observed, which was more than the loss due to the holding at 0.4 V (i.e. 7%). Note that repetitive CV cycling can also change the ECA due to CV cycles by 10% over a span of 30 min (70).

3.3.3. Example of contamination behavior: Effect of BOP materials (structural plastics) on ECA

Table 3.1 summarizes the contamination behavior of the electrolyte containing three balance-of-plant (BOP) materials such as Ultramid®, EMS Grivory® and Ryton® that may be used as structural plastic in PEMFCs. The column labeled time corresponds to a hold (at 0.4 relative to the RHE) of 10 min plus the time to perform 3 scans at 20 mV/s between ~0 and 0.5 V. Since the leachate contained both organic and inorganic materials, sufficient time was allowed to the leachate to reach equilibrium with Pt sites by repeating the hold at 0.4 V and subsequent 3 CV scans six times. The clean electrolyte (i.e. control experiment) showed some ECA loss due to cycling and holding which were 3, 8, 11, 14, 19, and 23% as the WE was cycled for three times after six successive holds for 10 mins. This loss of ECA from clean electrolyte can be attributed to the adsorbate species from the electrolyte (71).

The final concentration of carbon in the electrolyte due to addition of leachates was 180 μM. For comparison, there was a 33%, 22% and 5% loss for Ultramid®, EMS Grivory® and Ryton®, respectively, after the first hold cycle (before subtracting the loss due to holding and cycling from the control experiment). The final ECA loss after six holds for Ultramid®, EMS Grivory® and Ryton® were 62%, 52% and 12%, respectively. The value of ECA loss due to blank electrolyte was subtracted from the absolute values

of loss during contamination with any leachate to estimate the actual effects of contamination. It was found that after the fourth hold for 10 minutes (2700 s) the actual ECA loss for both cases of contamination got close to the saturation point. Therefore, the ECA loss due to the addition of leachates attained equilibrium after ~ 40 min. This also proved that contamination is a time dependent process. Figure 3.5 shows all saturation points as a function of concentration of the leachates (adsorption isotherm). It also illustrates that the effect of Ultramid® and EMS Grivory® on ECA loss was much more severe than that of Ryton®. This correlates with the TOC of the Ultramid®, EMS Grivory® and Ryton® (257 ppm, 282 ppm and 7 ppm, respectively). Due to the difference in TOC, 30 ml of Ryton® leachate was injected in the electrolyte while only 1.21 ml of Ultramid® and 1.1 ml of EMS Grivory® were injected to obtain a final concentration of 180µM of organic carbon concentration from the leachates in the electrolyte.

3.3.4. Effect of potential holding and cycling on recovery of the contaminated CVs

The recovery of Pt sites by holding the WE was measured with three partial CV scans performed immediately after each hold. The objective of performing the CV scans incrementally from 0.75 V, 0.85 V, 0.95 V and 1.05 V to ~0.025V and then finally to 0.5 V was to discover the correlation between the potential holding and degree of recovery. The potential limit to which the scan can be performed cathodically should be a voltage between 1.05 and 1.2 V. After 1.2 V, the Pt catalyst starts getting oxidized.

Figure 3.6 shows the effect of the holds at higher potential and the partial scans on the H_{upd} region as well as the Pt-O reduction region. As shown in figures 3.6 and 3.7, after the first part of potential holdings at higher voltages, the ECA loss decreased from

62% to 56%, from 52% to 38%, and from 12% to 8% for Ultramid®, EMS Grivory®, and Ryton®, respectively. These findings suggest that the potential holding helped recover the lost ECA to some extent. Further recovery was possible for each of the contaminated electrodes by simply cycling the WE to 1.05 V. Full recovery was observed in the case of Ryton®. Only partial recovery to 41% and 25% of initial ECA was possible for Ultramid® and EMS Grivory®, respectively.

This step-wise process (figure 3.6 and 3.7) is an efficient way to recover. It helped determine the potential at which recovery was most efficient. It also provided insight into the process of recovery. Since the properties of the contaminant molecules would be unknown most of the time, any electrochemical oxidation or reduction process undergone by the molecules during recovery can be captured from the current recorded during the holds. Earlier studies has shown that increased reduction current in the H_{upd} region close to 0V resulted from cycling to higher potential (72). So, in presence of contaminants, the same outcome can be expected by the removal of any contaminant species from the Pt sites.

Figure 3.8 demonstrates that charges increased with higher potential holds. These findings indicate a gradual recovery process (after contamination with leachates). The charges were always positive which suggested ongoing oxidation process during the holding at higher potentials. This oxidation facilitated recovery of the lost ECA among all the potential holds. Charges recorded during 1.2 V hold were highest among all the charges supporting the hypothesis that higher hold potential leads to higher recovery. For Ryton®, the charge passed during 0.75 V hold was more compared to the other two leachates indicating the higher of recovery at lower potential since Ryton® was a clean

material. For Ultramid® and EMS Grivory®, the charge was higher during hold at 1.2 V indicating difficulty of oxidizing the contaminant molecule at lower potential and need of holding the WE at a higher potential for higher recovery.

Figure 3.9 shows the final recovery CV after both potential holding and cycling. The recovery CV for Ryton® showed complete recovery while the recovery from contamination with Ultramid® and EMS Grivory® was partial. Therefore, only a fraction of the adsorbed Ultramid® and EMS Grivory® were completely oxidized and desorbed from the Pt sites leading to a partial recovery.

3.3.5. Part II. Experiments with organic compound to determine the impact on ECA and ORR of Pt/C catalyst

The leachates from the BOP materials can contain a variety of organic and inorganic materials. So, longer time was needed for the contaminants to come to equilibrium with the Pt sites. But since caprolactam was injected in directly from the 10000 ppm of caprolactam solution, there were no other impurities present. In the following sections, it will be shown that the time taken by caprolactam molecules to come to equilibrium with the Pt sites was comparatively much less. Accordingly, the experiments were designed with shorter hold times after injecting caprolactam.

3.3.6. Baseline experiments without any contaminants to benchmark ECA

As described in section 3.3.2, it is important to measure the loss in ECA due to potential cycling before adding any contaminants. These control experiments were performed before any experiments with caprolactam. The control experiments consisted of a baseline set of CV and ORR and three additional sets of the same corresponding to

sequential addition of contaminant. Note that contaminants were not added in the control experiments. The procedure for each set was described in section 2.5.2. Again, the set consisted of a partial CV, followed by an ORR LSV, followed by another partial CV. To report the change in ECA for each set, a normalized ECA was obtained by dividing each set's ECA by the baseline ECA (performed at the beginning of the experiment). The results of the control experiment are shown in figure 11 (points with * symbol) for four replicates (four electrodes) with error bars. Thus, it was observed that the ECA loss was 2%, 8% and 16% at the end of three steps. This may be due to adsorption of sub-surface oxygen that collected on the electrode during previous cycling or adsorption of anions from the electrolyte. Therefore, ECA depends to some extent on the potential cycling history as well as on the accumulation of adsorbate species from the electrolyte (72). The available ECSA of the electrode before and after ORR was calculated but no substantial change was observed between the two values. The electrochemical surface area (ECSA or ECA) was calculated from the area under the H_{upd} region using equation 1.

$$ECA = \frac{\frac{\int IdE}{v}}{210 * L_{Pt} * A_{geo}} \quad (1)$$

The charge of full coverage for clean Pt is 210 μCcm^{-2}. It is used as the conversion factor to calculate electrochemical surface area from the charge obtained from integrating the current (I) over the potential range (dE) under the H_{upd} region.

3.3.7. Benchmarking the ORR catalyst activity with TKK Pt/C catalysts

Recent studies have reported the guidelines for measuring ORR activities under different experimental conditions using adsorbing and non-adsorbing electrolytes (73-76). The catalysts evaluated in this study were commercially available TEC10E50E (high

surface area carbon or HSC, 46% Pt on C) and TEC10V50E (46% Pt on Vulcan carbon or VC XC-72C) manufactured by TKK, Japan. Both catalysts are carbon (graphite) based with 30 to 40 nm diameter carbon particles agglomerated to form a larger primary structure. The comparison of two catalysts is not a simple process and can only be done by estimating and comparing the ORR activities (77). The TEC10E50E is a higher surface area (75-80 $m^2g_{Pt}^{-1}$ (5)) carbon support catalyst compared to TEC10V50E (65-70 $m^2g_{Pt}^{-1}$, (73)) but exhibits poorer mass activities than the later. The higher surface area resulted from the larger pore volume in the TEC10E50E than TEC10V50E. The higher the pore volume, chances are the contaminant particle may enter the pores complicating the diffusion-adsorption processes on Pt sites. So, TEC10V50E was chosen as the catalyst for all the experiments over TEC10E50E, owing to its simple structure, low pore volume and high Pt surface area ($m^2g_{Pt}^{-1}$).

Here electrodes were prepared with different batches of inks to verify the reproducibility of the catalyst preparation technique. The ECA and ORR activities of Pt/VC were benchmarked using the electrodes prepared from seven batches of inks. After the seven electrodes were prepared, they were run in clean electrolytes each time at room temperature. The average ECA was ca.66 $m^2g_{Pt}^{-1}$, which is in agreement with earlier studies (73). The average mass and area specific activities were 231 $mAmg_{Pt}^{-1}$ and 351 μAcm_{Pt}^{2}.

To calculate specific activity (i_s) and mass activity (i_m), the diffusion limiting current (i_L) and the current at 0.9 V were recorded. The potential at which the current is

to be measured for calculating specific activities was determined by a simple relation – the current at 0.9 V has to be within 10% to 80% of the limiting current (77). The limiting current calculated using equation 2 was corrected for the partial pressure of oxygen which in Denver was 83 kPa and divided by the geometric electrode area 0.196 cm^2 to calculate the limiting current density as given in equation 2.

$$i_{lim} = \frac{i_{lim}}{\text{electrode area}} * \frac{101}{83} \quad (2)$$

All data were corrected for the resistance in the electrolyte. Specific activity (i_s, $\mu A/cm^2_{Pt}$) and mass activity (i_m, $mAmg^{-1}_{Pt}$), after the corrections for mass transport, electrolyte resistance, and partial pressure of oxygen, are given by equations 3 and 4:

Mass transport free current i_k is given by,

$$i_k = (i_{lim})\,(i)/(\,i_{lim}-i) \quad (3)$$

where, i_{lim} was the limiting current and i was the current at 0.9 V.

Mass specific activity or current can be calculated from equation 4,

$$i_m = \frac{i_k * 1.3 * 10^3}{\text{loading} * \text{geometric area of electrode}} \quad (4)$$

1.3 was the correction factor to account for the combined effect of low partial pressure of gases in Denver. Kinetic and thermodynamic aspects of lower partial pressures of H_2 and O_2 gases contribute to estimating the correction factor at Denver to be 1.3 (78).

The normalized activity follows the same trend as available ECA. The normalized mass activity graph follows the trend as ECA. The loss in mass activity for the control experiment (without contaminant) was around 4%, 6% and 11% for the three steps as given in table 3.2.

3.3.8. Determining the equilibrium time required for organic compounds

To characterize the time needed for molecules of caprolactam to reach equilibrium with the Pt catalyst, 1.36 ml of $1x10^{-3}$ M caprolactam was injected at 1.05 V (after 1.25 cycles, one full cycle then from 0.4 → 1.05 V) after conditioning the electrode as described in section 2.3. During this characterization, the WE was cycled between 0 and 1.05 V at a scan rate of 100 mV/s so that a complete scan was recorded in 20s. It took 0.7 cycles to observe the peaks due to contamination with caprolactam. After adding caprolactam, the first contamination peak was observed at 0.25 V (anodic). Thus, 12 s was recorded for the caprolactam molecules to reach Pt (figure 10). It took 12-13 cycles for the contaminant molecules to attain equilibrium with the Pt sites on the WE, which was approximately 240 s from the beginning of the contamination. Therefore, in the consecutive experiments quantifying the ECA and ORR loss due to addition of caprolactam, the WE was held for 300 s before CV scans.

3.3.9. Example of contamination effects from organic compounds on CV and ORR

The effect of contamination from the leachates was reported in the previous section of this paper. Experiments conducted in the following part attempt to assess the role of an organic compound found in the leachate of structural plastics that may be used in PEMFC. Since caprolactam, or dimer of caprolactam, was identified in the leachates

described in the previous part, it was chosen as the "model" compound for further contamination experiments.

After establishing a baseline for CV and ORR (section 3.2.5) caprolactam was injected in the clean electrolyte to achieve $1x10^{-3}$, $5x10^{-3}$ and $2x10^{-2}$ M concentrations in the RDE cell.

Caprolactam adsorbed on the Pt sites (figures 3.11 and 3.12) and showed distinctive poisoning behavior involving decrease in H_{upd} region to 81%, 76% and 74% of the initial value for the concentrations of caprolactam 1 mM, 5 mM and 20 mM. The "a" and "b" peaks at 0.22 V is due to proton adsorption/H_2 desorption on Pt (100). The black arrows in the H_{upd} region indicate the loss in ECA and its subsequent recovery.

The oxygen reduction reaction is known to be affected by contaminants present in air or fuel in a PEMFC (17). Some recent studies also suggest that irreversible poisoning characteristics of organic compounds from coolants (30) and additives (61) used in a PEMFC can inhibit the ORR activities. The ORR baseline was established in a clean electrolyte (section 3.2.5.2.). As caprolactam was injected in the electrolyte, the corresponding polarization curves showed (i) decreased diffusion limiting current and (ii) shift in current at 0.9 V. These two phenomena can indicate poisoning of the catalyst, adsorption of caprolactam on the Pt sites required for O-O bond breaking (colored lines in figure 3.12) as well as absorption on ionomer.

The mass transport limiting current decreased to 87, 85 and 78% of the initial value (table 3.3 and figure 3.13) whereas the ECA decreased to 81%, 76% and 74% i.e. the limiting currents after addition of contamination did not decrease in same extentand

proved to be beneficial for the ORR of Pt. Whereas, the available current at 0.9 V (80%, 76% and 74%) after adding caprolactam was found to be proportional to available ECA at that step. So no additional current loss (due to absorption on ionomer) effect was observed in case of caprolactam contamination.

The contamination of caprolactam suppresses ORR currents of Pt/C. The best way to quantify the ORR activities loss is by calculating the mass activity of the electrode. The mass activities were first calculated for each of the three steps of the contamination in a clean electrolyte without adding any contamination anytime during the experiments. These mass activities in the control experiment provided a perspective of the expected values of the mass activities at each step.

The baseline mass activities during the control experiments were close to 240 $\mathrm{mAmg}_{\mathrm{Pt}}^{-1}$ (figure 3.14). In the next set of experiments, where caprolactam was gradually added in three steps, the mass activities decreased to 125 $\mathrm{mAmg}_{\mathrm{Pt}}^{-1}$ as shown in figure 18. This is almost 51% of the value of mass activity at the beginning of the test. Therefore, 49% of mass activity was lost due to contamination. In an attempt to restore the lost mass activity, the electrode was rinsed in DI water and was moved into a second set of cell containing fresh electrolyte saturated with O_2. In that electrolyte, linear sweep voltammetry was performed and the recovered mass activity was 76% of the initial value.

3.4. Conclusions

This study summarizes comprehensive and sequential testing protocols to measure the impact of liquid phase contamination from BOP materials on Pt/C catalyst

used in a PEMFC. The protocols also included mitigating strategies that was partially successful in reversing the effect of contamination for some leachates.

The results were analyzed to reveal the following:

- To allow the contaminant molecules to reach equilibrium with the Pt sites, the WE electrode should be held at a potential less than the oxidation potential of the contaminants before performing a CV to measure contamination effects. This potential was chosen to be 0.4 V rather than the open circuit potential since it minimizes the loss of ECA.
- Due to time dependant nature of contamination, the ECA loss reached equilibrium with Pt sites after ~40 min although the majority of the contamination effect was observed in the first 10 min.
- From the quantitative analyses of ECA loss, it can be concluded that the contamination was more pronounced in the case of polyamide 6,6 (Ultramid® and EMS Grivory®) than polyphynelene sulfide (Ryton®). Even though all three of them are off-the-shelf BOP materials, the Ultramid® and EMS Grivory®) showed greater impact in poisoning the catalyst than Ryton®.
- The recovery strategies were more effective for Ryton® where full recovery was observed , whereas Ultramid® and EMS Grivory® contamination effects were partially recoverable, which mirrored the contamination effect of those three compounds.

In the second part (section 3.3.4 to 3.3.7), experiments were performed to report the contamination from the organic contaminant (caprolactam) detected in the leachate of

the BOP material Ultramid®. Caprolactam showed poisoning behavior comprising of loss of ECA and ORR currents and activities. Changing caprolactam concentration from 1 to 20 mM the ECA changed from 80 to 74%. The comparison of ORR activities between an uncontaminated and a contaminated (with caprolactam) electrode revealed up to 65% loss in mass activity of the catalyst, which was partially recovered at the end. ORR data showed no additional contamination effect resulting from absorption of caprolactam on ionomer. Also the contamination was recoverable by rinsing the electrode with DI water and cycling the electrode at higher potential.

Care must be exercised before measuring the ECA because the surface area of the thin film decreases with time and/or voltage cycling. So, it is imperative to benchmark several electrodes to establish a range of reproducible ECAs and ORR activities with the catalyst before assessing the effect of contaminants on it.

The data obtained in this study on the poisoning behavior of the structural materials may provide guidelines to the manufacturers of fuel cell with the specifications for concentration of the materials that can be safely used.

Table 3.1. Summary of comparison of ECA loss due to CV cycles and contamination (Ultramid®, EMS Grivory® and Ryton®) on Pt/C catalyst as evaluated in this paper

time, s	blank	Ultramid®		Ryton®		EMS Grivory®	
	% ECA loss	% ECA loss	Δ change	% ECA loss	Δ change	% ECA loss	Δ change
750	3	33	30	5	2	22	19
1500	8	57	49	10	2	34	26
2250	11	66	55	17	6	41	30
3000	14	72	58	27	13	64	50
3750	19	80	61	32	13	71	52
4500	23	85	62	35	12	75	52

Table 3.2. Summary of the average and standard deviation of mass activities during control experiments performed in three steps and after contaminating the electrolyte with 1, 5 and 20 mM of caprolactam corresponding to step 1, 2 and 3 in a different set of experiments (refer to figure 3.11 for the respective ECAs).

ORR activities after contamination	Normalized mass specific activity (%)	Normalized mass specific activity (%)
	control	caprolactam
Step 1	95.9 ± 3.0	51.2
Step 2	93.9 ± 3.6	48.4
Step 3	88.6 ± 2.6	35.4
recovery	-	75.0

Table 3.3. Summary of ECA loss and ORR currents before and after adding contaminants.

	i_{lim}	$(i_c/i_p)_{lim}$	$i_{0.9V}$	$(i_c/i_p)_{0.9V}$	*ECA*	*Available ECA %*	*ionomer effect*$_{0.9V}$	*ionomer effect*$_{lim}$
	mA/cm^2	%	mA/cm^2	%	m^2/g_{Pt}	%	%	%
1E-3 M	*5.2*	*87*	*2.0*	*80*	*54*	*81*	*-1*	*-3*
5E-3 M	*5.1*	*85*	*1.9*	*76*	*51*	*76*	*0*	*-9*
2E-2 M	*4.7*	*78*	*1.8*	*74*	*50*	*74*	*0*	*-4*
recovery	*5.8*	*96*	*2.3*	*92*	*62*	*92*	*0*	*-4*

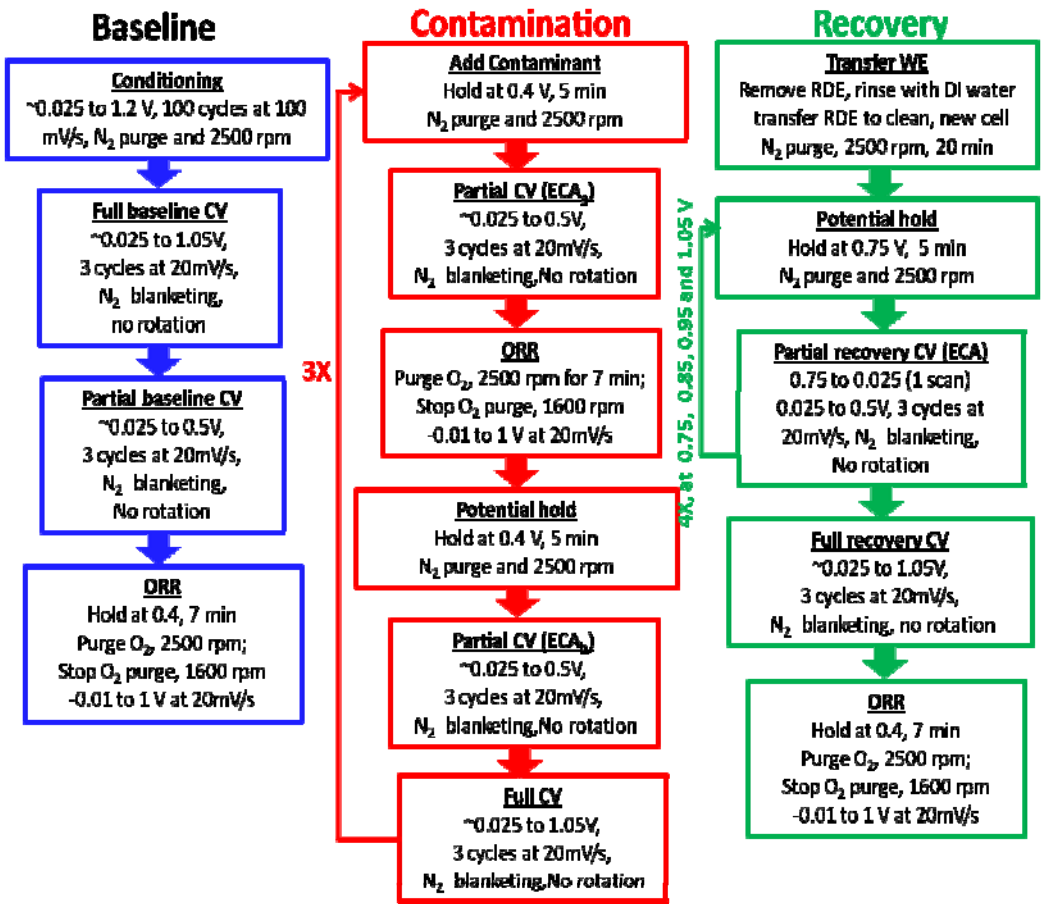

Figure 3.1. Schematic of the experimental protocol to investigate the impact of the organic contaminants found in the DI water soak of the materials used in a PEMFC. The loss of ECA and ORR activity of Pt/VC were measured using three electrodes TF-RDE apparatus at room temperature.

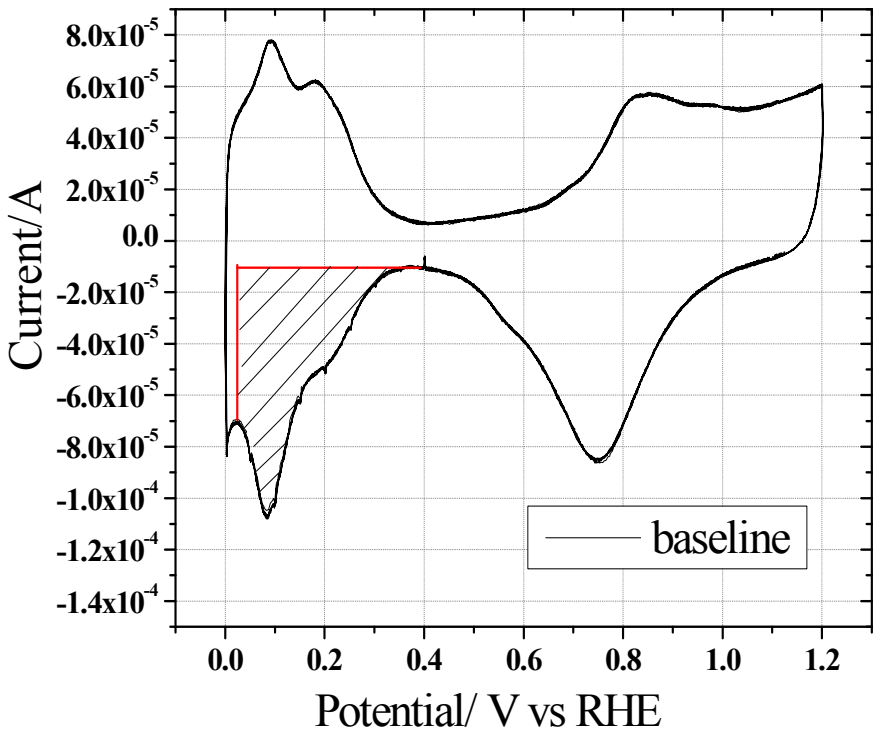

Figure 3.2. Figure showing the initial cyclic voltammetry in 0.1 M $HClO_4$ at room temperature. Conditions: scanned at $20mVs^{-1}$ without any rotation of the electrode in a well purged (with inert gas) clean electrolyte from 0.to 1.2 V after conditioning. The CV shows distinct peaks at 0.1 V cathodical (hydrogen adsorption).

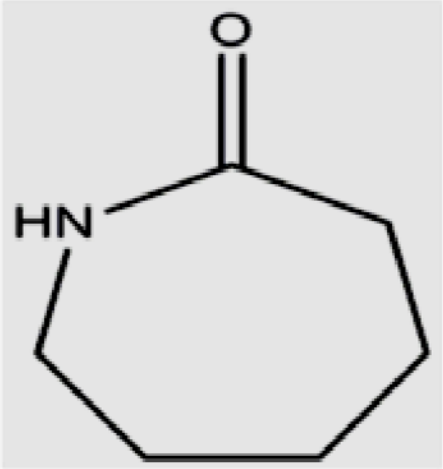

Figure 3.3. Schematic of the caprolactam molecule showing an aliphatic closed chain organic compound with =O and –HN group attached the ring.

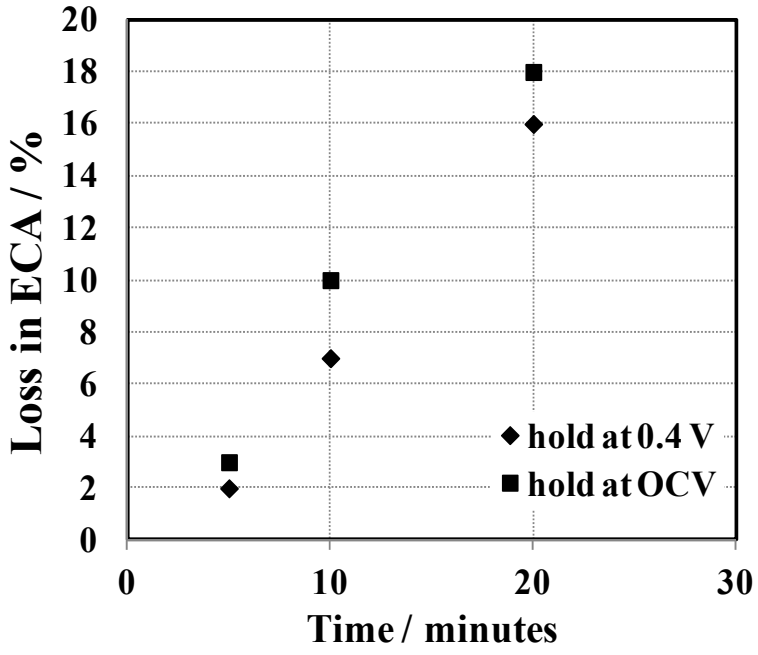

Figure 3.4. The loss in ECA after to holding the WE at 0.4 V and OCV potential (0.9V) from the initial ECA in clean 0.1 M $HClO_4$, at room temperature recorded at intervals of 5, 10 and 20 minutes.

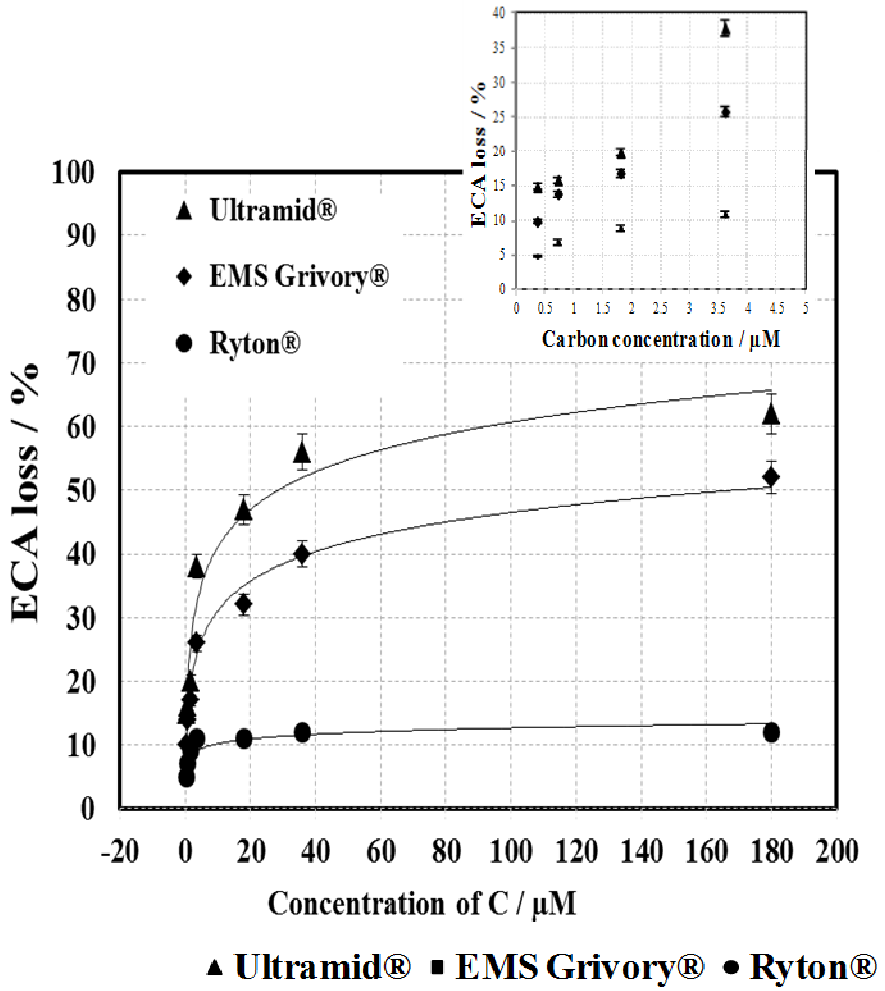

Figure 3.5. ECA loss due to contamination from the leachates at room temperature, in 0.1 M $HClO_4$.

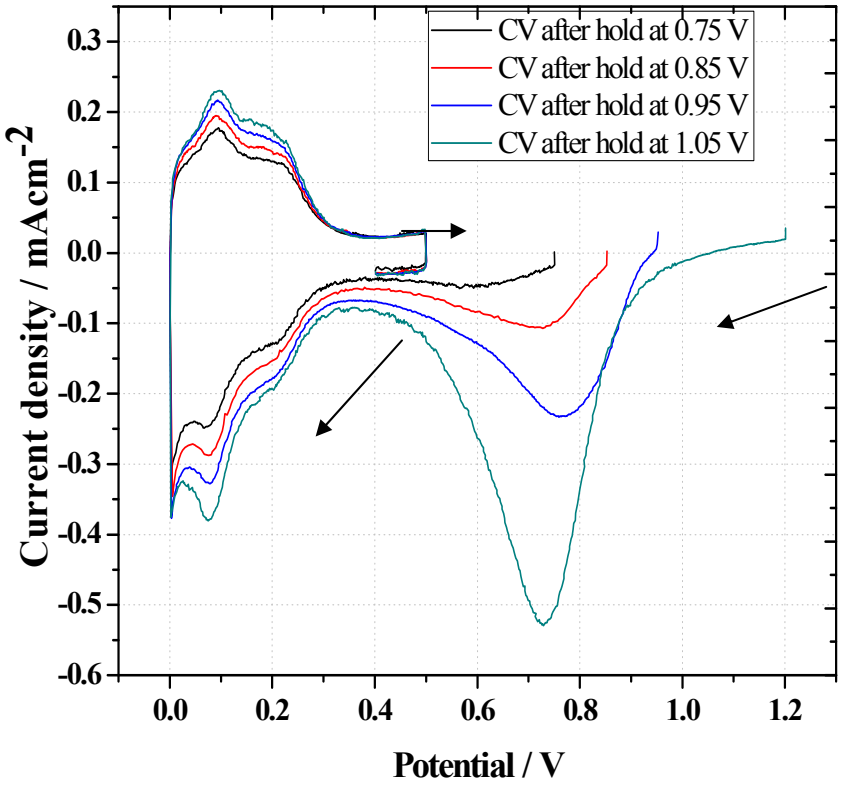

Figure 3.6. Example of the recovery of contaminated (Ultramid®) electrode at the end of potential holding at 0.75 V, 0.85 V, 0.95 V, 1.05 V in a clean electrolyte (0.1 M $HClO_4$) purged with N_2.

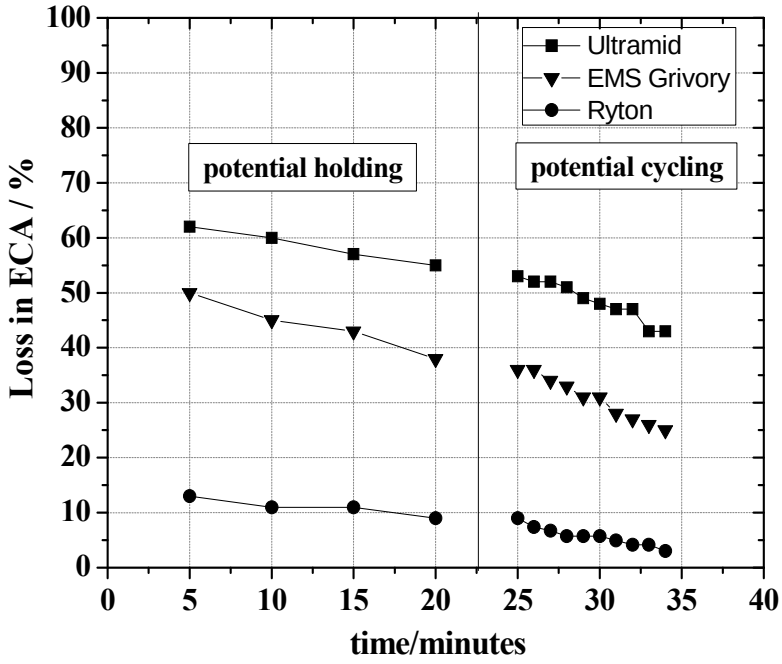

Figure 3.7. The recovery of lost ECA due to potential holding and potential cycling. The left side of the figure shows the recovery characteristic of potential holding on the lost ECA due to contamination from the fabrication plastics used in a fuel cell (Ultramid®, Ryton®) and DI water. The right side shows the further impact of potential cycling to a higher voltage (10 full CV cycles) on recovering the lost ECA after potential holding.

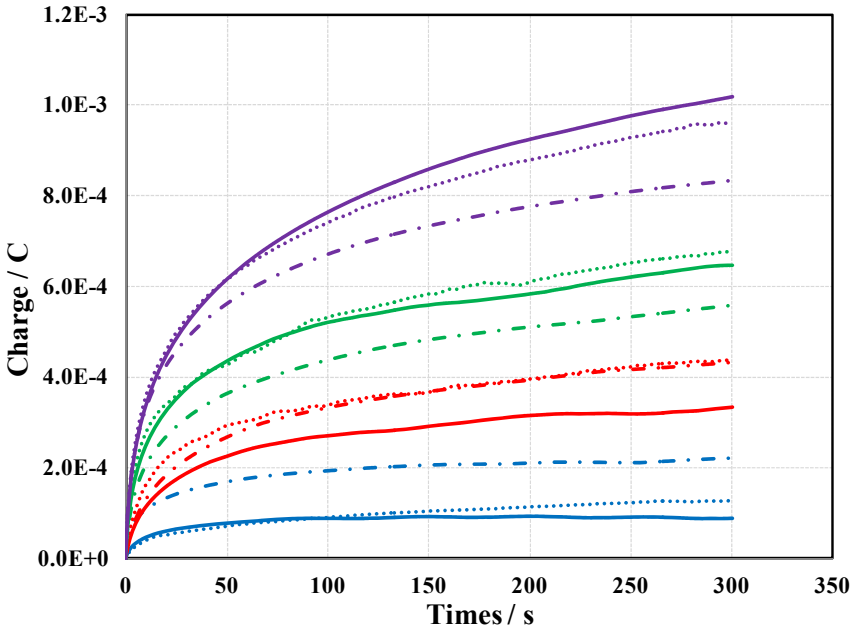

Figure 3.8. Charge recorded during 5 minutes holds at the time of recovery in a clean electrolyte after rinsing the WE in DI water. The holds were performed at 0.75 (blue), 0.85 (red), 0.95 (green) and 1.05 (violet) V. Legend: (…….. EMS Grivory, ¬¬—— Ultramid, –·– Ryton)

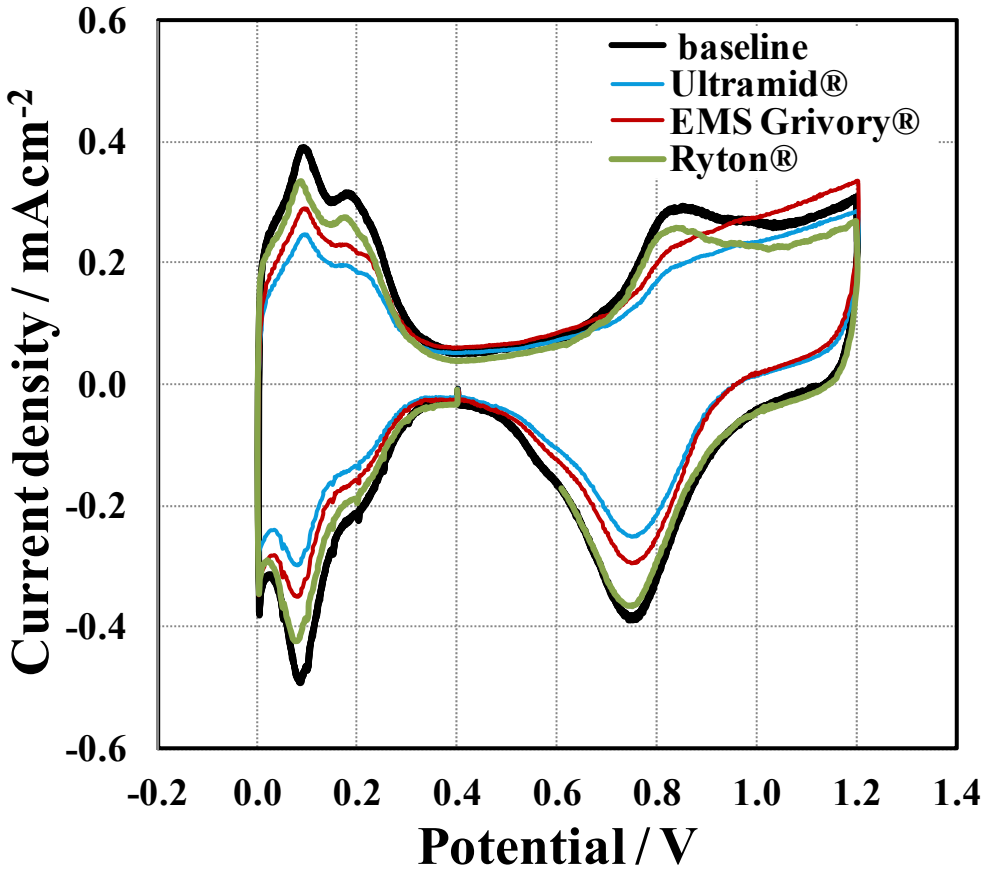

Figure 3.9. The baseline is the initial CV scans before adding any contaminants (black solid line). After the electrodes were contaminated with two leachates and recovered at higher potential, the CV scans after recovery was shown in red line for EMS Grivory®, blue line for Ultramid® and green line for Ryton®.

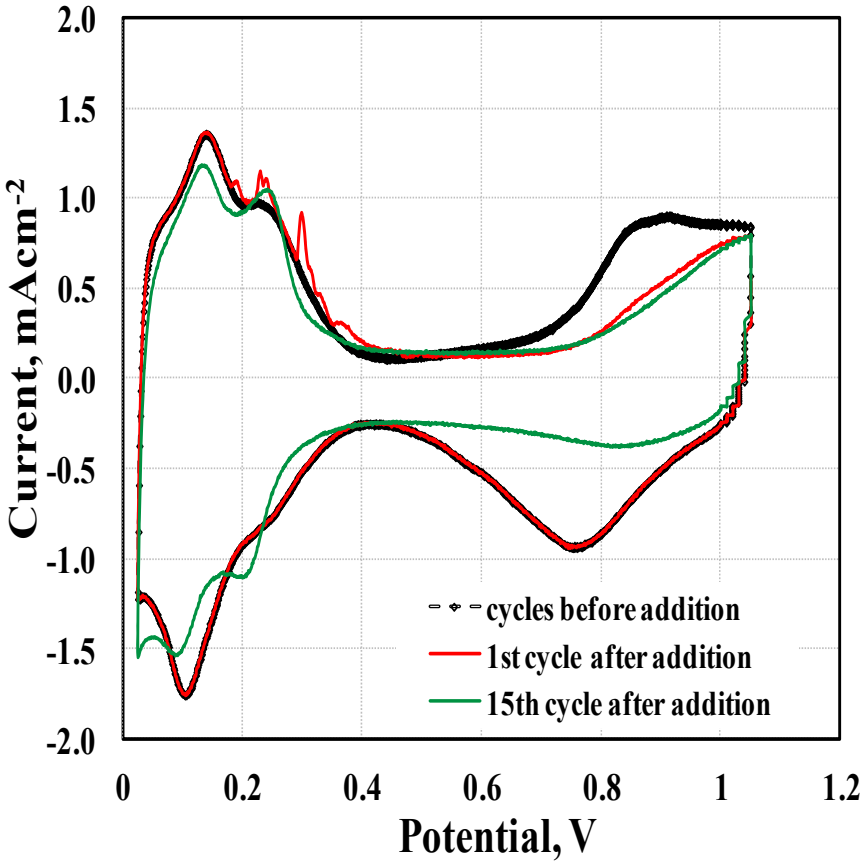

Figure 3.10. Cyclic voltammogram to determine time needed for caprolactam to adsorb on Pt sites. 1x10-3 M caprolactam was added to the electrolyte after conditioning of electrode at 1.05 V (a) and no change was observed in the Pt-O reduction region. In the first cycle (red line) the first peak (b) was observed at 0.3 V and the H_{upd} region (c) stayed the same. Then in the 15th cycle after the addition of caprolactam (green line), area under Pt-O region (d) as well as H_{upd} region (e) decreased. The arrows show the direction of cyclic voltammetry.

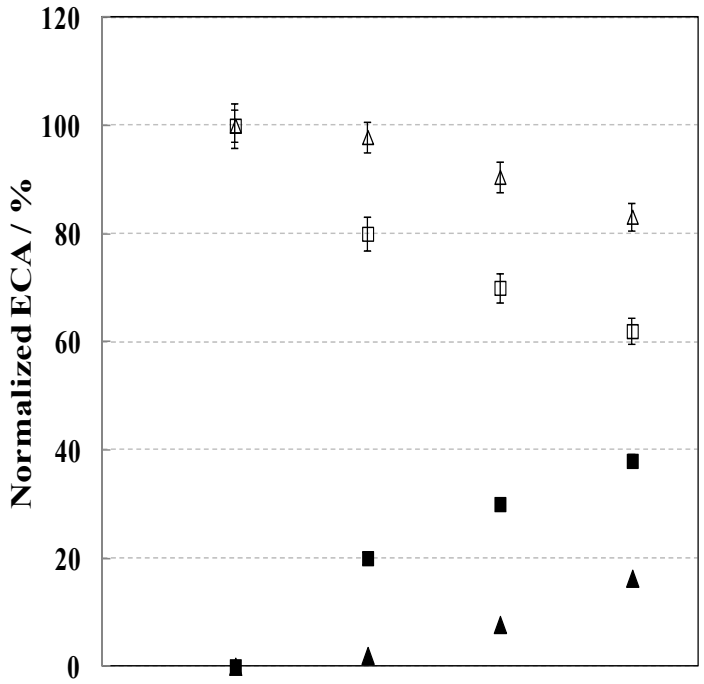

Figure 3.11. The loss in ECA during the control experiment (▲, Δ) in the clean electrolyte (0.1 M HClO4) and after injecting caprolactam (■, □). The y axis denotes normalized ECA. Sets 1 to 3 denote the three steps after contamination, which for caprolactam were 1, 5 and 20 mM. Legend: (open symbols: available ECA, solid symbols: loss in ECA)

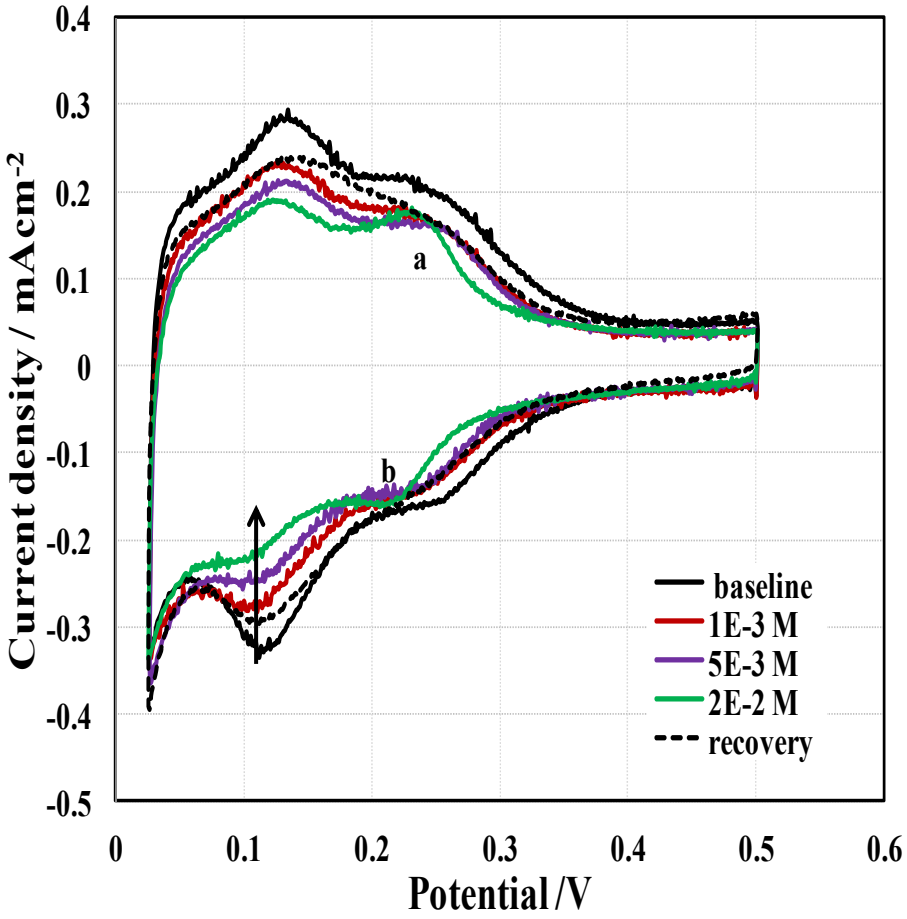

Figure 3.12. The effect of caprolactam on partial CV scans at room temperature. Conditions: scanned at 20 mVs^{-1} without any rotation of the electrode in a well purged (with inert gas) clean electrolyte.

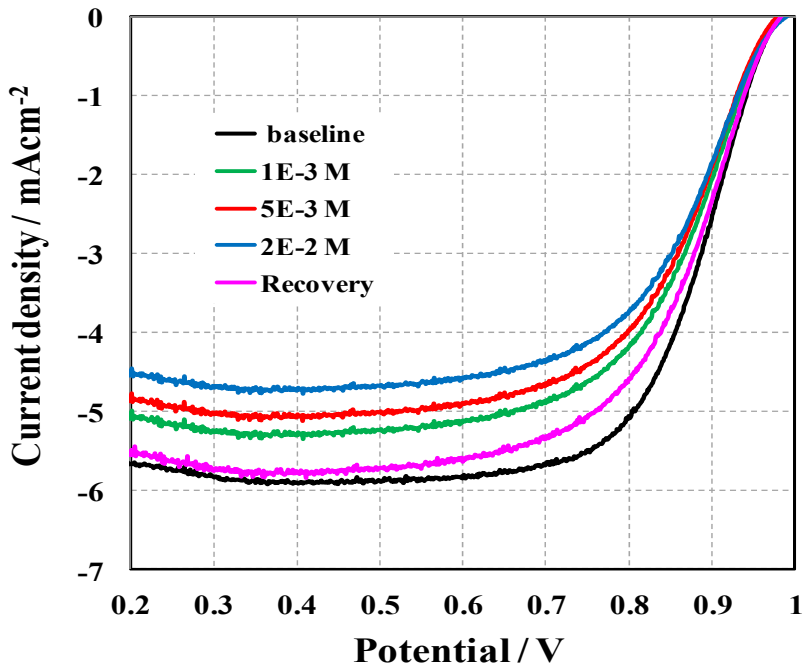

Figure 3.13. ORR polarization curves for Pt/VC in 0.1 M perchlric acid electrolyte: initial or baseline ORR (black solid line), with $1x10^{-3}$ M caprolactam (red solid line), with $5x10^{-3}$ M caprolactam (green solid line), with $2x10^{-2}$ M caprolactam (violet solid line).

Chapter 4. Screening of assembly aids using TF-RDE method

In this chapter the effect of off-the-shelf adhesives and lubricants (assembly aids) that may be used in PEM (proton exchange membrane) fuel cells affects the performance of Pt catalyst adversely. The impact on Pt, which is widely used in PEMFC was investigated using thin-film rotating disk (TF-RDE) method. The adhesives leach out in the PEMFC electrode and reduce electrochemical surface area (ECA) and oxygen reduction reaction (ORR) activities of platinum based catalysts leading to loss of performance. In this study liquid phase contamination effect on platinum supported on Vulcan carbon electro catalyst was shown using cyclic voltammetry and linear sweep voltammetry approaches. The effects of the leachant were compared to the effects of the organic compound present in it using rotating disk electrode (RDE) in 0.1 M perchloric acid. The loss in ECA and ORR activities (mass activities, mA/mgPt and specific activities, $\mu A/cm^2Pt$) are compared at the beginning of the test and after addition of different dosage of contamination.

The additional information on the methodology and background studies can be found in appendices D, E, F and G.

4.1. Introduction

Polymer electrolyte membrane fuel cell (PEMFC) is one of the cleanest sources among the available renewable technologies to be used in car industries. Success of fuel cell based vehicles depend on the performance of the electrocatalysts used in them, which

are widely known to be susceptible to various contaminants (15, 41, 79, 80) (air borne and liquid phase) resulting in poor performance and durability. When the contaminants reach the catalyst layer, they adsorb on the Pt sites preventing them to participate in oxygen reduction reaction ($O_2 + 4H^+ + 4e^- \rightarrow 2H_2O$).

The ORR reaction is usually the one of the most inhibiting processes for developing high performance electrocatalyst for fuel cell vehicles (81). So for the development of Pt electrocatalyst, understanding the process of contamination at the catalyst surface is necessary. The contamination of Pt electrode is a complex process, since the contaminants can modify the intrinsic catalyst properties. The common sources of contamination are air (cathode), fuel (anode), components of fuel cell (structural plastics, assembly aids, coolants, gaskets etc.). While there are many existing studies on air contaminants (15, 24, 44, 82) very few literature exists that quantifies and explains the contamination originating from the organic compounds used in a fuel cell as structural plastics, assembly aids (adhesives lubricants etc.) at the surface of the Pt catalyst.

Carbon supported Pt or Pt alloy of catalysts are mostly extensively used catalyst for low temperature fuel cells for vehicles. Air contaminants like SO_2, NH_3, CO, CO_2, H_2S etc. (15, 23, 24, 44, 56, 79) adsorb on Pt on cathode side and anode side in a PEMFC. While the impurity effect on hydrogen oxidation reaction (HOR) on anode side is well understood, the oxygen reduction reaction is still need to be studied with great detail since ORR inhibited by contaminants can result in high over potential and loss in fuel cell efficiency (44, 58). Therefore it is very important to understand the fundamentals of contamination process on Pt/C using ex-situ methods like rotating disk electrode to develop commercially viable catalyst with high ORR activities.

The performance of a fuel cell is degraded in presence of not only air contaminants. The contaminants leached out from the fuel cell stack are detrimental to Pt catalyst. The contaminants can leach from anywhere in a fuel cell stack, such as the plastics, coolant, gaskets, adhesives and assembly aids (31).

In situ and ex-situ voltammetric studies have been previously employed for studying and removal of adsorbed contaminants such as air contaminants (cathode and anode side) like SO_2, H_2S and CO from the Pt surface in the MEA (16, 56, 63). Recently ex-situ studies have revealed the significance for studying the liquid phase contaminant originating from commercially available coolant stream as they might contain additives which could poison the catalyst (30).

The off-the –shelf assembly aid materials are being considered by the manufacturer and may be used in PEM fuel cells since they possess excellent thermal stability and water resistant properties. But after prolonged use the assembly aids leach out inside the fuel cell and affects the catalyst performance. To study the effect on cathodic ORR due to contamination, these assembly aid materials were tested ex-situ using TF-RDE mimicking the same leaching condition.

Materials selection in this study was based on properties such as exposed surface area, utilization and integration in a PEMFC system, cost, and performance implications. They may be used for applications in hot and humid conditions such as in fuel cells. In this study it is shown that the leachant from adhesive used in a fuel cell stack adsorbs on Pt and reduces the available electrochemical surface area and also reduces the mass

activity of the catalyst layer. The ex-situ cyclic voltammetry data supports adsorption of contaminants on the Pt for the leachant aged for one week at 90°C.

Thin-film rotating disk electrode (TF-RDE) method was employed in this study to understand the fundamentals of oxygen reduction reaction (ORR) (47) and electrochemical area loss after injecting the contaminants leached out from the adhesives and lubricant. An attempt to recover the ECA and ORR activity loss was also explored in this study. RDE measurement technique was chosen for easy isolation of impact on ORR activities of the catalyst in presence of contaminants, which was not possible in-situ (in a PEMFC).

Our goal is to provide an increased understanding of fuel cell system contaminants and help provide guidance in the implementation, and where necessary, the development of system materials that will not lead to undesirable loss of fuel cell efficiency due to contamination. In addition to that, studying ORR in presence of those contaminants will facilitate development of high performance fuel cell catalysts.

In this paper, an in-depth study of broad spectrum of assembly aid (lubricant and adhesives) materials commonly used in PEMFC has been reported that will benefit the fuel cell manufacturers in selecting materials which will limit the contamination and develop cost-effective analysis technique of testing system components under contamination. It also provides valuable insights on estimating system derived contamination on the catalyst as well as the ionomer in a fuel cell.

4.2. Experimental

The off-the-shelf adhesives, sealants, and lubricants (i.e., assembly aids) were selected based on their properties and functionalities (i.e., thermally stable and chemically resistant) and can be categorized based on their original chemical groups as shown in figure 4.1. These assembly aid materials are not specifically designed for fuel cell and a wide range of function and applicability. Some of the most important characteristics of these adhesives, lubricants, and thread-locks are water resistibility and superior stability at elevated temperature. Although the materials were manufactured from same parent compounds and have same functional groups, the manufacturer added additives residue (solvent, reactant residues, anti-oxidants, flame retardants etc.) segregate them into different grades.

Data for the 19 assembly aids shown in Figure 1 can be found in (70) and six (6) of these (shown in Table 4.1) were selected (one from each group except the urethane where two were selected) for this paper to illustrate the contamination phenomena of ECA loss and the resulting changes in ORR performance as characterized by limiting current density, the Tafel slope, and kinetic current density. The results of the screening allow for categorization of the aids based on contamination and reversibility behavior.

Figure 4.2 shows that there were three essential parts of the experimental procedure: baseline, contamination, and recovery. Each electrode was subjected to the baseline first, followed by the contamination part, and finished with the recovery part. In each part, the ECA and ORR activities were measured. All experiments were performed at room temperature in 0.1M $HClO_4$ using a TF-RDE method (Ref dissertation). The details of experimental procedure including electrode preparation and conditioning were

reported in (59, 70). The contamination part was repeated three times for three different concentrations of the leachate. Since kinetics data were extracted from the ORR polarization curves, the background of ORR was recorded in N_2 gas saturated electrolyte.

For the baseline part, thin film electrodes were prepared as described in (59, 70) and mass activities were calculated and used to ensure quality of the electrode in terms of reproducibility of the catalysts. Conditioning involved 100 cycles from 0.025 to 1.2 V at 100 mV/s after a 20 min N_2 purge while the TF-RDE was rotated at 2500 rpm. The full baseline CV was obtained from three cycles between 0.025 and 1.05V at 20 mV/s under a N_2 blanket with no rotation. This full baseline allows calculation of the ECA according to typical procedures reported in 16, 17. In addition a partial baseline CV was obtained from three cycles between 0.025 and 0.50 V at 20 mV/s under a N_2 blanket with no rotation. Again the ECA was calculated and compared with the ECA from the full baseline CV. These two ECAs were within ±3% of each other with smaller ECA consistent with the fact that partial scans do not go higher up to the potential where PtO can be formed. Note the partial scan was used to be consistent need to limit the potential range for the contaminated ECA. Next, the WE was polarized at 0.4V for 7 min while purging with O_2 and rotating at 2500 rpm. Hydrodynamic voltammetry for the ORR current measurement was conducted by recording linear sweep voltammetry at 20 mVs^{-1} in an O_2 blanketing environment on the electrolyte and rotating at a speed of 1600 rpm. Finally, the electrolyte was saturated by sparging N_2 for 7 min then a background ORR scan was obtained in N_2 saturated electrolyte from -0.01 to 1.0 V at 20 mVs^{-1} while rotating at 1600 rpm. The sweep rate and rotation speed were the same as for the N_2 baseline. The

background was later subtracted from the ORR LSVs to correct for the pseudo capacity currents.

For the contamination part of figure 2 the initial leachate solution of known TOC concentration was 1.8 μM on a carbon basis which was added with a pipette directly to the electrolyte while purging the RDE cell with N_2 and while holding the working electrode at 0.4 V (to avoid any electrochemical change of the contaminant before it reached the Pt sites) and rotating at 2500 rpm. Then the ECA was measured from the cyclic voltammograms (full and partial, performed same way as described above for the baseline part). Next, the WE at 0.4V during a 7 min urge of O_2 during rotation at 2500 rpm followed by recording of linear sweep voltammetry (ORR current) at 20 mVs^{-1} with O_2 blanketing on the electrolyte and rotating at a speed of 1600 rpm. Note that the electrolyte was saturated by sparging N_2 for 7 min then a background ORR scan was obtained in N_2 saturated electrolyte from -0.01 to 1.0 V at 20 mVs^{-1} while rotating at 1600 rpm. The linear sweep voltammetry in N_2 is measured to subtract the background to obtain kinetic data (Tafel slope). Then the required volume of leachate was added to the 1.8 μM contaminated electrolyte to achieve 18 and 180 μM carbon concentration and the contamination part was repeated.

Recovery part includes the potentiostatic hold at higher potentials followed by potential cycles from the holding potential (0.75 V, 0.85 V, 0.95 and 1.05 V) to low potential (0 V) finally to 0.5 V. The partial CVs allowed calculating ECA after each hold, presenting the % of ECA recovered due to the holds. Finally recovery CV (3 cycles of full CVs - 0.025 V to 1.05 V at 20mVs^{-1}) and ORR (-0.01 to 1.0 V at 20mVs^{-1}at 1600 rpm) was performed using the same procedure as described in the baseline section. The

linear sweep voltammetry in N_2 is measured as the background to obtain kinetic data (Tafel slope) after recovery.

The contaminant solutions for the experiments were prepared by spreading the paste material on PTFE strips with the volume to surface area ratio of 150 cm^{-1}, then aged at 90^0C (close to fuel cell operating temperature) in DI water for one week inside an air tight PTFE bottles. The aging process at high temperature facilitates the organic compositions of the adhesive to leach out in the water. The water was decanted and analyzed for total organic carbon (Thermo Scientific), solution conductivity (Thermo Scientific) and pH. It was also subjected to GCMS, IC (Dionex ICS-90 Ion Chromatography System) and ICP-OES (Perkin Elmer Optima 5300 DV) to qualitatively detect the organic and inorganic compositions present in it. In GCMS the most detectable peaks are presented in table 4.1.

A material is selected from each group to demonstrate loss in ECA and effect on ORR activities on Pt/C catalyst at room temperature using TF-RDE method.

4.3. Results and discussions

4.3.1. Characterization of the leachate using GCMS, TOC, ICP

The ECA and ORR losses were attributed to the functional groups adsorption on Pt catalyst or absorption on ionomer. The TOC and the organic groups identified in the leachates for the six materials as determined by GCMS are listed in table 4.1. The concentration of organic carbon (given by TOC, ppm) in the leachates tested were as low as 10 ppm for Krytox® (fluorocarbon lubricant) and as high as 1695 ppm for Bond It (epoxy adhesive) leachate. To study the effect of those leachates the volume added to the

rotating disk electrode cell, were adjusted depending on the level of TOC so that the final concentration of carbon in the electrolyte from the leachate equaled to 1.8 μM, 18 μM and 180 μM. The cations identified in the leachates using ICP-OES for the six materials are listed in table 4.2.

4.3.2. Determining time required for the organic contaminant molecule to reach Pt sites

The effect of contamination was observed immediately after adding the contamination at 1.05V. As the CV proceeded cathodically a noticeable decrease in Pt-O reduction region. The first cycle (in red) shows decrease in H_{upd} region ($H^+ + e^- \leftrightarrow H_{upd}$) and for the case of Loctite®39916 and the green lines show the gradual decrease in ECA which finally comes to equilibrium after 12-13 cycles (figure 4.3).

The TOC of Loctite® 39916 was calculated to be 260 ppm. The solution was injected at 1.05 V after first 10 cycles and was scanned cathodically. The effect is seen immediately in the first cycle (red line) for both cases. It took ca. 8 cycles for the CV to come to a steady state. Therefore it took 20.5*8= 164s or over 3 minutes for the molecules to reach catalyst surface and adsorb on (block) the Pt sites.

4.3.3. Screening of BOP assembly aids

The screening was based on the contamination and reversibility of contamination – as depicted in the figure 4.4 were categorized as clean (green bucket), contaminates but recovers and contaminates but doesn't recover.

Due to potential cycling, the initial electrochemical surface area decreases. The initial ECA is denoted by first point on the graph. The ECAs are normalized by baseline

ECA. The cyclic voltammetries and linear sweep voltammetries were repeated three times to mimic the addition of contaminants in three steps. The ECA 2, 3, and 4 were performed after break in and baseline to measure the change in available ECA. During the control experiment, decline in available ECA was observed. It was up to 17% (normalized ECA or NECA was 83%, given by the third point in the graph) till the end of the experiment.

This loss in ECA was taken into account while calculating the NECA and ECA loss.

4.3.4. Analysis of ECA and ORR activities after contamination

4.3.4.1 DupontKrytox 206 (Lubricant)

The CVs before adding (baseline) and after adding contaminants (at the end of the experiments) are shown in figure 4.5. Both limiting current and currents at 0.9 V are very close with respective ECAs. Loss due to contamination adsorption on Pt. No loss due to contaminants absorbing on ionomer ECA loss is very low. Enough Pt sites available for O-O breaking needed for ORR since the ECA loss were negligible. The recovery steps were not performed.

Nothing was detected in the leachates of krytox (table 4.3) which is consistent with low contamination effects on Pt catalyst as well as ionomer. So this material is concluded to be a clean material based on the screening criteria.

4.3.4.2 3M silicone 8664 (assembly aid)

The figure 4.6 shows the cyclic voltammogram response (under Hupd region) and the currents from oxygen reduction reactions under clean, contaminated and recovery conditions.

Three organic compounds were identified in 3M silicone leachate by GCMS (83) 2-(2-ethoxyethoxy)ethanol, 2-(2-ethoxyethoxy)ethanol acetate and benzyl alcohol The structures of the functional groups are given in figure 4.7. The COO- (carboxylate) group, OH- (hydroxyl) group and benzene ring adsorb on Pt and decrease the ECA. But the ECA loss was somewhat recoverable, since the aliphatic groups oxidized and desorbed from the Pt sites at higher potential during recovery process.

The ICP results showed very low (11.5 ppm) metal ions (Li, K, Si etc) concentration in the leachate as supported by the ionomer contamination data (table 4.4).

4.3.4.3 Henkel Loctite 39916

Three organic compounds were identified in Loctite 39916 leachate by GCMS (83) –methyl benzene diamine (MBDA), 4-methylbenzensulfonamide (4MBSA) and Butyric acid N'-m-tolyl-hydrazine. The structures of the functional groups are given in figure 4.9. Loctite 39916 is a polyurethane adhesive, synthesized through polymerization between monomers of a 2,4 and 2,6 toluene diisocyante and a polyol through a catalyst. When trapped residual monomer from the synthesis reaction leached into solution at 90°C, which was later hydrolyzed to form methyl benzenediamine, the species identified via GCMS in leachates. 4-methylbenzensulfonamide comes through additive added to the adhesive for water scavenging.

The ICP results showed very high total ICP count (117 ppm) with significant amount of various metal cations (Ca) and non-metals (S) present in the leachate. The organic functional groups along with free or bound sulfur adsorb on Pt to decrease the ECA upto 56% at 180 μM carbon concentration. The ICP-MS data showed high but reversible ionomer contamination as supported by the ionomer contamination data. At high concentration of loctite 39916 leachate, the ionomer contamination was as high as 27%, which recovered to 2% (table 4.5).

4.3.4.4 Other assembly aids

Other assembly aids tested were 4000 fast cure white, loctite 567, bond it b 45

4000 fast cure white (urethane)

The ICP results showed high (109 ppm) metal ions (Zn, K etc). The ICP-MS data showed high ionomer contamination as supported by the ICP-MS data.

Three organic compounds were identified in the leachate of 4000 fast cure white by GCMS –Ethanol, 2-(2-ethoxyethoxy), Ethanol, 2-(2-ethoxyethoxy)- acetate, Benzyl Alcohol, Methyl-Benzenediamine. The structures of the functional groups are given in figure 4.11.

In addition to the metal ions the $-NH_2$ group from the methyl benzenediamine gets protonated and forms NH_3^+ which attacks the ionomer. Therefore the additional ionomer effect observed during the ORR (current at 0.9 V) was attributed to both the metal cations in the leachate as well as the NH_3^+ from the aromatic organic compound. Due to the strong affinity of Zn^{2+} and NH_3^+ towards the ionomer the ionomer effect was

only partially recoverable. Also this was the only leachate to show partially recoverable ionomer effect due to the combined effects of metal ions and NH_3^+ from the leachate.

Loctite 567 (acrylic)

Three organic compounds were identified in the leachate of loctite 567 by GCMS – Ethanol, 2,2'-[oxybis(2,1-ethanediyloxy)]bis-, Pentaethylene glycol, PEG dimethacrylate. The structures of the functional groups are given in figure 12. All these organics are result of dissociation of Polyethylene Glycols [PEG's] which act as emulsifiers, plasticizers, water soluble lubricants, solvents, and dispensing agents. All these three organic contain essentially same functional groups and they affect the Pt same way.

The ICP results showed total ICP of 74 ppm mostly from S and Si, with low metal ions (Na, Zn^{2+}, K^+ etc) present. The ICP-MS data showed lowionomer contamination as supported by the ORR current data. The structures of the functional groups are given in figure 4.12. The COO^- and OH^- groups from the aliphatic organic compounds adsorbed on the Pt sites to decrease the ECA. In addition to the organic groups, S (elemental or in the form of $-SO_2$ or $–SO_3$) also adsorbed on Pt, which was also seen in the other loctite (39916) adhesive.

Bond It b45 (epoxy)

Three organic compounds were identified in the leachate of bond it b45 white by GCMS - Benzyl Alcohol, [p or m]-tert-butyl- Phenol, Benzaldehyde. The aromatic benzene ring as well as –OH group of benzyl alcohol contributed to the ECA loss due to adsorption. The structures of the functional groups are given in figure 4.13.

The ICP results showed very low metal ions concentration. The total ICP (71 ppm) was due to the presence of Si, which do not absorb or ion-exchange with the ionomer. The ICP-MS data showed lowionomer contamination as supported by the ionomer effect extracted from the ORR data.

4.3.5. Contamination effect on oxygen reduction reaction (ORR) activities of Pt/C

A set of control experiments were performed without adding any contaminants to observe any loss in electrochemical surface area due to the running cyclic voltammograms on the Pt/C electrode.

The effect of contamination on ORR of Pt/C is presented in table 4.3 to 4.8. Table 4.9 draws conclusions based on the ECA and ionomer contamination. Krytox (lubricant) did not show any effect on the ORR currents or ECS loss. Rest of the assembly tested (adhesives and sealants) showed ECA and/or ionomer contaminations and each of those contaminations was either entirely recoverable or partially recoverable (table 4.9)

4.3.6. Tafel slopes

The Tafel slopes were calculated at high potential for the purpose of comparison between initial clean and contaminated electrolyte. The electrode potential plays an important role in changing the Pt surface structure in the presence of O_2, due to the mixed potential. At higher potentials (> 0.8 V), the electrode surface is a mixture of Pt and PtO, while at lower potentials, the Pt surface is pure Pt. Thus, the kinetics of O2 reduction on Pt is not expected to be the same in different potential ranges. Figures 4.14-4.17 showed the two Tafel slopes observed for ORR on a Pt electrode surface. At a low current density range (high potential), a Tafel slope of 60 mV/dec was obtained. At a high current

density range (low potential), a value of 120 mV/dec was observed. The difference in Tafel slope indicates that the mechanism on a Pt/PtO surface is different from that on a pure Pt surface. On a Pt/PtO surface, the rate determining step is a pseudo 2-electron procedure, which gives a Tafel slope of 60 mV/decade. However, on a pure Pt surface, the first electron transfer is the rate determining step, resulting in a Tafel slope of 120 mV/decade (84). The tafel slope changes were compared after addition of leachates and the comparison is given in table 4.11.

4.4. Conclusions

This study showed that contaminants leached from adhesives used in PEM fuel cell have detrimental effect of ORR activities and ECA. Table 4.9 summarizes the impact of leachates on ECA and ORR of the Pt/C catalyst as found in ex-situ RDE studies with additional remarks on the recoverability of contaminates ECA or ORR currents.

1. The selection of the materials was based on their adhesive and lubricant properties inside the fuel cell. One material from each group of materials was selected for ORR studies.
2. The ECA drop (100 - % normalized ECA) for the loctite 39916 and bond it b45 was more than the others. This effect can be attributed to the model compounds present in them (p-toluenesesulfonamide, methyl-benzenediamine, benzyl alcohol, p-tert benzyl alcohol). The order of ECA loss is loctite 39916 > bond it b45 > 4000 fast cure white >loctite 567 > 3m silicone 8664 >krytox.
3. Two fold effects observed on electrode – Pt catalyst and ionomer contamination

a. Pt and/ or ionomer contamination may or may not be recoverable
b. Krytox (lubricant, fluro carbon) is clean – no effects on Pt or ionomer
c. 3m silcone 8664 (silicone) showed recoverable Pt and ionomer contamination
d. Loctite 39916 (urethane) showed high contamination; low Pt and complete ionomer recovery
e. 4000 fcw (urethane) showed high contamination; low Pt and partial ionomer recovery
f. Loctite 567 showed moderate contamination; high Pt and complete ionomer recovery
g. Bond It B45 showed high contamination; low Pt and no ionomer contamination
h. Urethane group assembly aids showed higher Pt and ionomer contamination

Presence of different organic functional groups and cationic and anionic species in the leachates alters the performance characteristics of ORR of Pt.

This study will help the manufacturer of the assembly aids to select the solvents and eliminate any potential source of contamination.

Table 4.1. Organic (aromatic and aliphatic) compounds identified using GCMS in the leachates of the assembly aids tested in this paper.

Chemical Description	Name	GCMS: Liquids				TOC (ppm)
Urethane	3M® 4000 fast cure white	A	B	C	D	1280
Silicone	3M® # 8664 black	A	B	C		197
Urethane	Loctite® 39916	E	F	D		266
Acrylic	Loctite® # 567	G	H	I		750
Epoxy	Reltek® Bond-IT B45	C	J	K		1695
PFAE/PTFE	Krytox® XHT-SX	None Detected				10

A = Ethanol, 2-(2-ethoxyethoxy)

B = Ethanol, 2-(2-ethoxyethoxy)-acetate

C = Benzyl Alcohol

D = Methyl-Benzenediamine

E = p-toluenesesulfonamide

F = Butyric acid N'-m-tolyl-hydrazide

G = 2-Propenoic acid

H = 2,2'-[oxybis(2,1-ethanediyloxy)]bis-Ethanol

I = Diethylene glycol dimethacrylate

J = [p or m]-tert-butyl- Phenol

K = Benzaldehyde

Table 4.2. Inorganic constituents identified using ICP-MS in the leachates of the assembly aids tested in this paper

Chemical Description	Name				Total ICP count
Urethane	3M® 4000 fast cure white	Zn	K	Ca	109
Silicone	3M® # 8664 black	K	Na		11
Urethane	Loctite® 39916	S	Ca		98
Acrylic	Loctite® # 567	Na	K	S	74
Epoxy	Reltek® Bond-IT B45	K	Ca	P	2.7
PFAE/PTFE	Krytox® XHT-SX	-			-

Table 4.3. Analysis of current and ECA loss to demonstrate the effect of contamination due to addition of Krytox lubricant.Platinum ECSAs and ORR currents were determined before and after contamination, for thin films of 46 wt.%Pt/VC, 17.4 µgPt cm^{-2}, 0.1M $HClO_4$, 25°C

	i_{lim}	$(i_c/i_p)_{lim}$	$i_{0.9V}$	$(i_c/i_p)_{0.9V}$	*ECA*	*Available ECA %*	*ionomer effect*
	mA/cm^2	*%*	mA/cm^2	*%*	m^2/g_{Pt}	*%*	*%*
Baseline	***6***	***100***	***2.7***	***100***	***67***	***100***	***0***
1.8 µM	***5.8***	***97***	***2.7***	***97***	***65***	***97***	***0***
18 µM	***5.8***	***96***	***2.6***	***95***	***64***	***95***	***0***
180 µM	***5.7***	***95***	***2.54***	***95***	***64***	***95***	***0***

Table 4.4. Analysis of current and ECA loss to demonstrate the effect of contamination due to addition of 3M silicone 8664.Platinum ECSAs and ORR currents were determined before and after contamination, for thin films of 46 wt. % Pt/VC, 17.4 µgPt cm^{-2}, 0.1M $HClO_4$, 25°C

	i_{lim}	$(i_c/i_p)_{lim}$	$i_{0.9V}$	$(i_c/i_p)_{0.9V}$	*ECA*	*Available ECA %*	*ionomer effect*$_{0.9V}$
	mA/cm^2	%	mA/cm^2	%	m^2/g_{Pt}	%	%
Baseline	***6***	***100***	***2.6***	***100***	***66***	***100***	***0***
1.8 µM	***5.5***	***92***	***2.0***	***77***	***48***	***78***	***1***
18 µM	***5.3***	***88***	***1.8***	***69***	***42***	***69***	***0***
180 µM	***4.8***	***80***	***1.7***	***65***	***39***	***65***	***0***
recovery	***5.7***	***95***	***2.4***	***92***	***53***	***94***	***2***

Table 4.5. Analysis of current and ECA loss to demonstrate the effect of contamination due to addition of Loctite 39916.Platinum ECSAs and ORR currents were determined before and after contamination, for thin films of 46 wt.%Pt/VC, 17.4 μgPt cm^{-2}, 0.1M $HClO_4$, 25°C

	i_{lim}	$(i_c/i_p)_{lim}$	$i_{0.9V}$	$(i_c/i_p)_{0.9V}$	ECA	Available ECA %	ionomer effect$_{0.9V}$
	mA/cm^2	%	mA/cm^2	%	m^2/g_{Pt}	%	%
baseline	6	100	3	100	66	100	0
1.8 μM	4.4	73	1.7	57	48	72	15
18 μM	3.9	65	1.4	47	42	64	17
180 μM	3.5	58	0.9	30	39	56	26
recovery	5.0	83	1.9	63	53	63	0

Table 4.6. Analysis of current and ECA loss to demonstrate the effect of contamination due to addition of 4000 fast cure white. Platinum ECSAs and ORR currents determined before and after contamination, for thin films of 46 wt.%Pt/VC, 17.4 μgPt cm^{-2}, 0.1M $HClO_4$, 25°C

	i_{lim}	$(i_c/i_p)_{lim}$	$i_{0.9V}$	$(i_c/i_p)_{0.9V}$	*Available ECA %*	*ionomer effect*$_{0.9V}$
baseline	***6.0***	***100***	***2.8***	***100***	***100***	***0***
1.8 μM	***4.8***	***80***	***2.0***	***73***	***78***	***5***
18 μM	***4.3***	***72***	***1.6***	***57***	***70***	***13***
180 μM	***3.7***	***62***	***1.2***	***42***	***63***	***21***
recovery	***4.4***	***73***	***1.5***	***55***	***69***	***14***

Table 4.7. Analysis of current and ECA loss to demonstrate the effect of contamination due to addition of Loctite 567. Platinum ECSAs and ORR currents determined before and after contamination, for thin films of 46 wt.%Pt/VC, 17.4 μgPt cm^{-2}, 0.1M $HClO_4$, 25°C

	ilim	$(ic/ip)_{lim}$	$i_{0.9V}$	$(ic/ip)_{0.9V}$	***Available ECA %***	$ionomer\ effect_{0.9V}$
Baseline	6	100	2.7	100	100	0
1.8 μM	5.27	88	2.3	85	87	2
18 μM	4.9	82	1.65	61	64	3
180 μM	4.4	73	1.25	46	50	4
recovery	5.57	93	2.1	78	81	3

Table 4.8. Analysis of current and ECA loss to demonstrate the effect of contamination due to addition of Bond it b45. Platinum ECSAs and ORR currents determined before and after contamination, for thin films of 46 wt.%Pt/VC, 17.4 μgPt cm^{-2}, 0.1M $HClO_4$, 25°C

	i_{lim}	$(i_c/i_p)_{lim}$	$i_{0.9V}$	$(i_c/i_p)_{0.9V}$	*Available ECA %*	*ionomer effect*
Baseline	***6***	***100***	***2.8***	***100***	***100***	***0***
1.8 μM	***5.2***	***87***	***2.3***	***80***	***80***	***0***
18 μM	***4.9***	***81***	***1.7***	***61***	***62***	***1***
180 μM	***4.5***	***75***	***1.6***	***57***	***58***	***1***
recovery	***5***	***83***	***1.9***	***68***	***69***	***0***

Table 4.9. Summary and comments on the contamination process by leachates – based on extent of ECA loss during contamination (column 3), recovery of ECA (column 4), ionomer contamination (column 5) and recovery of ionomer contamination (column 6)

Name	*Group*	*ECA (Pt) contamination*	*ECA (Pt) contamination recovery*	*Ionomer contamination*	*Ionomer contamination recovery*	*Remarks*
Krytox	***Fluro carbon***	***very low***	***yes***	***no***	***-***	***clean***
3M silicone 8664	***silicone***	***moderate***	***yes***	***no***	***-***	***dirty but recoverable***
Loctite 39916	***urethane***	***high***	***partial***	***yes***	***yes***	***dirty and not recoverable***
4000 fast cure white	***urethane***	***high***	***partial***	***yes***	***partial***	***dirty and not recoverable***
Loctite 567	***acrylic***	***moderate***	***yes***	***yes***	***yes***	***dirty but recoverable***
Bond it B45	***epoxy***	***high***	***partial***	***no***	***-***	***dirty and not recoverable***

Table 4.10. Analysis of mass activities to demonstrate the effect of contamination due to addition of leachates. Platinum ECSAs and ORR currents determined before and after contamination, for thin films of 46 wt.%Pt/VC, 17.4 μgPt cm^{-2}, 0.1M $HClO_4$, 25°C

4000 fcw	*loctite 567*	*bond it b45*	*3m silicone*	*loctite 39916*	*krytox*
100	***100***	***100***	***100***	***100***	***100***
65	***83***	***75***	***71***	***46***	***99***
49	***51***	***50***	***69***	***36***	***98***
34	***36***	***47***	***70***	***20***	***93***
43	***69***	***55***	***91***	***51***	***-***

Table 4.11. Tafel slope (in mV/decade) measured from iR-free polarization curve at 23°C in 0.1 M perchloric acid at a scan rate of 20mV/s (range of polarization being -0.01 to 1.0V) with two parts. In the higher over potentials (typically above 0.8) it is around -65 to -75 mV/decade, but in the lower over potential region it is around -118 to -130 mV/decade for carbon supported Pt

	baseline	1.8μM	18 μM	180 μM	recovery
3Msilicone 8664	67	63	68	70	65
Loctite 39916	69	72	77	80	75
400 fast cure white	70	74	76	81	80
Loctite 567	70	72	78	82	75
Bond It b45	68	71	73	74	74

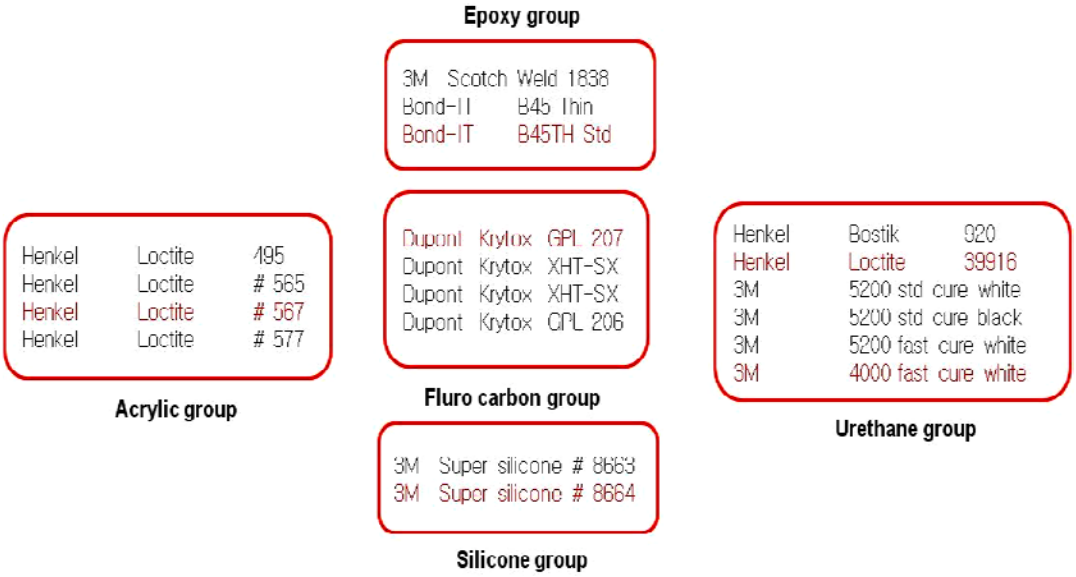

Figure 4.1. Assembly aids selected for screening based on the contamination and recovery characteristics. The assembly aids have different groups and the assembly aids highlighted may are presented in this paper.

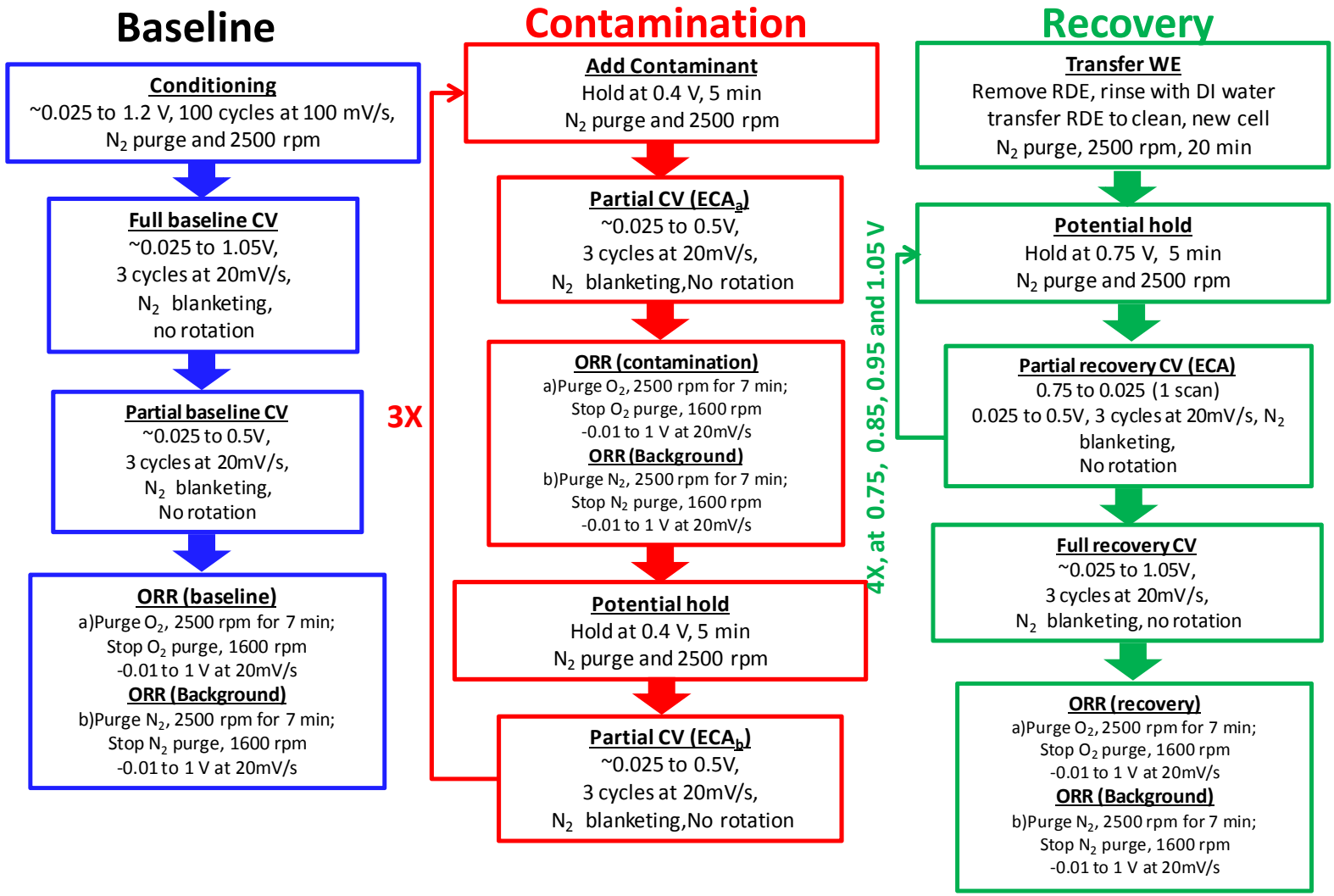

Figure 4.2. Schematic of contamination experiments consisting ECA and ORR measurement procedures

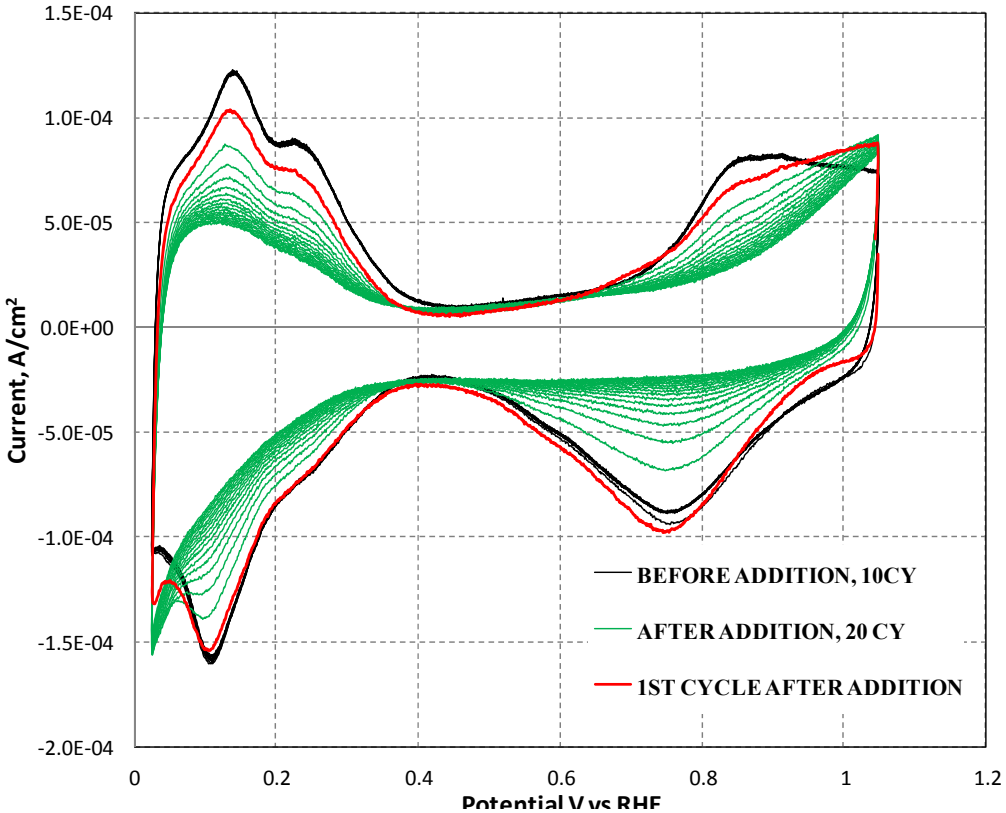

Figure 4.3. Votammograms showing effect of adding 1.2 ml of Loctite® 39916 on Pt/C (Vulcan) at room temperature in 0.1 M $HClO_4$, scanned from 0.025 to 1.05 V

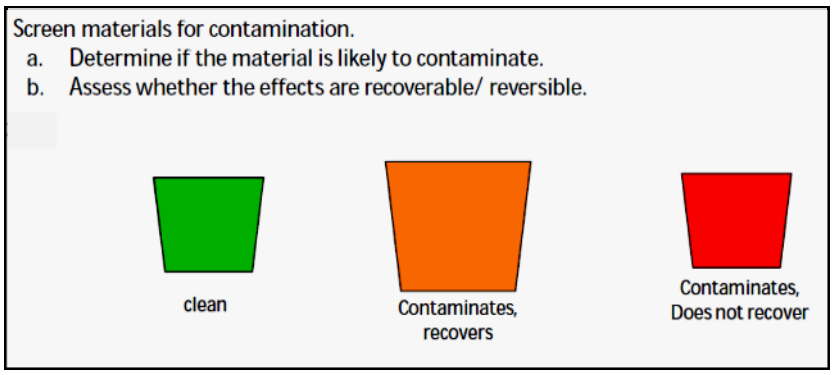

Figure 4.4. Contamination criteria: After selecting potential materials they were injected in the RDE electrolyte to observe the impact on the electrochemical surface area – which determined the characteristic of the leachate

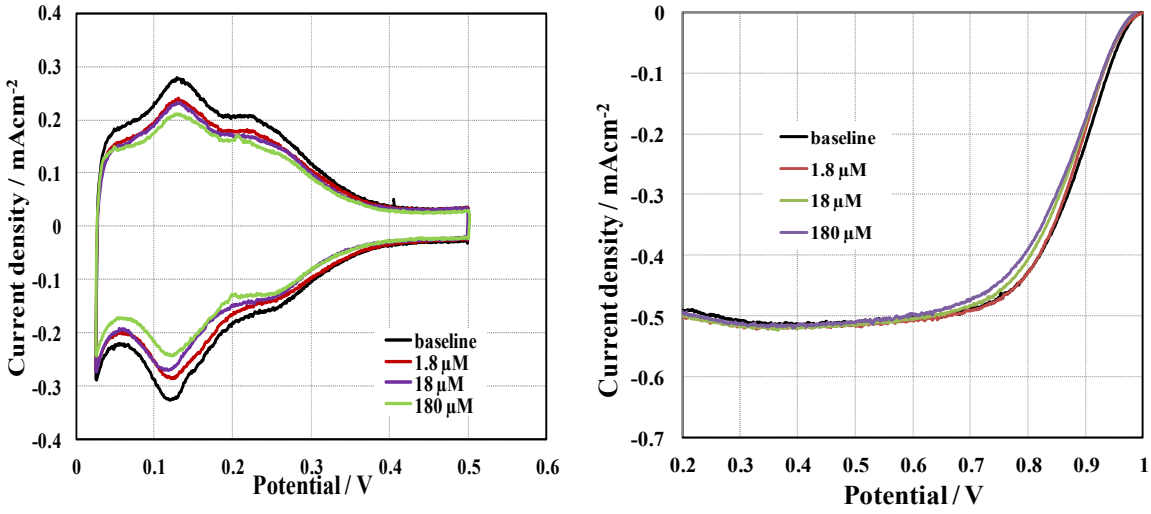

Figure 4.5. The CV and ORR curves before (baseline) and after adding Krytox leachate (1.8 µM, 18 µM, 180 µM). Change in surface coverage by contaminants (loss of ECA due to adsorption of contaminant molecules on Pt sites) with CV cycles from 0.025 to 0.5 V at a scan rate of 20mV/s as measured under the H_{upd}.

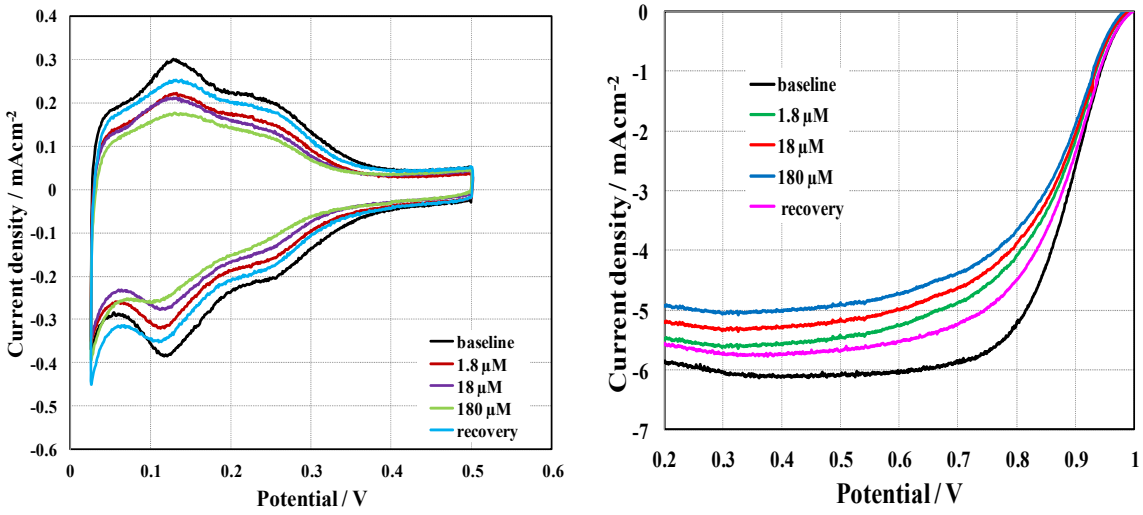

Figure 4.6. The CV and ORR curves before (baseline) and after adding 3M silicone 8664 leachate (1.8 µM, 18 µM, 180 µM). Change in surface coverage by contaminants (loss of ECA due to adsorption of contaminant molecules on Pt sites) with CV cycles from 0.025 to 0.5 V at a scan rate of 20 mV/s as measured under the H_{upd}.

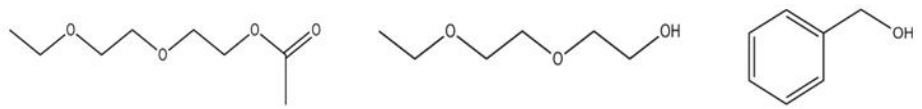

Diethylene glycol monoethyl ether acecate

Di (ethylene glycol) ethyl ether

Benzyl alcohol

Figure 4.7. Organic functional groups found in leachate of 3M Silicone 8664 using GCMS (83)

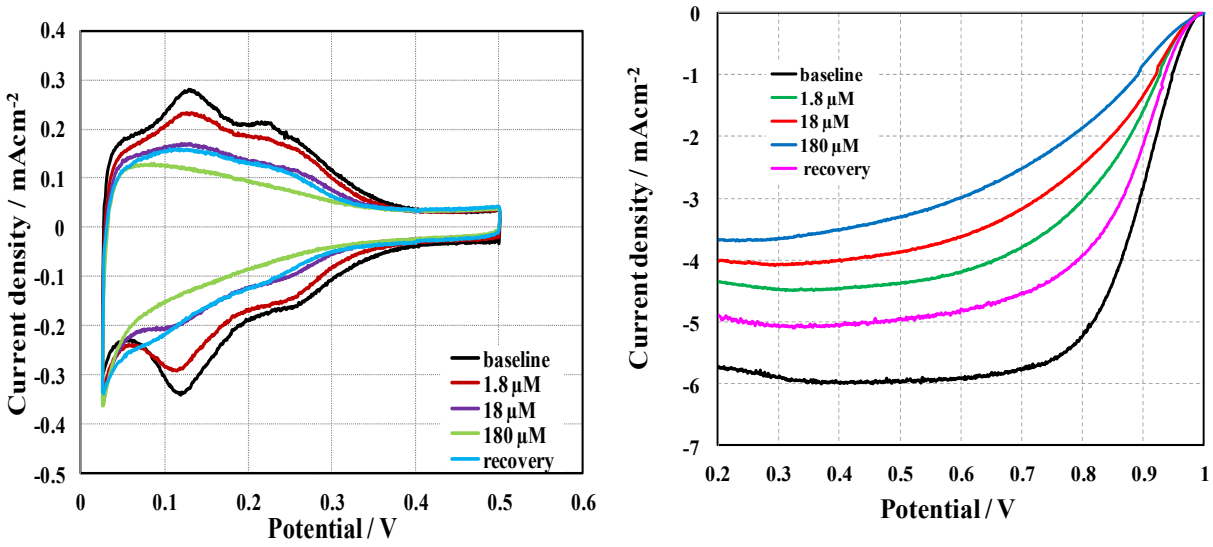

Figure 4.8. The CV and ORR curves before (baseline) and after adding Loctite leachate (1.8 µM, 18 µM, 180 µM).Change in surface coverage by contaminants (loss of ECA due to adsorption of contaminant molecules on Pt sites) with CV cycles from 0.025 to 0.5 V at a scan rate of 20 mV/s as measured under the H_{upd}.

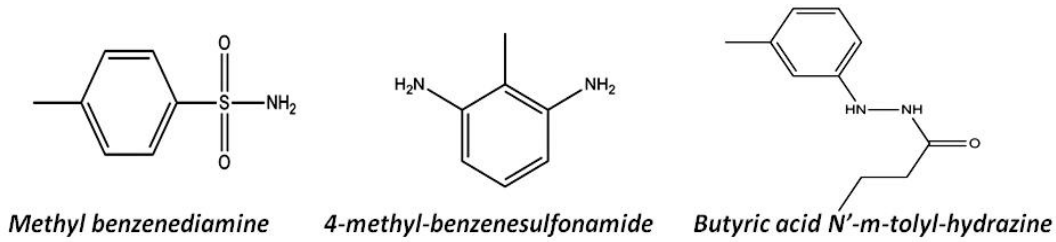

Figure 4.9. Organic functional groups found in leachate of Loctite 39916 using GCMS (83)

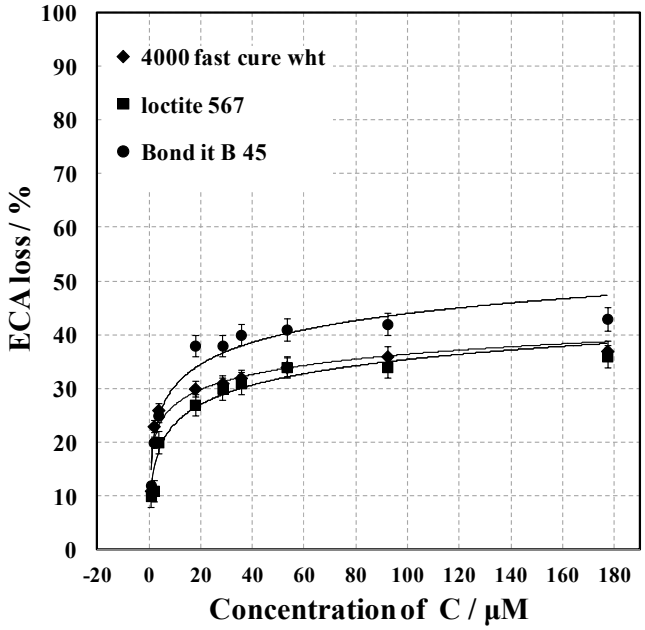

Figure 4.10. Changes in available ECA due to effect of contamination from the assembly aids

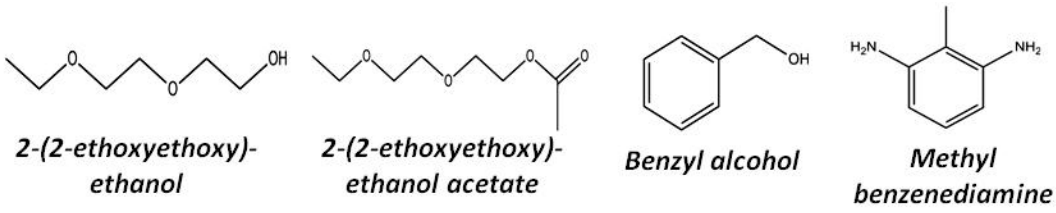

Figure 4.11. Organic functional groups found in leachate of 4000 fast cure white using GCMS (83)

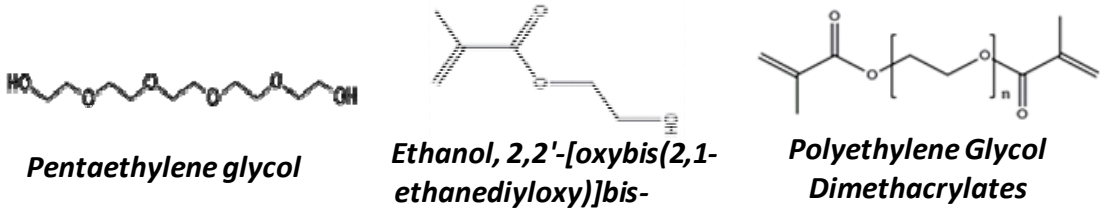

Pentaethylene glycol

Ethanol, 2,2'-[oxybis(2,1-ethanediyloxy)]bis-

Polyethylene Glycol Dimethacrylates

Figure 4.12. Organic functional groups found in the one week soak leachate of Loctite 567 using GCMS (83)

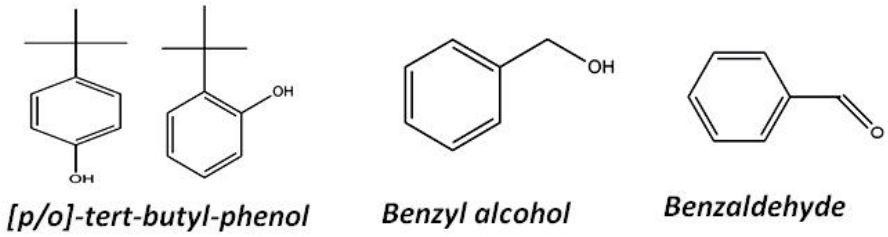

Figure 4.13. Organic functional groups found in the one week soak leachate of Bond it b45 using GCMS (83)

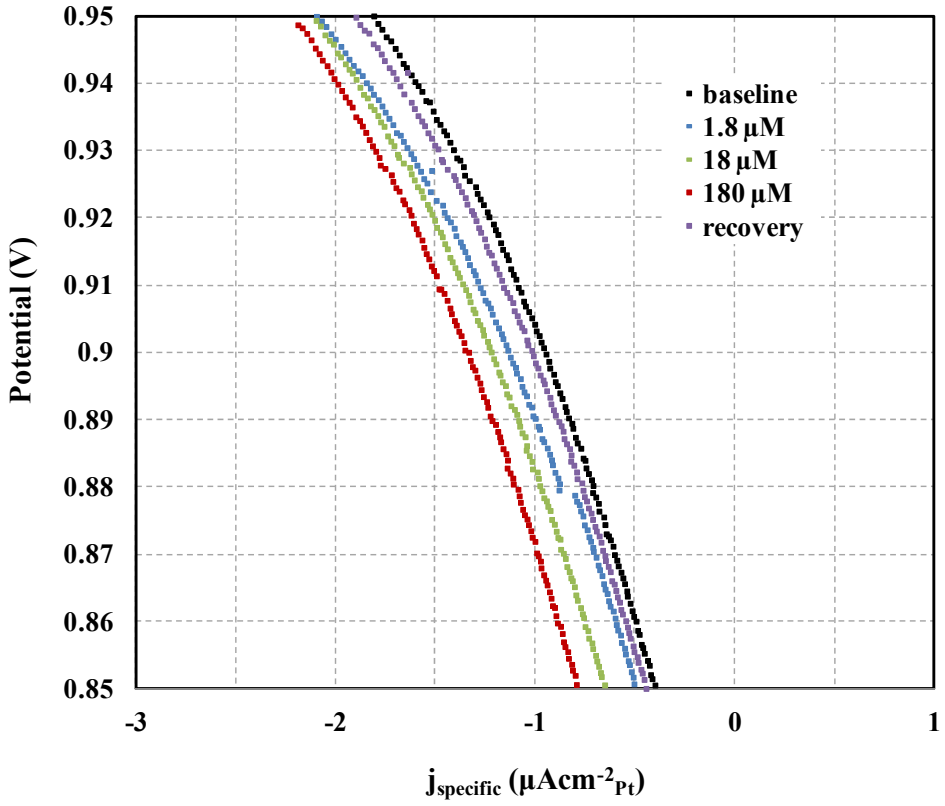

Figure 4.14. Tafel plots of the log of kinetic currents, for O_2 reduction during potentiodynamic scans in on Pt/C after adding 3M Silicone 8664. The oxidation rate was measured in a flow cell (scan rate 20 mVs^{-1}, electrolyte as indicated in the figure). The measurements were initiated at -0.1 V and ended at 1.0 V. Tafel slopes corresponding to −60 and −120 $mVdec^{-1}$ are shown as solid lines for comparison.

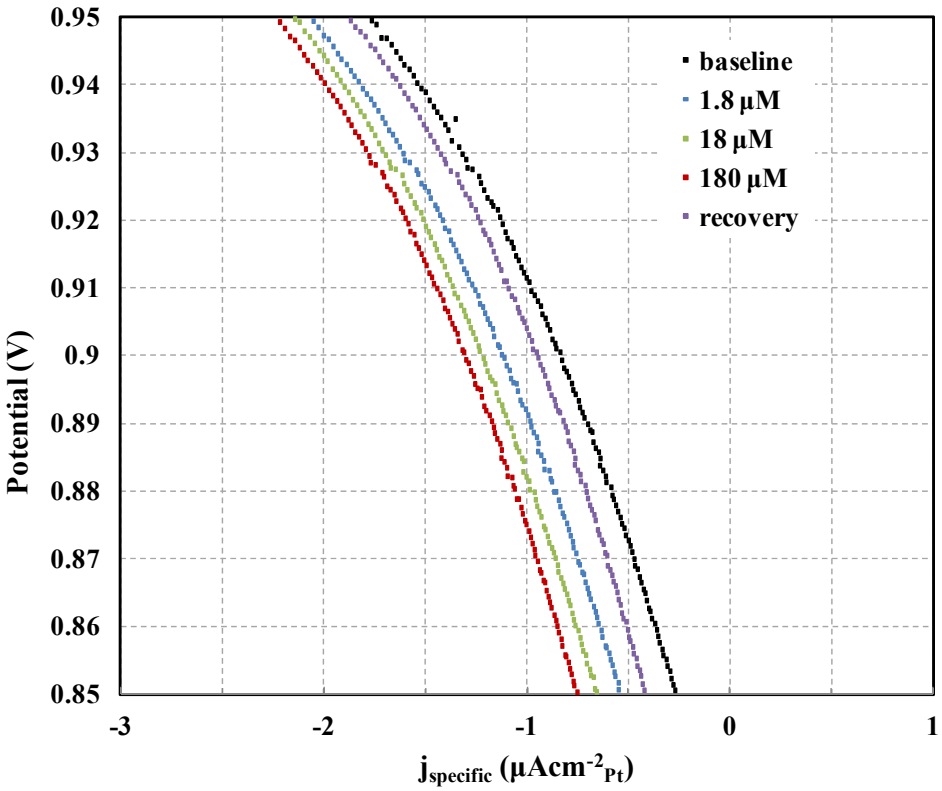

Figure 4.15. Tafel plots of the log of kinetic currents, for O_2 reduction during potentiodynamic scans in on Pt/C after adding Loctite 39916. The oxidation rate was measured in a flow cell (scan rate 20 mVs^{-1}, electrolyte as indicated in the figure). The measurements were initiated at -0.1 V and ended at 1.0 V. Tafel slopes corresponding to −60 and −120 $mVdec^{-1}$ are shown as solid lines for comparison.

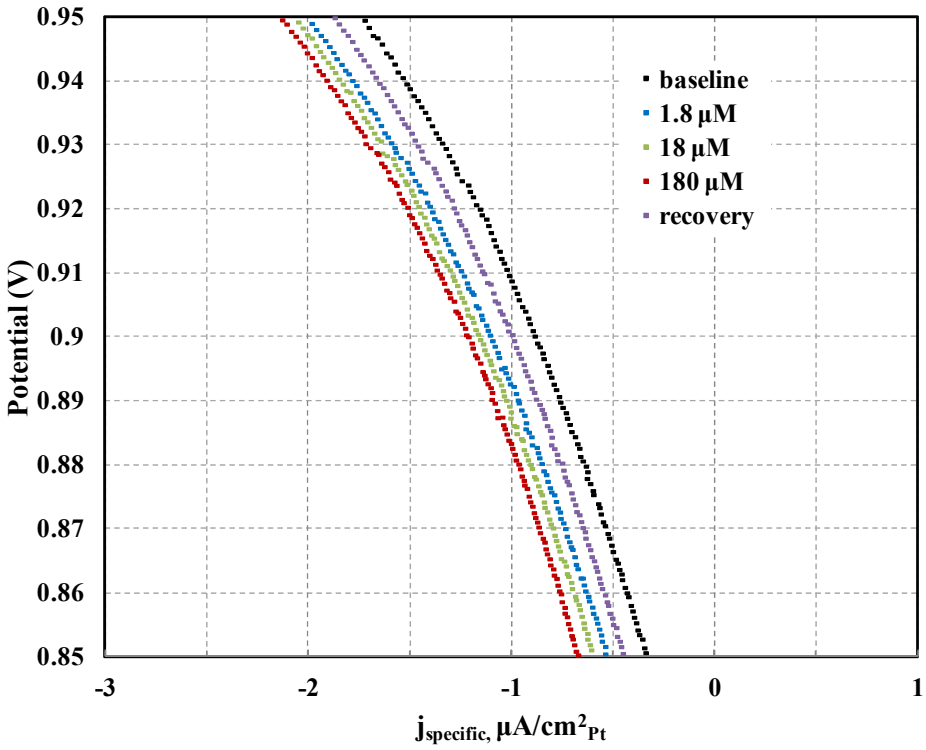

Figure 4.16. Tafel plots of the log of kinetic currents, for O_2 reduction during potentiodynamic scans in on Pt/C after adding 4000 fast cure white. The oxidation rate was measured in a flow cell (scan rate 20 mVs^{-1}, electrolyte as indicated in the figure). The measurements were initiated at -0.1 V and ended at 1.0 V. Tafel slopes corresponding to −60 and −120 $mVdec^{-1}$ are shown as solid lines for comparison.

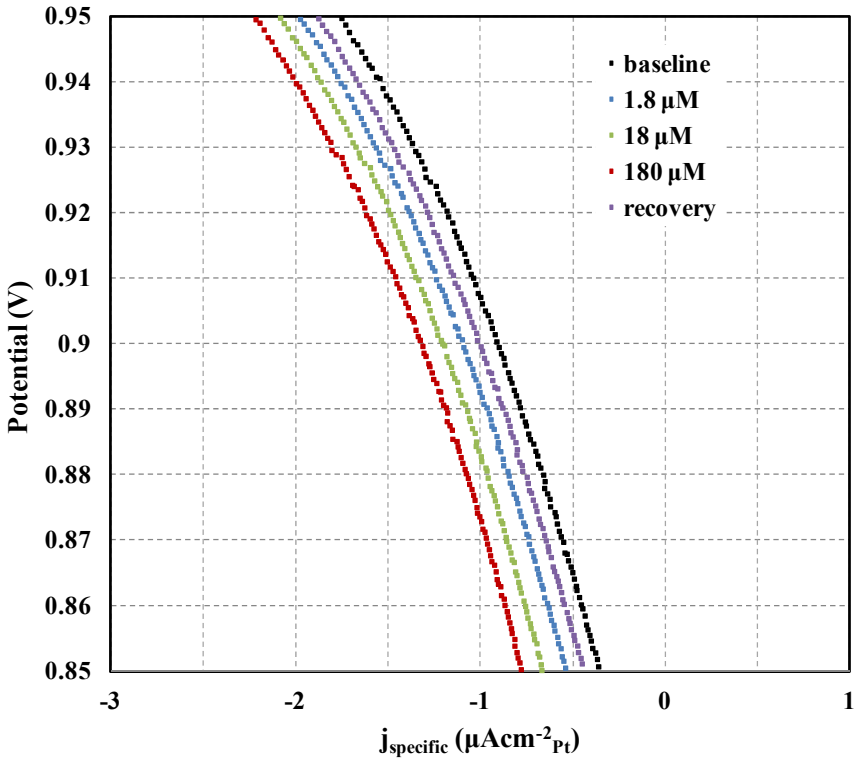

Figure 4.17. Tafel plots of the log of kinetic currents, for O_2 reduction during potentiodynamic scans in on Pt/C after adding Loctite 567. The oxidation rate was measured in a flow cell (scan rate 20 mVs^{-1}, electrolyte as indicated in the figure). The measurements were initiated at -0.1 V and ended at 1.0 V. Tafel slopes corresponding to −60 and −120 $mVdec^{-1}$ are shown as solid lines for comparison.

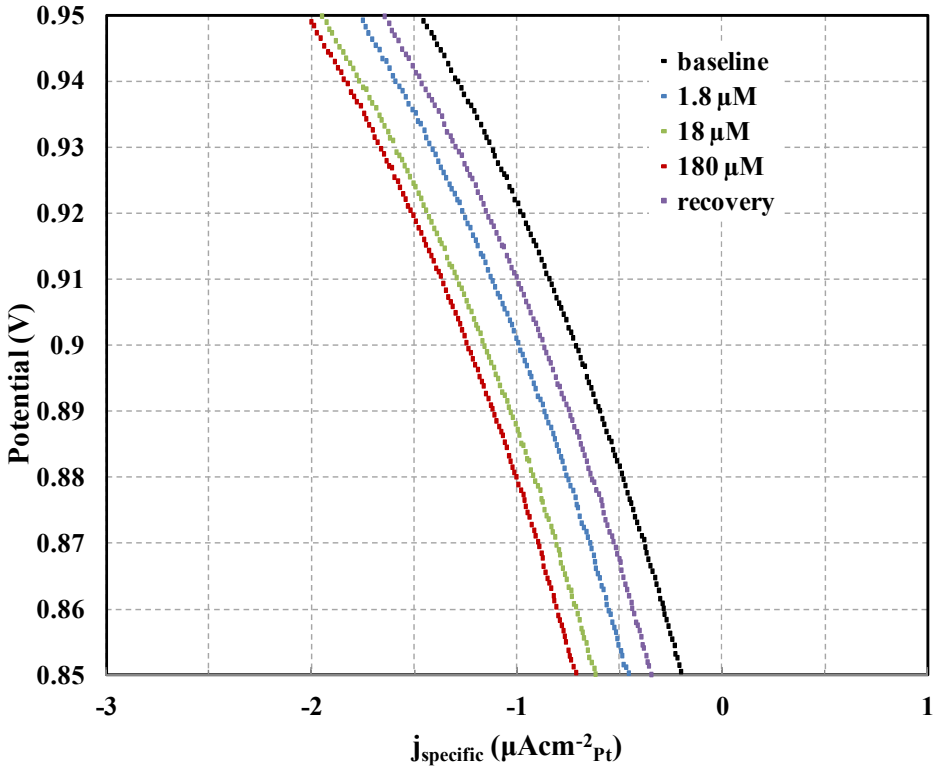

Figure 4.18. Tafel plots of the log of kinetic currents, for O_2 reduction during potentiodynamic scans in on Pt/C after adding Bond it b45. The oxidation rate was measured in a flow cell (scan rate 20 mVs^{-1}, electrolyte as indicated in the figure). The measurements were initiated at -0.1 V and ended at 1.0 V. Tafel slopes corresponding to −60 and −120 $mVdec^{-1}$ are shown as solid lines for comparison.

Chapter 5. Effect of a leachate and its constituents on Pt catalyst

In this chapter cyclic and linear sweep voltammetry methods were employed to show contamination effects on Pt by leachate from a urethane type adhesive that may be used in the assembly in PEMFC systems, using thin film rotating disk electrode (TF-RDE) method. TF-RDE method was employed to compare the extent of contamination with three low concentrations of the leachate and the organic constituents and rotating ring disk electrode (RRDE) method was used to quantify and compare the oxygen reduction reaction (ORR) losses due to the organic (p-toluenesulfonamide) and inorganic (chloride ion) constituents detected in the leachate independently and collectively. The first part of the study with low concentrations of leachate and organic compounds, quantified the ECA and ORR losses of Pt with partial recovery and in the second part of the study, effects of inorganic and organic constituents were investigated in the original high concentrations as detected in the leachate. For example, with carbon concentrations as low as 180 μM (0.02 mM of p-toluenesulfonamide), the ECA loss observed in case of leachate and p-toluenesulfonamide were 52% and 58% respectively. But at 1.3 mM concentration (equivalent to the original concentration of C detected in the leachate) of p-toluenesulfonamide, the ECA loss increased to 64%. Peroxide formation was observed during the experiments with higher concentrations of the constituents (p-toluenesulfonamide, chloride ion) indicating an interacting contamination effect on ORR.

The additional information on the methodology and background studies can be found in appendices E, F and H.

5.1. Introduction

Polymer electrolyte membrane fuel cell (PEMFC) has received attention from the vehicle manufacturing industry to reduce carbon emissions by generating electricity from electrochemical reaction between hydrogen and oxygen instead of burning fossil fuels. Commercialization and sustainability of such a power source is currently limited as the electrocatalysts used for the hydrogen and oxygen reaction in PEMFCs are susceptible to poisoning by various contaminants (15, 40, 41, 80) (air borne and liquid phase) resulting in higher cost and declining performance. When the contaminants reach the catalyst layer, they readily adsorb on the Pt sites preventing the oxygen reduction reaction (ORR) (O_2+ $4H^+$+ $4e^-$ → $2H_2O$). The ORR reaction is usually one of the most inhibiting processes for developing high performance electrocatalyst for fuel cell vehicles (85). For the development of PEMFC electrodes which are less susceptible to contamination, understanding the process of adsorption of the contamination at the catalyst surface is necessary. The contamination of Pt electrode is a complex process since the contaminants can modify the intrinsic catalyst properties. The common and established sources of contamination are air (cathode) and fuel (anode) until much recently when components of fuel cell (e.g. structural plastics, assembly aids, coolants, membranes and gaskets) were also identified as the potential contamination sources. To reduce the fabrication cost of a PEMFC stack and assembly, off-the-shelf adhesives and sealants (assembly aids) and structural plastics which are not specifically designed to be used in the hot and humid condition of a PEMFC are currently being considered by the PEMFC manufacturers (1,

31). While there are many existing studies on air contaminations (15, 24, 43, 86) very little literature exists that quantifies and explains the contamination at the surface of the Pt catalyst originating from the organic compounds that may leach from those assembly aids.

The performance of a fuel cell has been found to degrade over time in the presence of not only air contaminations but also system derived contamination in a PEMFC (11). For example, recent studies on the additives of the glycol based coolants have shown detrimental effects on Pt on Vulcan carbon catalyst. These contaminants originate from ethoxylated nonylphenol surfactant, and azole- and polyol-based corrosion inhibitors which are frequently added to the commercially available BioGlycol coolants to enhance specific functionalities. K.E. Swider Lyons et al has conducted a study with three above mentioned additives and glycol mixtures and have observed that the lost ECA could be fully recovered in clean electrolyte for the mixture with the surfactant pure glycol-water, glycol-water-surfactant mixtures and glycol mixture containing the polyol corrosion inhibitor, while coolant mixtures with the azole corrosion inhibitor caused irreversible losses to the ECA and oxygen reduction reaction (ORR) activity. The ECA and ORR activity could be recovered to 70% of its initial values after voltammetric cycling to 1.50 V in case of azole poisoning (30).

As a part of managing water content during polyurethane synthesis (attains the desired properties in urethane sealants) p-toluenesulfonyl isocyanate [PTSI] is frequently used as an additive for water scavenging. The cyanate groups of PTSI hydrolyzed to form CO_2 and p-toluenesulfonamide PTS, the species that was identified in the one week soak leachate from Bostik 920 (83). This study focuses on connecting and comparing the

effect of leachate (Bostik® 920) to the organic and inorganic constituent (p-toluenesulfonamide or 4 methyl benzyl sulfonamide and chloride ion). Bostik® 920 is a Urethane assembly aid that is being considered to be used in PEMFC in place of metal components for cost reduction purposes. Bostik® 920 was spread very thin on 2"x4" (5.1 cm x 10.1 cm rectangular pieces) Teflon sheet and dried for 24 hours. Then it was soaked in DI water at 90°C for 1 week, so that the surface are of the adhesive to the volume of water ratio was 1.5cm^{-1} (i.e., 150 mm^2/ml of DI water). The Teflon sheets coated with the sample were removed from the bottles at the end of the soak and the leached solution was subjected to TOC, GCMS, IC and ICP-OES measurements which would be needed during the ex-situ experiments. In the laboratory, p-toluenesulfonamide (4MBSA) was detected as the major organic compound using GCMS and chloride ion as the major anionic constituent when Bostik® was soaked at 90°C. The TOC of the leachate was 110 ppm and the chloride ion concentration was 22 μM.

The first part of the study compares the effect of the leachate from the adhesive with the identified model compound in the 1 week soak of the leachate after adding three low concentrations of both using TF-RDE method. Under the operating conditions of a PEMFC (80°C and humidity) the assembly aids may leach organic and inorganic compounds or ions which may mix into the fluid stream and enter the fuel cell and poison the catalyst and ionomers. Both Bostik® and p-toluenesulfonamide adsorbed on Pt catalyst, leading to reduced electrochemical surface area (ECA) and an inhibited ORR on the catalyst.

The paper also compares the effects of ions and organics separately and collectively in the second part using thin film RRDE studies after adding 110 ppm

equivalent of 4MBSA and 22 μM of Cl^- ions and a mixture of 110 ppm equivalent of 4MBSA and 22 μM of Cl^- ions in three different sets of experiments. The purpose of this study is to provide quantitative evidence of the poisoning characteristics of different types of contaminants originating from the assembly aids so that they can be investigated before using them in a PEMFC. These details will also assist the manufacturer to provide a guideline to limit the concentration of the materials to be used in a PEMFC based on the surface area to volume ratio of exposure in PEMFC restricting the contamination.

Liquid phase contaminants may adsorb on Pt on both the cathode (where ORR takes place) and the anode (where hydrogen reduction reaction or HOR takes place) in a PEMFC much like air contaminations (SO_2, NH_3, CO, CO_2, H_2S etc.) (15, 23, 24, 40, 44, 56). Since the contamination effect on the HOR is less pronounced compared to the ORR, it requires detailed investigation because its slower kinetics combined with the effects of contaminants can result in high over potential and loss in fuel cell performance (44, 58). So it will be useful to develop protocols (59) for systematic understanding of the contamination process from the liquid phase contamination such as chemicals leached out from the stack, on Pt/C using ex-situ methods like rotating disk electrode to develop commercially viable catalyst with high ORR activities with specific application in PEMFC.

Thin-film rotating disk electrode (TF-RDE) method is employed in this study to understand the change in of oxygen reduction reaction (ORR) and electrochemical surface area (ECA) after injecting contaminants leached out from commercially available assembly aids which are considered for being used in a PEMFC. These assembly aids have a wide range of properties and functionality and are not manufactured specifically

for the hot and humid operations in a fuel cell. TF-RDE method was chosen for easy isolation of ORR activities of the catalyst in the presence of contaminants, which was not possible in-situ (in a PEMFC).

5.2. Experimental

5.2.1. Determining time required for the organic contaminant molecule to reach Pt sites

The leachate and its major organic constituent 4MBSA were injected in the electrolyte at 1.05 V during a fast scanning ($100mVs^{-1}$) cyclic voltammetry experiment. The purpose of this experiment was to determine the amount of time that the contamination molecules need to reach equilibrium with Pt sites. This experiment was done before doing any ORR experiments. The detailed experimental procedure is given in ref. (59, 70).

5.2.2. Rotating disk experiments to measure ECA and ORR activity of Pt/C

The details of experimental procedure including electrode preparation and conditioning were reported in (59, 70). Additionally, the schematic of the ORR is presented in figure 5.1. Figure 5.1 shows the three essential part of the experimental procedure – baseline, contamination and recovery. The contamination part was repeated three times for three different concentrations of the leachate and 4MBSA. Since kinetics data was extracted from the ORR polarization curves, the background of ORR was recorded in N_2 gas saturated electrolyte.

The off-the-shelf adhesive Bostik ® 920 (Henkel) is analyzed by GCMS and the most prevalent model compound was identified to be p-toluenesulfonamide. Bostik ®

920 was aged at 90°C (close to fuel cell operating temperature) in DI water for one week inside an air tight PTFE bottles. The aging process at high temperature facilitates the organic compositions of the adhesive to leach out in the water. The water was decanted and analyzed for total organic carbon (Thermo Scientific), solution conductivity (Thermo Scientific) and pH. It was also subjected to GCMS, IC (Dionex ICS-90 Ion Chromatography System) and ICP-OES (Perkin Elmer Optima 5300 DV) to qualitatively detect the organic and inorganic compositions present in it. In GCMS the most detectable peak was due to p-toluenesulfonamide. 220 ppm solution of 99.9% pure (Sigma Aldrich) p-toluenesulfonamide or 4-methylbenzene sulfonamide was prepared with DI water and was used for the RDE experiments.

The total organic carbon (TOC) of the leachate from a 1 week soak was 110 ppm and Cl^- concentration was 22 μM detected by ICP-OES. Note that, Cl^- was the only anion identified in the leachate. To study the effect of concentrations we used dilutes of this leachate corresponding to 0.02, 0.2 and 2 ppm which corresponds to 1.8, 18 and 180 μM of carbon inside the electrolyte. Those three concentrations were chosen for 4MBSA in terms of C atoms concentration which translates to 1.8, 18 and 180 μM. Alternately, these concentrations were 0.26, 2.6 and 26 μM of 4MBSA in 145 ml of electrolyte (i.e. from a stock solution of 3300 ppm of 4MBSA and assuming 7 carbon/4MBSA). Similarly, in those three concentrations of leachate the Cl^- concentration was 0.004, 0.04 and 0.4 μM respectively.

This organic compound (p-toluenesulfonamide) and Cl^- anions are investigated for their individual and combined effects with a concentration of 1.3 mM and 22 μM respectively in the second part of the paper. The p-toluenesulfonamide was purchased

from Sigma Aldrich (99% purity) and the Cl^- was injected in the form of HCl acid from Sigma Aldrich.

5.2.3. RRDE experiments with constituent organic compound and anion (original higher concentration)

For the RRDE experiments, thin electrodes were prepared on the glassy carbon disk (5 mm dia) as described in ref. (59, 70). A reference hydrogen electrode, a Pt gauge spot welded on a Pt wire counter electrode in 145 ml electrolyte were used with a Pine instruments bi-potentiostat. First RRDE experiments were performed in uncontaminated electrolyte to obtain baseline value of ECA and the ORR. Then the same were performed on contaminated electrodes (contaminated with Bostik® 920 and p-toluenesulfonamide) at room temperature and fraction of peroxide was calculated using equation 1.

$$X_{H2O2} = \frac{2I_R/N}{I_D + I_R/N} \quad [1]$$

Where, I_R is the ring current and I_D is the disk current and N is the collection efficiency. The experimental conditions were same as RDE experiments. Please see figure 5.1 for detailed steps of ORR experiments.

5.3. Result and discussion

5.3.1. Study and compare the effects of the leachate and the organic constituent found in the leachate

5.3.1.1 Determining time required for the organic contaminant molecule to reach Pt sites

The experiments were performed with controlled final concentration of carbon (180 μM) inside RDE cell (inside 145 ml electrolyte). Figure 5.2 shows that the effect of contamination was observed immediately after adding the leachate at 1.05 V. As the CV proceeds cathodically, a noticeable decrease in the Pt-O reduction region can be observed. The first cycle (in red) shows decrease in H_{upd} region ($H^+ + e^- \leftrightarrow H_{upd}$) and in the case of Bostik® 920 (figure 5.2) – the shape of the CV changes around 0.5 V in the H_{upd} region highlighted in the rectangle. In the case of p-toluenesulfonmide (figure 5.2), however, this feature is absent. This is due to the different nature of adsorption interaction between the adsorbed species and Pt (87) in presence of two different contaminants. The leachate from Bostik® 920 has some inorganic contaminations.

In the first cycle, the area under the Pt-O reduction region is not affected much during the cathodic sweep. However, the area under Pt oxidation region decreases as lot during the anodic sweep. From 2nd cycle onwards the area under the Pt-O reduction loss is much steeper. Figure 5.3 shows the comparison of the loss in ECA (%) obtained from integrating the H_{upd} (empty symbols-H_{upd}) and oxide (solid symbols-oxide) region as a function of cycles. The solution was injected at 1.05 V after first 10 cycles and was scanned cathodically. The effect is seen immediately in the first cycle (red line) for both

cases. It took ca. 8 cycles for the CV to come to a steady state. Therefore it took 20.5*8= 200s or over 4.1 minutes for the molecules to reach catalyst surface and adsorb on (block) the Pt sites. However, it takes a couple of seconds (ca.2.5 s) for the contaminant molecules to be transported from the bulk to the surface, which is around 0.8 V in the cathodic sweep. This can be supported by the fact that ECA-H_{upd} is lower than ECA-oxide (% loss of pt sites = 100 –NECA), i.e. the loss calculated from H_{upd} region is greater than that of oxide region during the first cycle. In consecutive cycles, the loss in ECA-H_{upd} curve is much steeper than ECA-oxide. The Pt-oxide region current is due to the oxidation of Pt by OH from H_2O molecules ($Pt + OH^- \rightarrow Pt\text{-}OH + e^-$, followed by $Pt\text{-}OH + OH\text{-} \rightarrow Pt\text{-}O + H_2O + e^-$). During the 2nd cycle, the contaminant molecules have enough time to adsorb on the electrode and thereby hindering the chemisorptions of OH_{ads} on Pt at 0.55 V (anodic sweep). This decreases the amount of Pt-O formed during the anodic sweep, which in turn decreases the reduction of Pt-O. Since the H^+ is much smaller in size than OH, adsorption of proton on the Pt sites was more favored than that of OH on Pt sites in presence of contaminant molecules. Therefore, the % ECA loss in H_{upd} was less than ECA-oxide region.

The height of Pt-O reduction peak is independent of the contamination concentration, it only depends on the condition under which the scan in the oxide region was performed (88). In this study, the contamination was added after formation of oxide peak during the first cycle, so the reduction peak was very prominent and unaffected by contamination, during the cathodic cycling of the first cycle. But in later cycles, it decreased since the oxide peak couldn't form in the presence of contamination.

5.3.1.2 Effect of contaminants on electrochemical Surface area determined by CVs

The CV was measured after injecting the leachate and the model compound in two different set of experiments while the electrode was held at 0.4 V (vs. RHE) to avoid any potential oxidation of the contaminants. The CVs were performed at room temperature. The CVs before (baseline) and after adding contaminants (at the end of the experiments) are shown in figure 4. After the contaminations were added, the H_{upd} region decreased as shown with the upward arrows. Figure 5.4 shows that organic compound p-toluenesulfonamide (b) had more severe effects on H_{upd} region than the leachate (a).

5.3.1.3 Contamination effect on oxygen reduction reaction (ORR) activities of Pt/C

Table 1 shows the OOR mass activities for the Bostik and 4MBSA. The experiment was repeated twice with 5 mm and 6 mm diameter electrodes (0.196 and 0.283 cm^2 electrode area respectively). The continuous line represents experiment done using 0.196 cm^2 electrodes and the dotted line represents experiment done using 0.247 cm^2 electrode. The data fell within 5% of variance.

The normalized values of specific activities without any contamination in 0.1 M perchloric acid in three consecutive steps simulating the process of injecting three dosages of contaminants. In each step the Pt/C was pre-reduced at 0.4 V for 420s.

The effect of contamination on ORR activities of Pt/C is presented in columns 3-6. The loss in ECA and ORR activities observed during the control experiments are given in table 2. This loss of activities can be due to the adsorbing species from the electrolyte.

The normalized activity follows the same trend as available ECA. The normalized ECA (ECA at any point of time during the experiment divided loss in mass activity for

the control experiment (without leachate)) is around 4%, 6% and 12% for three steps (1.8, 18, 180 μMs of C). Both Bostik and the 4MBSA showed decreased mass activities.

Figure 5.5 and 5.6 present the family of polarization curves obtained during the contamination experiments with Bostik® and 4MBSA as a function of concentrations of the contaminants. The black line is the initial ORR performed on clean Pt/VC in O_2 saturated electrolyte. The initial ORR (black line) starts at 0.97 V and the ORR proceeds entirely through $4e^-$ pathway (89). The region between 0.98 and 0.5 V is kinetic diffusion controlled while between 0.45 and 0.3 is diffusion controlled with a limiting current of -6 $mAcm^{-2}$. When the three different concentrations of the contaminants were injected in three steps (1.8 μM, 18 μM and 180 μM) to the electrolyte, the diffusion limiting current started getting smaller corresponding to $3.2e^-$ and $3e^-$ transfer processes for Bostik and 4MBSA respectively. But in a 0.1 M $HClO_4$ electrolyte, the amount of peroxide formation is as low as 22% for an ORR involving 2.7 to 3.9 e^- transfer (90). So, the contamination process did not entirely proceed through $2e^-$ pathway but there might be around 10 to 20% peroxide below 0.3 V. Therefore, no significant peroxide formation was observed at the ring electrodes during the contamination experiments (not shown in the figures 5.5 and 5.6).

Figure 5.5 shows gradual loss in ORR current due to addition of Bostik® at 0.9 V but figure 5.6 shows at higher concentration of 4MBSA, the polarization curve lost the flat region in the diffusion limited potential region, indicating depletion of oxygen layer on the Pt sites in presence of adsorbed contaminants. Still, the current was not low enough for the ORR to completely proceed through the $2e^-$ pathway to form peroxides.

Since determining the coverage of contamination by ex-situ analyses does not provide decisive information on the extent of catalyst poisoning mass activity remains the more important parameter to compare between contaminant exposed Pt catalysts (91). Mass activities after contamination with the leachate of Bostik® decreased to 87%, 60%, 28% respectively (ORR in figure 5, the polarization curves for 1.8, 18 and 180 μM of C in the leachate). Similarly, after the Pt sites were contaminated with 4MBSA mass activities decreased to 85%, 46%, 23% from 100%.

5.3.1.4 Comparison of Tafel Slopes

The Tafel slope was calculated for higher potential (0.85-0.95 V, kinetic region) and lower potential (0.65-0.85 V, mass transfer limited region). In Tafel plot the x-axis is the current given by:

$$I_{Tafel} = \frac{i_k * 1.3 * 10^5}{\text{loading} * \text{ECA} * \text{area of electrode}}$$

Figure 5.7 shows the double Tafel slope in log scale observed during the contamination experiments. The Tafel slope in the higher potential region for the baseline, or uncontaminated, polarization curve was around 68-70 mV/decade which is as expected in 0.1 M perchloric acid. Figure 5.7 and table 5.2 also suggest that at a given potential the kinetic currents for contaminated polarization curves were lower compared to the clean ones.

The Tafel slope measured from iR-free polarization curve at room temperature in 0.1 M $HClO_4$ at a scan rate of 20mV/s (range of polarization being -0.01 to 1.0V) has two parts. In the higher over potentials (typically above 0.8) it is around -118 to -130

mV/decade, but in the lower over potential region it is around -65 to -70 mV/decade for carbon supported Pt nanoparticles (Pt/C) (72, 92, 93).

The Tafel slope was calculated for both high and low potential region and given in table 5.2. Above 0.85 V the Tafel slopes extracted from the ORRs performed in contaminated electrolytes were around -90 mV/decade. Since the tafel slope changed with addition of contamination, it can be concluded that contamination changed the ORR mechanism. The exchange current densities were also lower in the case of contaminated electrolyte.

Adzic et al. proposed that the adsorbed OH (from H_2O and not from O_2) could alter the adsorption energy of the ORR intermediates, which causes an additional energetic effect on the ORR kinetics. This, in turn, results in the variation of Tafel slope (94).

Adzic et al. has also projected an ORR model defining the Tafel slope in an absorbate free single crystal (Pt(111)) surface in $HClO_4$ so that OH adsorption cannot interfere with the model. Separating the anion adsorption effects (site blocking and electronic) from OH adsorption effect on Pt(111) helped them determine the cause of double Tafel slope. The adsorption of OH increases with coverage of OH ions on Pt site changing the slope of the polarization curve in the mixed kinetic-diffusion control region (around 0.8V vs RHE) (72).

Adzic et al further analyzed the cause of change in Tafel slope from the kinetic region (higher Tafel slope) to the diffusion control region (lower Tafel slope) by

developing kinetic equations (double trap kinetic model) for all the reaction steps (electro catalyzed reactions occurs in multi-step, forming reaction intermediates).

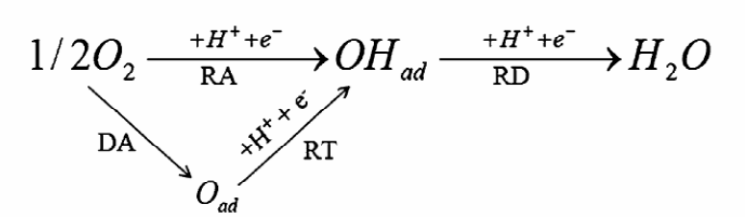

Where, RA = reductive adsorption

RD = reductive desorption

DA = dissociative adsorption

RT = reductive transition

The kinetics equation developed by them is shown above. The equation shows the intermediate steps.The variance of Tafel slope is explained to be roughly due to the change in OH coverage with potential. OH coverage increases at low potential as O coverage increases and then becomes constant making the Tafel slope -118 mV/decade. The lower Tafel slope at small overpotentials implies faster increase in current by decrease of highest activation barrier for the forward reaction (RT) as well as by the increase of lowest barrier for the backward reaction (-RT). Thus, the net reaction rate at higher potential region doubles that in the lower potential region. Since the RT and –RT has the highest and lowest barriers at zero overpotentials respectively the transition of Tafel plot is determined by the conversion of O/OH (72).

For higher potential region, after addition of Bostik® 920 the slopes increased slightly, but after addition of p-toluenesulfonamide the slopes increased to almost double the baseline value. For lower potential region it was difficult to extract the Tafel slope,

since some of the data points in log plots were undefined after reaching the limiting current. Therefore, Tafel slopes extracted at higher potential is much more relevant (figure 5).

5.3.2. Effects of organic and anionic constituents of leachate from Bostik 920® on ORR of Pt/C

Rotating Ring disk electrode (RRDE) study was employed to measure the peroxide formation before and after addition of contaminants. The reduction of oxygen proceeds through a four electron pathway to H_2O or a two electron pathway to H_2O_2 (95).

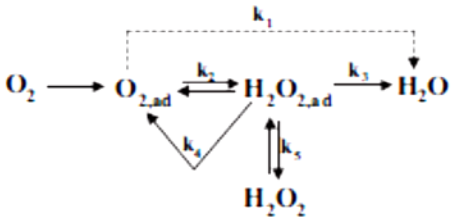

Although ORR via four electron transfer is the major pathway for oxygen reaction for Pt (111) and Pt (100) surfaces at H_{upd} region (< 0.3 V) , a substantial amount of H_2O_2 (upto 22%) also detected in the ring electrode using rotating ring disk electrode (RRDE) method (47) indicating the deviation of $4e^-$ to up to $2.7e^-$ (96) in 0.1 M $HClO_4$. Since carbon supported Pt catalysts typically consists of crystals with large fraction of Pt (111) and Pt (100), they can be expected to behave like single crystals (47). Therefore, RRDE method will help determine the reaction pathway in the presence of contaminants on high surface area Pt on carbon.

5.3.2.1 Effect of 4MBSA and chloride ions

The GCMS showed that Bostik® 920 (TOC= 110 ppm) has p-toluenesulfonamide (4MBSA) and Cl- (0.8ppm) as the only important anion among other anions searched

(NO_3^-, SO_4^{2-}, F^-) (83). An experiment was designed to determine the effect of organics and anions. To investigate the effects of all the components (organic and inorganic) of the leachates together, first we needed to obtain an insight on the effects of the individual components. Therefore, Cl^-, 4MBSA and mixture of Cl^- and 4MBSA were injected in the electrolyte solution at room temperature in three separate experiments and effects of each component were compared against the collective effects of organic and anion (mixture of 4MBSA and Cl^-). The purpose of this experiment was to create the same concentration condition inside the electrolyte as found in Bostik® 920 to capture the entire effect of the main constituents of the leachate separately and collectively. The data provides quantitative insight to any assembly aids of similar grade that may leach similar organic and inorganic compounds when used in a fuel cell at high temperature.

A. Baselining with organics

The first part of the experiment focused on the impacts of the organic compound alone. The total organic carbon content found in the 1 week soaked leachate of Bostik® 920 was 110 ppm. Since no other organic compounds were detected by GCMS in that leachate, a solution of 4MBSA was prepared and injected in the electrolyte so that the final concentration inside the cell was same as the TOC found in the leachate. There was a severe reduction of the area under the peaks in hydrogen adsorption/desorption region and Pt-oxidation and Pt-O reduction region. A distinct peak at 1.0 V was observed and the size of the peak increased with current proceeding to the cathodical part of the scan. That peak was also observed in the CVs performed with Bostik® 920 and low concentration of 4MBSA (described in sec. 5.3.2. in this paper). This peak is characteristic of aromatic compounds having amine groups. There wasn't any significant

change in the capacitance region, indicating the organic molecules are unable to displace any adsorbed perchlorate anions from the Pt surface. The electrochemical surface area (ECA) was decreased by 64%. 4MBSA is a sulfonamide with an S=O group. In 4MBSA the adsorption on Pt takes place through either S=O or $–NH_2$ group. The S atom is tetrahedral in 4MBSA and the adsorption is hindered. So the molecule adsorbs on Pt with $–NH_2$ group.

Figure 5.8 shows the uncontaminated partial and full CVs (red and black lines) along with CVs in the contaminated solution (blue and purple). The ORR activities were significantly affected. A small amount of peroxide was detected beyond 0.3 V in the ring (figure 5.9).

B. Baselining with Cl^- anion

The 1 week extract of Bostik® 920 was found to contain chloride as the only anion. To analyze the role of anions on ORR of Pt/C, chloride was added in the $HClO_4$ to make the final concentration of chloride ions same as detected in the extract of Bostik® 920. The objective of this experiment was to uniquely identify the effect of anion and then compare with the overall effect of anion and organic compound. The ECA loss after adding 22 μM Cl^- anion was calculated and compared against the uncontaminated solution (black and red lines) in 0.1 M $HClO_4$. There were three small peaks, centered at ca. 0.15, 0.2 and 0.3 V in the H_{upd} potential region. These peaks correspond to coupled processes of hydrogen desorption with Cl- anion adsorption on the Pt sites (77) as shown in figure 5.10.

The effect of anion on ORR activities on Pt/C is given in figure 5.11. The disk and ring currents were measured and plotted against disk potential. There was a large

decrease in the current at 0.9 V after addition of Cl^- anion. This is a characteristic of anion effect on ORR. This feature is not seen with organic compounds. The ring current increases after 0.3 V and then decreases after 0.5 V. these findings suggest that between 0.3 and 0.5 V the ORR proceeds through the 4 e^- pathway and after 0.5 V peroxide formation decreases gradually to almost 0 (figure 9).

Even if the ECA did not change much, the ORR activities in presence of Cl^- anions decreased a lot. Due to adsorption of Cl^- on Pt sites, the O_2 molecule could not reach the Pt sites, resulting in surpassed ORR activities (figure 9).

C. Effect of organic and anion

The third and final part of the experiment was mixing the anion and the organic to make a solution with same anion and model compound concentration as found in the leachate of Bostik® 920. This experiment was important because the leachate is a mixture of organic and inorganic (cationic and anionic) species. The adsorption process was not clear from the data obtained from the individual model compound and the anion. When the mixture was added to the electrolyte, depending on the effect seen in the cyclic voltammograms and the linear sweep voltammgroams, some insight was gained on the process of adsorption in presence of anion and organic compound. Earlier, we have seen that the leachates have fewer effects than same concentration mixtures of organic compounds due to the presence of other contaminating species. This experiment will prove if the anion effect is enhanced or suppressed in presence of organics.

Figure 5.12 presents the effect of mixture of 4MBSA and Cl^- on ECA. The characteristic features (peaks of Cl^- in H_{upd} region) of Cl^- were entirely absent in the contaminated CVs (blue and green dotted lines). The hydrogen adsorption/desorption

areas and the Pt-oxidation and reduction regions decreased. Even after recovery, the features of the initial CVs (red and black lines) were not retrieved.

Figure 5.13 shows the effect mixture of 4MBSA and Cl- on ORR of Pt/C. The figures on the left hand sides show the ring and disk currents and the right hand side figure shows the amount of peroxide formed detected by the ring. The black lines show the currents and peroxide formation in the uncontaminated electrolyte in the beginning of the test and the red lines show the effect of the mixture of the contaminants. The recovery was performed at the end of the test by holding the electrode at higher potentials (0.75, 0.85, 0.95 and 1.05 V) and cycling up to 1.05 V. The purple lines display the recovery.

The current at 0.9 V decreased to 6% of the initial value. Therefore, the characteristic of Cl^- anion was retained in the case of ORR as opposed to the CVs. There was significant amount of peroxide formation that started at very low potential. The ORR is strongly inhibited under the diffusion control region. Up to 0.7 V the peroxide formation was between 50 to 20%.

The current at 0.9 V and the ECA loss were summarized in figure 5.14. The mass activities were not compared since the Cl^- and 4MBSA are very dissimilar in nature and in their individual effects on the ECA. The current at 0.9 V was divided by the current at 0.9 V in the beginning of the test to give the percentage 0.9 V currents. Two contrasting features were clearly observed. The addition of organic 4MBSA resulted in higher ECA loss but lower loss in current at 0.9 V. The opposite trend was observed when only Cl^- was added. So, 4MBSA adsorbs faster in the Pt sites compared to Cl^-. The conclusions of the experiments with organic and anionis species can be summarized as:

1. The contamination loss is
   i) due to adsorption of contaminants on Pt (Loss in ECA, ORR)
   ii) due to absorption of contaminants on ionomer (Loss in ORR currents)
2. Effect of organic 1.3 mM 4MBSA: Pt contamination > ionomer contamination
3. Effect of anion 22 uM Chloride: loss in 0.9 V ORR current due to Cl^- by blocking Pt-O intermediates. This is not ionomer effect, this is entirely anionic effect.
4. Effect of anion and organic, 1.3 mM 4MBSA + 22 uM Cl–: Pt adsorption + ionomer absorbtion + Chloride ion inhibiting Pt-O formation
5. Ionomer effect from 4MBSA: after contamination ≈ after recovery, therefore ionomer effect is not recoverable, but chloride effect is.

5.4. Conclusions

This study showed that contaminants (organic or inorganic) leached from adhesives used in PEM fuel cell has detrimental effect on ORR activities and ECA. The poisoning effect is more prominent for the model compound than the leachate. This effect was supported by reduction in ECA and mass activities of contaminated electrodes. The loss in ECA and ORR activities (mass activities, mA/mg_{Pt} and specific activities, μAcm_{Pt}^{-2}) is compared at the beginning of the test and after addition of different dosage of contamination for both the leachate solution and the organic compound present in it.

- The decreases in ECAs due to poisoning with leachate and model compound were very similar.
- Due to contamination, the formation of Pt-OH and then Pt-O was hindered severely. But the decrease in ECA measured at H_{upd} is less than that measured at oxide region.
- The mass specific activities due to the contamination from the model compound were more than that of the leachate even though they both showed very similar

reduction in ECA. After adding 1.8, 18 and 180 µM of C equivalent of Bostik 20 and 4MBSA, the effect on ECA loss and ORR activities were very similar. For 180 µM of C equivalent of Bostik® 920 the ECA loss was 52%, and for 180 uM of 4MBSA – 58%. This indicates that other components compete with organics in adsorption on Pt. Consequently, the final loss of ECA by leachate is lower than that by its constituent organic compounds.

- The Tafel slope was measured at higher and lower potential region. The higher potential region yielded Tafel slopes below100 mV/decade whereas at lower potential region the slopes were very high. Also, the Tafel slopes increased with increase in contamination concentrations.

The total effect of all the components (organic and inorganic) was quantified by ECA loss of 60%, whereas the loss for adding 1300 µM (equivalent to 110 ppm of TOC) 4MBSA showed higher ECA loss – around 58%. In the presence of anion, the ORR activity was suppressed a lot. This feature was observed in both cases – anion with organic and anion alone.

- The mass activity decreased to 31% for 4MBSA alone, to 9% for Cl^- alone and 7% for a mixture of 4MBSA and Cl^-. After recovery, the mass activity came up to 68%. This proves that anion has more effect on ORR activity measured at 0.9 V than the organic compound.
- Ring current was detected in three cases with a significant amount of peroxide (50 to 60%) formed beyond 0.3 V only in case where a mixture of both organic and anion was injected. There is an interaction between the anion and the organic compound which is modifying the contamination characteristic of the individual

components. The detection of peroxide supports the hypothesis that ORR pathway changes from $4e^-$ to $2e^-$ in presence of organic and inorganic contaminants.

Table 5.1. Normalized mass activities of Pt/C at room temperature in 0.1 M perchloric acid before, during and after recovery of contamination

ORR activities after contamination	Normalized ECA	Normalized mass specific activity	Normalized ECA	Normalized mass specific activity	Normalized ECA	Normalized mass specific activity
	(%)	(%)	(%)	(%)	(%)	(%)
	control		Bostik®		4MBSA	
Step 1	98 ± 0.5	95.9 ± 3.0	76.16 ± 1.3	87.0 ± 2.6	71.4 ± 0.7	84.5 ± 3.5
Step 2	92 ± 1.4	93.9 ± 3.6	55.4 ± 0.6	59.8 ± 1.1	50.1 ± 2.1	45.6 ± 1.1
Step 3	84 ± 0.4	88.6 ± 2.6	48.0 ± 1.4	28.6 ± 5.0	42.3 ± 0.8	23.0 ± 0.2
recovery	-	-	70.2 ± 0.7	77.2 ± 4.2	60.1 ± 3.5	82.0 ± 2.5

Table 5.2. Comparison of Tafel slope before and after addition of contaminants from the leachate (Bostik® 920) and the model compound (p-toluenesulfonamide) of pre-reduced Pt in higher and lower potential region (interpreted from figure 5.7)

	Bostik® 920		p-toluenesulfonamide	
	high potential	low potential	high potential	low potential
0.1 M $HClO_4$ (baseline)	65	90	64	85
0.1 M $HClO_4$ + 1.8 µM compound	68	95	73	92
0.1 M $HClO_4$ + 18 µM compound	72	105	78	100
0.1 M $HClO_4$ + 180 µM compound	74	110	82	108
0.1 M $HClO_4$ (recovery)	70	95	72	90

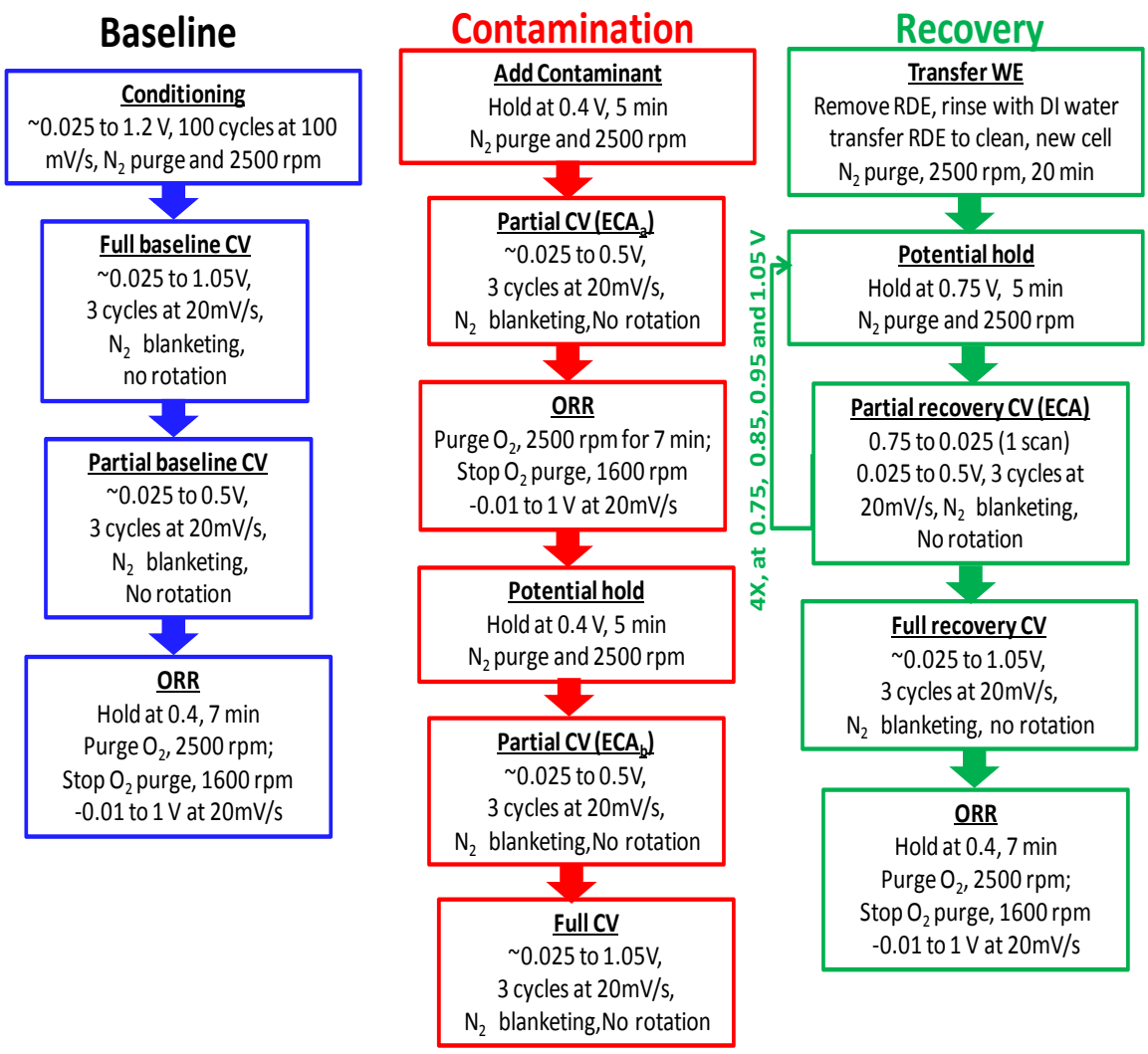

Figure 5.1. Schematic of the experimental protocol to investigate the impact of the organic contaminants found in the DI water soak of the materials used in a PEMFC. The loss of ECA and ORR activity of Pt/VC were measured using three electrodes TF-RDE apparatus at room temperature.

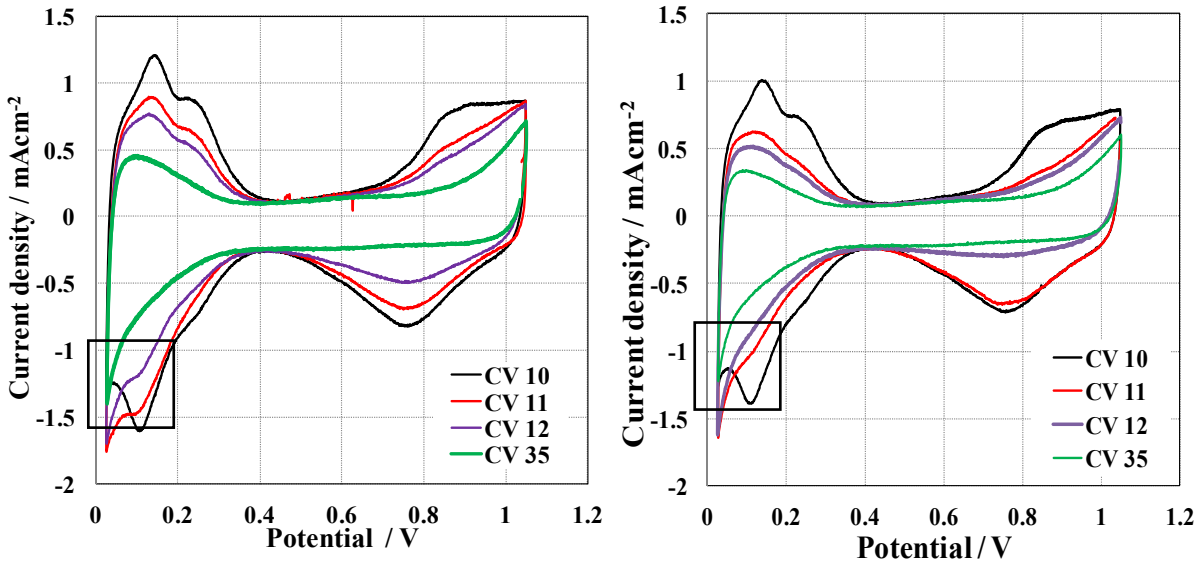

Figure 5.2. Votammograms showing effect of adding 28.3 µl of each of the contaminants Bostik®920 (left) and p-toluenesulfonmide (right) on Pt/C (Vulcan) at room temperature in 0.1 M $HClO_4$, scanned from 0.025 to 1.05 V. The TOC of Bostik®920 and p-toluenesulfonmide was 110 ppm. Original concentration of p-toluenesulfonmide was 220 ppm. The final carbon molecule concentration for both molecules was 180µM inside the RDE cell.

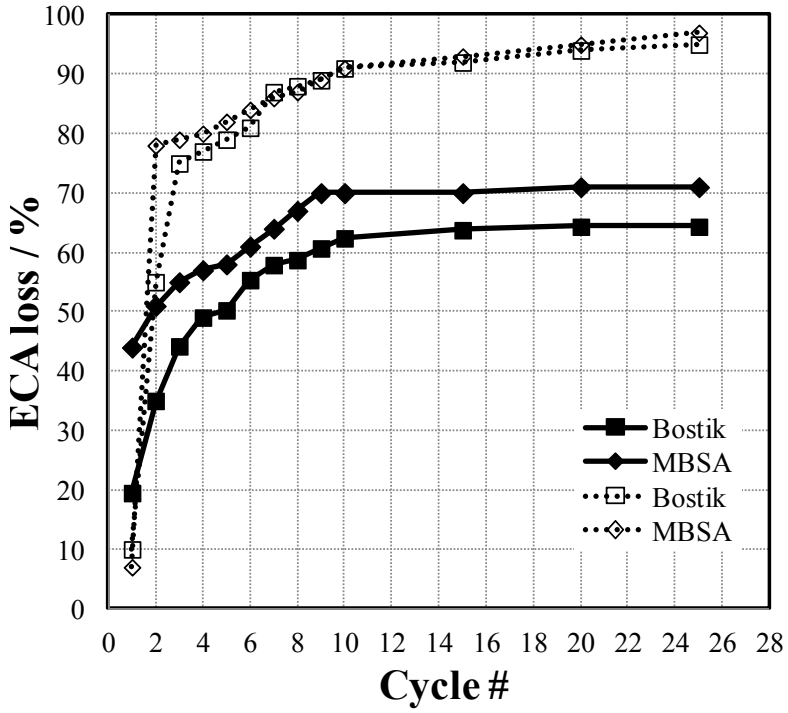

Figure 5.3. The change in surface coverage by contaminants (loss of ECA due to adsorption of contaminant molecules on Pt sites) with CV cycles from 0.025 to 1.05 V at a scan rate of 100 mV/s as measured under the H_{upd} (open symbols) and oxide region (solid symbols) of the voltammograms normalized by initial available surface in the clean electrode

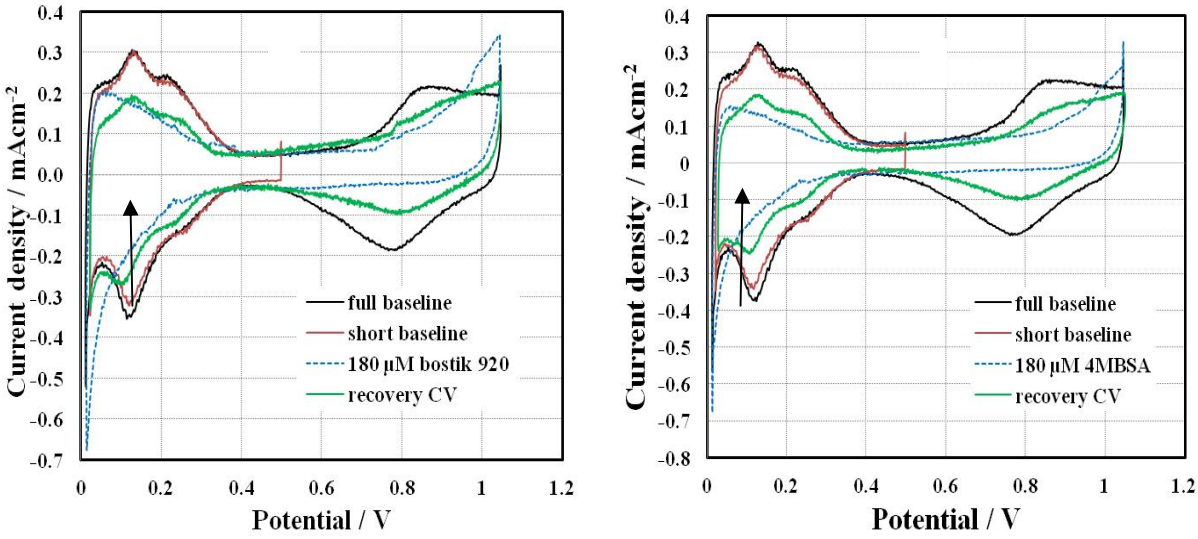

Figure 5.4. Cyclic Voltammetry to 1.05 V of uncontaminated contaminated (a. with bostik 920 and b. with 4MBSA) and contamination recovered Pt/C at room temperature in 0.1 M $HClO_4$ at 20 mVs^{-1}.

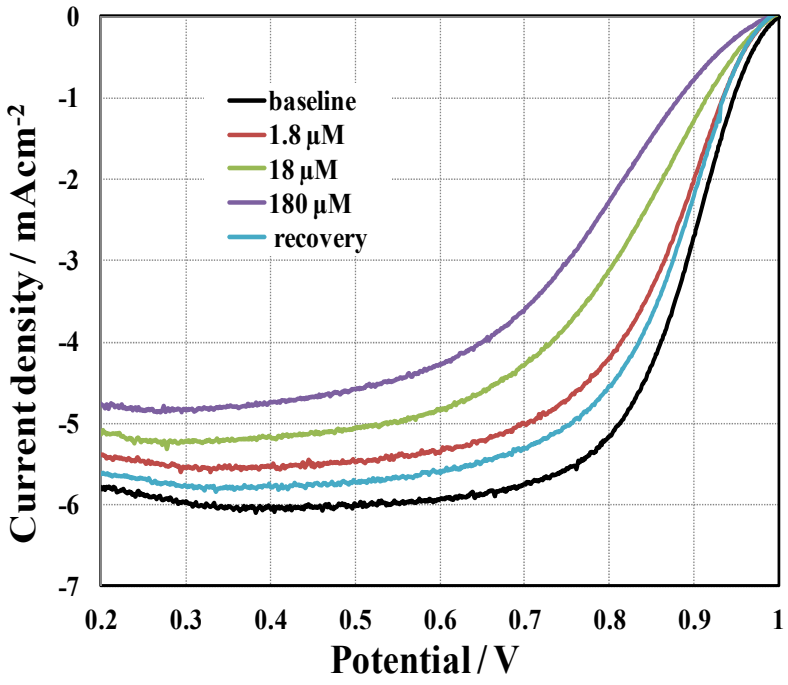

Figure 5.5. ORR polarization curves for Pt/VC in 0.1M $HClO_4$ as electrolyte: initial or baseline ORR (black solid line), with $1.8x10^{-3}$ mM Bostik® (red solid line), with $18x10^{-3}$ mM Bostik® (green solid line), with $18x10^{-2}$ mM Bostik® (violet solid line). The WE was transferred to a second set of cell with clean electrolyte after contamination to attempt recovery. The blue solid line was obtained during recovery. Conditions: scanned at 20 mVs^{-1} with electrode rotation at 1600 rpm of the electrode in a well O_2 saturated electrolyte at room temperature.

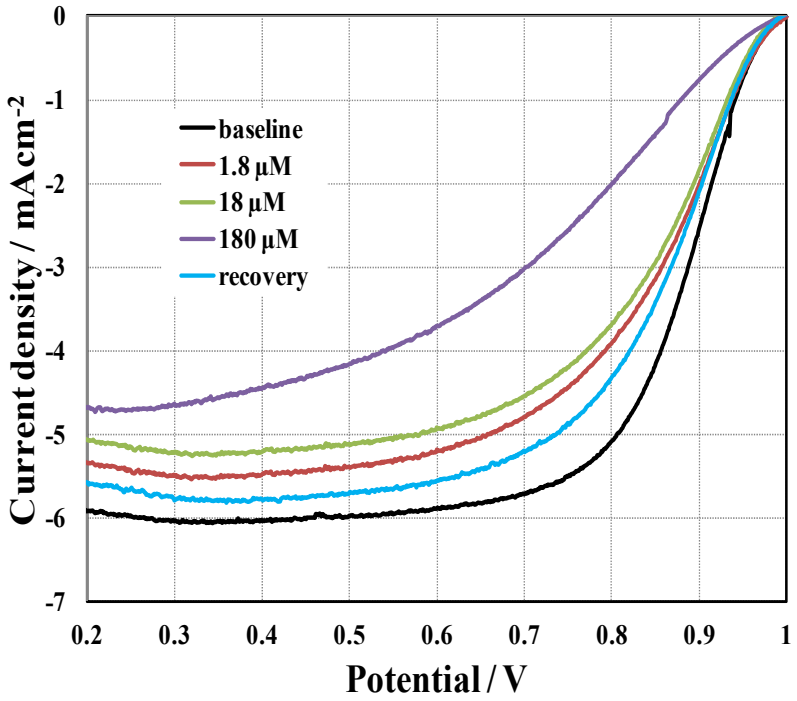

Figure 5.6. ORR polarization curves for Pt/VC in 0.1M $HClO_4$ as electrolyte: initial or baseline ORR (black solid line), with $1.8x10^{-3}$ mM 4MBSA (red solid line), with $18x10^{-3}$ mM 4MBSA (green solid line), with $18x10^{-2}$ mM 4MBSA (violet solid line). The WE was transferred to a second set of cell with clean electrolyte after contamination to attempt recovery. The blue solid line was obtained during recovery. Conditions: scanned at 20 mVs^{-1} with electrode rotation at 1600 rpm of the electrode in a well O_2 saturated electrolyte at room temperature.

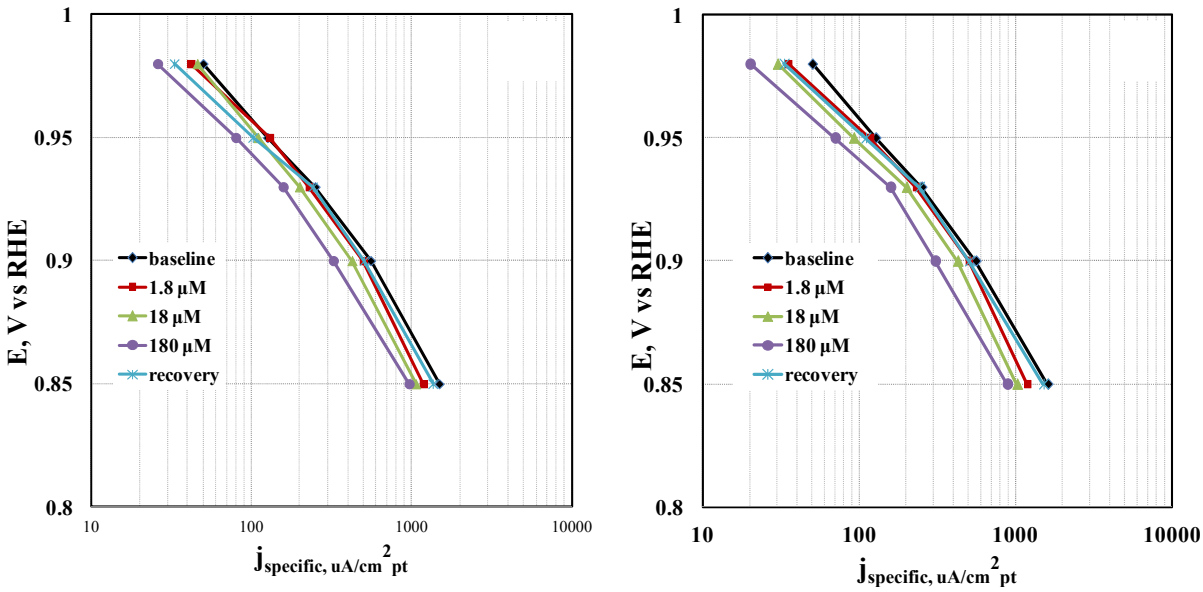

Figure 5.7. Tafel plots on pre-reduced Pt after addition of (a) Bostik 920 and (b) p-toluenesulfonamide. The ORR data were corrected for mass transfer limitations, elevation effect (due to the altitude of Denver, the partial pressure of oxygen over the RDE cell is 83 kPa instead of 101 kPa. Legend: black- baseline, dark blue -1.8 µM, green 18 µM, light blue -180 µM and violet- recovery. Experimental condition: pre-reduced Pt/C (17.37 µgPt/cm^2) i.e. 400 S at 0.4 vs. RHE before the sweep at 20 mV/s from -0.01 to 1 V in oxygen saturated 0.1 M perchloric acid at 1600 rpm.

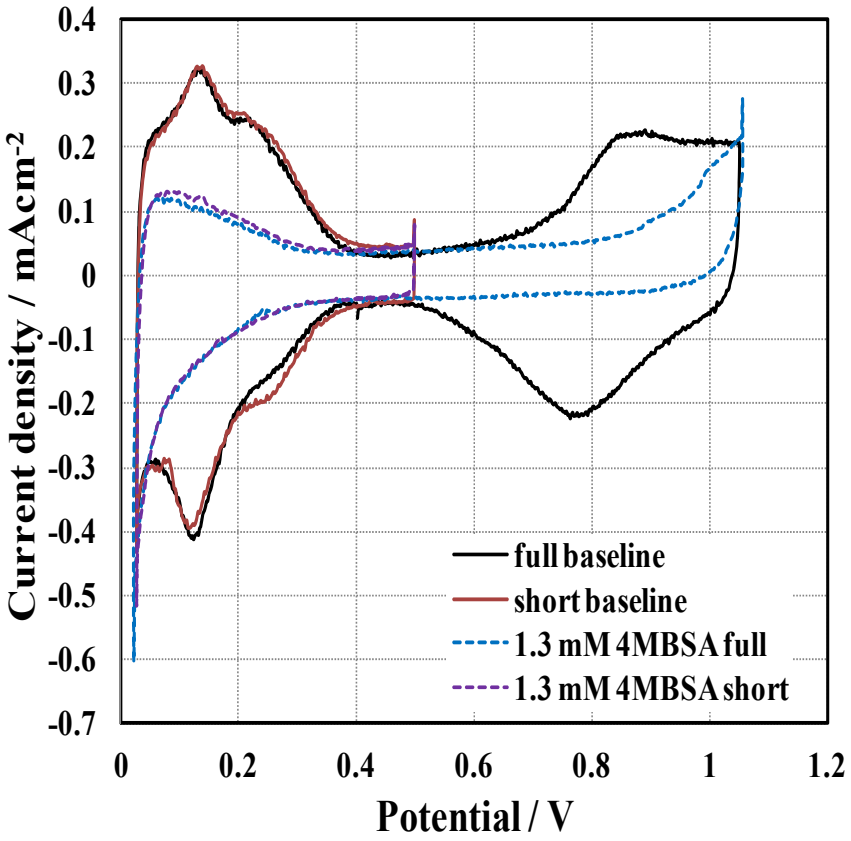

Figure 5.8. Cyclic Voltammetry to 1.05 V of contaminated electrolyte with 1.3 mM 4MBSA on Pt/C at room temperature in 0.1 M $HClO^4$ at 20 mVs^{-1}

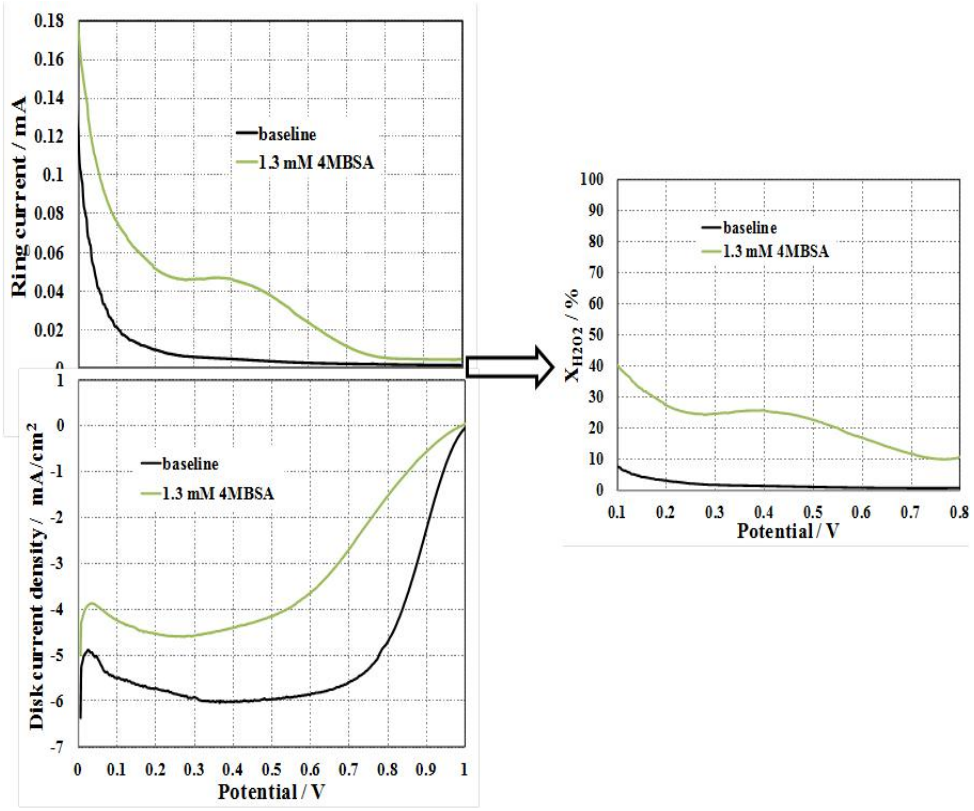

Figure 5.9. Role of 110 ppm equivalent of 4MBSA on ORR activities of Pt/C in O_2 saturated 0.1 M $HClO_4$, rotating WE at 1600 rpm. The Left hand side figure depicts the ring and disk currents during ORR and the right hand side figure shows the corresponding fraction of hydrogen peroxide formation. The black line shows ORR in clean electrolyte, while the green line shows the LSVs in contaminated electrolyte.

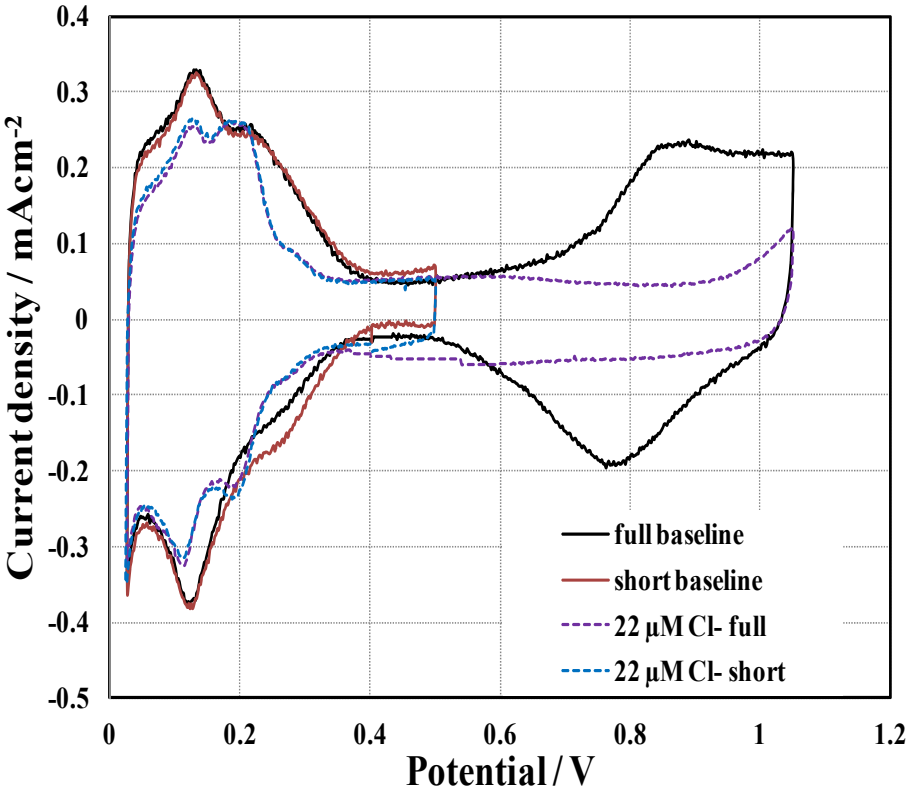

Figure 5.10. Cyclic Voltammetry to 1.05V of contaminated electrolyte with 22 µM Cl- on Pt/C at room temperature in 0.1 M $HClO_4$ at 20 mVs^{-1} in a N_2 saturated electrolyte.

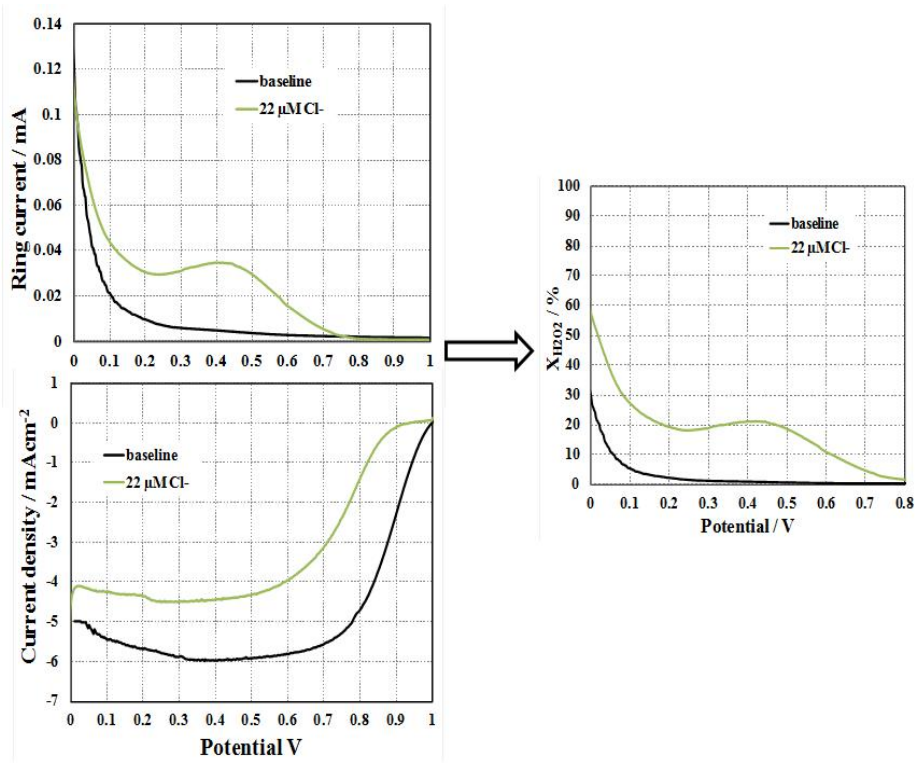

Figure 5.11. Role of 22 µM Cl^- on ORR activities of Pt/C in O_2 saturated 0.1 M $HClO_4$, rotating WE at 1600 rpm. The left hand side figure depicts the ring and disk currents during ORR and the right hand side figure shows the corresponding fraction of hydrogen peroxide formation. The black line shows ORR in clean electrolyte, while the green line shows the LSVs in contaminated electrolyte.

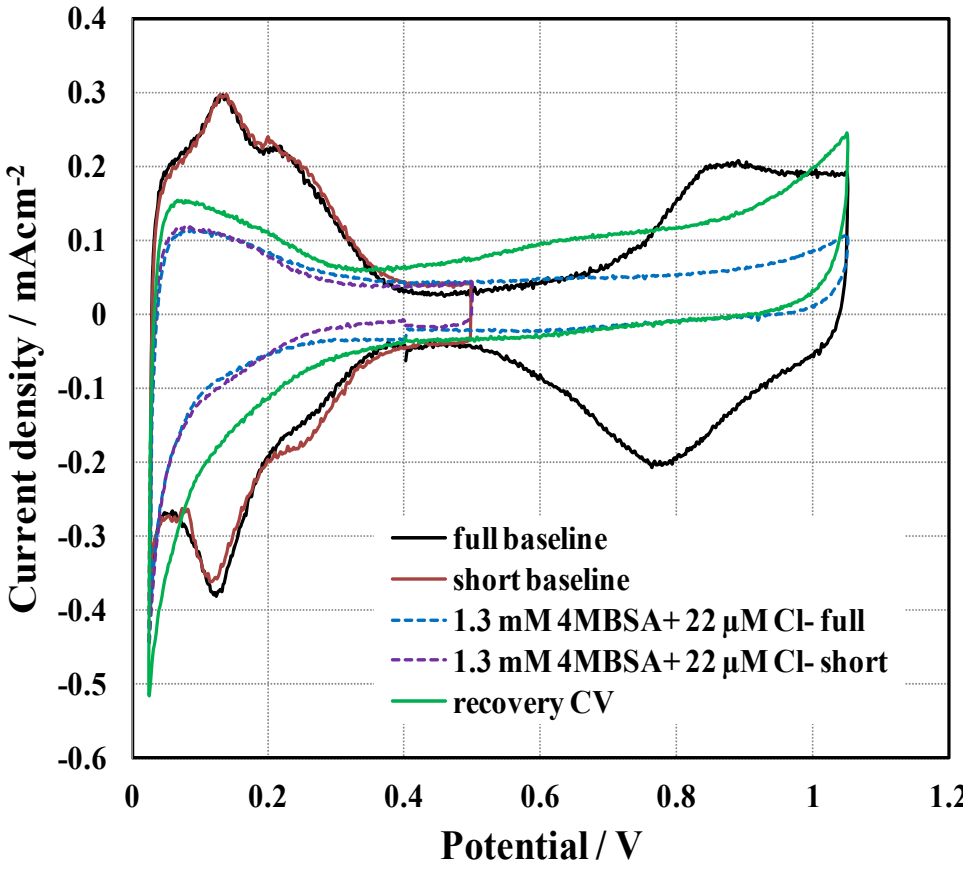

Figure 5.12. Cyclic Voltammetry to 1.05 V of contaminated electrolyte with 640 µM 4MBSA and 22 µM Cl^-, on Pt/C at room temperature in 0.1 M $HClO_4$ at 20mVs^{-1} in a N_2 saturated electrolyte.

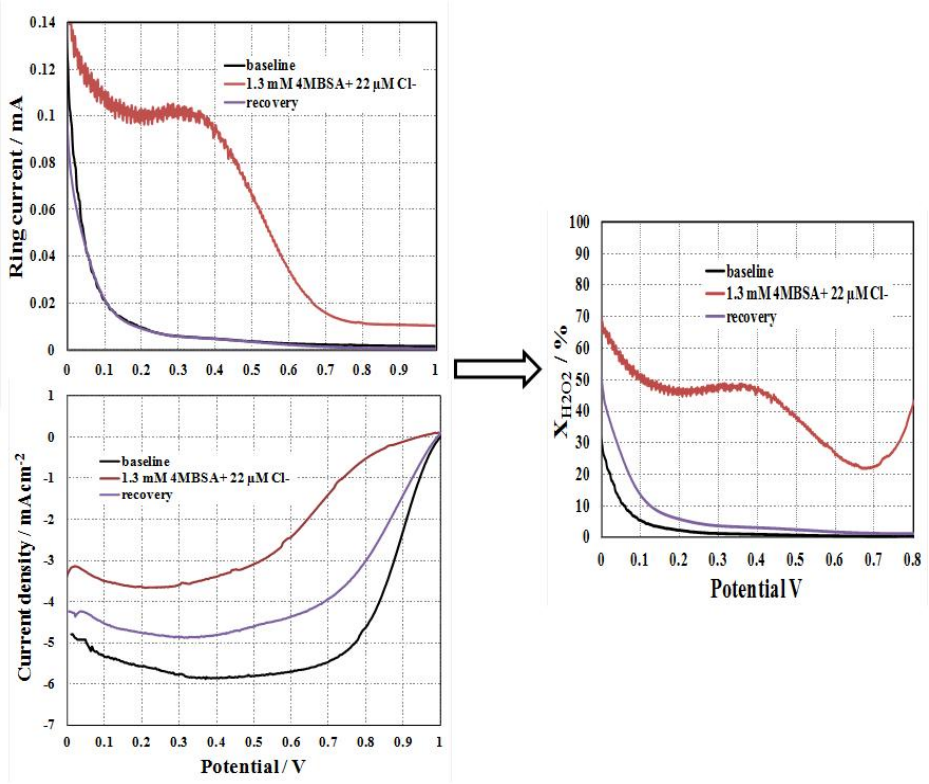

Figure 5.13. Role of 110 ppm equivalent of 4MBSA and 22 µM Cl^- on ORR activities of Pt/C in O_2 saturated 0.1 M $HClO_4$, rotating WE at 1600 rpm. The Left hand side figure depicts the ring and disk currents during ORR and the right hand side figure shows the corresponding fraction of hydrogen peroxide formation. The black line shows ORR in clean electrolyte, while the red line shows the LSVs in contaminated electrolyte and the red line shows the recovery in a clean electrolyte after rinsing the contaminated electrode in DI water.

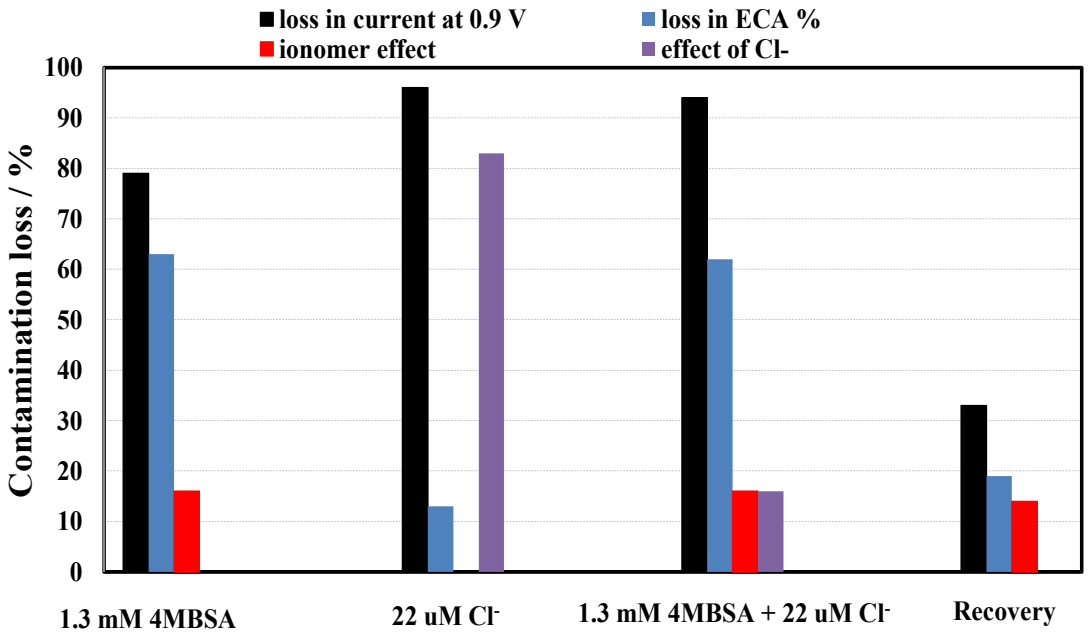

Figure 5.14. Comparison of normalized available ECA (%) and current 0.9 V (%) in pristine electrolyte with contaminated electrolytes (4MBSA, Cl^-, and mixture of 4MBSA and Cl^-).

Chapter 6. Study of the effects of organic compounds on PEMFC electrode

In this chapter the detrimental effect of leachates from off-the-shelf BOP materials (all categorized as assembly aids), which may be used in PEM fuel cells, on electrode was correlated to the contamination from the organic and inorganic species in the leachates. In this study the organic compounds (aliphatic, aromatic and polumeric) in the adhesives (identified in GCMS) were investigated for their role on the degradation of catalyst layer (carbon supported Pt) and ionomer by recording the loss in electrochemical surface area (ECA) and oxygen reduction reaction (ORR) currents using thin film rotating disk electrode (TF-RDE) method. The organic contaminants (model compounds) adsorb on Pt sites of the electrocatalyst, reducing the surface area available for electrochemical reactions and the oxygen reduction reaction activities. The ECA loss was more in case of aromatics than that of aliphatics, as the contaminant molecules block the Pt sites. For higher dosage of contamination, the oxygen reduction goes through 2 electrons pathway instead 4 electrons and generates peroxide which was detected at the ring during ring rotating disk experiment. Recovery of the lost ECA and ORR activities was partially possible by holding and cycling to a higher potential well in the range of an operating fuel cell.

The additional information on the methodology and background studies can be found in appendices D, F and G.

6.1. Introduction

Polymer electrolyte membrane fuel cell (PEMFC) converts chemical energy generated due to combination of hydrogen and oxygen directly to electrical energy which can used to run vehicles (97). In pursuit of commercialization of PEMFC in vehicles replacing the internal combustion engines, a large number of studies have been conducted in last one decade on fundamental hydrogen oxidation reaction (HOR) in anode and oxygen reduction reaction (ORR) in cathode. Overpotential losses of ca. 400mV were observed in proton exchange membrane (PEM) fuel cell cathodes due to poor oxygen reduction kinetics (74). Since the carbon supported Pt catalysts used in a fuel cell is susceptible to contamination from air such as SO_2 (17, 44, 56, 63, 98-100) in cathode and from fuel (40, 101-103) in anode it was necessary to conduct comprehensive studies to document the severity of contamination in both anode and cathode and explore the mitigation strategies which are cost effective. The structural materials, conduits and hoses, coolants, adhesives and lubricant used in a fuel cell also contribute to the contamination of the catalyst (both anode and cathode side) , change in the hydrophobicity of the gas diffusion layer, membrane degradation resulting in poor performance of the fuel cell. These materials are often chosen from the off-the-shelf materials to keep the cost of manufacturing low, and therefore eliminating the source of contamination may not be cost effective for the manufacturers of those materials. This study strives to provide an appropriate and all-inclusive study of some of the organic compounds found in the one week soak of leachants of the assembly aids (adhesives, thread lockers, grease etc.) used in a fuel cell. These organic compounds can come from the solvent, antioxidants, plasticizers, filling for the assembly aids and degrade or combine among themselves to

form the organic compounds under investigation. When the contaminants reach the catalyst layer, they get readily adsorbed on the Pt sites preventing them to participate in oxygen reduction reaction ($O_2 + 4H^+ + 4e^- \rightarrow 2H_2O$) and HOR ($H_2 \rightarrow 2H^+ + 2e^-$). Since catalyst loading at the cathode (where ORR takes place) contributes more to the overall cost effectiveness of the fuel cell stack than anode (where HOR takes place) catalyst (0.05 $mg_{Pt}cm^{-2}$ at anode vs. 0.35 $mg_{Pt}cm^{-2}$ at cathode (74)), this study focuses on evaluating the ORR activities of Pt/C catalyst in presence of the organic contaminants.

The ORR reaction is usually a four electron process resulting in formation of water. For this reaction to take place, the oxygen molecule must adsorb on the Pt sites where the O-O bond breaking occurs resulting to oxygen reduction reaction. ORR is associated with 0.35 to 0.4 V overpotential losses due to kinetic limitations (52, 104). So for the development of Pt electrocatalyst, understanding the mechanism of contamination at the catalyst surface is necessary. The contamination of Pt electrode is a complex process, since the contaminants can modify the intrinsic catalyst properties.

The reaction kinetics of ORR depends on the surface coverage of Pt by different species such as underpotentially deposited hydrogen (H_{upd}), adsorbed oxygenated species (OH_{ad}) and anions from supporting electrolyte (62, 105, 106). Therefore the ORR activity only depends on the available Pt surface on the electrode (53). To develop commercially viable catalyst with high ORR activities, understanding the fundamentals of contamination on Pt/C using ex-situ methods like rotating disk electrode is important.

This study has been supplemented with ring-rotating disk electrode (RRDE) study as well. The activity of oxygen reduction reaction decreases with increasing adsorbed

contaminants. From previous studies (53) it is known that decrease in disk current with simultaneous increase in ring current strictly reflects two electron reduction of oxygen and formation of peroxide. This phenomenon occurs in presence of impurity molecules (15) due to unavailability of Pt sites for O-O bond breaking.

Recovery of the ECA and ORR activity loss was also performed on the contaminated electrodes in this study. Ex-situ RDE technique was chosen to isolate the impact of contaminants on ORR activities and catalyst poisoning, which was not possible in-situ (in a PEMFC). In-situ studies has revealed the slow kinetics at the cathode (compared to anode) is greatly influenced by activation losses due to presence of contaminants (air borne and fuel, chemical degradation products from seals, coolants, assembly aids and plastics) in the fluid streams in addition to other factors like catalyst layer characteristics (107). Similarly the ohmic losses originating from the electrolyte (membrane) can also be predisposed to contaminations from alkali and alkaline earth metal ions (displaces protons of ionomers decreasing proton conductivity) altering the proton conducting properties of the MEA (108). The integral components of a fuel cell like membrane electrode assembly (MEA) could also serve as a source of contamination. As delineated in previous studies, the membrane degradation product can often cause poisoning of the electrodes by forming peroxide or peroxide radicals (107). Various similar sources can contribute to the efficiency loss and or degradation of the fuel cells. Liquid phase contamination is one of major concern due to its role in poisoning the catalyst thereby increasing the chances of poor performance in a PEMFC.

In this paper, experimental data was obtained and analyzed to gather insights on fundamental understanding contamination from organic compounds on PEMFC electrode.

When a molecule is adsorbed on the surface, the nature of adsorption is determined by the bonding and electronic state of the molecule. With no or very little change in electronic structure of the molecule the bond between the molecule and the surface is weak and it is called physio-adsorption. Or the bonding can be strong making it a chemi-adsorption. During chemi-sorption there is electronic interaction between the molecule and the metal. Most of the chemi-sorption takes place through Langmuir-Hinshelwood kinetics.

Monitoring adsorbates on the surface of a catalyst can offer great insight to the reactions that cause contamination and could help in the area of catalyst development. Also the recovery procedure could help mitigate the effect of the organic contaminants to the Pt electrocatalyst.

6.2. Experimental

The rotating disk method was employed in all the measurements, using three electrodes cell setup. The electro-chemical cell setup was cleaned in concentrated H_2SO_4 for 24 hours followed by cleaning in concentrated H_2SO_4 and nochromix solution for another 24 hours. After the acid cleaning, the cell setup was boiled in DI water for 2 hours.

6.2.1. Catalyst ink and thin film electrode preparation ORR on Pt/C

7.4 mg of TEC10V50E (Vulcan carbon) was dissolved in 7.6 ml DI water and 2.4 ml IPA in a small glass vial. 40 µl of Nafion (5wt%) was added to the vial. The ink solution was sonicated in an ice bath for 40 min. The ice was changed every 3-4 minutes as it started melting. A 5mm diameter glassy carbon tip on Teflon cylinder (Pine

Instruments) was chosen as the electrode. It was polished using 0.05 μm alumina polish suspension and a few drops of DI water on a Buehler MicroCloth for 5 minutes followed by rinsing in DI water. The electrode was then sonicated in Nanopure water (18MΩ) and diluted isopropyl alcohol (Sigma Aldrich) respectively for 15 minutes each. After sonication, 10 μL of ink was dispensed carefully at once on the electrode glassy carbon tip to build an evenly dispersed thin film (for less mass transport resistance). The tip was then dried in an oven at 40^0C for 20 min. the Pt loading was 18 $\mu g_{Pt} cm^{-2}$.

6.2.2. E-chem Cell preparation

The electrochemical glassware was filled with 0.1 M Perchloric acid from GFS chemical (maximum level of Chlorides of 0.00001%). A Pt wire (inside a glass insert, connected to hydrogen gas) serves as the reference electrode (Reversible Hydrogen Electrode). The counter electrode was also made of Pt wire and gauge (spot welded on the wire). N_2 gas was purged during baseline CV and while contaminating to remove excess oxygen from the electrolyte. The N_2 or O_2 (research grade purity, by Air products) gas goes through water trap before entering the cell to eliminate any other contaminants.

6.2.3. Preparation of the solutions with organic contaminants

The stock solutions of the organic compounds were prepared by diluting the organic compounds purchased from Sigma Aldrich. The purity of the purchased compounds was 99%.

6.2.4. RDE experiments protocol to measure ECA and ORR

Figure 2 shows that there were three essential parts of the experimental procedure: baseline, contamination, and recovery. Each electrode was subjected to the baseline first,

followed by the contamination part, and finished with the recovery part. In each part, the ECA and ORR activities were measured. All experiments were performed at room temperature in 0.1M $HClO_4$ using a TF-RDE method. The details of experimental procedure including electrode preparation and conditioning were reported in (59, 70).The contamination part was repeated three times for three different concentrations of the leachate. Since kinetics data were extracted from the ORR polarization curves, the background of ORR was recorded in N_2 gas saturated electrolyte.

For the baseline part, thin film electrodes were prepared as described in (59, 70) and mass activities were calculated and used to ensure quality of the electrode in terms of reproducibility of the catalysts. Conditioning involved 100 cycles from 0.025 to 1.2 V at 100 mV/s after a 20 min N_2 purge while the TF-RDE was rotated at 2500 rpm. The full baseline CV was obtained from three cycles between 0.025 and 1.05V at 20 mV/s under a N_2 blanket with no rotation. This full baseline allows calculation of the ECA according to typical procedures reported in 16, 17. In addition a partial baseline CV was obtained from three cycles between 0.025 and 0.50 V at 20 mV/s under a N_2 blanket with no rotation. Again the ECA was calculated and compared with the ECA from the full baseline CV. These two ECAs were within ±3% of each other with smaller ECA consistent with the fact that partial scans do not go higher up to the potential where PtO can be formed. Note the partial scan was used to be consistent need to limit the potential range for the contaminated ECA. Next, the WE was polarized at 0.4V for 7 min while purging with O_2 and rotating at 2500 rpm. Hydrodynamic voltammetry for the ORR current measurement was conducted by recording linear sweep voltammetry at 20 mVs^{-1} in an O_2 blanketing environment on the electrolyte and rotating at a speed of 1600 rpm. Finally, the

electrolyte was saturated by sparging N_2 for 7 min then a background ORR scan was obtained in N_2 saturated electrolyte from -0.01 to 1.0 V at 20 mVs^{-1} while rotating at 1600 rpm. The sweep rate and rotation speed were the same as for the N_2 baseline. The background was later subtracted from the ORR LSVs to correct for the pseudo capacity currents.

For the contamination part of figure 2 the initial leachate solution of known TOC concentration was 1.8 μM on a carbon basis which was added with a pipette directly to the electrolyte while purging the RDE cell with N_2 and while holding the working electrode at 0.4 V (to avoid any electrochemical change of the contaminant before it reached the Pt sites) and rotating at 2500 rpm. Then the ECA was measured from the cyclic voltammograms (full and partial, performed same way as described above for the baseline part). Next, the WE at 0.4V during a 7 min urge of O_2 during rotation at 2500 rpm followed by recording of linear sweep voltammetry (ORR current) at 20 mVs^{-1} with O_2 blanketing on the electrolyte and rotating at a speed of 1600 rpm. Note that the electrolyte was saturated by sparging N_2 for 7 min then a background ORR scan was obtained in N_2 saturated electrolyte from -0.01 to 1.0 V at 20 mVs^{-1} while rotating at 1600 rpm. The linear sweep voltammetry in N_2 is measured to subtract the background to obtain kinetic data (Tafel slope). Then the required volume of leachate was added to the 1.8 μM contaminated electrolyte to achieve 18 and 180 μM carbon concentration and the contamination part was repeated.

Recovery part includes the potentiostatic hold at higher potentials followed by potential cycles from the holding potential (0.75 V, 0.85 V, 0.95 and 1.05 V) to low potential (0 V) finally to 0.5 V. The partial CVs allowed calculating ECA after each hold,

presenting the % of ECA recovered due to the holds. Finally recovery CV (3 cycles of full CVs - 0.025 V to 1.05 V at $20mVs^{-1}$) and ORR (-0.01 to 1.0 V at $20mVs^{-1}$at 1600 rpm) was performed using the same procedure as described in the baseline section. The linear sweep voltammetry in N_2 is measured as the background to obtain kinetic data (Tafel slope) after recovery.

6.2.5. Determination of time taken by contamination molecules to reach Pt surface

To determine the time taken by the organic molecules to reach the surface of the electrode, the CVs were performed at 100mV/s and the electrolyte was contaminated at 1.05 V in a separate set of experiments with Loctite® 39916. Completion of one full cycle (1.05 V→0.025 V→1.05 V) requires 20 s. Therefore, after injecting the contaminant at 1.05 V, time taken by the contaminants to reach electrode surface can be calculated by counting the number of cycles before observing any impurity effect on the CV scan.

6.3. Results and discussions

6.3.1. Characterization of the leachant using GCMS

Systematic identification and selection of model compounds provide the basis for ex-situ RDE experiments to quantify effects of these system contaminants ECA and ORR currents loss which leads to determining the potential degradation mechanisms.

Lubricants, adhesives and thread locks/sealants fall under the broad category of assembly aids. There are five categories of materials tested and reported in my previous paper, such as urethane, epoxy, fluorocarbon, silicone and acrylic groups. These materials were leached in polypropylene bottles at 90^0C for a week and the leachates were analyzed

using GCMS to identify the organic species as furnished in table 6.1. For detailed leaching process, please refer to my previous paper.

6.3.2. Structure of the organic contaminants

The assembly aid materials chosen for this study are commercially available (off-the-shelf) with wide range of properties and have specific functions in a fuel cell stack operation. These materials are not specifically designed for fuel cell applications and hence they may contain additives that are not needed for fuel cell applications. The cost of off-the-shelf assembly aids vary but are within the range of affordability of a fuel cell stack manufacturer. The contamination effect of the assembly aids including the adhesives and lubricants has been expansively described in my previous paper. These assembly aids were analyzed using GCMS (109), ICP-OES, and IC to provide a qualitative insight on their organic, inorganic and anionic components. The GCMS identifies the most prevalent organic compounds using NIST library and fairly specifies the source of contamination. The assembly aids were soaked at an elevated temperature for a week and the solution separated from any solid particle at the end of the soak was tested by GCMS and found to contain the organic compound as described in table 1. All the component organic compounds found in those assembly aids are present as solvent, filler, antioxidants, pigments, flame retardants, product of polymer degradation and residues (109). The extent of contamination of the assembly aids varies with the surface area of contact with the gases inside the fuel cell. After determination of this subset of model compounds, pure standards of each were purchased from Sigma-Aldrich. One assembly aid was down selected for further probing from each group of the assembly aids and analyzed using GCMS. The organic compounds listed in table 1 were referred to as

model compounds and tested for their role in contamination during oxygen reduction reaction in this paper.

6.3.3. Surface chemistry between Pt and organic molecules

The contaminant organic molecules Pt sites depending on the crystal structure. Carbon supported electrocatalysts mainly consists of Pt (111) and Pt (110), and the organic molecules can adsorb to the surface in three general positions – atop, bridge, or multi-fold (Figure 6.3) (110).

During the atop configuration the entire molecule covers a Pt site), during bridge configuration the pi bond (electron donation from the pi bond) or the side chains spread over two Pt sites side by side and during the threefold the pi bond and or the side chains spread over three Pt sites side by side occur as shown in the figure 6.3. Depending on this orientation, one single molecule of an organic compound can reduce the original available Pt sites of the catalyst by one or by two or by three. ORR needs O-O bond breaking by two Pt sites. Therefore the adsorption of contamination molecules not only decreases the Pt sites but also inhibits oxygen reduction reaction ($O_2 + 4H^+ + 4e^- \rightarrow 2H_2O$).

The surface chemistry between Pt sites and organic compounds depends on the potential of the electrode. Electrocatalysis happens in two distinct parts: first, a molecule adsorbs on the surface and forms a bond with the Pt (chemical adsorption). Secondly, the molecule must exchange a charge with the metal surface by changing its chemical structure (electrochemical reaction). However, catalyst sites of a metal surface are always covered with adsorbed species (either water or adsorbate ions from the electrolyte), where the water molecules are denoted by blue circles and the contaminant by red circle.

When perchloric acid is used as an electrolyte due to weaker adsorption strength of perchlorate ions, the adsorption of organic molecules starts as early as at 0.2 V. If no potential is applied to the electrode, the surface will stay covered by water molecules and the adsorption of other molecules is repressed. When more positive potential is applied to the electrode adsorption of the water molecules becomes less favored in presence of organic polar molecules and gradually the organic molecules replace the water molecules and attach to the Pt sites). At these free catalyst sites other molecules, e.g. organic compounds, can adsorb, however, the electrochemical reaction cannot occur until the electrochemical potentials of the electrons in both phases are equal. Therefore, even if the potential of the electrode is positive enough to allow the adsorption to occur, it is not necessarily suitable for the electrochemical reaction. When more positive potentials than PZC are applied, organic molecule will adsorb on the Pt electrode with more negative part towards the metal surface.

In this study definitive proof of adsorption of the organic molecules will be presented at a potential upto 1.05V, but the occurrence of any parallel electrochemical reaction (i.e. exchange of electrons from the organic to the metal electrode) may not be observed in all cases. As suggested by a study conducted by A. Santasalo (111), the chances of contaminant molecule to attach to Pt (111) and Pt (100) are much higher than Pt (110). Since Pt/C resembles in behavior that of Pt (110 and Pt (111), we will see a higher affinity of the organic molecules towards Pt than as can be seen towards poly crystalline Pt.

6.3.4. Effect of aliphatics on electrochemical surface area determined by CVs

The CV was measured after injecting the leachant and the model compound in two different set of experiments while the electrode was held at 0.4 V (vs. RHE). Organic molecules are neutral (not positively or negatively charged like ions), and therefore they adsorb very well near the PZC of the metal electrode. At PZC, the water or any adsorbed species on the electrode is the least layered. So it is easy to displace the initial adsorbed species by the organic molecules. As mentioned before the PZC of Pt is 0.35 V so at 0.4 V organic molecules can adsorb on the electrode. Also at 0.4V the original uncontaminated CV shows adsorption/ desorption peaks. Between 0.4 to 0.5V the region is known as double layer region where no oxidation or reduction reactions take place. Therefore holding the working electrode at 0.4 V ensures the foreign contaminant molecules will not undergo any electrochemical change and will therefore, manifest the impact of contamination on consecutive cyclic voltammetric scans.

Two aliphatic compounds- 2-(2-ethoxyethoxy) ethanol and 2-(2-ethoxyethoxy) ethanol acetate were chosen for testing on the Pt/VC using thin film RDE. Each of the compounds contains two ethoxy groups ($-CH_2-O-CH_2-$).

No additional peaks were found in the CVs performed from 0.025 to 0.5 V but for full scans (0.025 to 1.05V) some additional peaks were observed. As discussed before the hydrophobicity of the organic molecules assist the adsorption process, but due to the large size of the molecules (bulk hindrance), the adsorption process slows down after the initial rapid phase. It is experimentally proven in the previous section that highest amount of adsorption and therefore decrease in ECA took place in first 5 minutes of injection. The CVs were performed at room temperature. The CVs before adding (baseline) and

after adding contaminants (at the end of the experiments) are shown in figures 6.4 and 6.6. It is clear from these figures that electrochemical surface area decreased after addition of the model compounds. The contaminants were injected at an increment of an order of magnitude of strength. The final dosage calculated inside 145 ml of electrolyte were 0.005mM, 0.05mM, 0.5mM, 1mM, 5mM and 20mM. For the initial lower concentration no interesting feature were found. However when the strength of the model compounds increased different features were observed in the contamination CVs.

The peak at 0.8V during the first cycle of the CV was due to oxidation of DME (dimethoxy ethane, $C_4H_{10}O_2$). The DME comes from the hydrolysis of the DEGEE and it is oxidized at 0.8 to form ethanol, which adsorbs on Pt as a contaminant (112).

The full cyclic voltammetric scans were performed for higher concentrations of the contaminants (0.1 M, 0.5M and 20 mM). In the uncontaminated solution the cyclic voltammogram shows peaks at 0.1 V (hydrogen adsorption/ desorption on Pt (111)), and at 0.85 V (Pt oxidation and Pt-O reduction) which are the key features observed in a CV conducted in 0.1 M perchloric acid. After adding the organic compounds (final concentration in 145 ml perchloric acid being 0.1 M) a peak at 0.8 V (anodic) was observed at the first cycle of the scan. The peak disappears in the consecutive scans and reappears when the concentrations of the organic compounds were increased to 0.5 M (final concentration inside the cell). But when the concentration was increased even more the peak didn't come back. At 20mM concentration, the DEGEE CV showed an interesting feature. No reduction was current observed at 0.8-0.85 V (Pt-O reduction region). The CV after the double layer region shifted above the 0 current, making the entire process contributing to oxidation current. This feature was not observed in case of

DGMEA, although there was an upward shift of the CV after double layer region, not as prominent as seen in case of DEGEE (figure 6.4, 6.5).

The DME electrooxidation occurs through hydrolysis first and then by dissociative adsorption as given below:

The last aliphatic compound tested was Polyethylene Glycol Dimethacrylates (PEG). It is essentially a polymer containing repeating -OCH_2CH_2- (ehtoxy) groups (average molecular weight = 750). This compound showed highest loss in ECA compared to the other compounds.

6.3.5. Effect of aromatics on electrochemical surface area determined by CVs

Four aromatic compounds were tested for their impacts on the Pt/VC catalyst on room temperature. Among them 2,6-diamino toluene (2,6-DAT) or methyl benzenediamine contain $–NH_2$ (amine) group. The amine groups adsorb on the Pt through the lone pair of electrons on N atom. Both are primary amines and are inclined to nucleophilic substitutions. 2,6-DAT has two amine groups attached in the meta positions of the ring. 2,6-DAT has two $–NH_2$ groups, they also bonds with Pt same way. In presence of electron withdrawing group-CH_3, 2-6-DAT molecule is stabilized increasing the basicity. Therefore, in weak acidic medium it reacts and anodical and cathodical peaks centered at around 0.5V was seen due to quinine-hydroquinone reversible reaction of the amine groups (figure 6.7). This peak was also observed in the earlier research with aromatic amines. One sharp peak at 1.05V was observed which is due to oxidation of the quinone-hydroquinone which was produced on Pt. The peak at 0.8V (Pt oxidation on Pt

(111)) was suppressed in presence of contaminants. The recovery showed increase in H_{upd} region, but no recovery in the Pt oxide or reduction regions (113).

The peaks at 0.14 V and 2.2 V which is a common feature of CVs on Pt disappear in presence of contaminant molecules.

The contaminant effects of two aromatic compounds having –OH. For the p-tert butyl phenol the –OH group is directly attached to the aromatic ring, but for benzyl alcohol, the –OH group is attached to the alkyl group, next to the aromatic ring. Due the size of the molecule both of them show almost same loss of ECA. There is a small reversible around 0.65 V.

6.3.6. ECA loss due to contamination

The loss of ECA is higher for the aromatic compounds than aliphatic compounds. Due to addition of two aliphatic compounds 2-(2-ethoxyethoxy) ethanol and 2-(2-ethoxyethoxy) ethanol acetate at high concentration as 20mM, the ECA loss was up to 50 ± 10%. The ECA losses (figure 6.9) in case of aromatics were observed to be steeper than any aliphatics, with an exception of dimethacrylate. It is hypothesized that the loss of ECA depends on the size of the molecules. Since dimethcrylate is a long chain polymer when it adsorbs on Pt it occupies more than one site. It may also be due to affinity of dimethcrylate to fuse together and form longer chains in weak acidic conditions.

6.3.7. Example of recovery of ECA

Recovery was performed by holding the electrode in a clean electrolyte at higher potentials. This helped the contaminant molecules to oxidize and or desorb from the Pt/C electrode surface. Prior to cyclic voltammetric scans, the working electrode was held at

0.75V, 0.85V, 0.95V and 1.05V. The partial scans were started at the potential the WE had been held. With each scan from a higher potential, the electrochemical surface area started recovering gradually (figure 6.10).

6.3.8. Contamination effect on oxygen reduction reaction (ORR) activities of Pt/C

The baseline ORR curve was performed prior to the contamination in a clean O_2 saturated 0.1 M $HClO_4$ at 20 mVs^{-1}, while rotating the working electrode at 1600 rpm. The poisoning was performed in two separate experiments. In the first set of experiments three concentrations (5 x 10^{-6} M, 5 x 10^{-5} M, 5 x 10^{-4} M) of organic contaminant solution were added. In the second set of experiments three higher concentrations (1 x 10^{-3} M, 5 x 10^{-3} M, 2 x 10^{-2} M) of organic contaminant solution were added.

The initial ORR polarization curve had a diffusion limiting current of -5.7 $mAcm^{-2}$. The first scan of ORR at a contaminant concentration of 5x10^{-4} M shows decrease in onset potential and diffusion limiting current. The higher the contamination the diffusion limiting current region loses the feature of the flat region between 0.2 and 0.6 V. Also the current density at 0.9 V decreases with contamination. The diffusion limiting current becomes as low at -3.5 $mAcm^{-2}$, with a similar decrease in current at 0.9V with higher overpotential losses. The recovery scan in the clean electrolyte almost overlaps the baseline scan in the mixed kinetic-diffusion region (0.8 to 1 V) and the diffusion limiting current also increases to -5.4 $mAcm^{-2}$ recovering the flat section at the diffusion controlled region. The decline in diffusion limiting current and current at 0.9 V was the most common feature in the ORR polarization curves after contamination (30).

Aliphatic compounds:

2-(2-ethoxyethoxy) ethanol

The ORR currents after adding 2-(2-ethoxyethoxy) ethanol is given in figure 6.11. No peroxide formation was observed during the ORR experiments.

2-(2-ethoxyethoxy) ethanol acetate

The ORR currents after adding 2-(2-ethoxyethoxy) ethanol acetate is given in figure 6.12. The ORR polarization curves after adding 2-(2-ethoxyethoxy) ethanol acetate show similarities in contamination features of the diffusion limiting currents, current at 0.9 V.

Polyethylene glycol dimethacrylates

The ORR polarization curves after adding polyethylene glycol dimethacrylates is shown in figure 6.13. The limiting current between 0.3 to 0.5 V and the current at 0.9 V decreased and the ORR changed from 4 electrons to 2 electrons pathway producing peroxide. This peroxide was detected in the ring of a ring disk electrode and the fraction of peroxide formation increased with potential. This feature is unique to the polymer and was not observed in case of the two ethoxy compounds tested earlier. The correlation between the ECA loss and ORR currents observed during the contamination experiment is given in table 6.4.

Aromatic compounds

2,6 DAT or dimethyl toluene

The ORR polarization curves after adding 2,6 diamine toluene is shown in figure 6.14. The limiting current between 0.3 to 0.5 V and the current at 0.9 V decreased and the

ORR changed from 4 electrons to 2 electrons pathway producing peroxide. This peroxide was detected in the ring of a ring disk electrode and the fraction of peroxide formation increased with potential. This feature is unique to the polymer and was not observed in case of the other aromatic compounds tested earlier.

The correlation between the ECA loss and ORR currents observed during the contamination experiment is given in table 6.5.

Benzyl Alcohol

The initial ORR curve has a well-defined diffusion limiting current region between 0.2 and 0.6 V, followed by a kinetic-mass controlled region with a current 2.4 $mAcm^{-2}$ (corrected for oxygen partial pressure) at 0.9 V. Post-contamination, the current at 0.9 V and limiting current decreases as shown in figure 6.15.

p-tert butyl alcohol

The initial ORR curve has a well-defined diffusion limiting current region between 0.2 and 0.6 V, followed by a kinetic-mass controlled region with a current 2.4 $mAcm^{-2}$ (corrected for oxygen partial pressure) at 0.9 V. Post-contamination, the current at 0.9 V and limiting current decreases as shown in figure 6.16, as observed in case of benzyl alcohol. No significant amount of peroxide was detected above 0.3 V for either of benzyl alcohol or p-tert butyl alcohol.

6.4. Conclusions

This study showed that contaminants found in the leachants used in PEM fuel cell have detrimental effect of ORR activities and ECA. Analytical diagnostic tools were used

to qualitatively determine the organic components of the one week soak of the assembly aids at elevated temperature. Even though the organic indentified in via GCMS and other techniques are not documented to be present in the assembly aids, the possible explanation of existence of trace amount of organics in the leachants can be explained from the starting materials and process of synthesis. The effects of contaminants are three fold. In addition to reducing the catalyst area available for electrochemical reactions, it reduces the activities (mass and area specific) leads to performance loss and long term poisoning can lead to membrane degradation and ultimately failure of a fuel cell stack. Also the manufacturing cost of the stack increases if the assembly aids are to be specifically designed for fuel cells instead of "cheaper" off-the-shelf materials which are commercially available for use in more than one industry.

The testing of some of the very common organic compounds resulting from the degradation of the additives, monomers, fillers, antioxidants etc used in the assembly aids, gives an insight on the overall poisoning mechanism. The ORR activities decreases, resulting in poor catalyst utilization in an operating fuel cell.

The organic compounds tested were both aromatic and aliphatic. The aromatic compounds with strong nuclephilic groups (like $-NH_2$) adsorb on the Pt with N atoms or the aromatic ring (pi-bonds) and ECA loss depends on the size or the bulk of the molecule. The aliphatic compounds tested contained ethoxy group. The oxygen atom of the ethoxy group is very reactive as it has two lone pairs of electrons. For that reason, the highest amount of contamination was observed when polyethylene glycol dimethacrylates which contains repetitive chains of ethoxy groups.

The recovery procedure recommended that holding at higher potential can recover the lost ECA as the adsorbing molecules desorbed from the Pt sites at higher voltages. Therefore potential cycling to a higher voltage may be a promising technique for removing contamination from a fuel cell. Also cleaning the catalyst with DI water can partially recover the lost surface area.

Table 6.1. Organic (aromatic and aliphatic) compounds aids tested in this paper identified using GCMS in the leachates of the assembly

Chemical Description	Name	GCMS: Liquids				TOC (ppm)
Urethane	3M® 4000 fast cure white	A	B	C	D	1280
Silicone	3M® # 8664 black	A	B	C		197
Urethane	Loctite® 39916	E	F	D		266
Acrylic	Loctite® # 567	G	H	I		750
Epoxy	Reltek® Bond-IT B45	C	J	K		1695
PFAE/PTFE	Krytox® XHT-SX	None Detected				10

A = Ethanol, 2-(2-ethoxyethoxy)

B = Ethanol, 2-(2-ethoxyethoxy)-acetate

C = Benzyl Alcohol

D = Methyl-Benzenediamine

E = p-toluenesesulfonamide

F = Butyric acid N'-m-tolyl-hydrazide

G = 2-Propenoic acid

H = 2,2'-[oxybis(2,1-ethanediyloxy)]bis-Ethanol

I = Diethylene glycol dimethacrylate

J = [p or m]-tert-butyl- Phenol

K = Benzaldehyde

Table 6.2. Analysis of current and ECA loss to demonstrate the effect of contamination due to addition of 2-(2-ethoxyethoxy) ethanol. Platinum ECSAs and ORR currents determined before and after contamination, for thin films of 46 wt.%Pt/VC, 17.4 μgPt cm^{-2}, 0.1M $HClO_4$, 25°C.

	i_{lim}	Available i_{lim} %	$i_{0.9V}$	Available $i_{0.9V}$ %	Available ECA %	Ionomer effect
baseline	5.9	100	2.4	100	100	0
1E-3 M	5.1	86	1.3	52	53	1
5E-3 M	4.8	82	1.2	49	49	1
2E-2 M	4.5	75	1.0	42	48	6
recovery	5.3	90	1.9	78	78	0

Table 6.3. Analysis of current and ECA loss to demonstrate the effect of contamination due to addition of 2-(2-ethoxyethoxy) ethanol acetate. Platinum ECSAs and ORR currents determined before and after contamination, for thin films of 46 wt.%Pt/VC, 17.4 μgPt cm^{-2}, 0.1M $HClO_4$, 25°C

	i_{lim}	Available i_{lim} %	$i_{0.9V}$	Available $i_{0.9V}$ %	Available ECA %	Ionomer effect
baseline	6	100	2.5	100	100	0
1E-3 M	4.9	82	1.3	52	53	1
5E-3 M	4.8	80	1.2	48	50	2
2E-2 M	4.3	72	1.0	40	43	3
recovery	5.3	88	1.8	71	71	0

Table 6.4. Analysis of current and ECA loss to demonstrate the effect of contamination due to addition of PEG dimethacrylate. Platinum ECSAs and ORR currents determined before and after contamination, for thin films of 46 wt.%Pt/VC, 17.4 μgPt cm^{-2}, 0.1M $HClO_4$, 25°C

	i_{lim}	Available i_{lim} %	$i_{0.9V}$	Available $i_{0.9V}$ %	Available ECA %	Ionomer effect
baseline	5.8	100	2.10	100	100	0
1E-3 M	4	69	0.54	26	31	5
5E-3 M	3.6	62	0.32	15	28	12
2E-2 M	3	52	0.26	12	26	14
recovery	4.35	75	1.06	48	50	2

Table 6.5. Analysis of current and ECA loss to demonstrate the effect of contamination due to addition of 2,6-DAT. Platinum ECSAs and ORR currents determined before and after contamination, for thin films of 46 wt.%Pt/VC, 17.4 μgPt cm^{-2}, 0.1M $HClO_4$, 25°C.

	i_{lim}	Available i_{lim} %	$i_{0.9V}$	Available $i_{0.9V}$ %	Available ECA %	Ionomer effect
baseline	5.8	100	2	100	100	0
1E-3 M	4.5	77	0.8	37	38	1
5E-3 M	3.6	62	0.4	20	33	13
2E-2 M	2.8	48	0.0	2	32	30
recovery	4.7	81	0.8	40	43	3

Table 6.6. Analysis of current and ECA loss to demonstrate the effect of contamination due to addition of benzyl alcohol. Platinum ECSAs and ORR currents determined before and after contamination, for thin films of 46 wt.%Pt/VC, 17.4 μgPt cm^{-2}, 0.1M $HClO_4$, 25°C

	i_{lim}	Available i_{lim} %	$i_{0.9V}$	Available $i_{0.9V}$ %	Available ECA %	Ionomer effect
baseline	5.9	100	2	100	100	0
1E-3 M	4.3	73	0.7	35	44	9
5E-3 M	3.8	64	0.6	32	41	9
2E-2 M	3.5	60	0.6	28	38	10
recovery	5.3	90	1.4	70	67	-3

Table 6.7. Analysis of current and ECA loss to demonstrate the effect of contamination due to addition of p-tert butl alcohol. Platinum ECSAs and ORR currents determined before and after contamination, for thin films of 46 wt.%Pt/VC, 17.4 μgPt cm−2, 0.1M $HClO_4$, 25°C

	i_{lim}	Availabl e i_{lim} %	$i_{0.9V}$	Availabl e $i_{0.9V}$ %	Availabl e ECA %	Ionomer effect
baseline	5.9	100	2.1	100	100	0
1E-3 M	4.3	73	1.0	48	48	0
5E-3 M	4.0	68	0.8	37	44	7
2E-2 M	2.9	49	0.7	31	41	10
recovery	5.3	90	1.7	79	79	0

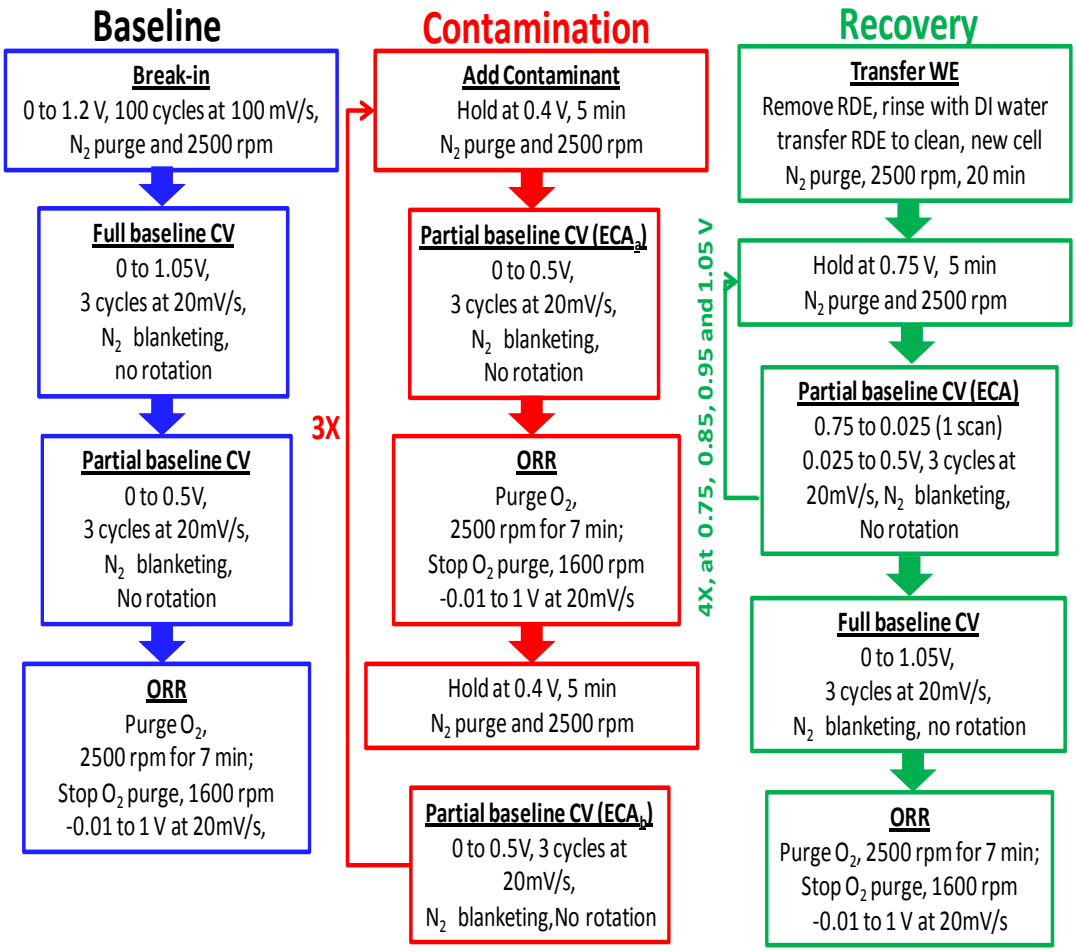

Figure 6.1. Schematic of the experimental protocol to investigate the impact of the organic contaminants found in the 1 week DI water soak of the assembly aids used in a PEM fuel cell, on loss of ECA and ORR activities of Pt/VC using three electrodes TF-RDE at room temperature.

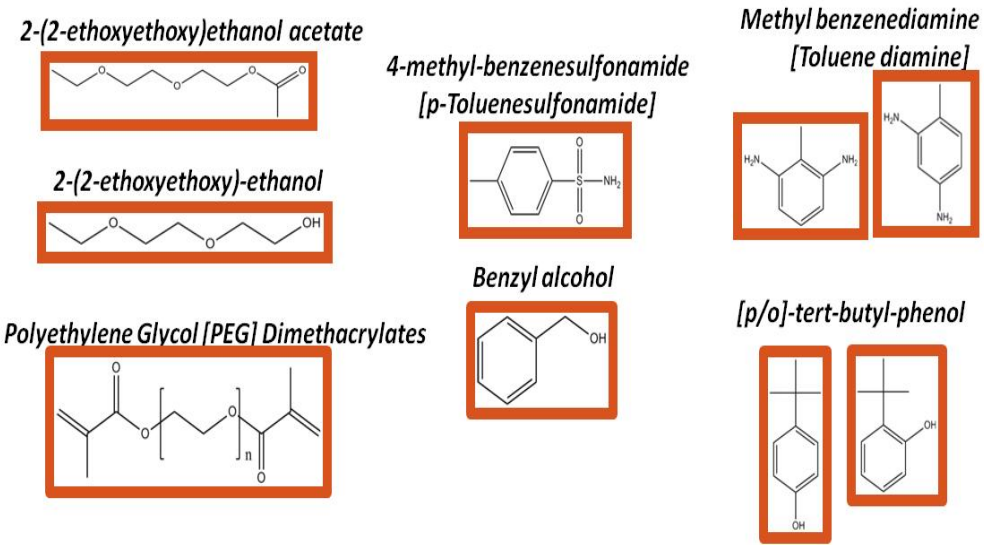

Figure 6.2. Structures of the organic compounds studied in this paper

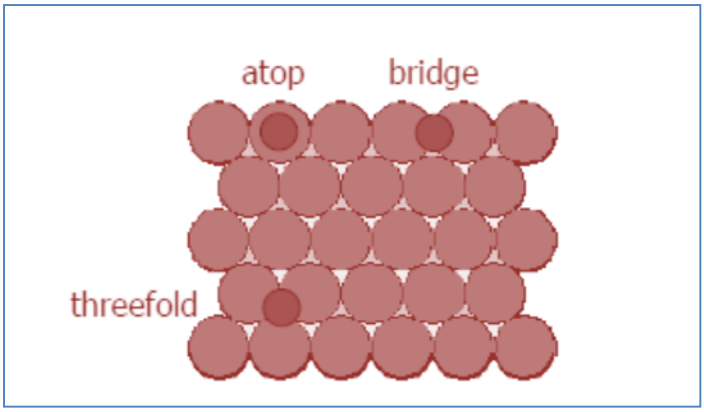

Figure 6.3. Schematic of the configurations of the adsorbed organic molecule on the Pt nanoparticles (Pt (111)).

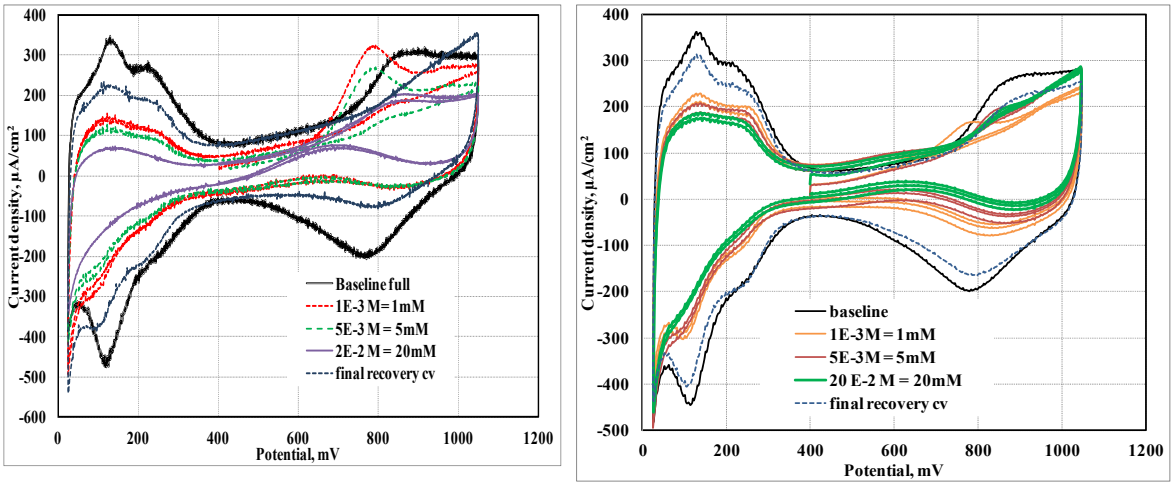

Figure 6.4. Example of the change in surface coverage by 2-(2-ethoxyethoxy) ethanol, and 2-(2-ethoxyethoxy) ethanol acetate (loss of ECA due to adsorption of contaminant molecules on Pt sites) with CV cycles from 0.025 to 1.05 V at a scan rate of 20 mV/s as measured under the H_{upd} normalized by initial available surface in the clean electrode.

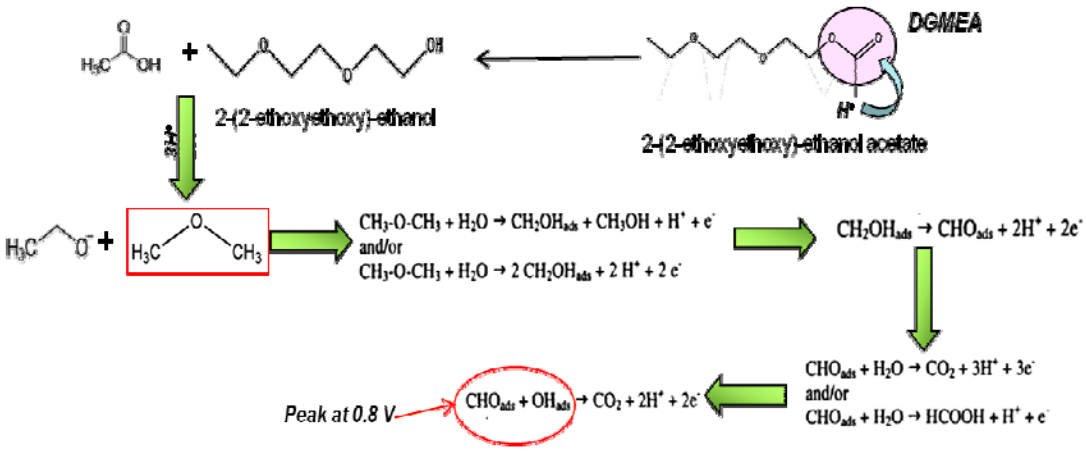

Figure 6.5. The peak at 0.8 V is a characteristic feature of both 2-(2-ethoxyethoxy) ethanol, and 2-(2-ethoxyethoxy) ethanol acetate, which is attributed to the adsorption of –CHO species on Pt after following a series of steps involving electrochemical reactions

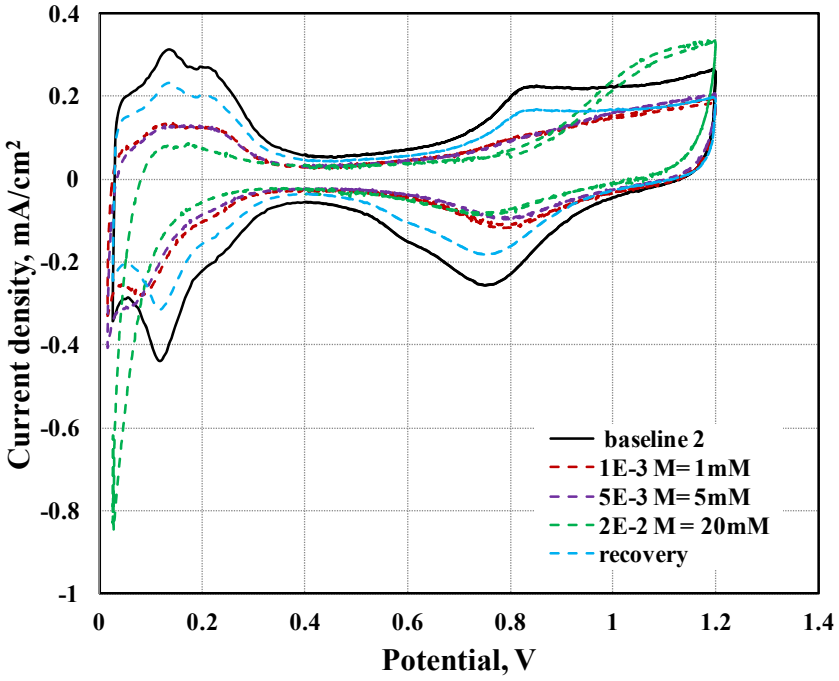

Figure 6.6. The effect of polyethylene glycol dimethacrylates (loss of ECA due to adsorption of contaminant molecules on Pt sites) with CV cycles from 0.025 to 1.05 V at a scan rate of 20 mV/s as measured under the H_{upd} normalized by initial available surface in the clean electrode.

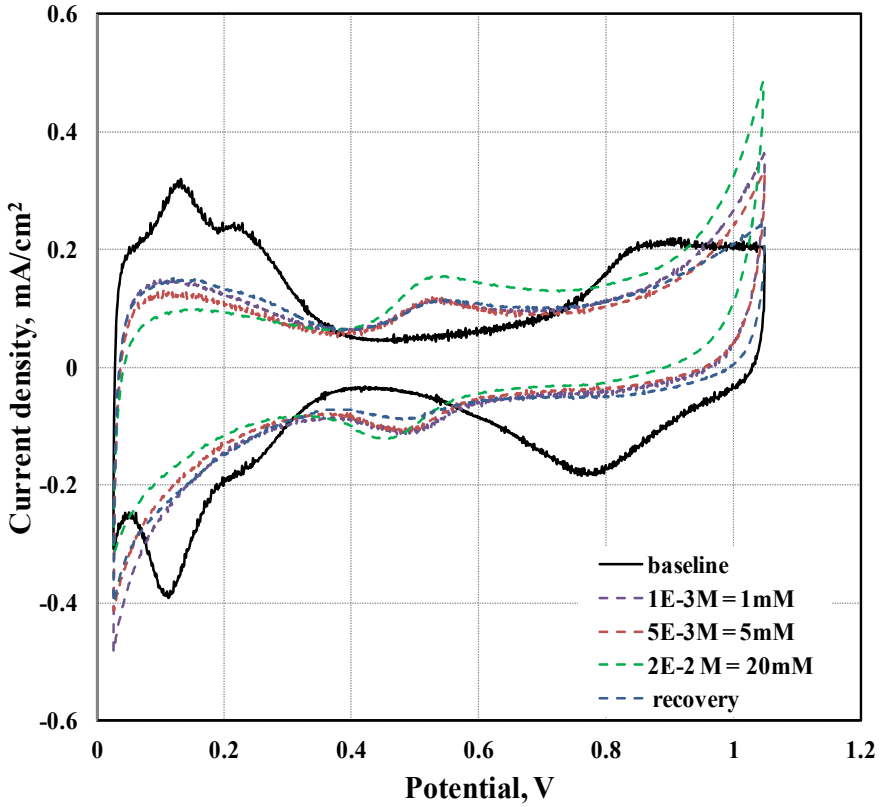

Figure 6.7. Example of effect of 2,6-DAT (loss of ECA due to adsorption of contaminant molecules on Pt sites) with CV cycles from 0.025 to 1.05 V at a scan rate of 20 mV/s as measured under the H_{upd} normalized by initial available surface in the clean electrode

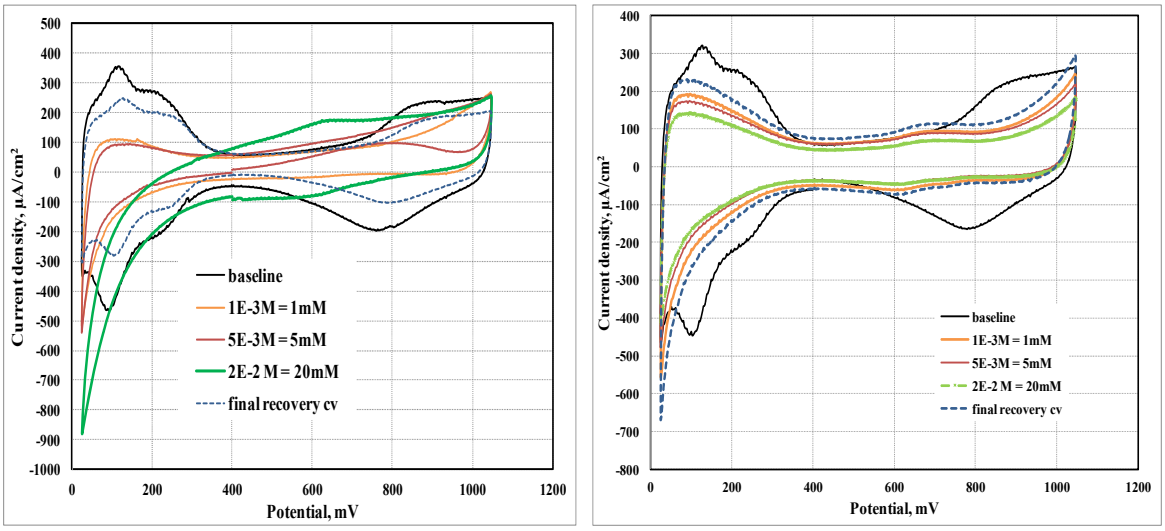

Figure 6.8. Example of the change in surface coverage by benzyl alcohol and p-tert butyl phenol (loss of ECA due to adsorption of contaminant molecules on Pt sites) with CV cycles from 0.025 to 1.05 V at a scan rate of 20 mV/s as measured under the H_{upd} normalized by initial available surface in the clean electrode.

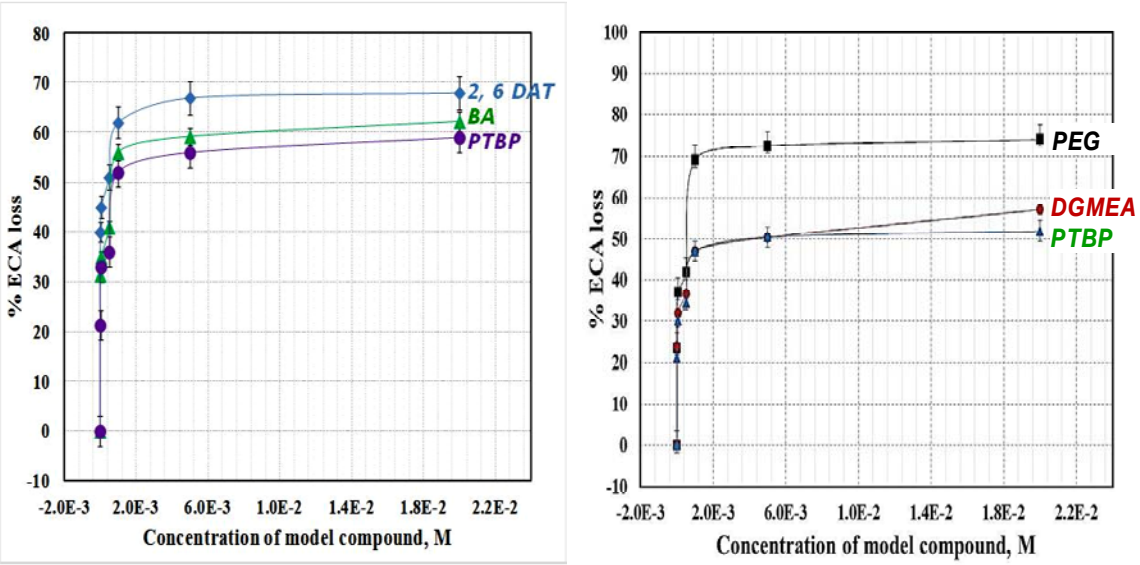

Figure 6.9. The ECS loss after adding organic compounds in the RDE electrolyte.

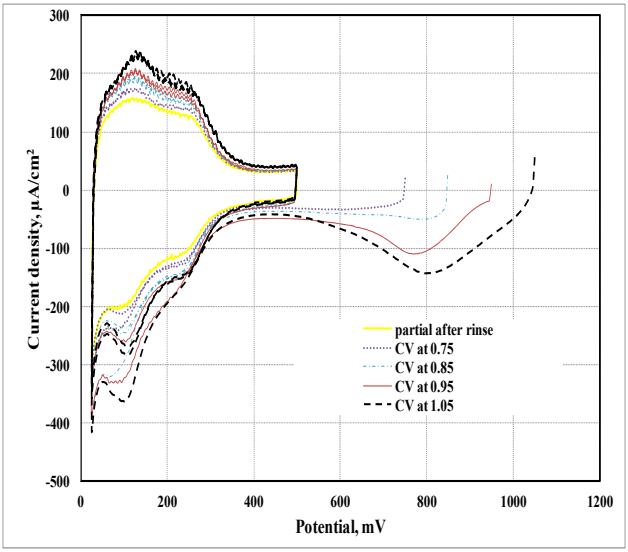

Figure 6.10. Recovery CV at room temperature after contaminating with 20 mM of DEGEE using partial scans from 0.75, 0.85, 0.95 and 1.05 V at 20 mVs^{-1}.

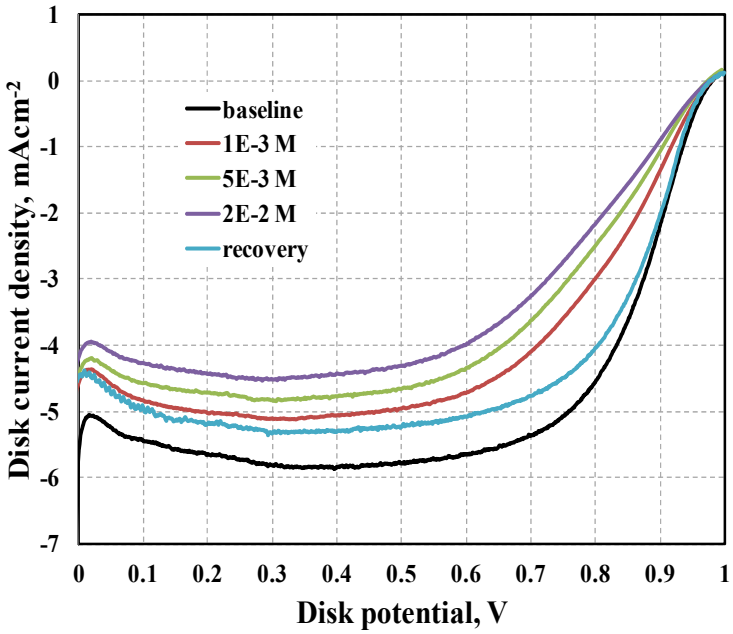

Figure 6.11. ORR polarization curves on a Pt/VC working electrode at different concentrations of 2-(2-ethoxyethoxy) ethanol after pre-reducing the Pt at 0.4 V for 400 s. The "baseline" curve denotes uncontaminated polarization curve.

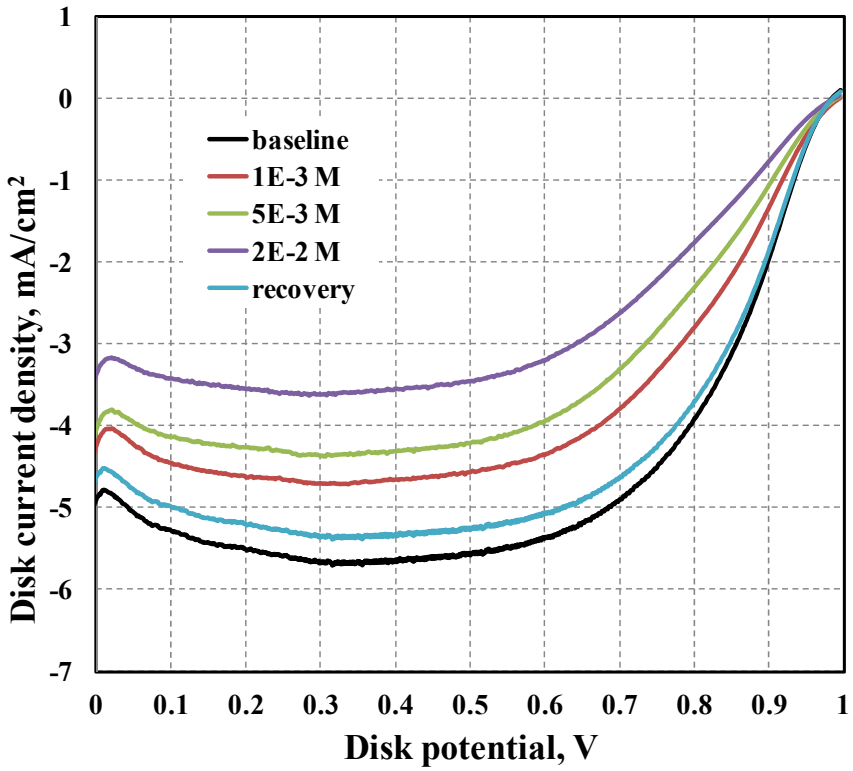

Figure 6.12. ORR polarization curves on a Pt/VC working electrode at different concentrations of 2-(2-ethoxyethoxy) ethanol acetate after pre-reducing the Pt at 0.4 V for 400 s. The "baseline" curve denotes uncontaminated polarization curve.

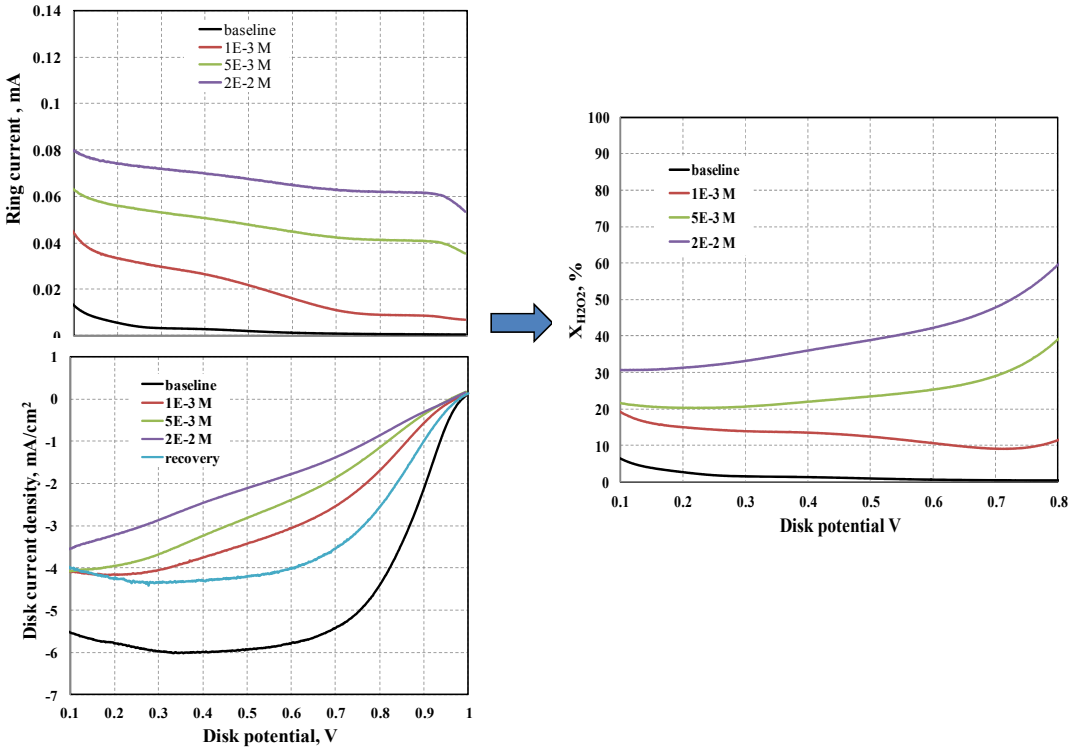

Figure 6.13. ORR polarization curves on a Pt/VC working electrode at different concentrations of polyethylene glycol dimethacrylates after pre-reducing the Pt at 0.4 V for 400 s. The "baseline" curve denotes uncontaminated polarization curve.

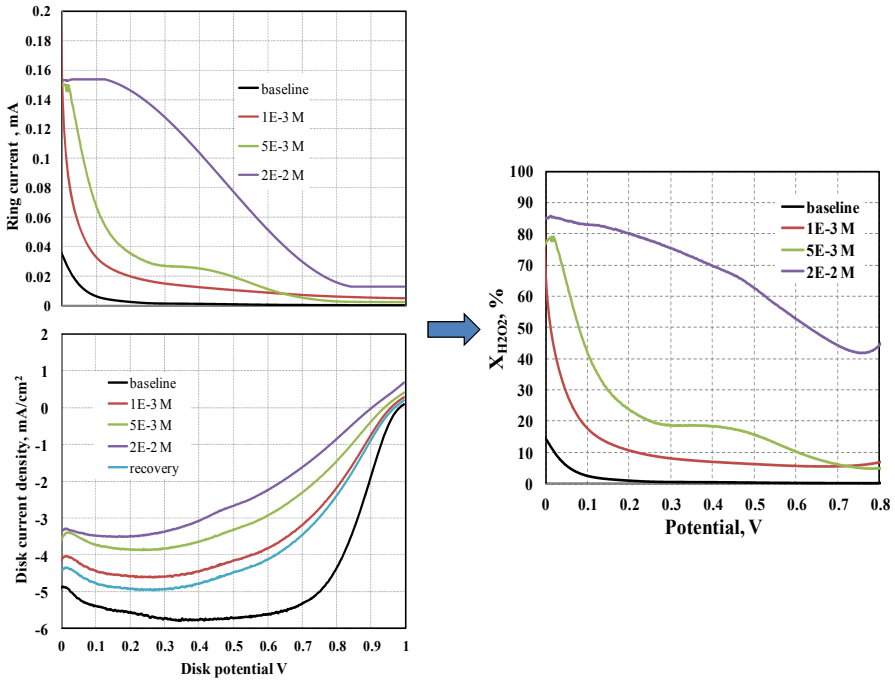

Figure 6.14. ORR polarization curves on a Pt/VC working electrode at different concentrations of 2,6-DAT after pre-reducing the Pt at 0.4 V for 400 s at room temperature. The "baseline" curve denotes uncontaminated polarization curve.

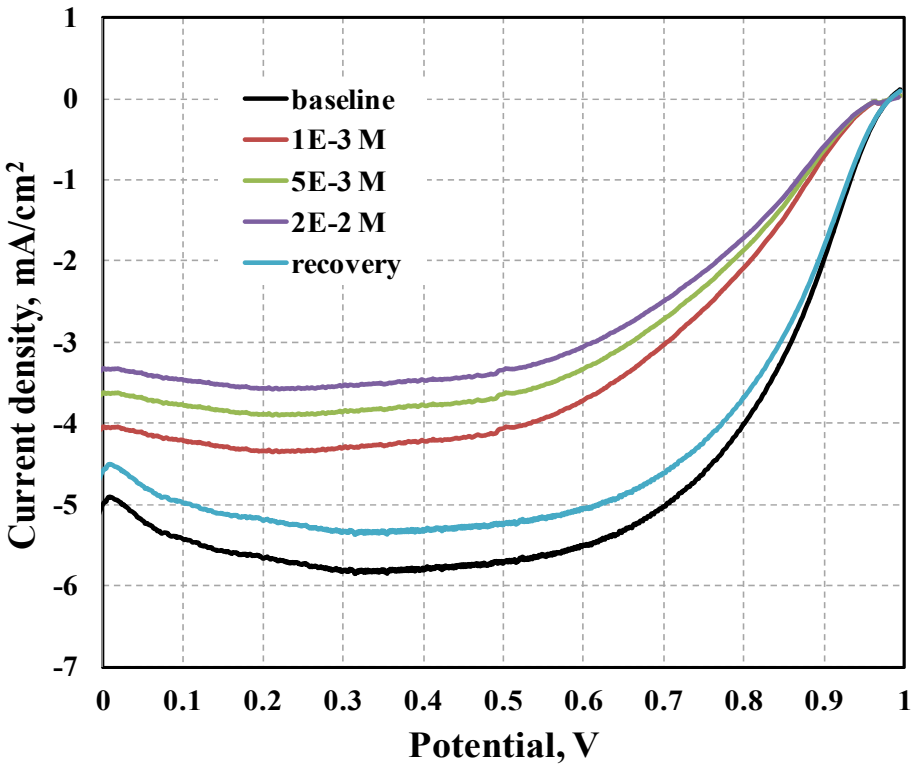

Figure 6.15. ORR polarization curves on a Pt/VC working electrode at different concentrations of benzyl alcohol after pre-reducing the Pt at 0.4 V for 400 s at room temperature. The "baseline" curve denotes uncontaminated polarization curve.

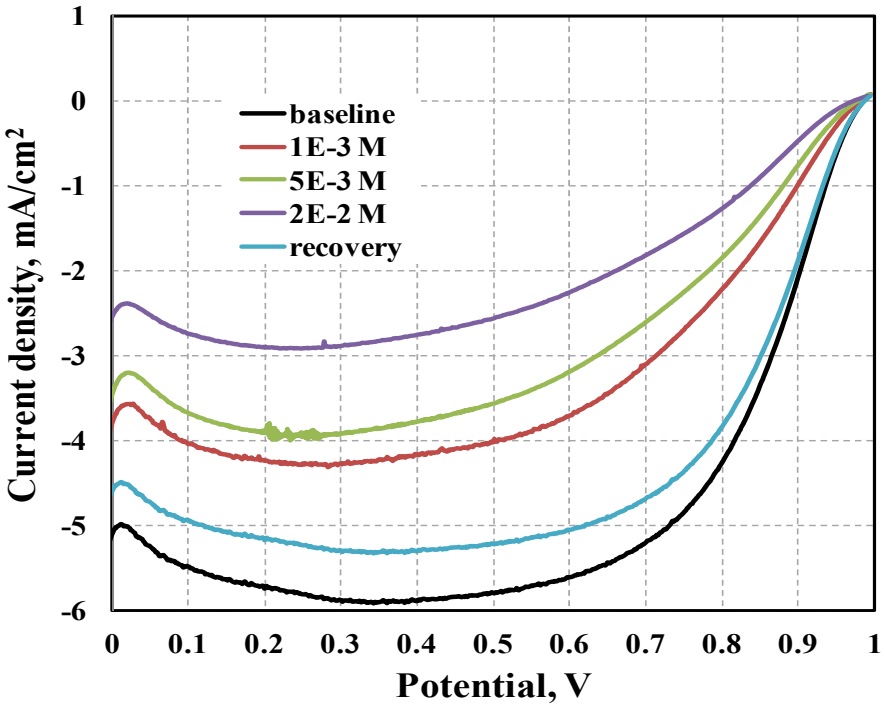

Figure 6.16. ORR polarization curves on a Pt/VC working electrode at different concentrations of p-tert butyl alcohol after pre-reducing the Pt at 0.4 V for 400 s at room temperature. The "baseline" curve denotes uncontaminated polarization curve.

References

1. H. Dinh, in *2010 Annual Merit Review and Peer Evaluation Meeting* (2010).

2. D. Papageorgopoulos, T. G. Benjamin, J. P. Kopasz and W. Podolski, *ECS Transactions*, **30**, 3 (2011).

3. R. Bashyam and P. Zelenay, *Nature*, **443**, 63 (2006).

4. F. Barbir, *PEM fuel cells: theory and practice*, Academic Press (2012).

5. H. A. Gasteiger, S. S. Kocha, B. Sompalli and F. T. Wagner, *Applied Catalysis B: Environmental*, **56**, 9 (2005).

6. A. Dicks and J. Larminie, Fuel cell systems explained, in, John Wiley & Sons (2000).

7. B. K. Gross, I. J. Sutherland and H. Mooiweer, *Hydrogen fueling infrastructure assessment*, General Motors Corporation, Research & Development Center (2007).

8. http://www.scientific-computing.com/features/feature.php?feature_id=126, in.

9. T. A. Zawodzinski Jr, T. E. Springer, F. Uribe and S. Gottesfeld, *Solid State Ionics*, **60**, 199 (1993).

10. A.-L. Rollet, O. Diat and G. Gebel, *The Journal of Physical Chemistry B*, **106**, 3033 (2002).

11. H. Li, S. Knights, Z. Shi, J. W. Van Zee and J. Zhang, *Proton Exchange Membrane Fuel Cells: Contamination and Mitigation Strategies*, CRC Press (2010).

12. J. Zhang, Y. Tang, C. Song, J. Zhang and H. Wang, *Journal of power sources*, **163**, 532 (2006).

13. J. Newman and K. E. Thomas-Alyea, Electrochemical systems. 2004, in, John Wiley and Sons, Inc., Hoboken, New Jersey.

14. L. R. F. Allen J. Bard, Electrochemical Methods: Fundamentals and Applications, in, 2nd ed., John Wiley & Sons (2010).

15. O. A. Baturina, Y. Garsany, B. D. Gould and K. E. Swider-Lyons, in *PEM Fuel Cell Failure Mode Analysis*, X. Z. Yuan Editor, p. 199, CRC Press (2011).

16. B. D. Gould, O. A. Baturina and K. E. Swider-Lyons, *Journal of Power Sources*, **188**, 89 (2009).

17. N. L. Zamel, X., *Progress in Energy and Combustion Science*, **30**, 1 (2010).

18. M. Steele, Information Report on the Development of a Hydrogen Quality Guideline for Fuel Cell Vehicles. Society of Automobile Engineers, in, SAE (2011).

19. T. Rockward, I. Urdampilleta, F. Uribe and F. Garzon, in *Meeting Abstracts*, p. 444 (2007).

20. B. Pivovar, B. Kienitz, T. Rockward, F. Uribe and F. Garzon, (2010).

21. B. D. Gould, G. Bender, K. Bethune, S. Dorn, O. A. Baturina, R. Rocheleau and K. E. Swider-Lyons, *Journal of the Electrochemical Society*, **157**, B1569 (2010).

22. X. Cheng, Z. Shi, N. Glass, L. Zhang, J. J. Zhang, D. T. Song, Z. S. Liu, H. J. Wang and J. Shen, *Journal of Power Sources*, **165**, 739 (2007).

23. N. Zamel and X. Li, *Progress in Energy and Combustion Science*, **37**, 292 (2011).

24. O. A. Baturina, B. D. Gould, Y. Garsany and K. E. Swider-Lyons, *Electrochimica Acta*, **55**, 6676 (2010).

25. T. Okada, H. Satou, M. Okuno and M. Yuasa, *The Journal of Physical Chemistry B*, **106**, 1267 (2002).

26. O. Baturina and K. Swider-Lyons, *Journal of The Electrochemical Society*, **156**, B1423 (2009).

27. R. Halseid, P. J. Vie and R. Tunold, *Journal of the electrochemical society*, **151**, A381 (2004).

28. T. Okada, *Handbook of fuel cells* (2010).

29. T. Okada, N. Nakamura, M. Yuasa and I. Sekine, *Journal of the Electrochemical Society*, **144**, 2744 (1997).

30. Y. D. Garsany, S.; Sweider-Lyons, K. E., *Journal of Power Sources*, **216**, 515 (2012).

31. K. O'Leary, M. Budinski and B. Lakshmanan, in *NRC-CNRC Workshop* (2009).

32. H. L. Wang, C. S. Macomber, K. O'Neil, G. Bender, B. Pivovar, R. Reid, B. Lakshmanan, K. O'Leary, M. Das, M. Ohashi, J. W. Van Zee and H. N. Dinh, *Abstr Pap Am Chem S*, **242** (2011).

33. K. E. Swider and D. R. Rolison, *Journal of The Electrochemical Society*, **143**, 813 (1996).

34. M. J. Martínez-Rodríguez, E. B. Fox, W. D. Rhodes, C. S. McWhorter, S. Greenway and H. R. Colón-Mercado, *Journal of The Electrochemical Society*, **158**, B698 (2011).

35. H. Wang, S. Coombs, C. Macomber, K. O'Neill, G. Bender, B. Pivovar and H. N. Dinh, *ECS Transactions*, **33**, 1617 (2010).

36. D. Papageorgopoulos, in *Annual Merit Review*, Washington D. C. (2011).

37. http://www.pineinst.com/echem/viewproduct.asp?ID=45651,

38. F. Garzon, E. Brosha, B. Pivovar, T. Rockward, F. Uribe, I. Urdampilleta and J. Valerio, *Annual Progress Report, DOE Hydrogen Program, US Department of Energy, Washington, DC*, 905 (2006).

39. Y. Nagahara, S. Sugawara and K. Shinohara, *Journal of Power Sources*, **182**, 422 (2008).

40. R. Mohtadi, W. k. Lee, S. Cowan, J. W. Van Zee and M. Murthy, *Electrochemical and Solid-State Letters*, **6**, A272 (2003).

41. T. Okada, in *Polymer Electrolyte Fuel Cell Durability*, F. N. Büchi, M. Inaba and T. J. Schmidt Editors, p. 323, Springer New York (2009).

42. H. J. Soto, W.-k. Lee, J. Van Zee and M. Murthy, *Electrochemical and solid-state letters*, **6**, A133 (2003).

43. J. J. Pietron and K. E. Swider-Lyons, *ECS transactions*, 103 (2006).

44. R. Mohtadi, W. K. Lee and J. W. Van Zee, *Journal of Power Sources*, **138**, 216 (2004).

45. F. Xiea, Z.-G. Shao, G. Zhanga, J. Zhaia, W. Lua, X. Qina, W. Linc and B. Yi, *Electrochimica Acta*, **67**, 50 (2012).

46. B. Kienitz, B. Pivovar, T. Zawodzinski and F. H. Garzon, *Journal of the Electrochemical Society*, **158**, B1175 (2011).

47. U. A. Paulus, T. J. Schmidt, H. A. Gasteiger and R. J. Behm, *Journal of Electroanalytical Chemistry*, **495**, 134 (2001).

48. W. Vielstich, *Handbook of Fuel Cells*, John Wiley and Sons (2003).

49. H. A. Gasteiger, S. S. Kocha, B. Sompalli and F. T. Wagner, *Appl Catal B-Environ*, **56**, 9 (2005).

50. N. M. Markovic, H. A. Gasteiger and N. Philip, *journal of physical chemistry*, **100**, 6715 (1996).

51. N. M. Markovic and P. N. Ross, *Surf Sci Rep*, **45**, 121 (2002).

52. U. A. Paulus, A. Wokaun, G. G. Scherer, T. J. Schmidt, V. Stamenkovic, N. M. Markovic and P. N. Ross, *Electrochimica Acta*, **47**, 3787 (2002).

53. N. M. Markovic, H. A. Gasteiger and P. N. Ross, *Journal of Physical Chemistry*, **99**, 3411 (1995).

54. Y. S. Garsany, I. L.; Sweider-Lyons, K. E., *Journal of Electroanalytical Chemistry*, **662**, 396 (2011).

55. N. M. Markovic, T. J. Schmidt, V. Stamenkovic and P. N. Ross, *fuel cells*, **1**, 105 (2001).

56. M. Chen, C. Du, J. Zhang, P. Wang and T. Zhu, *Journal of Power Sources*, **196**, 620 (2011).

57. B. James, in *2012 US DOE Annual Merit Review and Peer Evaluation Meeting, FC018, Washington, DC* (2012).

58. K. E. Swider-Lyons, *Journal of Physical Chemistry* (2010).

59. M. Das, K. C. Neyerlin, H. Dinh and J. W. V. Zee, *Electrochimica Acta* (2013).

60. F. A. Uribe, S. Gottesfeld and T. A. Zawodzinski, *Journal of the Electrochemical Society*, **149**, A293 (2002).

61. T. Okada, H. Satou and M. Yuasa, *Langmuir*, **19**, 2325 (2003).

62. T. J. Schmidt, U. A. Paulus, H. A. Gasteiger and R. J. Behm, *Journal of Electroanalytical Chemistry*, **508**, 41 (2001).

63. Y. Garsany, O. A. Baturina and K. E. Swider-Lyons, *Journal of The Electrochemical Society*, **154**, B670 (2007).

64. K. A. O'Leary;, R. Reid; and B. Lakshmanan, in *ECS Meeting*, Boston, MA (2011).

65. W. Vielstich, *Handbook of fuel cells-fundamentals, Technology and applications*, **2**, 155 (2003).

66. D. Pillay, Johannes, M. D. , Y. Garsany and K. E. Swider-Lyons, *J Phys Chem C*, **114**, 7822 (2010).

67. J. St-Pierre, in *Polymer Electrolyte Fuel Cell Durability*, F. N. Büchi, M. Inaba and T. J. Schmidt Editors, p. 289, Springer New York (2009).

68. C. S. Macomber, H. Wang, K. O'Neill, J. Christ, G. Bender, B. Pivovar and H. N. Dinh, *Abstr Pap Am Chem S*, **242** (2011).

69. C. Macomber, H. Wang, K. O'Neill, S. Coombs, G. Bender, B. Pivovar and H. N. Dinh, *ECS Transactions*, **33**, 1637 (2010).

70. M. Das, in *Department of Chemical Engineering*, University of South Carolina (2013).

71. D. Tripkovic, D. Strmcnik, D. Van der Vliet, V. Stamenkovic and N. Markovic, *Faraday discussions*, **140**, 25 (2009).

72. J. X. U. Wang, F. A.; Springer, T. E.; Zhang, J; Adzic, R. R., *Faraday discussions*, **140** (2008).

73. Y. Garsany, O. A. Baturina, K. E. Swider-Lyons and S. S. Kocha, *Anal Chem*, **82**, 6321 (2010).

74. I. Takahashi and S. S. Kocha, *Journal of Power Sources*, **195**, 6312 (2010).

75. M. Uchimura, S. Sugawara, Y. Suzuki, J. Zhang and S. S. Kocha, *ECS Transactions*, **16**, 225 (2008).

76. S. S. Kocha, in *Polymer Electrolyte Fuel Cell Degradation*, M. M. Mench; E. C. Kumbur; T. N. Veziroglu Editor, p. 89 (2012).

77. K. J. J. Mayrhofer, D. Strmcnik, B. B. Blizanac, V. Stamenkovic, M. Arenz and N. M. Markovic, *Electrochimica Acta*, **53**, 3181 (2008).

78. K. Neyerlin, W. Gu, J. Jorne and H. A. Gasteiger, *Journal of the Electrochemical Society*, **153**, A1955 (2006).

79. R. Mohtadi, W. K. Lee, S. Cowan, J. W. Van Zee and M. Murthy, *Electrochem Solid St*, **6**, A272 (2003).

80. H. J. Soto, W. K. Lee, J. W. Van Zee and M. Murthy, *Electrochemical and Solid State Letters*, **6**, A133 (2003).

81. V. R. Stamenkovic, B. Fowler, B. S. Mun, G. F. Wang, P. N. Ross, C. A. Lucas and N. M. Markovic, *Science*, **315**, 493 (2007).

82. K. E. Swider-Lyons, *ecs transactions* (2006).

83. C. S. Macomber, J. Christ, H. Wang, B. S. Pivovar and H. N. Dinh, in *Meeting Abstracts*, p. 1292 (2012).

84. J. Zhang, *PEM fuel cell electrocatalysts and catalyst layers: fundamentals and applications*, Springer (2008).

85. B. B. Blizanac, V. Stamenkovic and N. M. Markovic, *Z Phys Chem*, **221**, 1379 (2007).

86. R. Mohtadi, W. K. Lee and J. W. Van Zee, *Appl Catal B-Environ*, **56**, 37 (2005).

87. R. Subbaraman, D. Strmcnik, V. Stamenkovic and N. M. Markovic, *J Phys Chem C*, **114**, 8414 (2010).

88. W. G. Pell, A. Zolfaghari and B. E. Conway, *Journal of Electroanalytical Chemistry*, **532**, 13 (2002).

89. P. Wang, Z. Ma, Z. Zhao and L. Jia, *Journal of Electroanalytical Chemistry*, **611**, 87 (2007).

90. J. Maruyama and I. Abe, *Journal of Electroanalytical Chemistry*, **545**, 109 (2003).

91. Y. Garsany, O. A. Baturina and K. E. Swider-Lyons, *Journal of The Electrochemical Society*, **156**, B848 (2009).

92. A. M. Damjanovic, O.J.; Srinivasan, S, *Electrochemistry in Transition, From the 20th to the 21st Century*, Plenum Press (1992).

93. R. Halseid, T. Bystron and R. Tunold, *Electrochimica Acta*, **51**, 2737 (2006).

94. J. X. Wang, N. M. Markovic and R. R. Adzic, *J Phys Chem B*, **108**, 4127 (2004).

95. J. J. Baschuk and X. G. Li, *International Journal of Energy Research*, **25**, 695 (2001).

96. H. Wang, X.-Z. Yuan and H. Li, *PEM Fuel Cell Diagnostic Tools*, CRC PressI Llc (2011).

97. F. Barbir, *PEM Fuel Cells Theory and practice* Elesvier Academic Press (2005).

98. F. N. Jing, M. Hou, W. Y. Shi, J. Fu, H. M. Yu, P. W. Ming and B. L. Yi, *Journal of Power Sources*, **166**, 172 (2007).

99. K. Punyawudho, J. R. Monnier and J. W. Van Zee, *Langmuir*, **27**, 3138 (2011).

100. J. X. Zhai, M. Hou, H. B. Zhang, Z. M. Zhou, J. Fu, Z. G. Shao and B. L. Yi, *Journal of Power Sources*, **196**, 3172 (2011).

101. W. K. Lee, J. W. Van Zee and M. Murthy, *Fuel Cells*, **3**, 52 (2003).

102. M. Ciureanu and H. Wang, *J New Mat Electr Sys*, **3**, 107 (2000).

103. M. Murthy, M. Esayian, W. K. Lee and J. W. Van Zee, *Journal of the Electrochemical Society*, **150**, A29 (2003).

104. H. A. Gasteiger, *Journal of Electroanalytical Chemistry* (2001).

105. N. M. Marković, *Faraday discussions* (2008).

106. V. Stamenkovic, N. M. Markovic and P. N. Ross, *Journal of Electroanalytical Chemistry*, **500**, 44 (2001).

107. P. Rama, R. Chen and J. Andrews, *Proceedings of the Institution of Mechanical Engineers, Part A: Journal of Power and Energy*, **222**, 421 (2008).

108. K. Hongsirikarn, J. G. Goodwin Jr, S. Greenway and S. Creager, *Journal of Power Sources*, **195**, 7213 (2010).

109. C. S. M. J. C. H. W. B. P. H. N. Dinh, *ECS Transactions* (2012).

110. R. L. Behrens, Electrochemical and spectroscopic interfacial investigations of small organic molecule electrooxidation on platinum electrodes, in *Chemistry*, University of Illinois at Urbana-Champaign (2010).

111. A. Santasalo, Electrocatalysis of organic molecules on platinum catalyst surfaces: from the fundamentals to the polymer electrolyte fuel cell applications, in *Faculty of Chemistry and Materials Sciences*, p. 81, HELSINKI UNIVERSITY OF TECHNOLOGY, Helsinki (2009).

112. G. M. Brisard, *Electrocatalysis- Proceedings of the international symposium* p. 351, The Electrochemical Society (ECS) (2006).

113. R. S. Deinhammer, M. Ho, J. W. Anderegg and M. D. Porter, *Langmuir*, **10**, 1306 (1994).

Appendix A. Calculation of ECA using samples data

Principle

The ECA was calculated by integrating the area under the H_{upd} region (the hashed area in figure) where the protons (H^+) adsorb on Pt sites (between 0.04 and 0.4 V) during the cathodic sweep. Hydrogen adsorbs and desorbs on Pt sites after the capacitive region, on the negative sweep. If the WE is scanned more negative close or beyond 0V hydrogen gas evolves.

$$ECA = \frac{\frac{\int IdE}{\nu}}{210 * L_{Pt} * A_{geo}} \quad (1)$$

In the hydrogen region, protons interact with the catalyst surface, adsorbing to the surface in the cathodic scan and desorbing in the anodic scan. In the oxygen region, hydroxide ions oxidize the surface in the anodic scan and are reduced from the surface in the cathodic scan. Between these regions is the double layer region, in which only double layer charging occurs.

In the equation, ν denotes the scan rate (ECA depends on scan rate), I is the current integrated over potential range of E, L_{pt} denotes the Pt loading in $\mu g_{Pt}/cm^2_{elec}$, A_{geo} is the geometric area of the WE with the catalyst ink coating.

The area under the H_{upd} region could be calculated using the inbuilt program of the AfterMATH® by Pine Instruments, or the data can be imported into the excel and

using a macro program the area under the curve can be calculated by simple numerical methods like triangle rule or trapezoid rule. This area not only gives the ECA but also calculates the moles of available Pt on the surface of the catalyst as given by equation 4 in appendix B.

For our experiments the H_{upd} region is integrated using Excel Macro® program using Trapezoidal rule. The program in Macro, supplied by General Motors Fuel Cell Program, as follows:

Function: Output Calculation

```
Option Explicit
Sub OutputCalcs()
Dim macwb, macMain, macCyc, macECA
Dim EStt!, EStp!, EStt2!, EStp2!, EStt3!, EStp3!, ScR!, hi!, lo!
Dim sumM1!, sum0!, isumM1!, isum0!, isumP1!, avgM1!, avg0!, iavgM1!, iavg0!,
iavgP1!
Dim m1#, m2#, Rshort#, avg1#, avg2#, i_x_over#, i_dbl_layer#
Dim rend&, r&, rarray&, a&, a1&, b&, b1&, lowerboundrow&, lstc&, numcycs&, cyc&
Dim cyc1_E_array(), cyc1_i_array(), cyc1_icorr_array(), lowerbound
Dim cntA%, cntB%, Ec%, ic%
Dim short_E_up(), short_i_up(), short_E_down(), short_i_down() As Single
Dim area#, E#, EM1#, i#, iM1#, subtractor_i_plus#, subtractor_i_minus#, base1#, base2#,
height_#, ECA#, _
   ECA2#, area2#, area3#, ECA3#, area4#, ECA4#
Dim sub_i_missing As Boolean
'Background Info
   Set macwb = Workbooks(ThisWorkbook.Name)
   Set macMain = macwb.Sheets("Main")
   Set macCyc = macwb.Sheets("CycleData")
   Set macECA = macwb.Sheets("ECAData")
   EStt = macMain.Cells(25, 2)
   EStp = macMain.Cells(27, 2)
   EStt2 = macMain.Cells(29, 2)
   EStp2 = macMain.Cells(31, 2)
   EStt3 = macMain.Cells(33, 2)
```

```
    EStp3 = macMain.Cells(35, 2)
    ScR = macMain.Cells(7, 2)

'determine number of cycles
    lstc = macCyc.Cells(2, 13).End(xlToRight).Column
    numcycs = macMain.Cells(2, 5).End(xlDown).Row - 1       '(lstc - 12) / 3

'Must redim here so I can redim later to the correct (cntA & cntB) length
ReDim short_E_up(1024), short_i_up(1024), short_E_down(1024), short_i_down(1024)
As Single
num_avg_pts = 3
For cyc = 1 To numcycs
    Ec = 7 + cyc * 3
    ic = 8 + cyc * 3
    rend = macCyc.Cells(2, ic).End(xlDown).Row
ReDim cycl_E_array(rend), cyc1_i_array(rend)
    cyc1_E_array = Range(macCyc.Cells(2, Ec), macCyc.Cells(rend, Ec))
    cyc1_i_array = Range(macCyc.Cells(2, ic), macCyc.Cells(rend, ic))
    'subtractor_i = 0
    sub_i_missing = True
    For r = 2 To rend - 1
        E = cyc1_E_array(r, 1)
        EM1 = cyc1_E_array(r - 1, 1)
        i = cyc1_i_array(r, 1)
        iM1 = cyc1_i_array(r - 1, 1)
       If E <= EStp And EM1 >= EStp And i < 0 Then subtractor_i_minus = i  'And
sub_i_missing
        If E >= EStp And EM1 <= EStp And i > 0 Then subtractor_i_plus = i

    Next r
  '*************************Area Calculation*****************************
'For cyc = 1 To numcycs
    area = 0
    area2 = 0
    area3 = 0
    area4 = 0
        'cyc1_E_array = Range(macCyc.Cells(2, Ec), macCyc.Cells(rend, Ec))
    'cyc1_icorr_array = Range(macCyc.Cells(2, ic), macCyc.Cells(rend, ic))
    For r = 2 To rend - 1
        E = cyc1_E_array(r, 1)
```

```
        EM1 = cyc1_E_array(r - 1, 1)
        i = cyc1_i_array(r, 1)
        iM1 = cyc1_i_array(r - 1, 1)
        If i < 0 And E > EStt And E <= EStp Then
           base1 = i - subtractor_i_minus
           base2 = iM1 - subtractor_i_minus
           height_ = Abs(E - EM1)
           area = Abs(base1 + base2) / 2 * height_ + area
        End If
              If i > 0 And E > EStt And E <= EStp Then
           base1 = i - subtractor_i_plus
           base2 = iM1 - subtractor_i_plus
           height_ = Abs(E - EM1)
           area2 = Abs(base1 + base2) / 2 * height_ + area2
        End If

If i > 0 And E > EStt2 And E <= EStp2 Then
           base1 = i
           base2 = iM1
           height_ = Abs(E - EM1)
           area3 = Abs(base1 + base2) / 2 * height_ + area3
        End If

        If i < 0 And E > EStt3 And E <= EStp3 Then
           base1 = i
           base2 = iM1
           height_ = Abs(E - EM1)
           area4 = Abs(base1 + base2) / 2 * height_ + area4
        End If

      Next r
      ECA = area * 1000 '/ 210 / ScR * 1000000000 '/ AA / PtL
      macMain.Cells(cyc + 1, 6) = ECA
      ECA2 = area2 * 1000 '/ 210 / ScR * 1000000000
      macMain.Cells(cyc + 1, 7) = ECA2
      ECA3 = area3 * 1000 '/ 210 / ScR * 1000000000
      macMain.Cells(cyc + 1, 8) = ECA3
      ECA4 = area4 * 1000 '/ 210 / ScR * 1000000000
      macMain.Cells(cyc + 1, 9) = ECA4
    Next cyc
```

End Sub

Function : cycle splitting:

```
Option Explicit
Public num_avg_pts As Integer
Sub split_cycles()
Dim macwb, macMain, macCyc, macECA, datawb, dataws As Variant
Dim Ecol%, icol%, num_avg_pts%, cycle%
Dim First_Turn, Second_Turn As Boolean
Dim starting_potential, cycle_start_r
Dim rend&, rstart&, rnew&, rold&, r&, r2&, r3&, rarray&
Dim sumM1!, sum0!, sumP1!, avgM1!, avg0!, avgP1!
Dim fname As String, cellval As String
Dim E_array(), i_array()
Dim cycle_E0(0 To 65535, 0 To 0), cycle_i0(0 To 65535, 0 To 0)
Dim cycle_E(0 To 65535, 0 To 0), cycle_i(0 To 65535, 0 To 0) As Single
Dim corrected_i() As Single

   Application.ScreenUpdating = False
   Application.Calculation = xlCalculationManual
 fname = Cells(13, 1).Value
   If ISLIKE(fname, "*.cor") Then
      Workbooks.OpenText Filename:=fname _
      , Origin:=20127, StartRow:=1, DataType:=xlDelimited, TextQualifier:= _
      xlDoubleQuote, ConsecutiveDelimiter:=False, Tab:=True, Semicolon:=False, _
      Comma:=False, Space:=False, Other:=False, FieldInfo:=Array(Array(1, 1), _
      Array(2, 1), Array(3, 1)), TrailingMinusNumbers:=True
   Else
      Workbooks.Open Filename:=fname
   End If
'Background Info
   Set macwb = Workbooks(ThisWorkbook.Name)
   Set macMain = macwb.Sheets("Main")
   Set macCyc = macwb.Sheets("CycleData")
   Set macECA = macwb.Sheets("ECAData")
   Set datawb = Workbooks(ActiveWorkbook.Name)
   Set dataws = datawb.Sheets(ActiveSheet.Name)
   rend = Cells(1048576, 1).End(xlUp).Row      'subtract 1 if you un-comment delete
code on ln 20
   'macMain.Range("Cycles").ClearContents
   'macCyc.Range("A2:FZ65536").Clear
```

```
Do
        rstart = rstart + 1
        cellval = Cells(rstart, 1)
    Loop Until IsNumeric(cellval)  'ISLIKE(UCase(cellval), "END COMMENT*")

Ecol = 1            'the column with voltage values from the scan
icol = 2            'the column with current values from the scan
num_avg_pts = 3     'the number of points to average for finding cycles & peaks
First_Turn = False
Second_Turn = False

ReDim E_array(rend - rstart), i_array(rend - rstart)
E_array = Range(Cells(rstart, 1), Cells(rend, 1)).Value
i_array = Range(Cells(rstart, 2), Cells(rend, 2)).Value
worksheet
    rnew = 0
    cycle = 0
    For r = 1 + num_avg_pts * 2 To rend - rstart - num_avg_pts * 2
        sumM1 = 0
        sum0 = 0
        sumP1 = 0
        For rarray = r - num_avg_pts * 2 To r
            sumM1 = E_array(rarray, 1) + sumM1
            sum0 = E_array(rarray + num_avg_pts, 1) + sum0
            sumP1 = E_array(rarray + num_avg_pts * 2, 1) + sumP1
        Next rarray
avgM1 = sumM1 / (num_avg_pts * 2 + 1)
        avg0 = sum0 / (num_avg_pts * 2 + 1)
        avgP1 = sumP1 / (num_avg_pts * 2 + 1)
        If r = 1 + num_avg_pts * 2 Then
            starting_potential = avgM1
            cycle_start_r = r
        End If
              If avgM1 > avg0 And avg0 < avgP1 Then
            First_Turn = True
        End If
        If avgM1 < avg0 And avg0 > avgP1 Then
            Second_Turn = True
        End If
```

```
 If First_Turn And Second_Turn And (avg0 <= starting_potential Or r = rend - rstart -
num_avg_pts * 2) Then
        cycle = cycle + 1
        macMain.Cells(cycle + 1, 5) = "Cycle " & cycle
        For r2 = cycle_start_r To r
           cycle_E(r2 - cycle_start_r, 0) = "=" & E_array(r2, 1) & "+Main!$B$9"
           cycle_i(r2 - cycle_start_r, 0) = i_array(r2, 1)
        Next r2
        Range(macCyc.Cells(2, cycle * 3 + 7), macCyc.Cells(2 + r - cycle_start_r, cycle *
3 + 7)) = cycle_E
        Range(macCyc.Cells(2, cycle * 3 + 8), macCyc.Cells(2 + r - cycle_start_r, cycle *
3 + 8)) = cycle_i

        If cycle = 1 Then
           macCyc.Cells(1, 1) = "Cycle"
           macCyc.Cells(1, 2) = 1
           Range(macCyc.Cells(2, 1), macCyc.Cells(2 + r - cycle_start_r,
1)).FormulaR1C1 = "=OFFSET(RC7,0,R1C2*3)"
           Range(macCyc.Cells(2, 2), macCyc.Cells(2 + r - cycle_start_r,
2)).FormulaR1C1 = "=OFFSET(RC8,0,R1C2*3)"
           Range(macCyc.Cells(2, 3), macCyc.Cells(2 + r - cycle_start_r,
3)).FormulaR1C1 = "=OFFSET(RC9,0,R1C2*3)"
        End If
        cycle_start_r = r
        First_Turn = False
        Second_Turn = False
        r = r + num_avg_pts * 4
     End If
  Next r
     datawb.Close
     Application.Calculation = xlCalculationAutomatic
  Application.ScreenUpdating = True
End sub
```

This Macro enables to split the cycles of the CV and also integrate the area under the hydrogen adsorption region (0.04 to 0.4 V in the cathodic scan). This area is also divided by the scan rate and Pt loading to give the value of electrochemical surface area (ECA) or moles of Pt available.

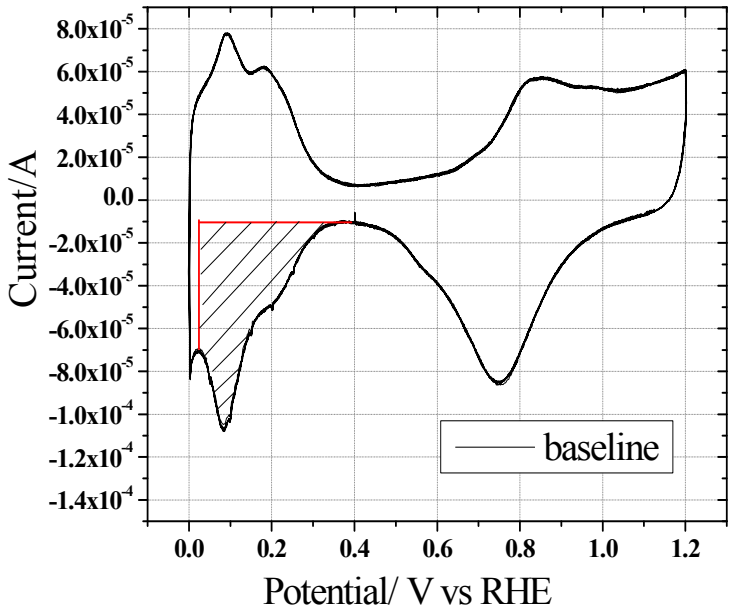

Figure A.1. Area under the curve in H_{upd} region used to calculate electrochemical surface area (ECA) and moles of available Pt

Appendix B. Monolayer equivalent of leachate solution calculation

The charge (Q) was calculated from integrating the current (I) over the potential range (E) diving by the scan rate (ν) under the H_{upd} region as shown in equation 1.

$$Q = \frac{\int IdE}{\nu} \quad (1)$$

For all the CV experiments depicted in this dissertation the value of ν is 20 mV/s or 100 mV/s.

The adsorption of hydrogen is governed by the following equation (2)

$$H_2 + Pt \leftrightarrow Pt\text{-}H_{ads} + H^+ + e^- \quad (2)$$

$$X + Pt \rightarrow Pt\text{-}X \quad (3)$$

For each mole of electron transfer one mole of H_2 adsorbs on Pt.

The magnitude of the charge of one mole of electrons is given by 96485. For Q amount of charge moles of Pt can be calculated from equation 3.

$$mol\ of\ Pt = \frac{Q}{96485} \quad (4)$$

Assuming one C from the leachate solution adsorbs in one Pt site, the monolayers of C atom was calculated using equations 4 and 5.

$$C\text{-}Pt = H\text{-}Pt \quad (5)$$

Though this assumption was not accurate for all organic species, it provided a manageable means of calculating an approximate surface coverage of unknown extract solution. A monolayer equivalent of surface coverage was assumed when enough moles of carbon in the leachate/extract solution was added to bond to every mole of active sites on the platinum surface. As shown in [4], a molar quantity of carbon was calculated by multiplying the desired number of monolayer equivalents of coverage by the number of moles of active sites as calculated in [2].

$$\text{Mol of C} = \text{monolayers x moles of Pt} \tag{6}$$

The volume added in the electrolyte can be calculated by equation 6.

$$\text{Volume in ml} = \frac{\text{mol C(mol)} * 12 \frac{\text{g}}{\text{mol}}}{1 \frac{\text{g}}{\text{ml}} * \text{TOC (ppm)} * 10^{-6}} \tag{7}$$

Concentration of C atoms in the leachate is given by equation 7.

$$\mu M = \frac{TOC}{12 * 1000} \tag{8}$$

Therefore, in 145ml of electrolyte the final concentration of C atoms from the leachates can be obtained from equation (8)

$$\mu M = \frac{\text{volume in ml} * \text{TOC}}{12 * 1000 * (145 + \text{volume in ml})} \tag{9}$$

A sample calculation for 50 MLs of carbon coverage on Pt is presented in table A.1, assuming 0.02 V/s sweep rate, charge (Q) calculated to be 0.0005 C and moles of Pt available in uncontaminated electrode to be 5.2×10^{-9} (calculated from the area under hydrogen adsorption region by integrating between 0.04 to 0.4 V, see appendix A), mol.

wt. of carbon being 12 mol/g, TOC of a leachate 750 ppm, density of leachate solutions 1g/cc, the equation 7 can be substituted as,

$$Volume\ in\ ml = \frac{50 * 12\ * 5.2 * 10^{-9}}{1 * 750 * 10^{-6}}$$

Volume in ml = 0.00412

Table B.1. Example of calculation of leachate volume added during the contamination experiments based on the initial moles of available Pt in the catalyst

MLs	Charge Q, C	Moles of Pt	Volume added, ml	Concentration of carbon, µM
50	0.0005	5.2×10^{-9}	0.00412	1.8
500	0.0005	5.2×10^{-9}	0.0412	18
5000	0.0005	5.2×10^{-9}	0.412	180

Appendix C. Effect of purging, hold and cycle time and DI water on ECA

Effect of purging before CV experiments

The purpose of purging the electrolyte before conditioning with inert gas was to make the electrolyte free of dissolved oxygen. Since presence of oxygen can interfere with the different peaks of the CV it is desirable to make the electrolyte free from any dissolved oxygen. The open circuit voltage (OCV) at the beginning of the experiment (before purging) was measured to be around 0.85-0.9 V. The OCV after purging the fresh electrolyte with N_2 for 15 minutes (900 s) came down to 0.45 V. The effect of purging was further observed after breaking in the electrode. During the break-in the OCV was recorded to decrease below 0.4 V. The significance of purging the fresh electrolyte with inert gas is evident in figure 4. The one way of detecting any dissolved oxygen inside the RDE cell is to measure the OCV of the cell before running cyclic voltammograms.

The effect of hold time on CV cycles

Prior to cyclic voltammetric scans, the potentiostatic hold experiments were performed for different amounts of time. The first row of table C.1 denotes the cumulative time of holds (total time of hold before performing the CV). For the first set of experiment, (CVs longer time), the working electrode was held initially for 10 minutes before running the first CV. It was subsequently held for another 10 minutes (total 20 minutes), 35 minutes (total 55 minutes) before transferring the electrode to the clean electrolyte in the second cell for recovery. The ECA loss was 8%, 11%, and 18%,

respectively. To isolate the effect of potentiostatic hold from that of the CV scans, a number of the longer hold times were broken down into small segments of shorter hold times. During the first set of experiments (exp. 1), the WE was held for 20 minutes and the ECA loss was only 8% after first 10 minutes compared to an ECA loss of 11% after another 10 minutes hold (i.e. after a total of 20 minutes hold). In another experiment (exp. 2) of total 20 minutes hold (without truncating the hold in two 10 minutes holds), the loss in ECA was 8%. This proved that the longer the hold time, the higher ECA loss and two 10 minutes hold had higher effects on ECA loss than one 20 minutes hold. Therefore, the CV cyclic had contributed to the extra loss of ECA during the exp. 1 (two 10 minutes hold). But these experiments did not specify whether holding the WE or the CV scanning had more effect on the ECA loss. In a third set of shorter time hold experiments (exp. 3), the WE was held for 5 minutes, then for 10 minutes (total 15 minutes hold), and finally – for another 5 minutes (total 20 minutes). Each hold was followed by 3 cycles of CV scans. The ECA loss was 1%, 4% and 11%, respectively. In this case, the final ECA loss was same as that of the after first two 10 minutes during the longer hold experiments. The final set of shorter hold experiments (exp. 4), were performed with six small 5-minutes hold segments with total holding time equal to 30 minutes. In this case also there was a gradual decrease in ECA and finally at the end of 30 minutes the ECA loss amounted to 20%, which was still less than the ECA loss due to longer holding time of total 55 minutes during the longer holds experiments. It is clear from the above mentioned experiments that the holding the WE at 0.4 V had more detrimental impact on ECA than CV scans. Also if the holds are broken into smaller segments, the ECA loss is higher than that of during one single hold for the same amount

of time, since each hold was followed by partial scans of CV and there was a loss due to the CV scans as well. This loss of ECA due to hold and cycling was attributed to the adsorbate species from the electrolyte [16] and also to the impurities from gas purging.

Effects of DI water on CV

Before introducing the contaminants in the electrolyte, it was important to explore the effects of DI water, since the assembly aids were soaked in DI water at an elevated temperature. Also, the process of adding the contamination can be simulated by adding DI water. Addition of contaminants increases the volume and therefore pH of the electrolyte. By adding DI water, all above mentioned effects could be studied, and appropriate measurements could be taken before adding the contaminants at liquid phase. To study the effect of DI water, the partial CVs were performed till 0.5 V after holding the electrode at 0.4 V for 10 minutes. This process was repeated 6 times so that the total time of hold was 60 minutes. The CVs recorded after 10, 20, 30, 40, 50 and 60 minutes are presented in figure C.2 as CVs 1 to 6.

When no DI water was added, there was some loss in ECA due to potential hold and potential cycling. The DI water had some effects as well. The partial CV scans after adding DI water is shown in figure 5.

The comparison of loss of ECA (in %) due to holding the electrode for 10 minutes and cycling 3 times at the end of hold without adding and after addition of DI water (1000ML, 31ml) was given in figure C.3. In the first case, the loss in ECA was 24% and in the second case – ECA decreased up to 32% at the end of 60 minutes, for partial scans at a scan rate of 20 mVs^{-1}.

Effects of plastic leachates on CV

Figure C.3 illustrates the contamination behavior of the leachant extracts from the two structural plastics. The control experiment with water showed some contamination. Therefore it is very important to subtract the loss due to addition of DI water from the absolute values of loss during contamination with any leachant (soaked in DI water).

The contamination effect of the balance of plant (BOP) materials such as Ultramid® and Ryton® used as structural plastic in a fuel cell was recorded after injecting the leachant extracts in RDE cell at room temperature. The WE was held for 10 minutes followed by partial CV scans. Figure C.3 shows the effect of the leachant addition on the electrochemical surface area. The effect of Ultramid® was much more severe than that of Ryton®. From the TOC of the Ultramid® and Ryton®,(Ultramid® being higher than Ryton®) it was apparent that the first leachant had more total organic carbon present in the leachant than that of the second leachant. Therefore the volume of the contaminants were adjusted to bring the final concentration of the total organic carbon in the electrolyte after injecting the leachants from Ultramid and Ryton will be the same (see equations 1 to 6 for detailed calculations). For detailed chemical analysis please refer to (32, 68). The source of the contamination may be from the degradation of the plastic pellets at higher temperature inside the DI water. The leachant obtained at the end of the soaking period was a mixture of organic, inorganic materials and ions. Future studies with the organic, inorganic and ions separately will enlighten about the exact cause of contamination.

Figure C.4 shows the CVs performed from 0 to 0.75, 0.85, 0.95, 1.05 V potentials to observe any improvement due to cycling to higher potentials. The figure also shows

increase in the area under the Pt-O reduction region as well as area under the H_{upd} with cycling to higher potentials. These CVs suggest that higher potential cycling helped increase adsorption and desorption currents because higher potential cathodical scans facilitated more Pt-O and then Pt-OH adsorption and oxidation after 0.8 V till 1.05 V consequently promoting an increase in reversible hydrogen adsorption and Pt-OH reduction current (shown with arrows).

This segmented recovery process is a proficient way to recover as it not only helped us determine the right potential at which recovery was most efficient, but also gave us insight about the process of recovery. Since the properties of the contaminant molecules would be unknown most of the time, any electrochemical oxidation or reduction process undergone by the molecules during recovery can be captured from the current recorded during the holds. Figure C.3 shows the effect of the holds at higher potential and the partial scans. The recovery of the Pt-O reduction region was significantly high. Recovery was observed in the H_{upd} region also. Figure 9 shows the final recovery of the ECA due to both potential holding and cycling. The lost Pt sites were almost completely recovered. Therefore, addition of DI in the electrolyte had fully reversible contamination effect.

Conditions: CVs were scanned at 20 mVs^{-1} without any rotation of the electrode in a well purged (with N_2 gas) clean electrolyte.

Table C.1. Summary of % loss of ECA due to holding and cycling of clean and conditioned working electrode in a fresh electrolyte.

% loss of ECA	After 5 minutes	After 10 minutes	After 15 minutes	After 20 minutes	After 25 minutes	After 30 minutes	After 55 minutes
Exp. 1- CVs after longer time hold		8		11			24
Exp. 2- CVs (after shorter time hold)				8			
Exp. 3- CVs (after shorter time hold)	1		4	11			
Exp. 4- CVs (after shorter time hold)	3	6	11	13	17	20	

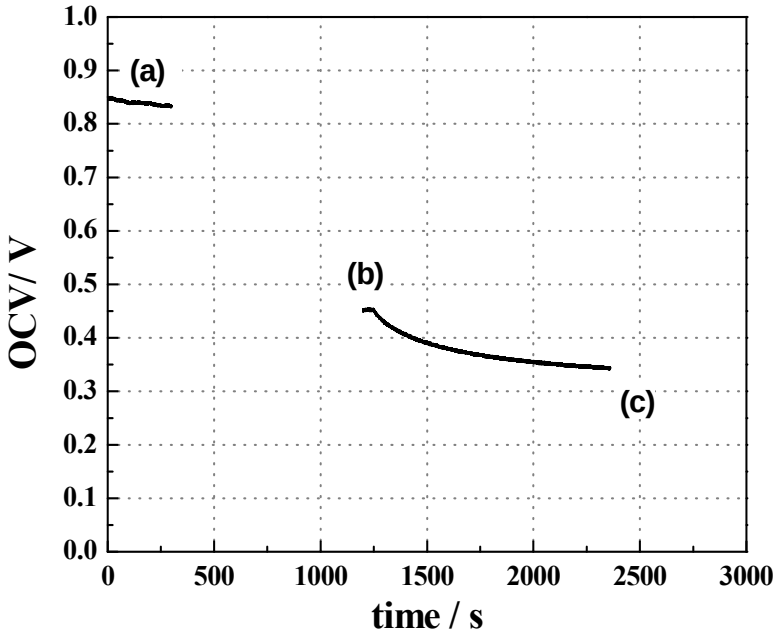

Figure C.1. Open circuit potential before purging the electrolyte with inert gas was as high as 0.85 V due to the presence of dissolved O_2 in the electrolyte (a). After purging for 15 minutes the OCV came down to 0.45 (b) and after conditioning (WE was subjected to potential cycling between 0 to 1.2 V at a rate of 100 mVs^{-1}) the OCV further reduced to 0.3 V (c).

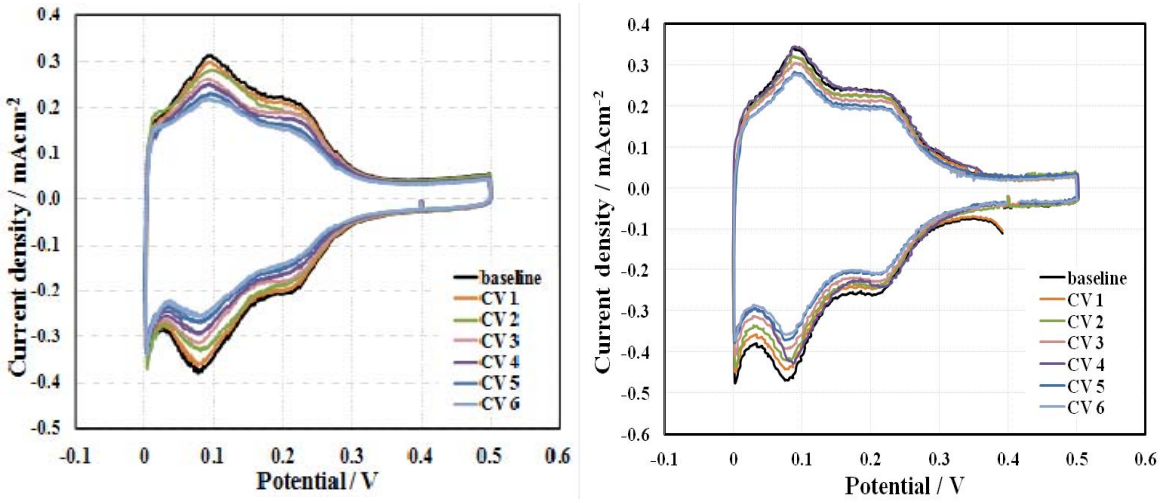

Figure C.2. Effect of DI water (left) on the partial cyclic voltammetries and baseline cyclic voltammetries during the control experiments, with no DI water added (right). CVs 1 to 6 correspond to the CVs at the performed at 10 minutes intervals.

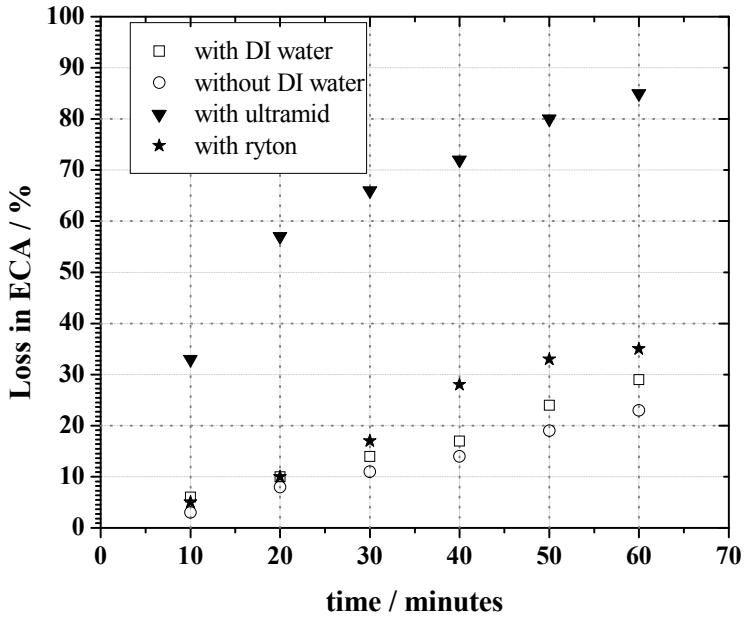

Figure C.3. The % loss in ECA before and after contaminating the electrolyte with DI water, Ultramid® and Ryton®. The scans were performed after 10 minutes intervals of holds.

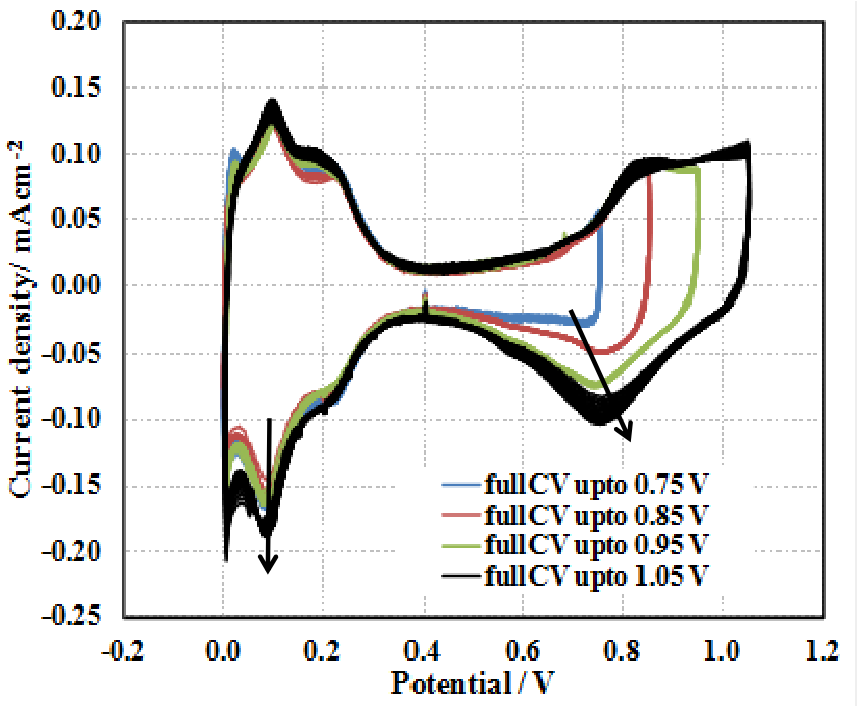

Figure C.4. Cycling to higher potential can restore the lost ECA. The figure shows the effect of potential scans on several higher potential regions of the CV.

Appendix D. Calculations for ORR mass and Pt area specific activities

Principle

The reduction of oxygen proceeds through a four electron pathway to H_2O or a two electron pathway to H_2O_2.

$$O_2 + 4e^- + 4H^+ \rightarrow 2H_2O \text{ } (4e^- \text{ transfer pathway}) \quad (1)$$

$$O_2 + 2e^- + 2H^+ \rightarrow H_2O_2 \quad (2)$$

$$H_2O_2 + 2e^- + 2H^+ \rightarrow 2H_2O \text{ } (2e^- \text{ transfer pathway}) \quad (3)$$

Although four electron is the major pathway for oxygen reaction for Pt (111) and Pt (100) surfaces H_{upd} region is <0.3 V, a substantial amount of H_2O_2 is generated[3]. Since carbon supported Pt catalysts typically consists of crystals with large fraction of Pt (111) and Pt (100), it resembles the single crystal properties.

The dissociative mechanism and the associative mechanism are proposed for a low current density range and a high current density range, respectively:

(1) Dissociative Mechanism:

$$1/2O_2 + * \rightarrow O* \quad (4)$$

$$O* + H^+ + e^- \rightarrow OH* \quad (5)$$

$$OH^* + H^+ + e^- \rightarrow H_2O + * \quad (6)$$

where * denotes a site on the Pt surface. In this mechanism, no H_2O_2 is produced. On a Pt surface, O_2 adsorption breaks the O-O bond and forms adsorbed atomic O, which further gains two electrons in the two consecutive steps, forming water.

Since there is no adsorbed O_2 on the Pt surface, H_2O_2 cannot be formed. This mechanism can be considered a detailed form of the direct 4-electron pathway.

(2) Associative Mechanism:

$$O_2 + * \rightarrow O_2^* \quad (7)$$

$$O_2^* + H^+ + e^- \rightarrow HO_2^* \quad (8)$$

$$HO_2^* + H^+ + e^- \rightarrow \quad (9)$$

$$O^* + H^+ + e^- \rightarrow OH^* \quad (10)$$

$$OH^* + H^+ + e^- \rightarrow H_2O + * \quad (11)$$

This mechanism also does not involve H_2O_2. Since adsorbed O2 is present, the O-O bond may not be broken in the following steps, resulting in the formation of H_2O_2. The H_2O_2 could either be further reduced to H_2O or be a final product (84).

Based on $4e^-$ reduction of oxygen to water specific activity (was) and mass activity (i_m) were calculated. The limiting current (i_{lim}) and the current at 0.9 V were recorded.

i_{lim} in theory should be 5-6 mA/cm^2 electrode. But it has to be corrected for 0.196 cm^2 electrode (5mm diameter, RDE) and also for the partial pressure of oxygen which in Denver was 83 kPa. Thus, the calculation follows equation 2.

$$i_{\text{lim corrected}} = \frac{\text{i lim}}{\text{electrode area}} * \frac{101}{83} \quad \text{..... (12)}$$

Correction for mass transport limitations is given by equation 3:

Mass transport free current

$$i_k = \frac{i_{lim} * i}{i_{lim} - i} \quad \text{..... (13)}$$

i_{lim} was the limiting current and i was the current at 0.9 V.

The data was corrected for the resistance in the electrolyte. Figure 3 shows the LSVs for iR corrected and as well as corrected for partial pressure of O_2 in Denver. Specific activity (was, $\mu A/cm^2_{Pt}$) and mass activity (i_m, mA/mg_{Pt}) after the corrections for mass transport, electrolyte resistance, partial pressure of oxygen are given by equations 4 and 5:

$$i_{s\ \text{corrected}} = \frac{i_k * 1.3 * 10^5}{\text{loading} * \text{ECA} * \text{area of electrode}} \quad \text{..... (14)}$$

$$i_{m\ \text{corrected}} = \frac{i_k * 1.3 * 10^3}{\text{loading} * \text{area of electrode}} \ldots \quad \text{. (15)}$$

1.3 was the correction factor to account for the combined effect of low partial pressure of gases in Denver.

The electrodes were prepared with different batches of inks and the ECA and ORR activities of Pt/VC as shown in figure D.1. Before performing ORR, the working electrode was held at 0.4 for ca. 7 minutes. During the ORR experiments, a short CV scan was performed before and after ORR to monitor any loss in ECA due to ORR.The seven electrodes were prepared and ran in clean electrolytes each time at room temperature. The average ECA was ca. 66 m^2/mg_{Pt}, average activity (I_m) was ca. 240 mA/mg_{Pt} and the average specific activity (I_s) was ca. 348 $\mu A/cm^2_{Pt}$.

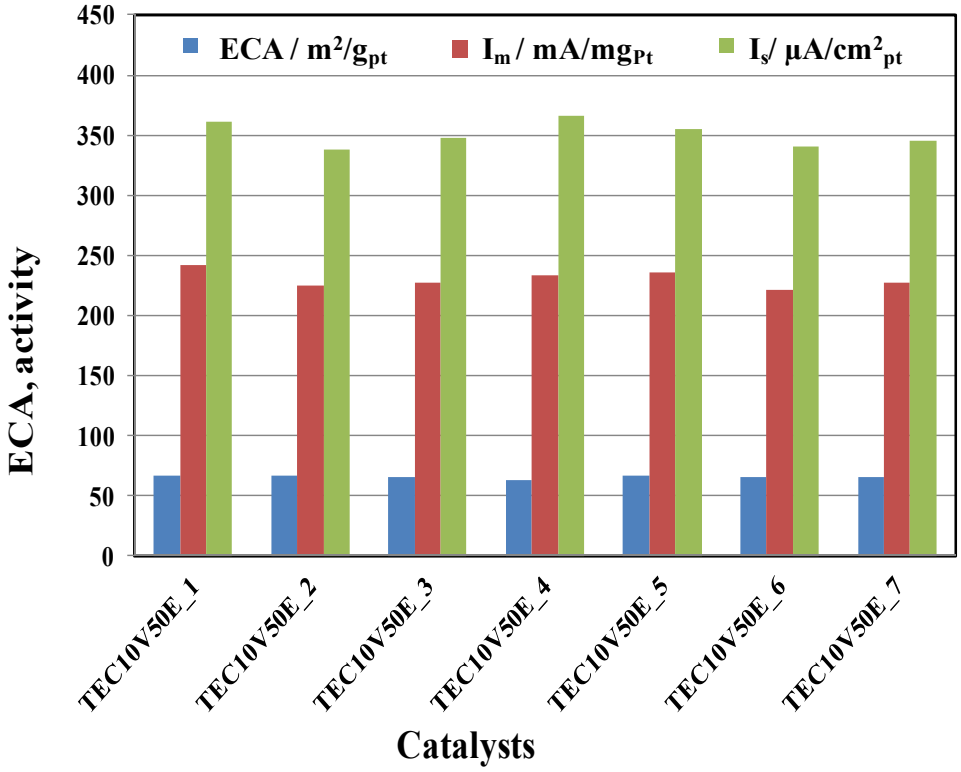

Figure D.1. Benchmarking the catalyst activities and ECA with seven batches of electrodes having inks made of catalyst TEC10V50E.

Appendix E. Calculations of Tafel Slope

Principle

The relationship between overpotential and te current is given by Butler Volmer equation (

$$i=i_0\left\{\exp\left[\frac{-\alpha_{rd}F(E-E_r)}{RT}\right]-\exp\left[\frac{\alpha_{ox}F(E-E_r)}{RT}\right]\right\} \quad (1)$$

In the case of a large cathodic current density the current as a function of overpotential η can be written

$$\eta=\frac{RT}{\alpha nF}\ln(i/i_0)$$

$$\text{or } \eta=b\ln(i/i_0)$$

$$\text{where, } b=\frac{2.303RT}{\alpha nF}$$

This corresponds to an early empirical equation by Tafel

$$\eta = a + b \log i$$

Below (Figure 1) is a plot of η vs. log of anodic current with a = 0.5. The linear plot is of the Tafel equation. The slope b is 2.3RT/anF. The intercept at η = 0 gives the exchange current density i_0. This is known as a Tafel plot.

The Tafel slope was calculated for higher potential (0.85-0.95 V, kinetic region) and lower potential (0.65-0.85 V, mass transfer limited region). With the increase of

contaminants the Tafel Slope increases because the mass specific current (i_m) decreases therefore for the same potential the kinetic current i_k increases with contamination.

The contamination changed the Tafel slope for both cases of contamination. The Tafel slope for the baseline or uncontaminated polarization curve was around 68-70 mV/decade which is as expected in 0.1 M perchloric acid. The Tafel slope was calculated for both high and low potential region and given in table 1.

For lower potential region it was difficult to extract the Tafel slope, since some of the data points in log plots were undefined after reaching the limiting current. Therefore Tafel slopes extracted at higher potential is much relevant.

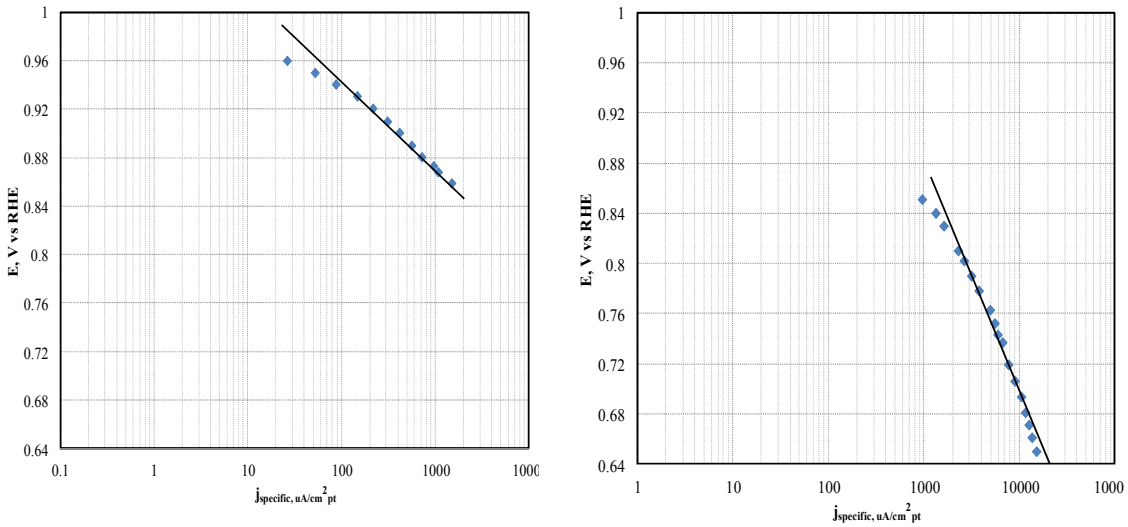

Figure E.1. Schematic showing the method of measuring Tafel slope. Due to the presence of double Tafel slope (94) the polarization curve was fitted in two different regions- higher potential region (0.95 to 0.85 V, left) and lower potential region (0.65 to 0.85 V, right).

Appendix F. Ring-rotating disk electrode (RRDE) experiments

Principle

In a rotating disk electrode a second working electrode in the form of a ring around the central disk of the first working electrode is added. The two electrodes are separated by a non-conductive barrier and connected to the potentiostat through different leads. To operate such an electrode it is necessary to use a bipotentiostat or some potentiostat capable of controlling a four electrode system.

Mechanism

The RRDE takes advantage of the form of the laminar flow created during rotation. As the system is rotated the solution in contact with the electrode is driven to the side of the electrode the same as with a rotating disk electrode. As the solution flows to the side it crosses the ring electrode and back into the bulk of the solution. If the flow in the solution is laminar then the solution is brought in contact with the disk quickly followed by the ring in a very controlled manner. This technique allows the surface concentration of reactants and products to be varied in a controlled manner through changes in the rotation rate and hence can be used to determine the reaction orders through the dependence of the current on the rotation rate without the necessity of varying the bulk concentrations.

An important extension of the rotating disc technique is the ring-disc configuration which consists of a disc surrounded by a closely placed concentric ring with its surface in the sane plane and separated from the disc by a thin insulating sleeve. The rotating ring-disc electrode is well suited to the study of electrode reactions involving unstable products or intermediates. Species produced electrochemically on the disc are monitored electrochemically on the ring as the liquid spirals out from the disc across the surface of the ring. The concentration of the species in question, averaged over the surface of the ring, can be determined in most instances by one of the following 2 procedures:

1. Maintain the ring potential at a iralue such as to reverse the 2rocess leading to the fornation of the species of interest and measure the ring current.
2. Construct the ring of a metal which is favorable for the completion of the overall electrode process yielding the intermediate in question on the disc or for the further oxidation or reduction of the product. Maintain the ring at a fixed potential favorable for such or scan through an appropriate range of potentials and measure the ring current.

The problem of mass transport by convective diffusion to a rotating disc electrode has been solved by Levich (1) for the case of a perfectly smooth, horizontal disc of infinite radius rotating at a constant angular velocity in an infinite liquid under conditions of laminar flow. In practice, a disc electrode can effectively meet these requirements if 1) the radius is very large compared to the momentum boundary layer.thickness, 2) all other surfaces within or bounding the liquid are at a distance large conpared to the radius of the rotating surface, 3) surface irregularities on the disc are small compared to the momentum boundary layer thickness, 4) the rotation rate for the particular disc is below

the critical Reynolds number for the onset of turbulence [i.e. Re = (r^2 w/v) < 10^5 where r = overall radius of the disc, w = angular rotation rate, v = kinematic viscosity].

O_2 on disk can either directly reduce to water or form intermediate H_2O_2 which further reduce to water. Production of peroxide undesired since loss of 2 electrons. Formed H_2O_2 desorbs from disk and can be detected in the ring (at 1.2 V) where it is oxidized back to O_2.

Appendix G. Characterization of leachates by TOC, GCMS and ICP-MS

Introduction

Leachate solutions were derived from the off the shelf plastic pellets and adhesives and lubricants. Leaching protocol involved soaking the assembly aid in water at elevated temperature for six weeks and then characterized analytically. The assembly aids were chosen for their variety of properties, as well as, their application as balance of plant [BOP] system components in PEM fuel cell systems.

Leaching Protocol

The leaching protocol was carried out using triply rinsed and capped polypropylene bottles. The assembly aids chosen are flowable and were spread out and allowed to cure on clean Teflon sheets, then peeled off of the sheets if possible and placed in the clean bottles of fresh DI water. A material surface area to volume of water ratio of 150mm2 / 1ml ratio was maintained for all samples. All bottles along with control blanks were placed in a calibrated oven at 90°C for 1 week. The exception was the Krytox lubricants, which were treated for 6 weeks due to their extremely low TOC and ICP total counts. Afterwards, the extract solutions were promptly removed and the solutions decanted off into clean bottles to separate the assembly aids from the leachant solution, to prevent and further leaching or re-adsorption. Aliquots (5ml) of the solution were taken at weekly intervals for pH and solution conductivity analysis.

Leachate characterization

Gas chromatography mass spectrometry (GCMS), total organic carbon (TOC), pH, solution conductivity, ion chromatography (IC) and inductively coupled plasma optical emission spectroscopy (ICP-OES) were used for characterization of leachates.

Total Organic Carbon (TOC) was determined using a GE Innovox, for levels up to 50,000 ppm and a TOC 900, for levels up to 50 ppm of total carbon. These systems employ a series of pumps and persulfate oxidation reactions to determine the total amount of carbon in a sample via CO_2 production. Samples were prepared in a 4:1 dilution of DI water to sample.

Leaching

GCMS was performed by a Thermo Scientific Trace/ISQ GCMS. 1.0 µl of liquid was injected into a SSL injector, volatilized and separated on a Thermo TG-5SILMS column with the resulting chromatogram generated by a total ion current [TIC] detector. The mass spectrometer was auto-calibrated to a perfluorotributylamine standard and each resulting peak/mass spectra underwent a NIST library spectral search of over 200,000+ molecules. High quality hits manually determined by the operator were reported as the species identified. After determination of model compounds selected for further study, pure standards were purchased from Sigma-Aldrich and run under the same conditions to verify molecular identification via comparison of retention time [RT] and mass spectrum.

ICP-OES was performed using a Perkin Elmer Optima 5300 DV axial radial instrument with a segmented array charge coupled device [SCD] and a shear gas of argon. Samples were acidified using nitric acid and the system was calibrated for 29 different

ions before and after runs. The ICP total value was calculated as the sum of the twenty nine individual values and is reported in Figure I.

IC was performed using a Dionex ICS-90 Ion Chromatography System with species separation on a Dionex Ion Pac AS14A IC column. The machine is calibrated for measuring six anions [F^-, Cl^-, Br^-, NO_3^-, PO_4^{3-}, and SO_4^{2-}]. The IC total value was calculated as the sum of the six measured values and is reported in Figure I.

Solution conductivity and pH were performed on aliquots removed from the leachant solutions with a Thermo Scientific Orion 4 Star pH/conductivity benchtop conductivity meter after calibration with a multi-point buffer standard solutions.

Appendix H. Baselining with Cl^- to study effect of anions

Principle

High-surface area fuel cell catalysts are often contaminated from the anions found in the leachates. It is well known from work on Pt single crystals, that anions can dramatically affect the kinetics of electrocatalytic reactions, e.g. the oxidation of small organic molecules or oxygen reduction. Although, the influence of specifically adsorbing anions on the ORR kinetics on high-surface area fuel cell catalysts is not widely researched.

In this study I investigated the anion effect on the ORR on a high-surface area Pt/Vulcan XC 72 catalyst, established a baseline before running experiments with mixture of chloride and organics as described in chapter 5.

ECA after addition of chloride

The baseline with chloride performed after adding 0.1 M HCl to the electrolyte to achieve 0.2, 2 and 20 ppm of final chloride concentration.

Volume added in electrolyte for 2 ppm = $\frac{2 \text{ x}145}{1000\text{x}35.5\text{x}0.1}$

The full and partial baseline CVs before adding the contamination showed usual peaks for Pt (111 and 100) in perchloric acid. When the first dose of contamination was added, the H_{upd} region region is suppressed as well as the Pt-OH region.

The decrease in activity due to the presence of chloride in solution is accompanied, but not quantitatively mirrored, by an increased formation of peroxide, as compared to the reaction in pure perchloric acid. Obviously, Clad acts mainly as a site-blocking species, which reduces the number of active sites for the orr to proceed. The double-layer region in the positive-going sweep and to a smaller extent in the negative sweep widens with increasing chloride concentration, caused by a strong retardation of oxide formation by adsorbed Cl^-. The reduced oxide formation in the presence of Cl^- is also demonstrated by the decreasing oxide reduction peak charge in the negative sweep (at ca. 0.8 V) with increasing chloride concentration

From the figure H.2, the onset for the ORR shifts to higher overpotentials with increasing chloride concentration in the solution. The ORR proceeded almost entirely as a 4 e^- reduction between 0.85 and ca. 0.3 V.

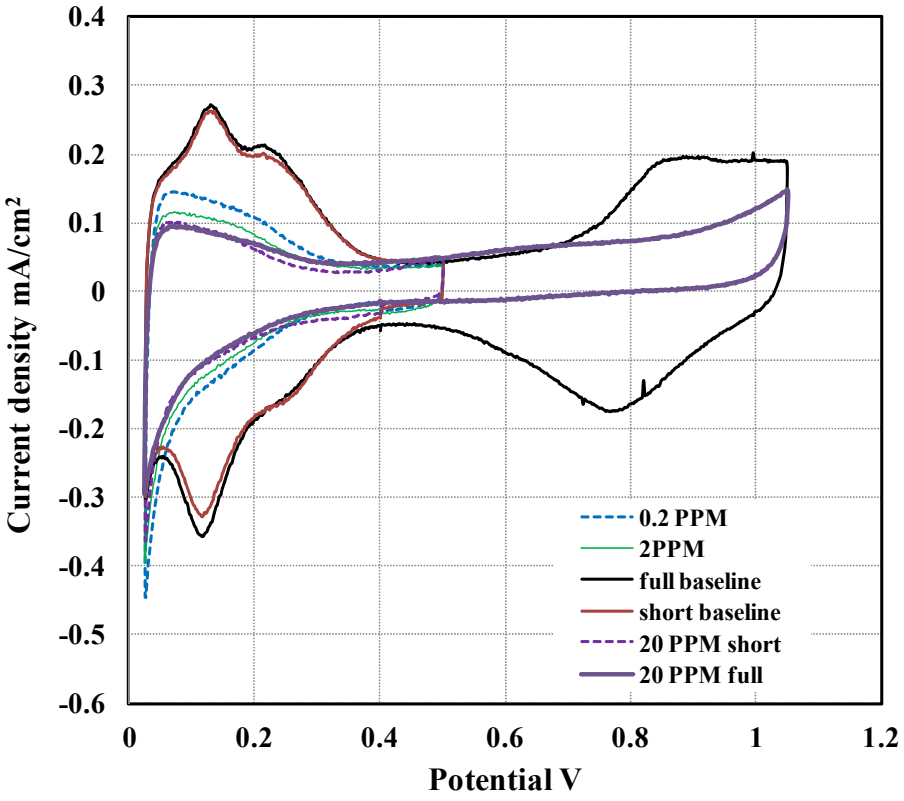

Figure H.1. Cyclic voltammograms before (black and red lines) and after adding different concentrations of chloride (0.2, 2 and 20 ppm)

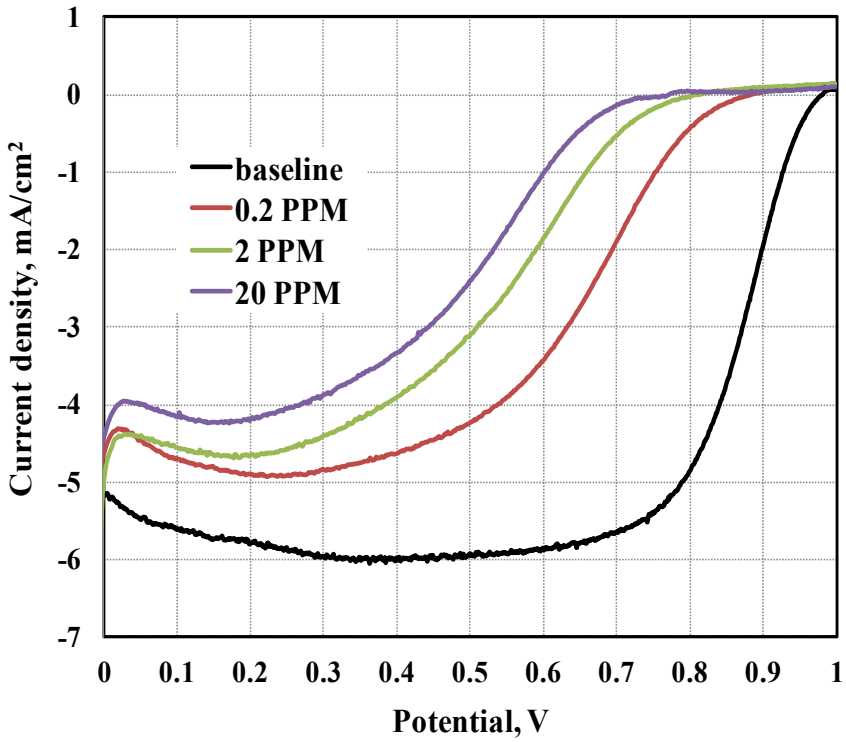

Figure H.2. ORR before (black line) and after adding different concentrations of chloride (0.2, 2 and 20 ppm)